INTERACTIONS OF THE PHOTOSYNTHETIC MACHINERY WITH THE PROTON MOTIVE FORCE: LIMITATIONS AND APPLICATIONS FOR IMPROVEMENT

By

Geoffry Austin Davis

A DISSERTATION

Submitted to
Michigan State University
in partial fulfillment of the requirements
for the degree of

Cell and Molecular Biology—Doctor of Philosophy

2018

ABSTRACT

INTERACTIONS OF THE PHOTOSYNTHETIC MACHINERY WITH THE PROTON MOTIVE FORCE: LIMITATIONS AND APPLICATIONS FOR IMPROVEMENT

By

Geoffry Austin Davis

The light reactions of photosynthesis convert harvested light into chemical energy that can be utilized by cells for metabolism. Through the translocation of protons across the thylakoid membrane coupled to electron transfer reactions, the photosynthetic proton motive force (*pmf*) is used to drive the production of ATP synthesis. Detailed studies have characterized the molecular processes of *pmf*–mediated feedback regulation of photosynthesis via changes in luminal pH from the light-induced proton gradient (ΔpH). While it is now well established that the photosynthetic *pmf* in higher plants consists of both a ΔpH and an electric potential ($\Delta\psi$), the impact that $\Delta\psi$ exerts on photosynthesis *in vivo* is mostly unstudied.

The $\Delta\psi$ component, however, influences the relative free-energy between redox mediators of electron transfer within membrane complexes. We found that in plants, a large *in vivo* $\Delta\psi$ increases photoinhibition through photosystem II (PSII) damage. High $\Delta\psi$ levels were observed in mutants with high steady-state *pmf* levels, as well as in wild type plants during light fluctuations. The increase in photoinhibition is primarily due to increased yields of electron recombination in PSII, which generate reactive oxygen species (ROS). The yield of PSII recombination when $\Delta\psi$ is large is mediated by ΔpH-dependent photosynthetic downregulation to decrease the concentration of reduced electron acceptors in PSII (Q_A^-) capable of recombining and generating ROS.

The ability to regulate photosynthetic light capture and electron transfer via pH–dependent processes as well as the need for photosynthetic organisms to mitigate a large $\Delta\psi$

leads me to propose that the photosynthetic organisms have evolved regulatory processes to mediate the bioenergetic limitations imposed by the $\Delta\psi$ effect on electron transfer. In a population of natural *Arabidopsis thaliana* accessions, variation in the kinetics of activating and deactivating pH-dependent downregulation of photosynthesis allowed the genetic loci responsible for the kinetics within this population to be mapped. These results suggest that photosynthetic organisms have evolved multiple mechanisms to regulate how rapidly photosynthesis is regulated by the *pmf*. The partitioning of *pmf* between $\Delta\psi$ and ΔpH allows a plant to balance the induction and relaxation of photoprotective mechanisms at the detriment of light utilization, while minimizing the impact of $\Delta\psi$-mediated PSII recombination and ROS production. The processes work in concert to minimize potential photodamage and loss of productivity that occurs due to biophysical alterations in electron transfer processes mediated by $\Delta\psi$.

ACKNOWLEDGEMENTS

My dissertation research has been tremendously impacted by the involvement of the Kramer lab as a whole, who have fostered a friendly, non-competitive environment full of creativity and, at times, weirdness. My mentor, Dr. David Kramer, has allowed me to grow as a scientist both in experimental work as well as communicating science. While at times challenging, I have greatly appreciated the determination for excellent science he pushes me towards.

I have had the pleasure to work on many projects with Dr. Mio Satoh-Cruz, from whom I have benefitted and learned her great organizational skills. Dr. Nicholas Fisher provides a wealth of knowledge for *in vitro* enzymology as well as all things tea and cricket. With Dr. Fisher, I had the pleasure of working with a former graduate student and postdoctoral researcher Dr. Deserah Strand on cyclic electron flow projects. The cyclic team was a great introduction to the Kramer lab during my rotation, and the energy and passion Dr. Strand has for research is inspiring.

Much of my work would not have been possible without the technical assistance of Dr. Jeff Cruz, Robert Zegarac, and Nathan Galbreath. The engineering assistance they have provided has allowed me to take instruments up to 11 for my experiments.

Linda Savage and David Hall, along with the undergraduate assistants they have employed, have been critical assistants in my many plant imaging experiments as well as resources for growing and managing Arabidopsis. Although my work did not often lead me into the algae group, I have appreciated the interest and feedback on experiments from Dr. Ben Lucker.

Many experiments were carried out in a timely and organized manner thanks in large part to the excellent assistance of Abigail Crampton while working as an undergraduate research assistant.

I have had the opportunity to conduct my dissertation research in the Michigan State University Department of Energy Plant Research Laboratory. The resources, expertise, and openness of the different lab groups has been an outstanding working environment. In particular, I have appreciated the opportunities to interact with Dr. John Froehlich, and learn from members of Dr. Tom Sharkey's carbon assimilation lab and Dr. Daniel Ducat's photosynthetic synthetic biology lab. Within my graduate department, I have enjoyed the weekly research seminars and the interactions with Dr. Sue Conrad and Dr. Kathy Meek. Outside of formal department affiliations, the interactions between labs at Michigan State University has allowed me to comfortably discuss questions with experts in many fields as they have occurred, and I am grateful for the openness that has been fostered.

Lastly, I would like to thank my partner Siobhan Cusack, who has worked with me as we have both navigated our dissertations. Your optimism and support have helped with the many difficulties graduate student life provides, and I think that after five years you now know what the proton motive force does.

TABLE OF CONTENTS

LIST OF TABLES

LIST OF FIGURES

KEY TO ABBREVIATIONS

$^1O_2$	Singlet oxygen
ΔG_{ATP}	Free-energy of hydrolysis of ATP
ΔpH	pH gradient
$\Delta\psi$	Electric field
ΦII	Quantum yield of photosystem II activity in the light
ΦDF	Quantum yield of delayed fluorescence
ϕ_f	Fluorescence yield
ATP	Adenosine tri-phosphate
ADP	Adenosine di-phosphate
ANOVA	Analysis of variance
DCMU	3-(3,4-dichlorophenyl)-1,1-dimethylurea
DF	Delayed fluorescence
e^-	Electron
ECS	Electrochromic shift
ECS_{inv}	Inversion of the electrochromic shift
ECS_{ss}	Electrochromic shift decay steady-state
ECS_t	Total amplitude of the electrochromic shift
F_o	Minimum chlorophyll fluorescence from dark-adapted sample
FRIP	Field recombination-induced photodamage
F_s	Fluorescence emission from sample in the light
F_V/F_M	Maximum quantum efficiency of photosystem II

g_H^+	Proton conductivity of the ATP synthase
H^+	Proton
K^+	Potassium cation
LEF	Linear electron flow
MAGIC	Multi-parent advanced generation inter-cross
NPQ	Nonphotochemical quenching
$NADP^+$/NADPH	Oxidized/reduced nicotinamide adenine dinucleotide phosphate
ODE	Ordinary differential equation
OEC	Oxygen-evolving complex
P	Primary reaction center donor
P_{680}	Primary photosystem II chlorophyll electron donor
P_{700}	Primary photosystem I chlorophyll electron donor
^1P	Singlet electron state of primary reaction center donor
^3P	Triplet electron state of primary reaction center donor
P^*	Excited state of primary reaction center donor
PAR	Photosynthetically active radiation
PC	Plastocyanin
Pheo	Pheophytin
P_i	Inorganic phosphate
pmf	Proton motive force
PMT	Photomultiplier tube
PQ	Plastoquinone
PQH_2	Plastoquinol

PSI	Photosystem I
PSII	Photosystem II
Q_A	Photosystem II primary electron acceptor quinone
Q_B	Photosystem II secondary electron acceptor quinone
q_E	Energy-dependent chlorophyll *a* fluorescence quenching
q_I	Photoinhibitory chlorophyll *a* fluorescence quenching
q_L	Fraction of photosystem II with Q_A
QTL	Quantitative trait locus
ROS	Reactive oxygen species
S_1/ S_2/ S_3/ S_0/ S_n	S-state of the oxygen-evolving complex
SNP	Single nucleotide polymorphism
SOSG	Singlet oxygen sensor green
VDE	Violaxanthin de-epoxidase
Y_Z	Photosystem II D1 protein tyrosine Z
ZEP	Zeaxanthin epoxidase

Chapter 1

Regulation of photosynthesis in higher plants by the thylakoid proton motive force

Geoffry A. Davis

1.1 Photosynthetic electron transfer is tightly coupled to the generation of a trans-thylakoid proton motive force.

Conversion of light into chemical energy in oxygenic photosynthetic membranes involves the capture of light and energy funneling through a series of redox intermediates to ultimately generate NADPH from $NADP^+$. These electron transfer steps are tightly coupled to proton transfer reactions across the membrane, stabilizing the electron transfer reactions via charge-coupled movement and generating a potential energy store in the form of the proton motive force (*pmf*) (1). Through the activity of the *pmf*, ATP synthesis via the rotary catalysis of the ATP synthase generates ATP for metabolic processes required for cellular proliferation. The *pmf* is composed of both a proton gradient (ΔpH) and an electrochemical gradient ($\Delta\psi$) created via redistribution of H^+ and other ion species between the thylakoid lumen and chloroplast stroma by photosynthetic processes (2). Both components are thermodynamically equivalent in driving the ATP synthase (3) and the total driving force for ATP synthesis can be described as:

$$pmf = \Delta\psi_{i-o} + \frac{2.3RT}{F}\Delta pH_{o-i} \qquad \text{(Eq. 1)}$$

where $\Delta\psi_{i\text{-}o}$ and $\Delta pH_{o\text{-}i}$ represent the electric field and proton gradient calculated as the difference in concentrations between the inside (lumen) and outside (stroma), *R* is the universal gas constant, and *F* is Faraday's constant. While both components of the *pmf* are thermodynamically equivalent drivers of ATP synthesis (3, 4), as can be seen from Eq. 1, $\Delta\psi$ and ΔpH are not kinetically equivalent, with a larger ΔpH required to reach an equivalent $\Delta\psi$ driving force. The *pmf* is primarily dissipated by H^+ efflux from lumen through the ATP synthase, but both *pmf* generation and dissipation are tightly regulated during photosynthesis, requiring coordination of the electron transfer processes with substrate acceptor availability in the chloroplast stroma (e.g.

$NADP^+$, ADP, P_i) to match the rapid processes of electron and proton transfer to the slower metabolic processes occurring in cells.

1.2 The photosynthetic *pmf* ΔpH is a key feedback regulatory loop.

During the course of oxygenic photosynthesis, the vectorial movement of electrons through membrane embedded proteins is tightly coupled to the deposition of protons into the thylakoid lumen (Fig. 1.1). This movement of protons both stabilizes the transfer of the electrons across the membrane and acts as a chemical store of potential energy through the generation of a proton gradient. While the *pmf* is dissipated through the ATP synthase to generate ATP, acidification of the thylakoid lumen during ΔpH generation acts as a feedback signal to various components of the light reactions (reviewed in 5).

As the ΔpH increases, protonation of violaxanthin deepoxidase occurs as the lumen pH decreases below ~6.5 and is fully active at pH ~5.8, leading to the accumulation of the carotenoid derivative zeaxanthin in the thylakoid membrane, which has a photoprotective role and is part of the energy-dependent nonphotochemical quenching (q_E) processes (Fig. 1.1) (6). Similarly, protonation of lumen-exposed glutamate residues of the peripheral antennae protein PsbS also contributes to q_E (7), which, in combination with zeaxanthin accumulation, contributes to the total q_E response (8). Following protonation of PsbS and accumulation of zeaxanthin, excitation energy is quenched in the antenna pigment protein complexes via energy transfer from singlet or triplet excited state chlorophylls to closely localized antenna carotenoid and zeaxanthin (9).

Acidification of the thylakoid lumen also acts as a thermodynamic limitation to the proton releasing steps of photosynthesis. Oxidation of plastoquinol by cytochrome b_6f results in the release of two protons into the lumen per plastoquinol oxidized, which is coupled to the

continuous activity of the Q-cycle, resulting in three protons transferred from the stroma into the thylakoid lumen per electron from PSII (10). As the lumen acidifies, the rate of plastoquinol oxidation at the cytochrome b_6f Q_o site decreases ten–fold from pH 7.5 to pH 5.5 (11, 12), limiting the rate of photosynthetic electron transfer (reviewed in (13, 14). Similarly, proton release from the PSII oxygen evolving complex (OEC) has also been shown to be kinetically limited by acidification of the lumen (15). Reduction of the primary PSII electron donor (P_{680}^+) is facilitated by redox intermediate states (S-states) of the Mn_4Ca OEC complex, during which changes in Mn oxidation status due to electron transfer to reduce P_{680}^+ are coupled to proton deposition in the lumen and water splitting (16, 17). Advancement of the of the OEC S-states becomes kinetically limited by the lumen pH *in vitro*, with the most alkaline pK_a (~4.6) associated with the S_3 to S_0 transition (15). Although a lumen pH of 4.6 is likely far below the physiological lumen pH limit (13), the pH limitation of water splitting would limit the amount of *pmf* that could be stored as ΔpH (15). This pH–mediated kinetic control allows the *pmf* to act as a feedback mechanism to the light capturing and electron transfer components of the thylakoid membrane to tune electron transfer processes to meet the capability of the thylakoid ATP synthase to generate ATP and relieve ΔpH, which is dependent upon substrate availability from metabolic processes (18, 19).

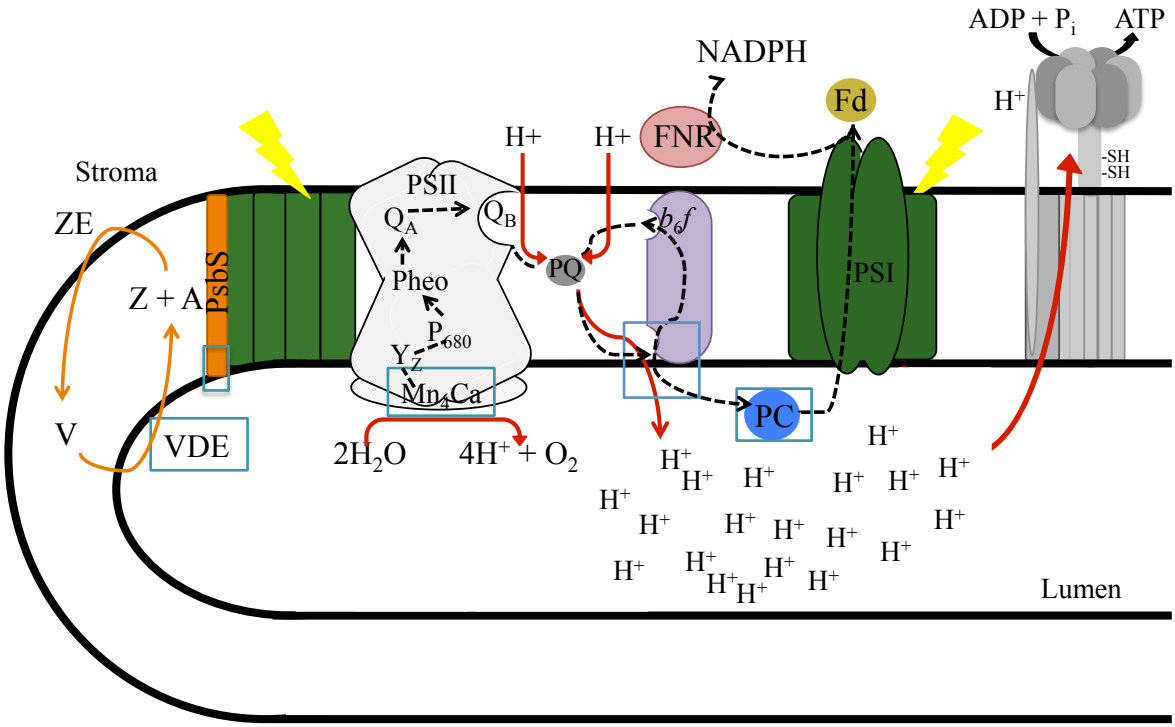

Figure 1.1: Electron and proton transfer steps of the photosynthetic light reactions. Schematic representation of the electron (black dashed lines) and proton (red sold lines) transfer reactions occurring across the thylakoid membrane during photosynthetic linear electron flow. Following absorption of light by antenna pigment protein complexes, excitation transfer and charge separation within photosystem (PS) II and I generates the oxidizing potential capable of splitting water at PSII. Electron transfer from the PSII primary donor P_{680} occurs vectorially across the membrane spanning protein through a pheophytin (Pheo) intermediate, the bound primary quinone Q_A, to the mobile quinone Q_B. P_{680}^+ is reduced by electron transfer from the Mn_4Ca oxygen-evolving complex (OEC) through a redox active tyrosine (Y_Z). Following two successive PSII turnovers, the doubly reduced quinone bound at Q_B forms the quinol by protonation and is release into the thylakoid membrane, followed by binding of a new quinone at Q_B from the quinone pool (PQ). Two more PSII turnovers are required to complete the oxidation of water by the OEC and deposition of protons into the lumen. Oxidation of plastoquinol by cytochrome *b*$_6$*f* reduces plastocyanin (PC) and translocates more protons into the lumen. Excitation and charge-separation in PSI allow electron transfer from PSI to ferredoxin (Fd) and re-reduction of PSI by PC. Fd is used to generate NADPH from $NADP^+$ via ferredoxin-$NADP^+$ reductase (FNR). The proton motive force generated by proton deposition is used to move protons from the lumen to the stroma through the ATP synthase *c*-subunit ring to generate ATP. Lumen acidification regulates multiple thylakoid proteins (blue boxes). Activation of pH-dependent nonphotochemical quenching occurs via protonation of violaxanthin de-epoxidase (VDE) and the conversion of violaxanthin (V) to zeaxanthin and antheraxanthin (Z + A), as well as protonation of PsbS (orange).

1.3 Trans–thylakoid Δψ regulation is poorly understood but is not without consequences to photosynthesis.

While the regulatory mechanisms of ΔpH generation have been well-characterized *in vitro* and *in vivo*, Δψ–mediated feedback on photosynthesis has been poorly studied. Due to a low electrical capacitance of the thylakoid membrane, generation of Δψ can occur rapidly from a dark-adapted (fully oxidized) state via the charge disequilibrium that occurs following charge separation within PSII and PSI complexes, producing anion electron acceptors closer to the stromal face and cation holes near the luminal edge within both complexes (20). This Δψ is rapidly replaced by the redistribution of ions between the stroma (or cytosol in cyanobacteria) and thylakoid lumen (21-25). Although the movement of ions across the thylakoid has been characterized for decades (26), how or if Δψ regulates photosynthesis *in vivo* has only recently emerged as a focus of study (2). In *Arabidopsis thaliana*, the use of knockout or knockdown mutants in putative chloroplast ion transporters has identified proteins that, when absent, alter the ΔpH/Δψ ratio *in vivo* (27-32), reviewed in (33-35). In mutants with a decreased ΔpH/Δψ ratio (*tpk3*, *kea1/kea2*, *clce*, *vccn1, pam71*), the kinetics of NPQ induction is delayed due to an inability to rapidly collapse Δψ and generate ΔpH as quickly as wild type plants (27, 29-31). This also led to a measured increase in PSII photoinhibition in *tpk3*, attributed to the decreased ΔpH failing to properly activate q_E and preventing proper photoprotection (27).

However, recent work with Arabidopsis ATP synthase activity mutants, in which only the buildup of total *pmf* was purposefully altered but other *pmf* regulatory proteins remained genetically unchanged, an alteration of the ΔpH/Δψ ratio was similarly seen under high total *pmf* conditions, suggesting *in vivo* regulation of *pmf* partitioning not previously identified that prevents over-acidification of the thylakoid lumen (13). Unlike ion transporter mutants, the

activation of NPQ through ΔpH generation is not impaired via constitutive mis-regulation of *pmf* partitioning, but PSII photoinhibition was still prominent when the ΔpH/Δψ ratio was low (36). This was shown mechanistically to be due to destabilization of charge-separated states during vectorial electron transfer, which decreases the free energy barrier for charge recombination, leading to an increase in singlet oxygen ($^1O_2$) production via PSII recombination when Δψ is large (37, 38). While this phenomenon was found during the steady–state in high *pmf* mutants, the same phenomenon was observed in wild type plants during light fluctuations similar to natural conditions, when a large, transient Δψ is present following the increase in excitation energy. These findings highlight the importance of Δψ not only for providing *pmf* to properly balance ATP synthesis (39), but also an emerging role for Δψ–mediated regulation of electron transfer events *in vivo*. As the core electron transfer protein complexes of photosynthesis (PSII, cytochrome b_6f, and PSI) are highly conserved across all oxygenic photosynthetic organisms, Δψ regulation of photosynthetic electron transfer, though poorly studied, is likely to be a prevalent phenomenon occurring under natural (non–static) conditions with substantial consequences for photosynthetic productivity.

1.4 The ATP synthase *c*–ring stoichiometry dictates the efficiency of *pmf*-generated ATP synthesis.

The dissipation of *pmf* through the rotary-coupled F_0F_1 ATP synthase is utilized in bioenergetic membranes throughout the tree of life, highlighting not only the utility of *pmf*–driven phosphorylation but also the highly conserved mechanism of ATP synthase activity (reviewed in 40). Rotational movement of the membrane embedded F_0 portion is driven by a single proton binding residue on each *c*–subunit, which is coupled to the catalytic turnover of the $\alpha_3\beta_3$ hexamer to release 3 ATP molecules per full turnover. Therefore, full turnover of the F_1

enzyme is coupled to complete 360° rotation of the *c*–ring, generating 3 ATP per *c*-subunits. This rotational catalysis mechanism is conserved across species and membranes of various bioenergetics processes, however, the subunit stoichiometry of the *c*–ring has been shown to vary from 8–15 subunits, although maintaining a single stoichiometry within a species, in turn leading to a wide range of H^+/ATP ratios and thus bioenergetic limitations between different species and various cellular compartments membranes.

The bioenergetic implications of *c*–ring stoichiometry have direct consequences on the amount *pmf* required to drive ATP synthesis (41, 42). While ΔpH and $\Delta\psi$ are thermodynamically equivalent drivers of ATP synthesis (Eq. 1), they are not kinetically equivalent. Using ATP synthases with different *c*–ring stoichiometries, the threshold of *pmf* activation for ATP synthesis has been shown to vary with the number of c-subunits, with larger values becoming active at lower potentials (43) and having higher activity at lower potential (44). This has been postulated to be due to a decrease in the total rotation required for each *c*–subunit step–wise movement as the stoichiometry increases, suggesting that larger *c*–ring stoichiometries allow those complexes to operate at a lower *pmf*. Remarkably, the chloroplast ATP synthase *c*–ring stoichiometry is on the high end of ATP synthase complexes with 14 *c*-subunits (42, 45).

Intriguingly, using published data to derive parameters for ATP synthesis, Silverstein (41) found that even at a nearly identical *pmf*, the *E. coli* and bovine mitochondrial ATP synthases (*c*-subunits=10 and 8, respectively) outperform the chloroplast ATP synthase in terms of efficiency by ~25%. This inefficiency specific to the chloroplast ATP synthase was hypothesized to be due to the increase in *pmf* storage as ΔpH component *in vivo* relative to other membranes, as well as the lower $\Delta\psi$ threshold for activation (43, 46). While both of these issues may address mathematically why the chloroplast complex is less efficient, they fail to consider

why chloroplasts evolved to utilize a higher ΔpH and lower Δψ. As described above and thoroughly discussed elsewhere (5, 47), acidifying the thylakoid lumen leads to pH–mediated downregulation of photosynthesis, while in other cellular compartments acidification may lead to enzyme damage, or be difficult to acidify due to a larger volume than the thylakoid lumen (48, 49). Chloroplasts, however, still do not solely maintain a ΔpH as their *pmf* source, but maintain a balance with Δψ, likely to avoid deleterious acid–induced damage to lumen-exposed proteins and protein residues (13, 36).

1.5 A large ATP synthase *c*-ring stoichiometry may help stabilize *pmf* partitioning into ΔpH to minimize Δψ.

If chloroplasts have evolved to supplement a ΔpH gradient with Δψ to avoid over–acidification, one could speculate as to why chloroplasts do not maintain a large Δψ while supplementing with a ΔpH gradient to activate q_E. A larger Δψ gradient would increase thermodynamic efficiency of chloroplast ATP synthase, but as noted above in chloroplasts, and likely cyanobacteria, due to the highly conserved core electron transfer proteins, a large Δψ decreases the free energy barriers for electron recombination, leading to increased $^1O_2$ production at PSII (36). Could photosynthetic ATP synthases have evolved to specifically mitigate this Δψ problem? It is intriguing that the number of *c*-subunits in photosynthetic organisms analyzed to date are all on the high end (13–15 subunits) of the determined *c*–ring stoichiometries (45, 50, 51). The energy required to catalyze the synthesis of ATP (ΔG_{ATP}) is given by:

$$\Delta G_{ATP} = n * \Delta \mu_{H+} \quad \text{(Eq. 2)}$$

where *n* is the H^+/ATP ratio required to generate each molecule of ATP dictated by the number of *c*–subunits. The high H^+/ATP ratio in chloroplasts (*n*=4.3) decreases the *pmf* required to

overcome ΔG_{ATP}, allowing photosynthesis to produce ATP at a lower relative *pmf* (52), reducing the requirement to maintain a either a large ΔpH or $\Delta\psi$ during steady–state photosynthesis.

The implications of large *c*–ring stoichiometry are evident if one considers the energetic consequences that decreasing the stoichiometry would have on photosynthesis. Assuming a ΔG_{ATP} of 40 kJ/mol (53), a decrease in the number of *c*–subunits from 15 to 9 would result in an increase in the *pmf* required to maintain ΔG_{ATP} equilibrium from ~83 mV to ~138 mV. If the energy is equally partitioned between $\Delta\psi$ and ΔpH, this leads to an equilibrium ΔpH of 0.7 units with a c_{15} stoichiometry and ΔpH of 1.2 units at c_9, enough to already begin activating q_E processes in the dark (39). Similarly, the $\Delta\psi$ required just to maintain ΔG_{ATP} equilibrium increases by nearly 30 mV. Further *pmf* generation during photosynthesis would therefore exacerbate these increases. Under this hypothetical smaller c_9 operating structure, photosynthetic *pmf* would either need to be limited to a lower total *pmf* capacity than its current c_{14} state, or require a dramatic shift in the partitioning into $\Delta\psi$ to avoid near immediate over-acidification of the thylakoid lumen below ~5.5 (ΔpH 2.6 units assuming stromal pH 7.8) (13, 39). As discussed above, the physical properties of the thylakoid membrane dictate the temporal partitioning of $\Delta\psi$ and ΔpH generation. A shift in partitioning in favor of $\Delta\psi$ could occur via genetic regulation of counter-ion movement through ion transport expression, or an increase in the buffering capacity of the lumen, which would require massive remodelling of thylakoids or the use of high concentrations of mobile buffering groups such as polyamines (54).

1.6 Photosynthetic regulation limits the influence of $\Delta\psi$ on electron transfer.

A shift of *pmf* partitioning into more $\Delta\psi$, however, will greatly influence the recombination frequency between charge-separated states in PSII. The recombination rate in PSII depends on the energetics of electron sharing between redox intermediates and changes

exponentially with changes in $\Delta\psi$. For the charge-separated state(s) forming $P^+Q_A^-$, where P^+ is the primary electron donor and Q_A the non-mobile PSII quinone, these changes correspond to:

$$v_{recombination} = [S_2Q_A^- + S_3Q_A^-] * k_r * 10^{\frac{-\Delta E_{stab}}{0.06}} \quad \text{(Eq. 3)}$$

where $[S_2Q_A^- + S_3Q_A^-]$ represents the fraction of PSII containing donor and acceptor side states capable of recombining from Q_A^-, k_r is the intrinsic rate of recombination from $S_2/S_3Q_A^-$, and ΔE_{stab} is the stabilization free energy of the charge separated state $S_2/S_3Q_A^-$, expressed in eV (36). As $\Delta\psi$ increases, the ΔE_{stab} of charge separated states decreases (37, 55), leading to an increase in the rate of recombination. Therefore, even with relatively small changes in the amount of energy stored as $\Delta\psi$, the velocity of recombination will increase dramatically. This likely limits the amount of energy that can be stored safely across photosynthetic membranes as $\Delta\psi$, as electron recombination through back–reactions can lead to generation of reactive oxygen species (ROS) (36, 56).

It therefore appears that a large *c*–ring stoichiometry, although energetically inefficient (41) may in fact be far more physiologically efficient for organismal survival in photosynthetic membranes. Additionally, the decrease in the chloroplast ATP synthase *pmf* activation threshold may have led to the additional advantage of photosynthetic ATP generation under even low light conditions (46).

The increased storage of *pmf* as ΔpH in photosynthetic organisms activates multiple regulatory processes that feedback into the amount of energy held by Q_A^-. As ΔpH builds and q_E is activated, excitation quenching in the antenna decreases the fraction of absorbed light transferred to PSII, decreasing the PSII excitation pressure to limit over-reduction and buildup of Q_A^-, which can recombine to generate ROS. Concurrently, downregulation of b_6f turnover regulates the redox state of the plastoquinone pool, balancing the PSII excitation pressure with

the availability of electron donors. Although pH-mediated activation of NPQ has been well characterized in multiple eukaryotic organisms (57), NPQ mechanisms vary between different photosynthetic lineages, and are not pH regulated in cyanobacteria (58). Comparatively, $\Delta\psi$ influences on electron transfer are likely to be experienced in all photosynthetic lineages, as the core electron transfer proteins are highly conserved from cyanobacteria to higher plants. Further investigation of *in vivo pmf* partitioning to mediate the $\Delta\psi$ component as well as the regulation of photosynthesis by $\Delta\psi$ will likely identify key factors that allow organisms to respond to the total *pmf* generated, as well as factors that allow organisms limit the impact of transient $\Delta\psi$ fluctuations experienced under natural conditions.

Chapter 2

Limitations to photosynthesis by proton motive force-induced photosystem II photodamage[1]

Geoffry A. Davis, Atsuko Kanazawa, Mark Aurel Schottler, Kaori Kohzuma, John E. Froehlich, A William Rutherford, Mio Satoh-Cruz, Deepika Minhas, Stefanie Tietz, Amit Dhingra, David M. Kramer[1]

[1] This chapter was published as:
Davis, GA, Kanazawa, A, Schottler, MA, Kohzuma, K, Froehlich, JE, Rutherford, AW, Satoh-Cruz, M, Minhas, D. Tietz, S, Dhingra, A, Kramer, DM. 2016 Limitations to photosynthesis by proton motive force-induced photosystem II photodamage. eLife, 5. doi: 10.7554/eLife.16921

2.1 Abstract

The thylakoid proton motive force (*pmf*) generated during photosynthesis is the essential driving force for ATP production; it is also a central regulator of light capture and electron transfer. We investigated the effects of elevated *pmf* on photosynthesis in a library of *Arabidopsis thaliana* mutants with altered rates of thylakoid lumen proton efflux, leading to a range of steady-state *pmf* extents. We observed the expected *pmf*-dependent alterations in photosynthetic regulation, but also strong effects on the rate of photosystem II (PSII) photodamage. Detailed analyses indicate this effect is related to an elevated electric field ($\Delta\psi$) component of the *pmf*, rather than lumen acidification, which *in vivo* increased PSII charge recombination rates, producing singlet oxygen and subsequent photodamage. The effects are seen even in wild type plants, especially under fluctuating illumination, suggesting that $\Delta\psi$-induced photodamage represents a previously unrecognized limiting factor for plant productivity under dynamic environmental conditions seen in the field.

2.2 Introduction

The thylakoid proton motive force (*pmf*), the transmembrane electrochemical gradient of protons generated during the light reactions of photosynthesis, is a fundamental entity of bioenergetics, coupling light-driven electron transfer reactions to the phosphorylation of ADP via the ATP synthase (59, 60). In oxygenic photosynthesis, light energy is captured by pigments in light-harvesting complexes and transferred to a subset of chlorophylls in photosystem I (PSI) and photosystem II (PSII), where it drives the extraction of electrons from water and their transfer through redox cofactors to ultimately reduce $NADP^+$. The vectorial transfer of electrons across the membrane is tightly coupled with the generation of the *pmf*, composed of both electric field ($\Delta\psi$) and pH (ΔpH) gradients.

In addition to its role in energy conservation, the *pmf* is also critical for feedback regulation of photosynthesis (61). Acidification of the thylakoid lumen activates the photoprotective energy-dependent exciton quenching (q_E) process, which dissipates excess absorbed light energy in the photosynthetic antenna complexes by the activation of violaxanthin deepoxidase (62) and protonation of PsbS (7). Lumen acidification also regulates the oxidation of plastoquinol by the cytochrome b_6f complex, slowing electron transfer from PSII and preventing the accumulation of electrons on PSI, which can otherwise lead to photodamage (11, 12). *In vitro* work has shown that excessive lumen acidification can inactivate PSII (63), decrease the stability of plastocyanin (64) and severely restrict electron flow through the cytochrome b_6f complex (13). Taken together, the *in vivo* and *in vitro* evidence of the susceptibility of photosynthetic components to acidification has led to the proposal that the extent of *pmf* and its partitioning into $\Delta\psi$ and ΔpH components is regulated to maintain the lumen pH above about 5.8, where it can regulate photoprotection. However, under environmental

stresses the regulation of photosynthesis may become overwhelmed, leading to PSII damage, or photoinhibition, from lumen over-acidification, although this has not been shown to occur *in vivo* (13).

PSII photoinhibition can be a major contributor to loss of photosynthetic productivity (65), particularly under rapid fluctuations in environmental conditions experienced in the field (66). However, the mechanisms and regulation of photoinhibition remain highly debated (67, 68). Though several mechanisms have been proposed for the photodamage process, it is not known which of these operate *in vivo* under diverse environmental conditions. In addition, there are differing views on whether the extent of photoinhibition is governed by the rate of photodamage to PSII or by regulation of PSII repair (69). Answering these questions is essential to understanding how plants respond to rapidly changing conditions and thus of critical importance to improving plant productivity.

The extent of the *pmf* can be modulated by altering the light-driven influx of protons into the lumen, i.e. by changing the rates of linear electron flow (LEF) or cyclic electron flow, or the efflux of protons through the ATP synthase (reviewed in 13). This latter mode of regulation is important for co-regulation of the light reactions with downstream metabolic processes. For example, under CO_2 limitations (19) as well as during stromal P_i limited conditions (18) the chloroplast ATP synthase activity is strongly down-regulated, decreasing the proton conductivity (g_{H^+}) of the thylakoid, leading to buildup of *pmf* and activation of q_E. Similar decreases in g_{H^+} and increases in *pmf* are seen when ATP synthase protein content is decreased (70) or in mutants with an altered ATP synthase γ-subunit (71).

2.3 Results

We took advantage of the effects of the ATP synthase on the photosynthetic proton circuit to probe how the *pmf* influences photoinhibition *in vivo*. We constructed a series of *Arabidopsis thaliana* mutants, which we termed *minira (mini*mum *r*ecapitulation of *A*TPC2), in which we complemented a γ_1-subunit (ATPC1) T-DNA knockout line (72) with γ-coding sequences containing site-directed mutations to specifically incorporate amino acid changes around the redox regulatory cysteines present in ATPC2 into ATPC1 (Figure 2.1A) (73). Each *minira* line is designated numerically based on amino acid position and independent transformation events; for example *minira* 4–1, *minira* 4–2, and *minira* 4–3 represent three independent transformation events of the same I201V mutation. The *minira* library was originally developed as part of an on-going 'domain swapping' approach to assess functional differences in the two ATPC paralogs in Arabidopsis, ATPC1 and ATPC2, but the *minira* mutants also shows a range of ATP synthase activities useful to the present work. As described below, we also confirmed key aspects of the work using previously characterized ATPC1 tobacco antisense lines (70). However, variations in ATP synthase suppression in the antisense lines between leaves and plant generations limited their experimental utility. The current mutagenesis approach was preferable as it allowed repeatable analyses of multiple photosynthetic parameters in stable, identical genetic backgrounds within each mutant line.

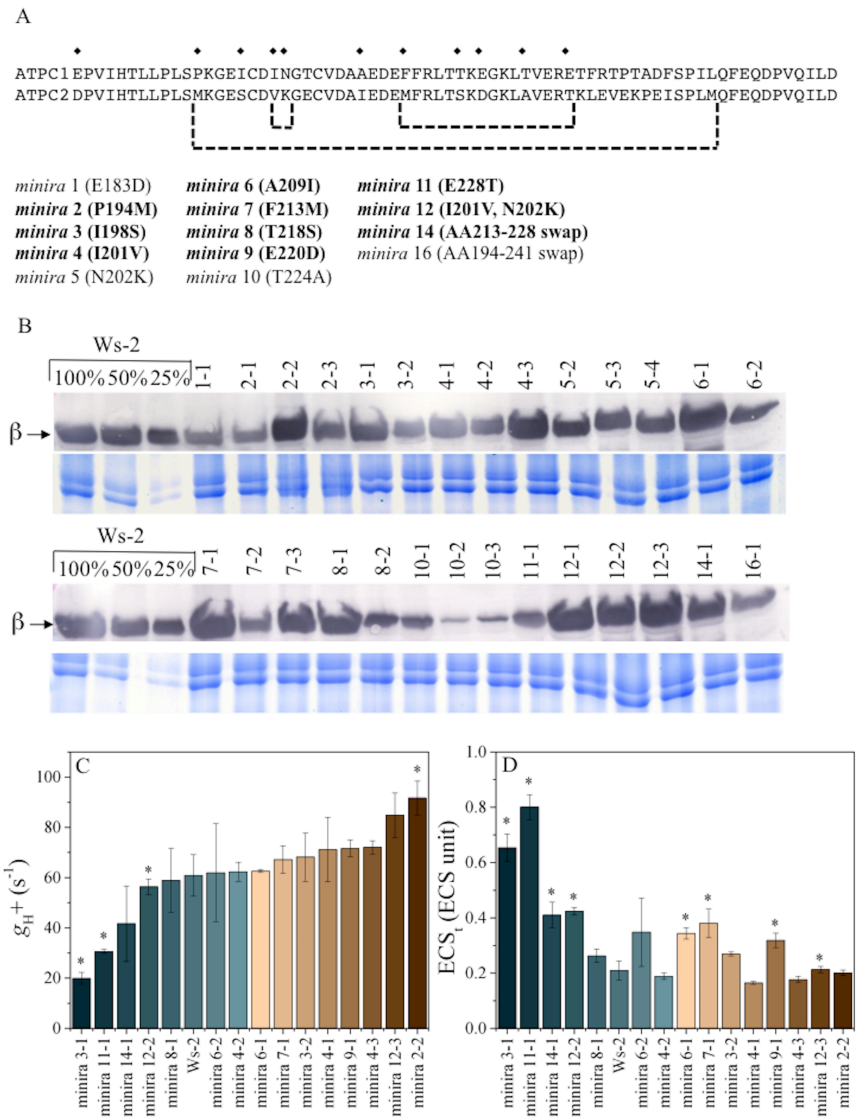

Figure 2.1: γ-subunit mutations alter photosynthetic proton efflux.
Sequence alignment of Arabidopsis ATPC1 and ATPC2 regulatory region (A). Amino acid differences incorporated into ATPC1 to generate *minira* are indicated by symbols (♦). Amino acid numbers are based on standard spinach positions, which *minira* numeric designations are based upon position within the amino acid primary sequence. Regions where multiple changes were incorporated from ATPC2 are outlined in brackets. Bold: mutations resulting in successful transgenic plants with stable phenotypes utilized for experiments. Accumulation of chloroplast ATP synthase complexes was verified across resulting transformant lines (B). Total leaf protein was probed for chloroplast ATP synthase β-subunit compared to a titration of wild type (Ws-2) accumulation. Gels run with identical samples stained with Coomassie Brilliant Blue are shown below to ensure equal loading to the 100% wild type samples. The conductivity of the ATP synthase for protons (g_H^+, C) and the light-driven *pmf* (ECS_t, D), calculated from the decay of the electrochromic shift at 100 µmol photons $m^{-2}s^{-1}$ actinic light (mean ± s.d, n = 3). Statistically significant differences (*$p<0.05$) from wild type were determined using a t-test. ECS units were defined as the deconvoluted ΔA_{520} µg $chlorophyll^{-1}$ cm^2.

We assessed the effects of *minira* modifications on g_H^+ and the extent of the light-driven *pmf in vivo* based on the decay kinetics of the electrochromic shift (ECS), which reports changes in the thylakoid electric field (74). The *minira* lines displayed a range of ATP synthase activities (Figure 2.1C), from about 30–120% that of wild type (Wassilewskija-2, Ws-2), resulting in similar variations in light-driven *pmf* (Figure 2.1D). Multiple independent transformations were utilized for the same *minira* mutation, as the g_H^+ changes likely reflect both intrinsic ATP synthase activity changes due to the mutations, as well as changes due to protein expression level or stability of the mutated subunit within the complex (Figure 2.1B). While some *minira* mutants display an increase in g_H^+ relative to the wild type and will acidify the lumen at a slower rate, others have a large decrease in total ATP synthase content. For the purpose of understanding how a high *pmf* impacts photosynthesis we have primarily focused on those mutants that modified g_H^+ while maintaining an ATP synthase content similar to wild type levels.

The *minira* library was then screened for photosynthetic phenotypes using whole plant chlorophyll fluorescence imaging (75) over a consecutive three-day photoperiod (Figure 2.2A). Photosynthetic parameters were calculated from these images (videos are shown in supplemental files 1-9) and shown as kinetic traces (Supplemental Figures 2.1-2.16) or as log-fold changes compared to wild type (Figure 2.2B-D). Under 'standard' laboratory growth chamber lighting on day one, most *minira* lines showed relatively small differences from wild type in LEF (Figure 2.2B), q_E (Figure 2.2C), and photoinhibitory quenching (q_I) (Figure 2.2D), with the exceptions of *minira* 3–1 and 11–1, which also showed the most severe decreases in g_H^+ (Figure 2.1C). Stronger photosynthetic phenotypes appeared on days two and three,

implying that the decreased g_H^+ and *pmf* effects were enhanced by intense or fluctuating illumination.

In general, LEF decreased with decreasing g_H^+ (Figure 2.2B, rows are ordered by increasing g_H^+) while q_E increased (Figure 2.2C). The increases in q_E were especially pronounced at higher light intensities on days two and three. These effects can be explained by slowing of proton efflux through the ATP synthase in the mutants that results in increased *pmf* for a given LEF. This is reflected in the higher lumen pH-sensitive q_E response for a given LEF (Figure 2.2E), which is strikingly similar to that attributed to ATP synthase regulation in wild type plants during limitations in carbon fixation (19) or decreases in ATP synthase content (70). The q_E sensitivities for the mutants remained similar throughout the experiments, i.e. the data for each mutant followed similar curves, implying that the ATP synthase activities were relatively constant within a particular line, consistent with a lack of light-dependent modulation of g_H^+ that has previously been observed (76). The extents of q_E did not exceed about 3.5 units in any of the lines, suggesting that either the lumen pH was restricted to a moderate acidity or that the capacity of the q_E response was saturated as light intensities increased.

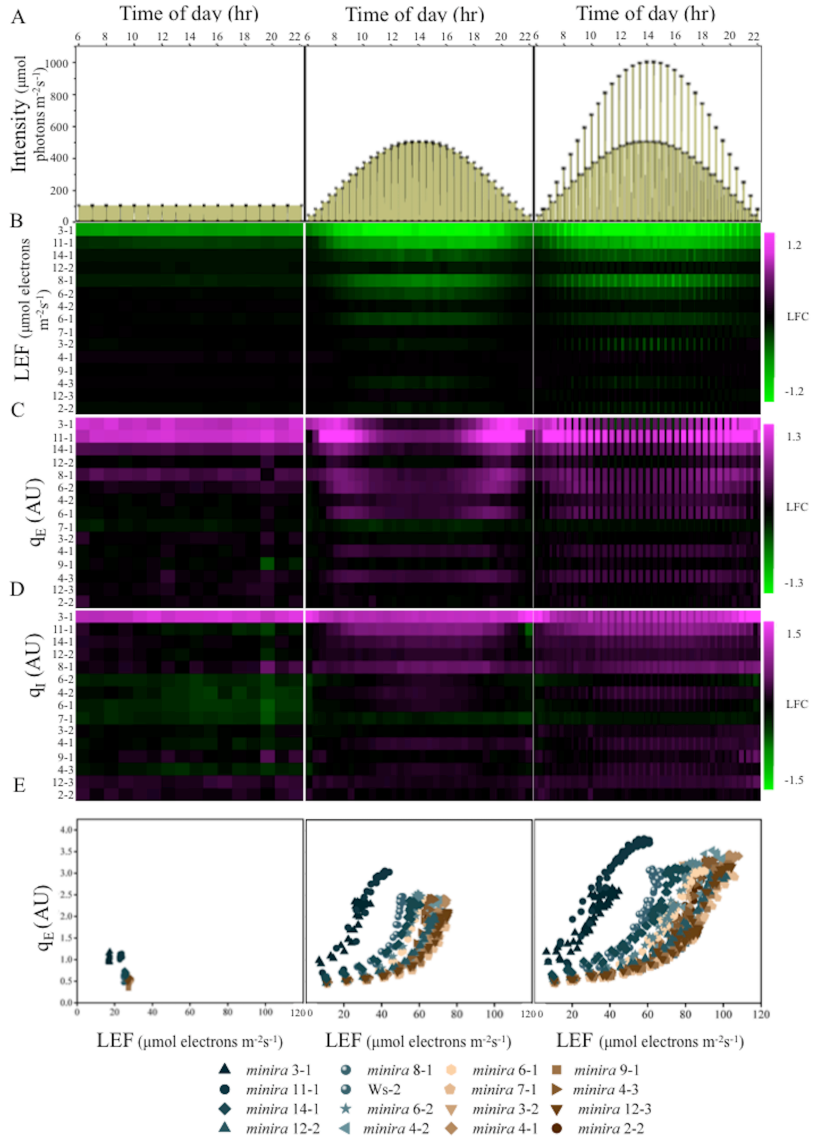

Figure 2.2: Dynamic light conditions enhance *pmf* dependent phenotypes.
Whole plant fluorescent images were captured over three days under the illumination conditions displayed in Panel A and listed in Tables 2.5-2.7. Plants were illuminated over the 16-hr photoperiod, shown as yellow filled areas representing the light intensity when present in A, under either a constant light intensity (day one), a sinusoidal photoperiod (day two), or a sinusoidal photoperiod interrupted by fluctuations in light intensity (day three). Square symbols in Panel A indicate each light intensity change. Steady-state fluorescence parameters were captured for each plant at the end of each light condition. Panels B, C and D represent the responses of LEF, q_E and q_I respectively ($n \geq 3$). Data are shown as $\log_2$-fold changes compared to the wild type. Kinetic data including wild type are shown in Supplemental Figures 2.1-2.16. The rows were sorted in order of ascending g_H^+ values measured as in Figure 2.1C. Panel E plots the dependence of the mean ($n \geq 3$) of q_E against the linear electron flow (LEF) for each time point measured for the day. For visualization purposes the error bars have been omitted from E.

We also observed a strong correlation between increased q_E and q_I, (for quantitative comparisons, see Supplemental Figure 2.2), implying that decreases in ATP synthase activity in the mutants led to not only higher photoprotection but also higher rates of PSII photoinhibition. This result appears counterintuitive, in that we would expect the photoprotective q_E response to prevent photoinhibition. Particularly striking was the relative loss in q_E near the peak light intensities on days two and three in the most strongly affected *minira* lines (Figure 2.2C). We attribute this effect to strong accumulation of PSII photoinhibition (Figure 2.2D) leading to the loss of photosynthetic capacity (see Figure 2.2B) that limited acidification of the thylakoid lumen.

The observed increases in photoinhibition at high *pmf* could be caused by several mechanisms. It has been proposed that photoinhibition is primarily controlled by modulating the rate of PSII repair, i.e. the rate of damage is dependent solely on light intensity but repair being inhibited by stress-induced ROS production (77). However, blocking PSII repair with the chloroplast translation inhibitor lincomycin (78) revealed that, when compared to wild type or *minira* lines with wild type like g_H^+ (e.g. *minira* 6–1), *minira* lines with low g_H^+ and high *pmf* (e.g. *minira* 3–1, Figure 2.1C, Figure 2.3) had higher rates of photodamage as reflected in both decreased maximal PSII quantum efficiency and loss of the capacity to perform charge separation in PSII (79-81) and significantly decreased levels of D1 protein (Figure 2.3C-E). Thus, decreasing ATP synthase activity led to increased PSII photodamage rather than decreased rates of repair, in contradiction with strict control of photoinhibition by repair (69).

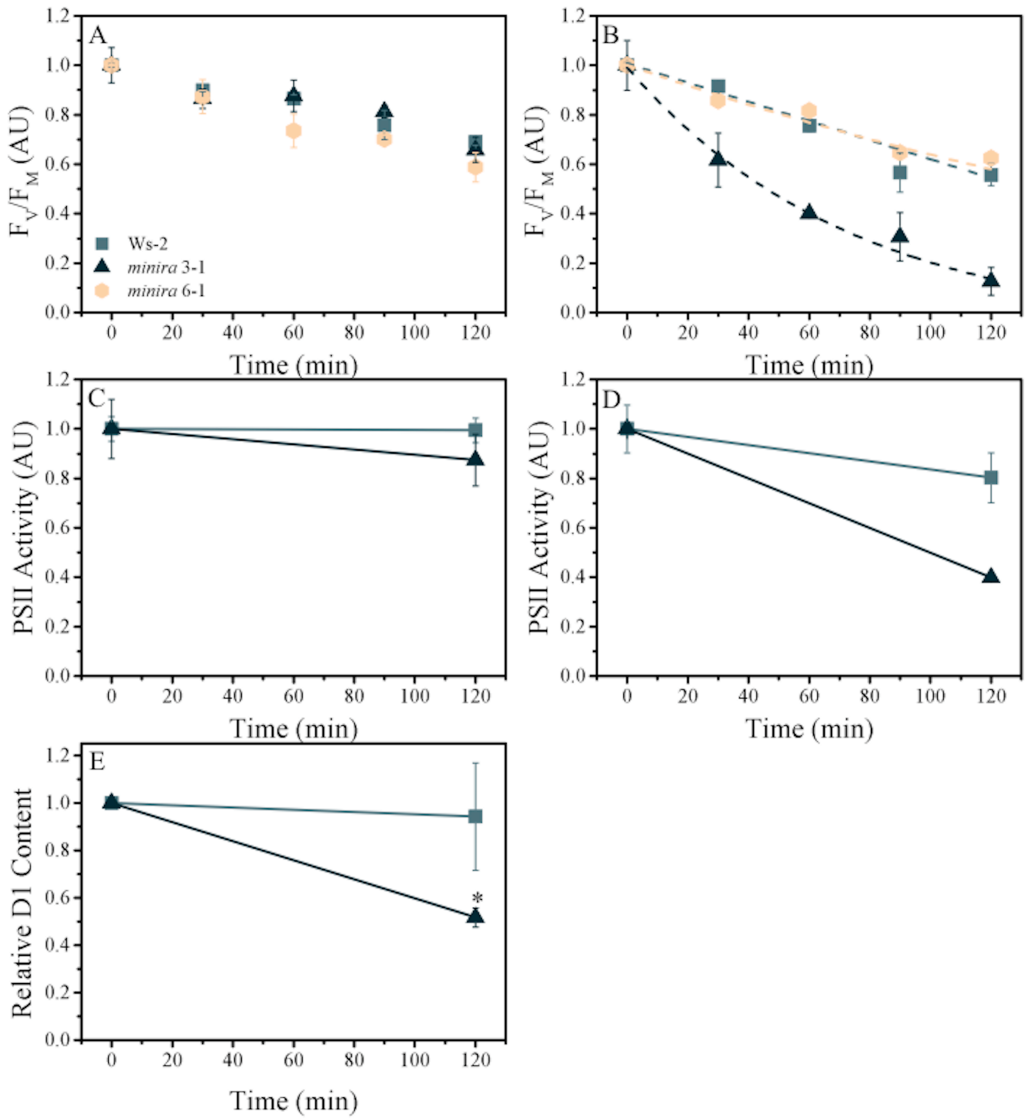

Figure 2.3: Elevated *pmf* leads to PSII photodamage.
Detached leaves were infiltrated with either water (A, C) or a 3 mM solution of lincomycin (B, D) and treated with 1000 µmol photons $m^{-2}s^{-1}$ red light for the times indicated. Following dark adaptation, F_V/F_M values were obtained (A, B) for treated leaves of wild type (square, initial F_V/F_M 0.75 ± 0.006 and 0.76 ± 0.012 for water and lincomycin, respectively), *minira* 3–1 (triangle, initial F_V/F_M 0.60 ± 0.07 and 0.54 ± 0.10 for water and lincomycin, respectively), and *minira* 6–1 (hexagon, initial F_V/F_M 0.72 ± 0.004 and 0.73 ± 0.01 for water and lincomycin, respectively) (mean ± s.d., n ≥ 3). Data were normalized to the initial dark-adapted F_V/F_M values to remove intrinsic differences between the three lines. In panel B, dashed lines represent the best fit curves for a single exponential decay. The ability of photoinhibited leaves to perform PSII charge separation was determined in Ws-2 and *minira* 3-1 by measuring the ECS absorbance changes following two consecutive single-turnover saturating flashes in the presence of DCMU (C, D). Leaves infiltrated with water (C, initial amplitudes of $8.88 \times 10^{-4} \pm 9.0 \times 10^{-5}$ and $9.59 \times 10^{-5} \pm 3.6 \times 10^{-5}$ for wild type and *minira* 3–1, respectively) or 3 mM lincomycin (D, initial amplitudes of $8.59 \times 10^{-4} \pm 1.2 \times 10^{-4}$ and $1.63 \times 10^{-4} \pm 3.1 \times 10^{-5}$ for

Figure 2.3 (*continued*): wild type and *minira* 3-1, respectively) were infiltrated with DCMU following the indicated light treatment time and dark adaptation. PSII activity was determined by subtracting the ECS amplitude induced by the second flash from the ECS amplitude induced by the first flash (mean ± s.d., $n \geq 4$). Loss of the PSII reaction center D1 protein over the time course of illumination in lincomycin treated wild type and *minira* 3-1 leaves (E). Leaves treated as in panel B were analyzed by western blot (n = 4) using an α-PsbA antibody and the 32 kDa band was quantified. Band intensities were normalized to the time zero point for each genotype within a single blot to control for differences in development intensities. Statistically significant differences (*$p<0.05$) from wild type were determined using a t-test.

Photodamage can be induced *in vitro* by excitation of PSII centers with previously reduced primary quinone acceptor (Q_A) leading to the formation of the doubly-reduced Q_AH_2 state (67). This situation might be expected if a high *pmf* slowed electron transfer through the b_6f complex, resulting in the accumulation of electrons on PSII acceptors. When data at a range of light intensities are compared, the relationship between the Q_A redox state (q_L) (82) and q_I is statistically significant (ANOVA, $p=2 \times 10^{-16}$) (Figure 2.4). However, both the light intensity ($p=3 \times 10^{-5}$) and q_E ($p=7 \times 10^{-3}$) are significant interacting factors. At any one light intensity, q_L was relatively stable, whereas q_I was strongly dependent upon the mutant background and underlining *pmf* changes, indicating that while Q_A reduction may be a contributing factor, it cannot by itself explain the observed extents of photoinhibition in the *minira* lines. On the other hand, this dependence is also consistent with an alternative model, proposed below, that involves effects on PSII recombination rates.

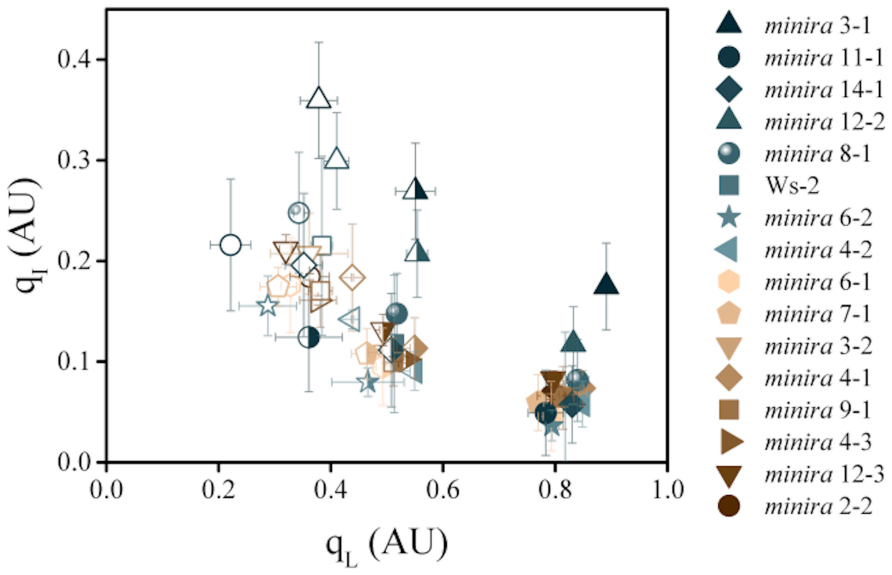

Figure 2.4: The dependence of photoinhibition on the redox state of Q_A.
The redox state of the primary electron acceptor Q_A was assayed using the q_L fluorescence parameter concurrently with photoinhibitory quenching q_I at 100 (solid symbols), 300 (half filled symbols), and 500 µmol photons $m^{-2}s^{-1}$(open symbols, mean ± s.d., n = 3). Plants were exposed to at least 10 min of actinic illumination prior to q_L measurement, and q_I measured after 10 min of dark relaxation. While the extent of q_I varies between plants, the relative redox state of Q_A remains similar between all plants within each actinic light intensity.

Changes in chlorophyll content have also been correlated with increases in PSII photoinhibition (83), likely due to less light being absorbed at the leaf surface and the subsequent increased light penetration into the leaf reaching more PSII centers. While the leaf chlorophyll content was altered in the *minira* mutants from wild type levels (Table 2.8), the leaf chlorophyll content does not fall below where (83) observed correlations between a lack of chlorophyll content and photoinhibition.

We next hypothesized that the most probable explanation for the increased photoinhibition is direct sensitization of PSII to photodamage by *pmf*. In the 'acid-damage' model (13), it was proposed that excessive lumen acidification at high ΔpH (i.e. low lumen pH) could sensitize PSII centers to photodamage. To test this possibility, we compared the rates of

photoinhibition with the extents of the ΔpH and Δψ components of the *pmf* by measuring the relaxation kinetics of the ECS signal (47). Surprisingly, increased extents of photoinhibition in low g_H^+ lines were not correlated with ΔpH, but were with Δψ (Figure 2.5), contrary to what was expected with the acid-damage model. Consistent with this result, the rates of P_{700}^+ reduction, which reflect the lumen pH-sensitive turnover of the cytochrome b_6f complex remained in a range consistent with a lumen pH above or near the pK_a for b_6f down-regulation, i.e. above about 6.0 (Supplemental Figure 2.17).

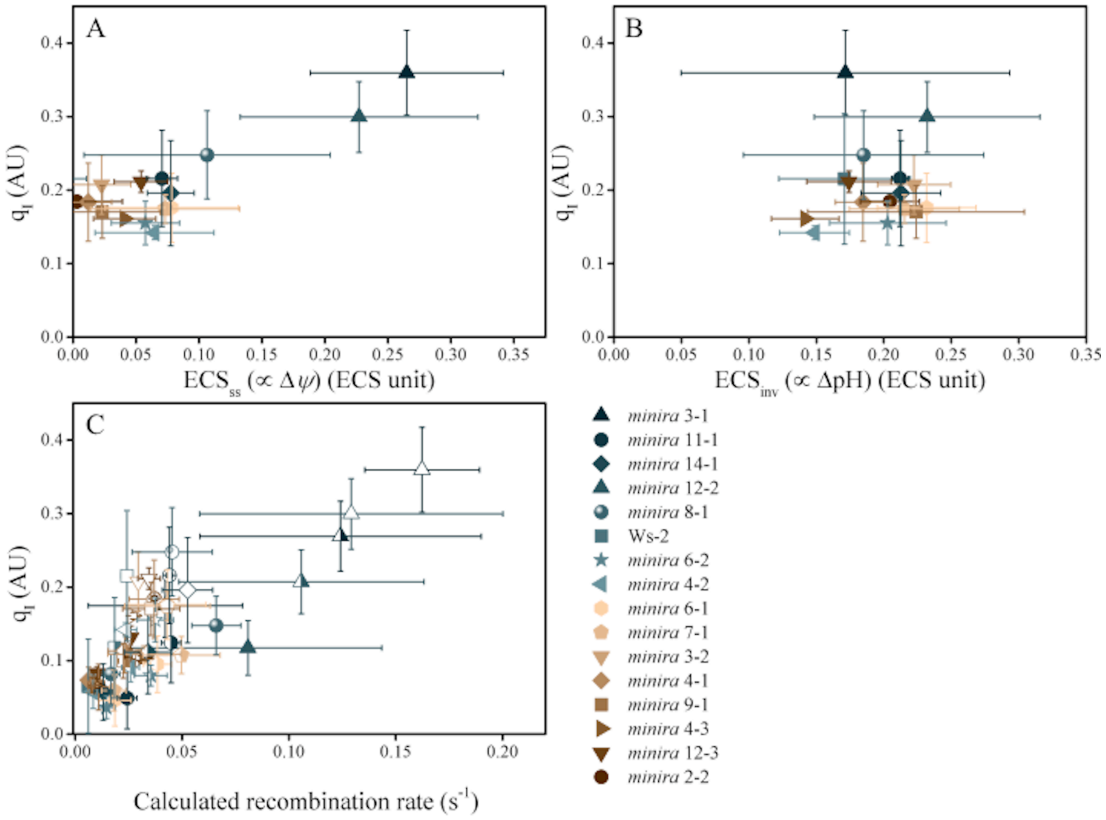

Figure 2.5: Photoinhibition is strongly correlated with Δψ but not ΔpH in *minira* lines. Photoinhibition, estimated by the q_I fluorescence parameter, is plotted against either the ΔpH or Δψ components of *pmf*, estimated by the ECS_{ss} (A) and ECS_{inv} (B) parameters, as described in Materials and methods. Measurements shown were taken during exposure to 500 µmol photons $m^{-2}s^{-1}$ actinic light (mean ± s.d., n = 3). Two-way analysis of variance (ANOVA) of all combined data, 15 *minira* lines and wild type, showed a stronger correlation between q_I and Δψ (F = 9.5, p=0.003) than ΔpH (F = 4.05, p=0.05). This correlation is also seen with the expected pH-dependent alterations of P_{700}^+ reduction for the observed partitioning differences from wild

Figure 2.5 (*continued*): type (Supplemental Figure 2.17) and an increase in the fraction of total *pmf* stored as $\Delta\psi$ at the expense of ΔpH over multiple light intensities (Supplemental Figure 2.18). Increased storage of *pmf* as $\Delta\psi$ is also observed in tobacco ATP synthase knock-down plants (Supplemental Figure 2.19). ECS units were defined as the deconvoluted ΔA_{520} μg chlorophyll^{-1} cm^2. The influence of $\Delta\psi$ on the rate of PSII recombination was estimated based on the change in the equilibrium constant for the sharing of electrons between pheophytin and Q_A (described in Materials and methods) (C). The influence of $\Delta\psi$ on the calculated recombination rate taking into account the fraction of reduced Q_A using the equations described in Materials and methods and described in the main text. Data were obtained at 100 (solid symbols), 300 (half filled symbols), and 500 μmol photons m^{-2}s^{-1} (open symbols) (mean ± s.d., n = 3).

These results are consistent with an increase in the partitioning of *pmf* into $\Delta\psi$ as the total *pmf* increased (Supplemental Figure 2.18), as have been observed previously (59), and are likely caused by alterations in ion movements across both the thylakoid and chloroplast envelope membranes (28, 29, 59). Our results suggest that *pmf* partitioning acts to maintain a permissible lumen pH during large *pmf* increases.

We observed similar results throughout the range of *minira* mutants with low g_H^+ as well as with tobacco γ-subunit antisense plants (70) with reduced ATP synthase complexes, finding that a large increase in total *pmf* was accompanied by increased partitioning of *pmf* into $\Delta\psi$ (Supplemental Figure 2.19), and increased rates of photodamage in the presence and absence of lincomycin (Supplemental Figure 2.19). These results suggest that low g_H^+ or high *pmf*-related PSII damage is a more general phenomenon, which is related to excess $\Delta\psi$ and likely to be independent of such factors as changes in the protein or supercomplex content (see also discussion in (70).

As described in Figure 2.8, we hypothesize that high $\Delta\psi$ accelerates photodamage by favoring recombination reactions within PSII (55, 84-86) that lead to the formation of chlorophyll triplet states that in turn generate $^1O_2$ (87).

To test this model, we studied the relationship between elevated $\Delta\psi$ and PSII charge recombination in isolated spinach thylakoids (Figure 2.6), which unlike Arabidopsis can be isolated as highly intact chloroplasts and tightly coupled thylakoids. Consistent with our model, we found that elevated $\Delta\psi$, produced by artificial decyl-ubiquinol mediated cyclic electron flow through PSI, increased the rate of charge recombination from the $S_2Q_A^-$ state compared to samples treated with gramicidin to dissipate $\Delta\psi$ (Figure 2.6A). This recombination reaction can also occur *in vivo* during normal turnover when the $S_2Q_A^-$ state is formed given that the equilibrium constant for sharing of electrons between Q_A and Q_B is small (88). The extent of $\Delta\psi$ generated in these experiments was similar to that observed in *minira* leaves under photoinhibitory conditions (Figure 2.6B), suggesting similar increases in recombination rates should occur *in vivo*.

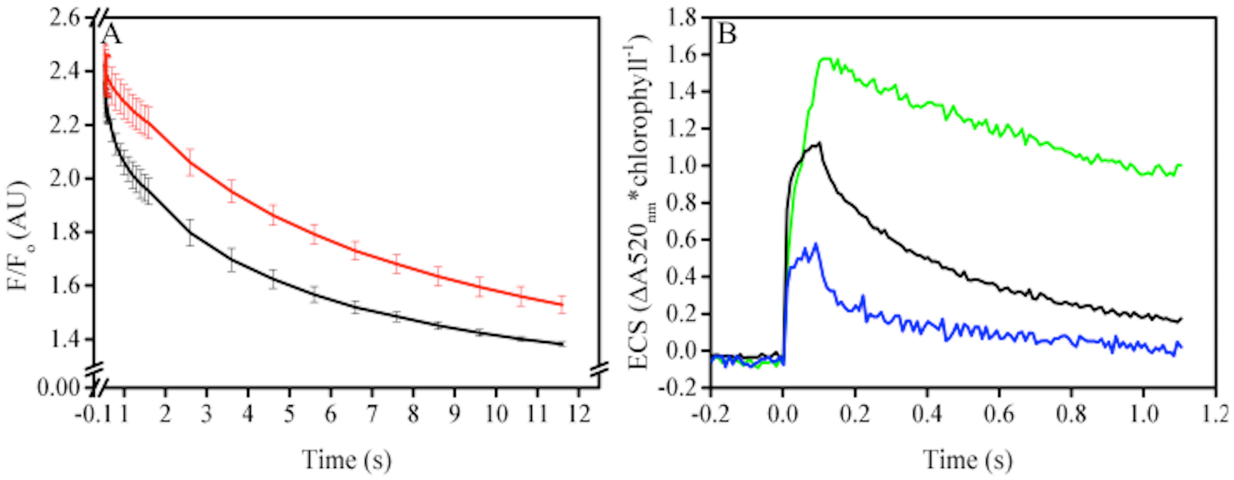

Figure 2.6: *In vitro* manipulation of the $\Delta\psi$ alters PSII $S_2Q_A^-$ recombination rates. Isolated spinach thylakoids in the presence of 5 µM spinach ferredoxin and 10 µm sodium ascorbate were treated with 3–3,4-dichlorophenyl 1,1-dimethylurea (DCMU) to block PSII forward electron transfer, and a trans-thylakoid *pmf* generated utilizing decyl-ubiquinol mediated PSI cyclic electron transfer (A). Recombination from the $S_2Q_A^-$ state was probed by observing the decrease in the high fluorescence state associated with Q_A^- following a short (100 ms) actinic flash to dark-adapted thylakoids (black line). Depletion of the *pmf*, which under these conditions is stored almost exclusively as $\Delta\psi$, in the presence of 25 µM gramicidin (red line) resulted in an approximate 5-fold increase in the initial rate of decay when $\Delta\psi$ was largest, and an overall 2-fold increase in the lifetime of the high fluorescence state. The extent of $\Delta\psi$ generated by the 100

Figure 2.6 (*continued*): ms light (B), estimated by the ECS signal measured at 520 nm and normalized to chlorophyll content. Thylakoids were assayed in the absence of inhibitors (green line), in the presence of DCMU (blue line), and in the presence of both DCMU and 50 μM decyl-ubiquinol (black line) to generate *pmf* through PSI turnover, corresponding to the condition used in panel A.

We next tested the predicted connection between elevated $\Delta\psi$ and singlet oxygen ($^1O_2$) generation (Figure 2.7D). In wild type leaves, moderate illumination (30 min of 300 μmol photons $m^{-2}s^{-1}$) resulted in no detectable light dependent changes in $^1O_2$ (Figure 2.7D) using Singlet Oxygen Sensor Green (SOSG) dye fluorescence (89-91). In contrast, the low g_H^+ *minira* 3–1 line showed a strong induction of SOSG fluorescence within the first 10 min of illumination, which saturated by about 30 min. Infiltration of leaves with valinomycin, a potassium ionophore that decreases the $\Delta\psi$ component of *pmf* (85), partially inhibited the rise in in SOSG fluorescence (Supplemental Figure 2.20). While care must be taken making quantitative estimates of $^1O_2$ from SOSG fluorescence (92), within the limits of these experiments the $\Delta\psi$-dependence of the SOSG fluorescence increases strongly support a role for $\Delta\psi$-induced $^1O_2$ production from photosynthesis.

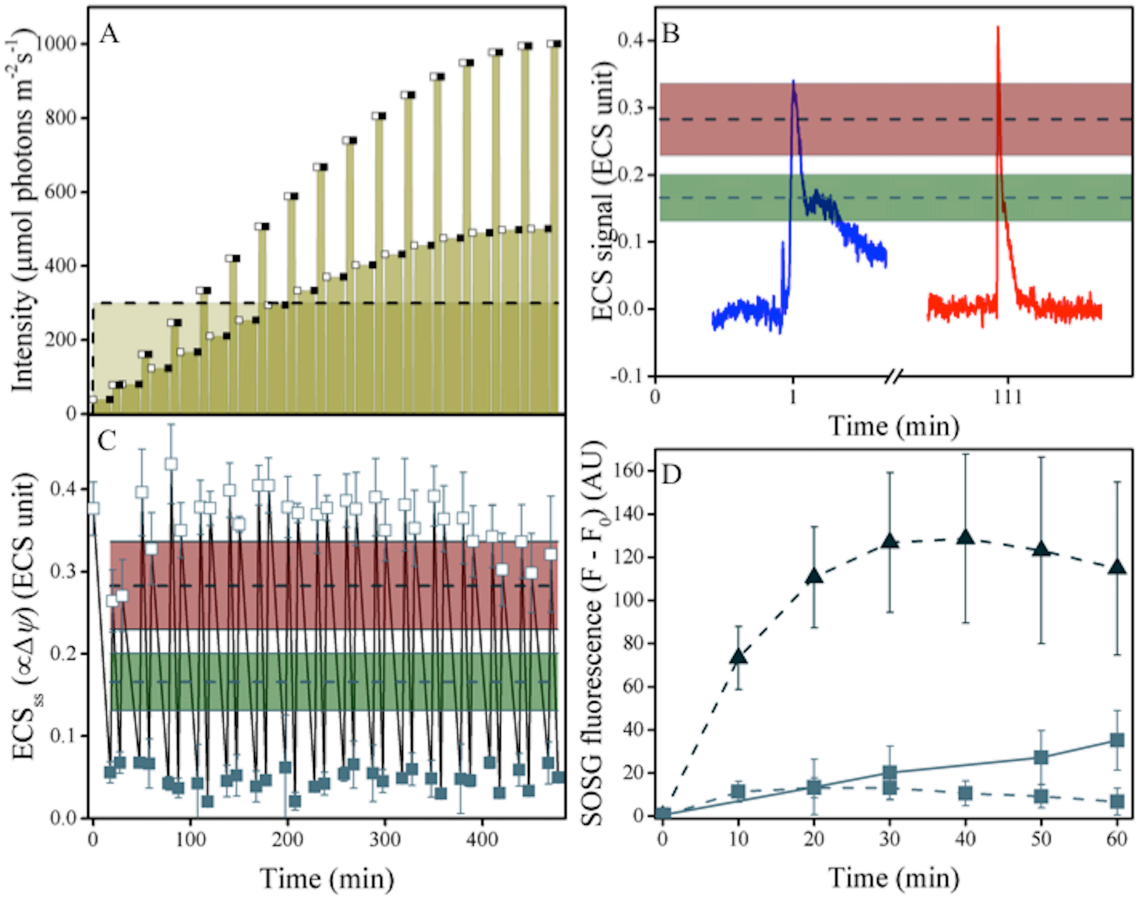

Figure 2.7: Induction of Δψ and $^1O_2$ production under fluctuating light in wild type plants. (A) Illumination conditions and measurement points used in the experiments. Fluctuating light conditions (replicating Figure 2.2 day three) are shown as connected points, with open squares representing measurements obtained 10 s after the light transition and closed squares the end of steady-state illumination. Constant illumination of 300 µmol $m^{-2}s^{-1}$ is represented as a dotted line. (B) Representative traces of the light-fluctuation induced ECS signals resulting in transient ECS 'spikes' are shown for the first fluctuation (dark to 39 µmol $m^{-2}s^{-1}$, blue) and the fluctuation from 167 to 333 µmol $m^{-2}s^{-1}$, red). A full set of ECS kinetic 'spikes' following increased light fluctuations can be found in Supplemental Figure 2.21. The extents of light-induced Δψ in wild type (green line and shaded box, indicating mean ± s.d) and *minira* 3-1 (red lines and box, indicating mean ± s.d) at 300 µmol $m^{-2}s^{-1}$ are shown for comparison. (C) The extents of light-induced Δψ, estimated using the ECS_{ss} parameter over the time-course of the fluctuating light experiment, compared to those obtained under continuous illumination in wild type and *minira*3-1 (green and red lines and boxes, respectively, as in Panel B). Open and closed squares correspond to the ECS_{ss} measurements taken at the timing designated in panel A. (D) Time-course of SOSG fluorescence changes for wild type (squares) and *minira* 3–1 (triangles) during exposure to constant 300 µmol $m^{-2}s^{-1}$ (dotted lines) and wild type leaves under the first hour of fluctuating light (solid line). A decrease in SOSG fluorescence occurs when Δψ is collapsed with the addition of the ionophore valinomycin (Supplemental Figure 2.20). All data in A, B, and C represent mean ($n \geq 3$) ± s.d. ECS units were defined as the deconvoluted ΔA_{520} µg $chlorophyll^{-1}$ cm^2.

Singlet oxygen is produced by the interaction of O_2 with triplet excited states of pigments, most likely from the $^3P_{680}$ chlorophyll within the PSII reaction centers generated by recombination reactions (93, 94), as further discussed below. It is unlikely that such triplets could be generated in the bulk light harvesting pigments because high NPQ in the mutants will decrease the lifetime of antenna excited states, and chlorophyll triplets generated in light harvesting complexes are efficiently quenched by carotenoids (95). We thus propose that elevated $\Delta\psi$ induces $^1O_2$ production by accelerating PSII recombination in low g_H^+ mutants when *pmf* is large. Keren et al. (96) suggested that recombination-induced triplet formation could explain the photoinhibitory effects of very low light, when PSII charge recombination is preferred over the forward electron transfer reactions. Our work implies that this type of phenomenon is greatly accelerated by high $\Delta\psi$, potentially making it relevant to photosynthesis under growth light conditions.

The effects of high $\Delta\psi$ would be expected to alter the rates of PSII recombination through P^+Pheo^- (where P^+ is the oxidized primary chlorophyll donor and Pheo the D1 subunit pheophytin) in an increasing dependence upon the fraction of Q_A^-, consistent with the observed correlation between q_I and q_L as the light intensity increased (Figure 2.4). To test this relationship, we estimated the recombination rates from $S_2Q_A^-$ through the P^+Pheo^- pathway, considering Q_A redox state (estimated by $1-q_L$) and the expected impact of $\Delta\psi$ on the equilibrium constant for sharing electrons between Pheo and Q_A (based on ECS_{ss} and the position of Q_A in the structure relative to the membrane dielectric). The basis of this estimate is described in more detail in Materials and methods. As shown in Figure 2.5C, we see a positive correlation between q_I and estimated recombination through P^+Pheo^- over both mutant variants and light intensities, indicating that the combined effects of $\Delta\psi$ and Q_A redox state can explain a large fraction of the

observed extents of photoinhibition. While it is likely that multiple mechanisms of photoinhibition exist, which may also explain some of the q_I variation, overall the greatest impact upon photoinhibition under these conditions can be explained by $\Delta\psi$-mediated changes in PSII electron recombination.

The obvious questions are: does $\Delta\psi$-induced photoinhibition occur in wild type plants and if so under what conditions? Photosynthesis is known to be particularly sensitive to rapid fluctuations in light intensity (66), at least some of this sensitivity is associated with photoinhibition of PSI, especially in cyanobacteria (97). However, such fluctuations should also result in large transient changes in $\Delta\psi$, as the thylakoid membrane has a low electrical capacitance and low permeability to counter-ions, while the lumen and stroma have high proton buffering capacity (2). The slow onset of q_E and other down-regulatory processes in photosynthesis should exacerbate these effects and allow for large fluxes of electrons when light levels are rapidly increased, resulting in large, transient $\Delta\psi$ 'pulses'.

We therefore hypothesized that $\Delta\psi$-induced photodamage may contribute to the increased photodamage seen under fluctuating light. To test this possibility, we measured light-driven *pmf* ($\Delta\psi$ and ΔpH) and $^1O_2$ generation in wild type Arabidopsis under fluctuating light conditions (Figure 2.7A, replicating the first 8 hr of Figure 2.2A day three). The initial dark-to-light transition resulted in an immediate, transient 'spike' in $\Delta\psi$, even though the light intensity was low (39 μmol photons $m^{-2}s^{-1}$, Figure 2.7B). The spike was transient, and decreased to steady-state levels within tens of seconds, as shown in the blue trace in Figure 2.7B. Spikes in $\Delta\psi$ of similar amplitudes were also seen upon each increase in light at the onset of each fluctuation, though the recovery kinetics tended to be more rapid than those seen at the first dark-light transient. An example of these transients, taken at the transition between 167 and 333 μmol

photons m^{-2} s^{-1} is shown in (Figure 2.7B). A more complete set of transient kinetics, over the entire course of the experiment is presented in Supplemental Figure 2.21. The amplitudes of these $\Delta\psi$ transients were similar to or larger than those seen in the *minira* 3–1 line under constant 300 μmol photons m^{-2} s^{-1} light, which also induced $^1O_2$ generation (see red horizontal bars in Figure 2.7B). These spikes reflect increases in $\Delta\psi$ above that already produced by steady-state photosynthesis, so the true extent of $\Delta\psi$ is likely considerably higher, and based on estimates of the calibration of the ECS signal likely range between 150–260 mV (see Supplemental Figure 2.21).

By contrast, wild type plants under constant 300 μmol photons m^{-2} s^{-1} produced much lower $\Delta\psi$ extents (Figure 2.7B green bars) and had no detectible $^1O_2$ generation (Figure 2.7D). These results suggest that even low amplitude light fluctuations are capable of inducing $\Delta\psi$ large enough to produce $^1O_2$ and PSII photodamage. Supporting this interpretation, wild type leaves under these fluctuating light conditions produced substantial amounts of $^1O_2$ during the first hour of fluctuating conditions compared to higher intensity, but constant illumination (Figure 2.7D).

The above results lead us to conclude that fluctuating light likely induces strong effects through $\Delta\psi$-induced recombination reactions in PSII (see below for considerations of potential contributions to PSI). In addition to direct damage to the enzymes of photosynthesis, $^1O_2$ can also activate plant light stress-related gene expression and programmed cell death (98), suggesting a possible physiological linkage between *pmf*-enhanced recombination and plant regulatory pathways that may result in long-term acclimation to fluctuating light.

At a mechanistic level, we propose that imposing a large $\Delta\psi$ across the PSII complex will decrease the standard free energy gap between the vectorial electron transfer steps and thus the back-reaction will be accelerated in competition with forward (energy-storing) reactions (37, 55,

87) (Figure 2.8). It is known that decreasing the energy gap between Pheo and Q_A favors recombination from $P^+Q_A^-$ via $Pheo^-$ (55, 87) rather than directly from Q_A^- to P^+ (56, 87, 99). The observed increased recombination rates *in vitro* (Figure 2.6) when $\Delta\psi$ is present, combined with $^1O_2$ production under high $\Delta\psi$ conditions *in vivo* suggest that the fraction of electrons recombining to P^+ through a $Pheo^-$ intermediate is greatly increased, as the recombination pathway via the $Pheo^-$ has a high yield for formation of the triplet state of P (^3P) that in turn can interact with O_2 to produce $^1O_2$ (56, 67, 87).

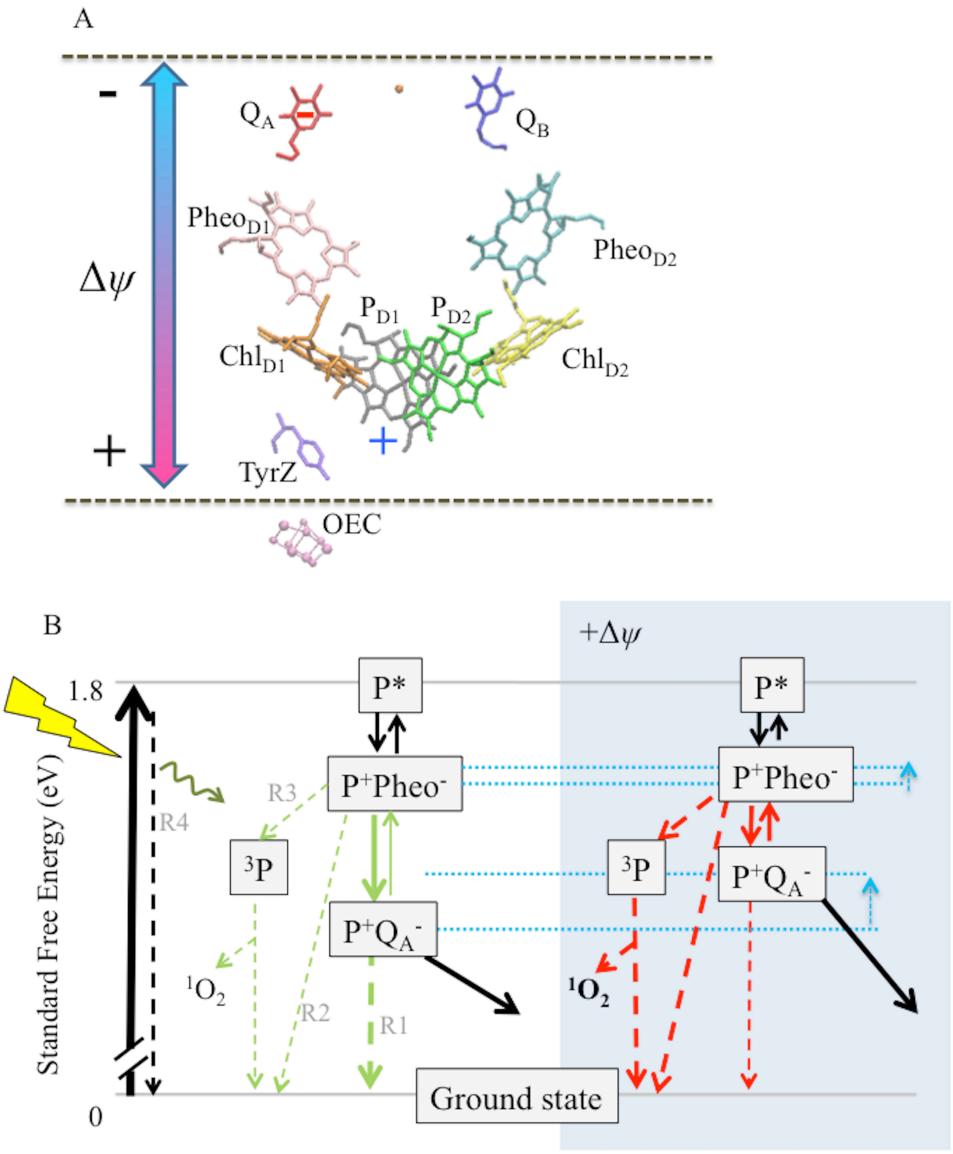

Figure 2.8: Schemes for the trans-thylakoid Δψ-induced acceleration of recombination reactions in PSII and subsequent production of $^1O_2$.
(A) The relative positions of PSII electron transfer cofactors with respect to the electric field (double-headed arrow) imposed across the thylakoid membrane (dotted lines). The red and blue arrows indicate the Δψ-induced changes in the equilibrium constant for the sharing of electrons (−) between Q_A and Pheo, and electron holes (+) among P^+ and the oxygen evolving complex. Excitation of PSII by light leads to formation of excited chlorophyll states (P*), the excitation is shared over the 4 chlorophylls and the 2 pheophytins. Charge separation occurs between more than one pair of pigments, so at short times the situation is not well defined, but $Chl_{D1}^+Pheo_{D1}^-$ appears to be the dominant radical pair. Secondary electron transfer events occur forming $P_{D1}^+Pheo_{D1}^-$, the second radical pair, which is present in nearly all centers. This radical pair is stabilized by electron transfer from $Pheo^-$ to Q_A forming $P_{D1}^+Q_A^-$. This radical pair is further stabilized by electron transfer from D1Tyr161 (TyrZ) forming a neutral tyrosyl radical,

Figure 2.8 (*continued*): which oxidizes the Mn cluster of the oxygen evolving complex to form the state $S_{n+1}Q_A^-$. Finally, Q_A^- reduces Q_B to form $S_{n+1}Q_B^-$. Upon a second PSII turnover the double reduced and protonated Q_B plastohydroquinone becomes protonated and is exchanged with an oxidized plastoquinone from the membrane pool (black arrows). The illustration was based on crystal structure 3WU2 (Umena et al., 2011). (B) The charge separation states described above are unstable and recombination competes with the energy-storing reactions. When P_{D1}^+ is present, recombination reactions can occur by several pathways as indicated by the dashed lines: (1) direct electron transfer from Q_A^- to P^+ (R1); (2) by the back reaction to form the P^+Pheo^- state, which can then recombine directly (R2) or, (3) when the P^+Pheo^- radical pair is present as a triplet state, $^3[P^+Pheo^-]$, the dominant state when formed by the back-reaction, $^3[P^+Pheo^-]$ charge recombination forms ^3P (R3), a long lived chlorophyll triplet that can easily interact with O_2 to form $^1O_2$; (4) complete reversal of electron transfer can also occur, repopulating P* (R4), which can return to the ground state by emitting fluorescence (luminescence) or heat. Route 3, the triplet generating pathway, is the dominant recombination route in fully functional PSII. For simplicity the $^3[P^+Phe^-]$ is not distinguised from the singlet form in this scheme. A $\Delta\psi$ across the membrane should destabilize $P^+Q_A^-$ relative to the other states (see dotted blue lines), affecting the rates of reactions indicated in the green versus red. A $\Delta\psi$ across the membrane should also destabilize P^+Pheo^-, but because of the smaller dielectric span across the membrane, to a lesser extent than $P^+Q_A^-$. Thus, the buildup of $\Delta\psi$ should shift the equilibrium constant for sharing electrons between Q_A^- and Pheo, favoring the formation of $Pheo^-$ and thus increasing the rate of recombination through R3 (as well as the R2 and R4), resulting in increased production of ^3P and $^1O_2$. Destabilization of $P^+Q_A^-$ will also increase the driving force for $P^+Q_A^-$ recombination via R1, however this recombination is already driven by 1.4eV and it is thus likely to be in the Marcus inverted region. Thus increasing the driving force will slow recombination by this route.

2.4 Discussion

This proposed mechanism of $\Delta\psi$-mediated photoinhibition has broad implications for the energy limitations of photosynthesis. Although the two components of *pmf* are energetically equivalent for driving ATP synthesis (3), they have distinct effects on the regulation of photosynthesis (13, 100, 101). It has thus been proposed that the partitioning of *pmf* into $\Delta\psi$ and ΔpH is regulated to maintain a balance between efficient energy storage and regulation of light capture (61). We demonstrate here another important constraint on this balance: the avoidance of photodamage caused by recombination reactions in PSII, and this may explain the need for complex ion balancing systems in chloroplasts (2, 28, 29).

The effect of $\Delta\psi$ on recombination and $^1O_2$ production may, at least in part, explain the severe effects of fluctuating light on photosynthesis, and thus could constitute a significant limitation to photosynthetic productivity. In the absence of a large $\Delta\psi$, the energy gap between the P^+Pheo^- and $P^+Q_A^-$ appears to be sufficient to keep detrimental recombination to a manageable level when the usual regulatory mechanisms are functional (56). During photosynthesis, and especially under fluctuating light, though, the energy gaps between the photo-generated radical pairs vary dynamically under the influence of the *pmf*, so that high $\Delta\psi$ renders the charge-separated states in the photosystems considerably less stable. The $\Delta\psi$ is also expected to influence the trap depth (i.e. the energy level between P^* and the first radical pair(s), the most relevant probably being P^+Pheo^-) and this could potentially affect the quantum yield of charge separation and the yield of radiative recombination (luminescence). Transthylakoid electric fields also influence recombination reactions in PSI reaction centers (102). It is thought that P_{700} triplet formation is minimized in PSI by the presence of the higher potential quinone in PsaA, making this side of the reaction center the safe charge recombination pathway (56). In light of the present findings, it is worth considering whether a transiently large $\Delta\psi$ could make this protective mechanism less efficient, though this question has yet to be addressed experimentally.

Over evolutionary time scales, the $\Delta\psi$-effect may have constrained other bioenergetics features of photosynthesis. It has long been known that oxygenic photosynthesis is limited, in most organisms, to wavelength ranges shorter than about 700 nm (the 'red limit'), resulting in the loss of a large fraction of the light energy hitting the plant (103). Gust et al. (104) proposed that the red limit may be the result of certain limitations imposed in part by key biochemical properties of life (e.g. the properties of energy storage molecules NAD(P)H and ATP, the use of

certain biochemical pathways, etc.) that evolved before the advent of photosynthesis. Milo (105) came to a different conclusion based on estimates of the theoretical wavelength dependence of energy conversion efficiency for plant photosynthesis, based on the Shockley and Queisser equation (106). The maximum efficiency was about 700 nm, similar to the red limit of oxygenic photosynthesis, suggesting that evolution has selected for photosynthetic energetics based on this fundamental limit, rather than any biological imperative. However, the predicted wavelength-dependence of the energy efficiency is very broad, with only about a 15% decrease from the peak at wavelengths out to 800 nm, far beyond the red limit, even in organisms with red-shifted reaction centers. Marosvolgyi and van Gorkom (107) drew a similar conclusion but with additional restraints and suggested a narrower maximum more closely overlapping with the red absorption of chlorophyll *a*.

Rutherford et al. (56) took a different view based on an analysis of the bioenergetics of reaction centers. They noted that PSII was in a uniquely difficult situation in energy terms: (1) it does multi-electron chemistry (at both sides of the reaction center) and so cannot prevent back reactions by kinetic control, (2) it has a very energy demanding reaction to do: water oxidation and quinone reduction with a ΔE ~920 meV in functional conditions, and requires a significant over-potential not just for attaining a high quantum yield of photochemistry but also for achieving water oxidation and quinol release, and (3) its chlorophyll cation chemistry is uniquely oxidizing and thus it cannot use carotenoids to protect itself from chlorophyll triplet formation at the heart of the reaction center. This situation means that unlike other type-II reaction centers, PSII is unable to prevent electrons from the bound semiquinones getting back to the Pheo and then recombining with P^+ and forming ^3P.

This lack of energy 'headroom' was seen not only as a major factor in PS II's susceptibility to photodamage but also as a reason why oxygenic photosynthesis is pinned to chlorophyll *a* photochemistry at around 680 nm as the red limit. The existence of efficient oxygenic photosynthesis at longer wavelengths seemed to question that view (108-111). However, it was pointed out that these species seem to exist in very stable environments that have very little variation in light conditions (112). Under such a narrow range of illumination conditions it is not unreasonable that less energy 'headroom' is required (112).

Clearly, these specific energy limitations of PSII will be exacerbated by spikes in the $\Delta\psi$ reported here. Indeed, it seems reasonable to suggest that the existing 'energy headroom' postulated in normal chlorophyll *a*-containing PSII, while too small to avoid photodamage altogether, exists quite specifically to mitigate the extra photodamage from back-reactions enhanced by spikes in $\Delta\psi$ due to variable light intensities. In this way, the extent of the variable light-induced $\Delta\psi$ may be considered to contribute to the position of the red limit of oxygenic photosynthesis.

The need to prevent $\Delta\psi$-induced recombination may also have guided the evolution of other photosynthetic components. Recent mechanistic models of the ATP synthase suggest that the ratio of protons passed through the ATP synthase per ATP synthesized depends on the number of subunits in the *c*-ring (41). The chloroplasts of green plants and algae thus far studied possess ATP synthase complexes with larger *c*-ring stoichiometries than their mitochondrial and bacterial homologues (45), imposing higher fluxes of protons to generate ATP and necessitating the engagement of additional bioenergetic processes, including cyclic electron flow, to make up the ATP deficit needed to sustain photosynthesis (76, 82). While this increased H^+ demand is often viewed as a bioenergetic limitation to photosynthetic electron and proton transfer, a high

H^+/ATP ratio decreases the *pmf* needed to maintain a given ATP free energy state (ΔG_{ATP}), thus allowing photosynthesis to operate at a decreased steady-state *pmf*. In this context, the deleterious electron recombination effects of a high *pmf* may have favored the evolution of ATP synthase complexes with high H^+/ATP ratios in chloroplasts.

2.5 Materials and Methods

2.5.1 Plant materials and growth conditions.

Wild type *Arabidopsis thaliana* (ecotype Wassilewskija-2) and ATP synthase γ-subunit mutants were germinated on Murashige and Skoog medium supplemented with 2% (w/v) sucrose, and 10 mg L^{-1} sulfadiazine for selection of transgenic *minira* lines (113). Following germination plants were grown on soil under a 16 hr photoperiod at 100 μmol photons m^{-2} s^{-1} at 22°C for three weeks.

Nicotiana tabacum wild type (cv Samsun NN) and *ATPC1* antisense lines were germinated and grown as in (70) under a 16 hr photoperiod at 300 μmol photons m^{-2} s^{-1}. Measurements were performed at the onset of flowering on the youngest, fully expanded leaves.

2.5.2 Generation of chloroplast ATP synthase γ-subunit minira (minimum recapitulation of ATPC2) mutants.

A T-DNA insertion mutant for ATPC1 (*dpa1*) (72) was used to introduce the mutated constructs as a complemented allele as in (71). Site-directed mutations in the redox-regulatory domain of ATPC1 were designed to incorporate amino acid differences from the redox inactive ATPC2 into the redox regulated ATPC1 (Figure 2.1A). The *Arabidopsis thaliana* AtpC1 gene was excised from binary vector pSex001 as a SmaI/XbaI fragment and cloned into SmaI/XbaI digested pBluescript plasmid. The resulting plasmid was named pDA15. The mutations were introduced into ATPC1 using a combination of three approaches.

The first approach used an adaptor ligation strategy. Oligonucleotides were designed to introduce desired mutations. Adaptors representing the 5' and 3' strand of DNA targeting specific mutations were obtained independently from Sigma Aldrich. A total of 5 ml of each oligonucleotide pair (10 mM) were mixed and denatured at 95°C for 10 min in a boiling water bath. The oligonucleotides were allowed to reach room temperature over two hours in the water bath allowing for efficient annealing of complementary strands. The adaptors thus obtained were utilized for adaptor ligation.

The target region from ATPC1 cDNA was removed using BglII/HpaI restriction enzymes. The larger linearized backbone of pDA15 was used for ligation with the adaptors (Table 2.1). The resultant vector was double digested with SmaI and XbaI to excise the mutated ATPC1 gene, which was then ligated back into the SmaI/XbaI digested binary vector, pSex001.

A second set of mutations was introduced by first digesting pDA15 with BglII followed by a partial digestion with TatI. The resulting plasmid backbone was used for ligation with the adaptors having the desired mutation (Table 2.2). As in the first adaptor ligation-mediated mutagenesis approach, the resultant vector was double digested with SmaI and XbaI to excise the respective mutated atpC1 gene and ligated into SmaI/XbaI digested binary vector, pSex001.

A second mutagenesis strategy used splicing by overlap extension (SOE) PCR. For each desired mutation, two sets of primers were designed to produce two overlapping fragments during amplification of atpC1 from pDA15 such that the mutation was generated in the region of overlap (Table 2.3). The two fragments were mixed together and the resulting DNA solution was used as a template for a subsequent PCR using primers that amplify the complete AtpC1 gene (DMP 45 and DMP 46). This led to the amplification of the entire atpC1 gene with the desired

mutation. The mutated atpC1 was digested with SmaI and XbaI and was sub-cloned into SmaI/XbaI digested pSex001.

The third mutagenesis approach involved swapping of target domains (delete swaps) using synthetic gene fragments synthesized at GenScript USA (Table 2.4). The synthetic gene was used to replace the ATPC1 redox regulatory domain in the native gene. To swap the domains, pDA15 was digested with BsrGI and XbaI to remove the native domain and ligated with the synthetic fragment derived from the synthetic gene construct after digestion with BsrGI and XbaI. To introduce a synthetic gene with a single nucleotide mutation, the synthetic gene construct for *minira* 3 and pDA15 were double digested with BsrGI and XbaI and the synthetic BsrGI/XbaI fragment with the mutation was ligated into pDA15 where the original BsrGI/XbaI fragment had been removed The resultant intermediate plasmid was digested with SmaI/XbaI to obtain the gene with swapped C domain. This gene was then sub-cloned into SmaI/XbaI digested pSex001. All of the introduced mutations were confirmed by Sanger sequencing of individual plasmids.

Following successful mutagenesis, *minira* constructs were mobilized into the binary vector pSEX001-VS under control of the Cauliflower mosaic virus 35S promoter. A single *minira* construct was transformed into heterozygous *dpa1* plants via *Agrobacterium tumefaciens*-mediated transformation (114). The resulting transgenic plants were screened for the *minira* insertion via PCR using the forward primer 5’ -GGTAATATCCGGAAACCTCC- 3’ and the reverse primer 5’ -GTACAAGAGCTCGACTTTCTCG- 3’ followed by *dpa1* screening using the forward primer 5’ -CACATCATCTCATTGATGCTTGG- 3’ and the reverse primer 5’ -GTACAAGAGCTCGACTTTGTCG- 3’. Transgenic plants containing both *minira* and *dpa1*insertions were self-pollinated until plants were homozygous for

both *dpa1* (Δ*atpc1*) and the correct *minira* mutation, which was subsequently confirmed by sequencing.

2.5.3 Isolation of tightly coupled chloroplasts and intact thylakoids.

Chloroplasts were extracted from market spinach with modifications to the method described in Seigneurin-Berny et al. (115). All centrifugation steps were carried out at 4°C and exposure to light was kept to a minimum. Briefly, approximately 20 g of spinach leaves were homogenized in a blender for 10 s with ice cold homogenization buffer of 50 mM HEPES (pH 7.6), 330 mM sorbitol, 5 mM $MgCl_2$, 2 mM EDTA and supplemented with 0.1% BSA for grinding. The homogenate was filtered through three layers of wetted Miracloth and one layer of wetted muslin followed by centrifugation at 4000 x *g* for 10 min. The pellet was resuspended in homogenization buffer and layered on top of a single step 80%–40% Percoll gradient. Intact chloroplasts were recovered after centrifugation for 20 min at 3000 x *g* in a swinging bucket rotor. The intact chloroplasts were diluted approximately 4-fold with homogenization buffer and centrifuged for 5 min at 4000 x*g*. The chloroplast pellet was resuspended in a minimal amount of homogenization buffer (<1 mL) and chlorophyll quantified in 80% acetone (116).

2.5.4 Spectroscopic measurements.

Near simultaneous chlorophyll fluorescence and electrochromic shift (ECS) measurements were performed on a custom made spectrophotometer (117). For *in vivo* spectroscopic measurements, following a 10 min dark acclimation the maximal PSII quantum efficiency, linear electron flow (LEF), energy-dependent exciton quenching (q_E), and photoinhibitory quenching (q_I) were estimated using saturation pulse chlorophyll *a* fluorescence as described previously (118). The extent of the q_I component of NPQ was determined following at least 10 min dark relaxation to eliminate the residual effects of q_E type quenching. Red actinic

illumination was used for all measurements to prevent incorrect assessment of chloroplast movement as q_I, as red light is ineffective in inducing chloroplast movements (119). A Stern-Volmer derivation of q_E ($q_{E(SV)}$) was used to minimize the contribution of q_I in the determination of q_E (120). Estimates of the relative redox status of Q_A (q_L) were performed as described in (100) after at least 10 min of actinic illumination. The relative extents of steady state *pmf* (ECS_t) and the conductivity of ATP synthase to protons (g_{H^+}) were measured using the dark interval relaxation kinetics of absorbance changes associated with the electrochromic shift (ECS) fit to a first-order exponential decay (74). Partitioning of the *pmf* was determined from deconvolution of the absorbance change at three wavelengths (505, 520 and 535 nm) around 520 nm during the dark interval ECS changes and the ECS steady-state ($\Delta\psi$) and ECS inverse (ΔpH) were determined as in (47). Briefly, the total amplitude of the deconvoluted ECS signal following a rapid light/dark transition was used to estimate the total light-induced *pmf* (ECS_t). The steady-state $\Delta\psi$ component was determined from the extent to which the inverted ECS signal during the dark interval decreased from the steady-state baseline. The steady-state ΔpH component was determined as the amplitude of the inverted ECS signal during the dark interval. The ECS measurements were corrected for pigment variations by normalizing to chlorophyll content determined from acetone extraction as above. For tobacco measurements, the ECS measurements were normalized to the xenon-flash induced extent of the $\Delta A_{520\ nm}$ ECS rise. P_{700}^+ reduction kinetics were measured from the dark interval relaxation kinetics of the absorbance change at 810 nm after subtracting the 930 absorbance change (121).

In vitro chloroplast measurements were performed on a similar instrument described above modified to measure a cuvette held sample. Chloroplasts were osmotically shocked on ice in buffer containing 10 mM HEPES (pH 7.8) and 10 mM $MgCl_2$ to a final chlorophyll

concentration of 20 μg ml^{-1} supplemented with 5 μM spinach ferredoxin and 10 μM ascorbate. Where noted, thylakoids were treated with 50 μM decyl-ubiquinol to catalyze PSI cyclic electron transfer and generate a *pmf*, 50 μM 3-(3,4-dichlorophenyl)-1,1-dimethylurea (DCMU) to block PSII forward electron transfer, and 25 μM gramicidin to decouple the *pmf*. Fluorescence measurements were performed as above, with variable fluorescence measured after a 20 min dark adaptation after which the thylakoids were excited with a single 100 ms subsaturating actinic pulse. From a dark-adapted state, the application of a single turnover pulse will lead to rapid accumulation of $\Delta\psi$, due to the high buffering capacity of the thylakoid lumen as well as the low capacitance of the thylakoid membrane, allowing gramicidin to decouple $\Delta\psi$, as the $\Delta\psi$ primarily composes the *pmf* under these conditions (2). The F_0 measurements for all samples were taken from the first measured point to avoid any actinic effects due to the measuring pulses themselves.

2.5.5 Estimation of recombination rate.

The $\Delta\psi$-induced enhancement of the rate of recombination from the $S_2Q_A^-$ state was estimated based on the change in the equilibrium constant for the sharing of electrons in the presence of $\Delta\psi$. Other states will also recombine (e.g. the $S_3Q_A^-$ state) but we use $S_2Q_A^-$ as a proxy because we expect most of these states to respond to changes in Q_A and $\Delta\psi$ in similar ways. The rate of recombination from $S_2Q_A^-$ was calculated as:

$$v_r = [\mathrm{S_2Q_A}^-] * k_r 10^{\frac{-\Delta E_{stab}}{0.06}} \quad (1)$$

where $[S_2Q_A^-]$ is the concentration of PSII centers with reduced Q_A, k_r the intrinsic rate of recombination from $S_2Q_A^-$, and ΔE_{stab} is the free energy for stabilization of the charge separated state, expressed in eV. In the absence of a field and in the presence of DCMU where all Q_A is reduced, v_r is measured to be about 0.3 s^{-1} (Figure 2.5), but in the uninhibited complex under

steady state photosynthesis, this rate will be decreased proportionally by oxidation of Q_A, while ΔE_{stab} will be decreased by $\Delta\psi$ so that:

$$v_r = 0.3 * (1 - q_L) * 10^{\frac{-\Delta\varphi_{light-dark}}{60}} \quad (2)$$

where 1-q_L is an estimation of the fraction of Q_A in the reduced form (100), and $\Delta\psi_{light\text{-}dark}$ is the light-dark difference in electric field in mV. From Takizawa et al. (47) we obtained a factor for estimating $\Delta\psi$ from the extents of ECS, and correcting for the chlorophyll content as performed here, we obtain:

$$v_r = 0.3 * (1 - q_L) * 10^{\frac{-ECS_{ss}}{60}} \quad (3)$$

where ECS_{ss} is the normalized ECS signal representing the light-dark difference in $\Delta\psi$ normalized to the chlorophyll content.

2.5.6 Chlorophyll fluorescence imaging.

In vivo whole plant chlorophyll a fluorescence imaging was performed in an imaging chamber equipped with 50W Bridgelux White LEDs (BXRA-56C5300, Bridgelux Inc., Livermore, California) for white actinic illumination (75). Pre-illumination values for F_0 and F_M were captured just prior to the beginning of the photoperiod and subsequent fluorescence parameters obtained using a 300 ms saturating actinic pulse at ~25,000 μmol photons m^{-2} s^{-1} and a Red LED matrix (Luxeon Rebel SMT High Power LED Red, LXM2-PD01-0050, Philips Lumiled, San Jose, California) to measure chlorophyll which was then captured by a CCD camera (AVT Manta 145 M) equipped with a near infrared long pass filter (RT-830, Hoya Glass). Plants were imaged over three consecutive 24 hr photoperiods (Figure 2.2A, Supplemental Files 1-9, timing and light intensities are described in Tables 2.5-2.7). During the first day, the actinic light intensity remained constant at 100 μmol photons m^{-2} s^{-1} to collect growth chamber conditions. Days two and three represented ramped lighting

perturbations. The photoperiod for day two was sinusoidal, beginning at 39 μmol photons m^{-2} s^{-1} and increasing in intensity by approximately 1.2 times every 30 min until midday where it peaked at 500 μmol photons m^{-2} s^{-1}, after which the light intensity decreased at the same rate every 30 min. The photoperiod for day three was sinusoidal with brief fluctuations in light intensity. Starting at 39 μmol photons m^{-2} s^{-1}, the light intensity was doubled after 15 min followed by 1.5-fold increase for 12 min and the cycle repeated until peak intensities of 1000 and 500 μmol photons m^{-2} s^{-1} were cycled through at midday, after which the sinusoidal fluctuations decreased at the same rate as the increases. Steady state values for NPQ parameters of chlorophyll fluorescence were captured prior to the ramp to the next light intensity on days two and three, or hourly on day one and calculated as noted above for the fluorescence spectroscopy. Sequences of images were captured with a 60 ms delay between images for a 15 frame total for each measurement pre- during and post-saturation flash followed by images taken to correct for artifacts due to residual electrons in the CCD array. Images were analyzed using open source software (ImageJ, NIH) modified in house to allow calculations of photosynthetic fluorescence parameters across selected regions of interest.

2.5.7 Photoinhibition of detached leaves.

Plant leaves were excised and incubated in the dark for 3 hr with their petioles submerged in either water or 3 mM lincomycin to inhibit chloroplast protein translation (78). The leaves were then illuminated with red light at 1000 μmol photons m^{-2} s^{-1} using a red actinic light for indicated periods of time. During illumination, the petioles of the leaves remained submerged in the treatment solution. Following illumination, leaves were allowed to dark adapt for 20 min, after which the F_0 and F_M values of chlorophyll fluorescence were measured in order to

determine F_V/F_M. For tobacco plants, leaf discs were soaked in a lincomycin solution and fluorescence parameters determined at 600 μmol photons m^{-2} s^{-1}.

To determine PSII activity, following photoinhibitory treatment, performed as above, leaves were dark adapted for 20 min and then vacuum infiltrated with a 50 μM DCMU solution. Analysis of PSII activity was determined from the amplitude of the $\Delta A_{520\ nm}$ ECS signal using two saturating single-turnover flashes provided by a xenon lamp spaced 200 ms apart. The amplitude of the second flash, corresponding to PSI centers capable of charge separation, was subtracted from the amplitude of the first flash, corresponding to both PSI and PSII centers capable of charge separation, to obtain the relative PSII photosystems capable of activity both before and after photoinhibition. Xenon flashes were judged to be fully saturating by ensuring that essentially identical results were obtained with a 50% weaker intensity.

2.5.8 Protein analysis.

Photoinhibited leaf samples were collected as described above and total leaf proteins were extracted as described in Livingston et al. (118). Analysis of chloroplast ATP synthase complexes was carried out on 20 μg of protein using leaves collected from 3–4 plants taken from the growth chamber. Analysis of PsbA (D1) protein levels during photoinhibitory treatment was carried out on 30 μg of total protein from 3–4 leaves sampled during the photoinhibitory treatment time points as described above. Proteins were separated by SDS-PAGE and the ATPB (β-subunit) and PsbA (D1) proteins detected using commercially purchased antibodies (Agrisera, Vannas, Sweden).

2.5.9 $^1O_2$ detection.

Plant leaves were excised and incubated in the dark for 3 hr in 250 μM Singlet Oxygen Sensor Green (SOSG, Life Technologies) prepared according to manufacturer's instructions.

Petioles were maintained below the liquid's surface during the infiltration and were wrapped in a Kimwipe soaked in water during imaging to prevent drying. For valinomycin treatments, leaves were vacuum infiltrated with either SOSG solution or with SOSG supplemented with 50 μM valinomycin and subsequently measured. Successful penetration of leaf epidermal and mesophyll cells, as well as SOSG penetrance throughout the cells was confirmed via confocal microscopy. The leaves were imaged in a chamber equipped with the same lighting as above. Qualitatively similar data were obtained for *minira* 3–1 leaves under both white and red (650 nm) LED illumination, ensuring that photosensitization of SOSG was not responsible for the signals obtained (122). Images were captured with a cooled CCD camera (AVT Bigeye G 132B-NIR) equipped with a 555 nm 10 nm band pass filter. Fluorescence excitation was provided via 458 nm LEDS (Cree Inc). Images were analyzed using ImageJ software.

2.5.10 Data analysis.

All spectroscopic data were analyzed and figures generated using Origin 9.0 software (Microcal Software). Statistical analyses of data were performed in R package, utilizing two-way ANOVA to test for significant effects on photoinhibition (q_I) from the interaction with either the ΔpH or $\Delta\psi$ component of the *pmf*.

2.6 Acknowledgements.

This work was supported by the U.S. Department of Energy (DOE), Office of Science, Basic Energy Sciences (BES) under Award number DE-FG02-91ER20021 and the MSU Center for Advanced Algal and Plant Phenotyping (CAAPP). AWR was supported by a Biotechnology and Biological Sciences Research Council (BBSRC) grant (BB/K002627/1) and the Royal Society Wolfson Research Merit Award.

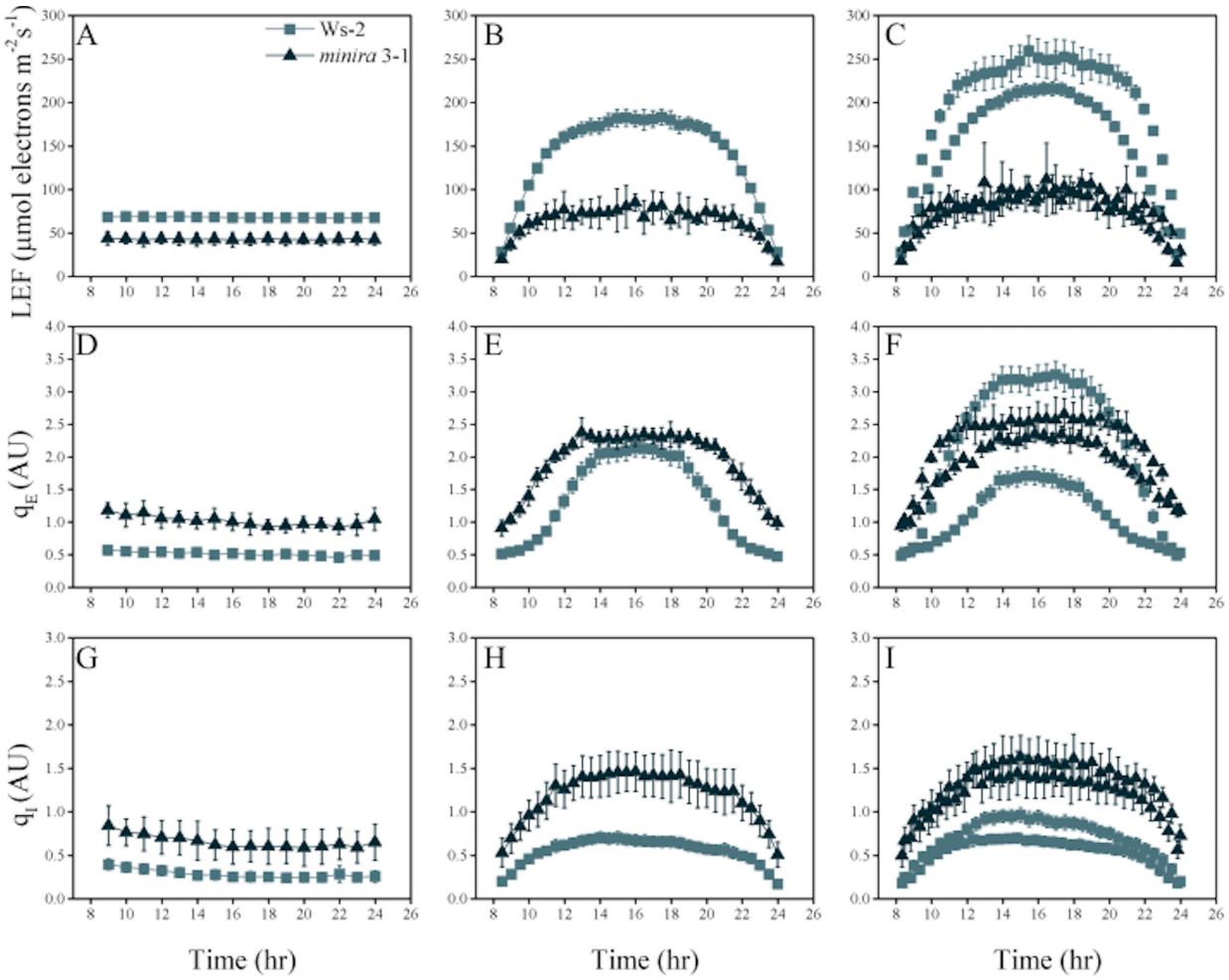

Supplemental Figure 2.1: Whole plant fluorescence imaging phenotyping of *minira* 3–1 mutant.

Three week old plants were imaged over three consecutive 16-hr photoperiods and fluorescent measurements taken at the end of each light transition for LEF (A–C), q_E (D–F), and q_I (G–I) for Ws-2 and *minira* 3–1. Values represent mean of $n \geq 3 \pm$ s.d., all of which were imaged in the same experiment. Timing and illumination are the same as Figure 2.2 and are detailed in Tables 2.5-2.7.

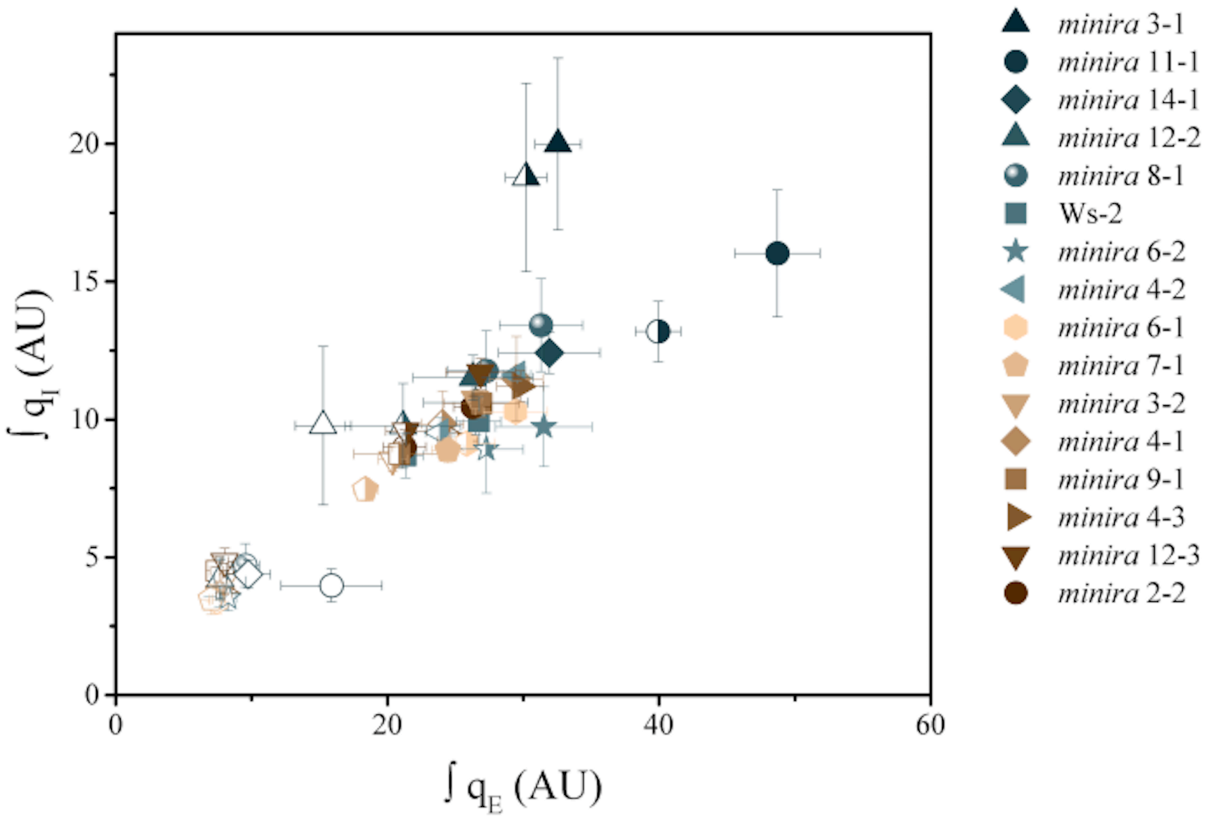

Supplemental Figure 2.2: Increased pH-dependent quenching correlates with increased photoinhibitory quenching.
Whole plant fluorescent phenotypes were measured over three consecutive photoperiods. Day one consisted of a single irradiance level (open symbols), day two of sinusoidal irradiance (half filled symbols), and day three of sinusoidal irradiance interrupted by bright fluctuations (closed symbols). The pH-dependent fluorescence quenching (q_E) and photoinhibitory quenching (q_I) were integrated over time for each plant for each photoperiod to determine how prolonged exposure to an increased pmf influences the extent of photoinhibition. Data represent the integrated total for each day ($n \geq 3$, ± s.d).

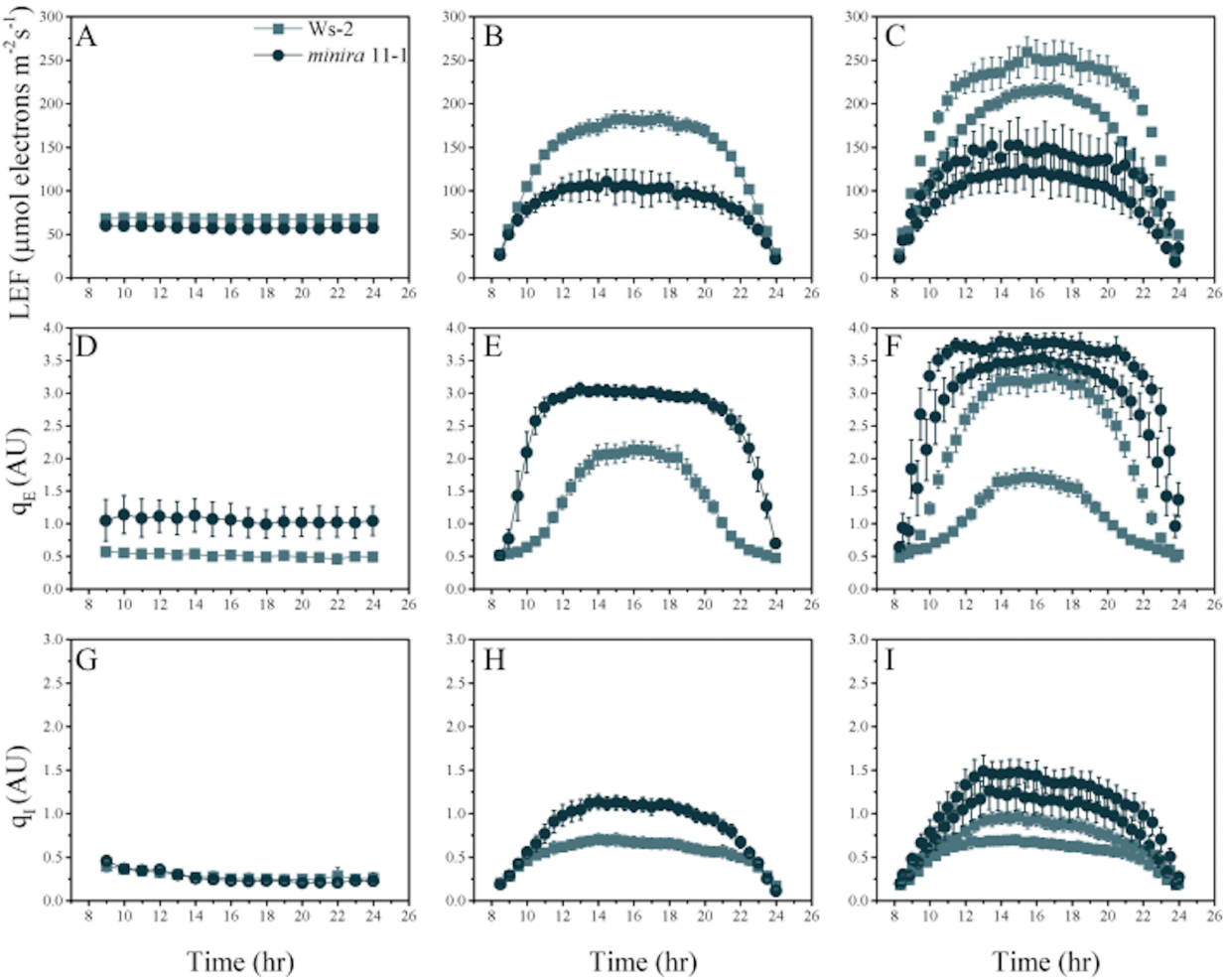

Supplemental Figure 2.3: Whole plant fluorescence imaging phenotyping of *minira* 11–1 mutant.

For details, please refer to the legend of Supplemental Figure 2.1.

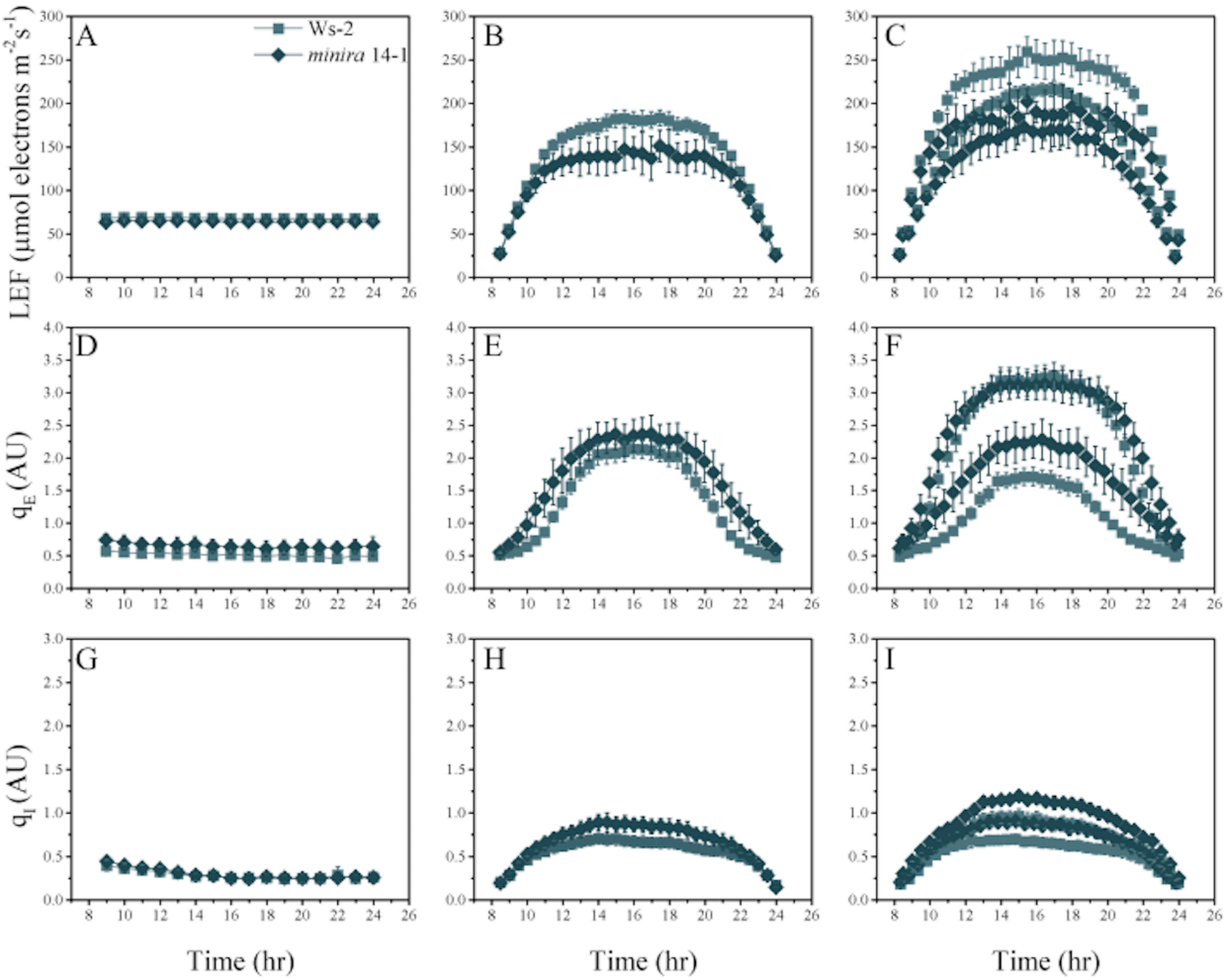

Supplemental Figure 2.4: Whole plant fluorescence imaging phenotyping of *minira* 14–1 mutant.

For details, please refer to the legend of Supplemental Figure 2.1.

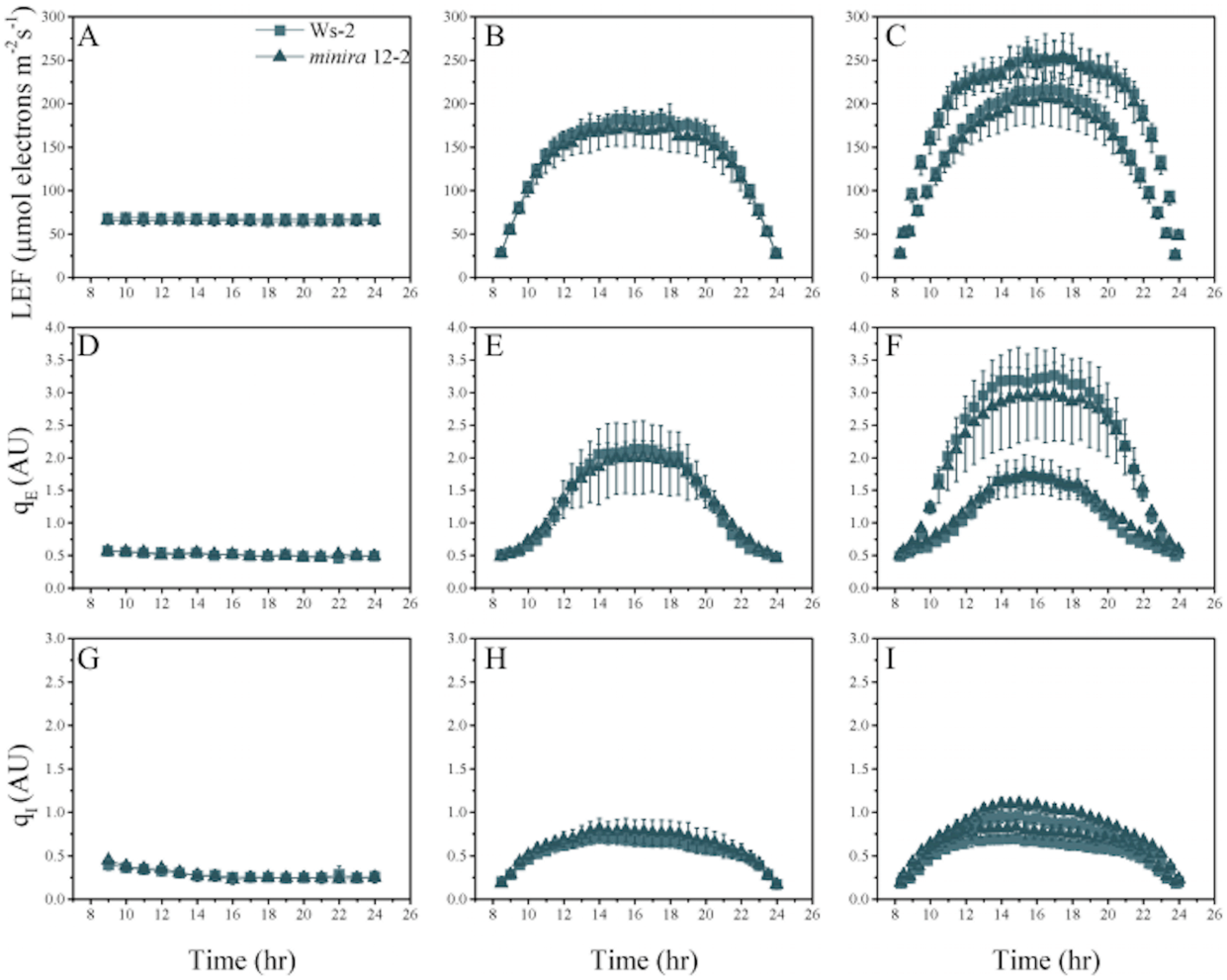

Supplemental Figure 2.5: Whole plant fluorescence imaging phenotyping of *minira* 12–2 mutant.

For details, please refer to the legend of Supplemental Figure 2.1.

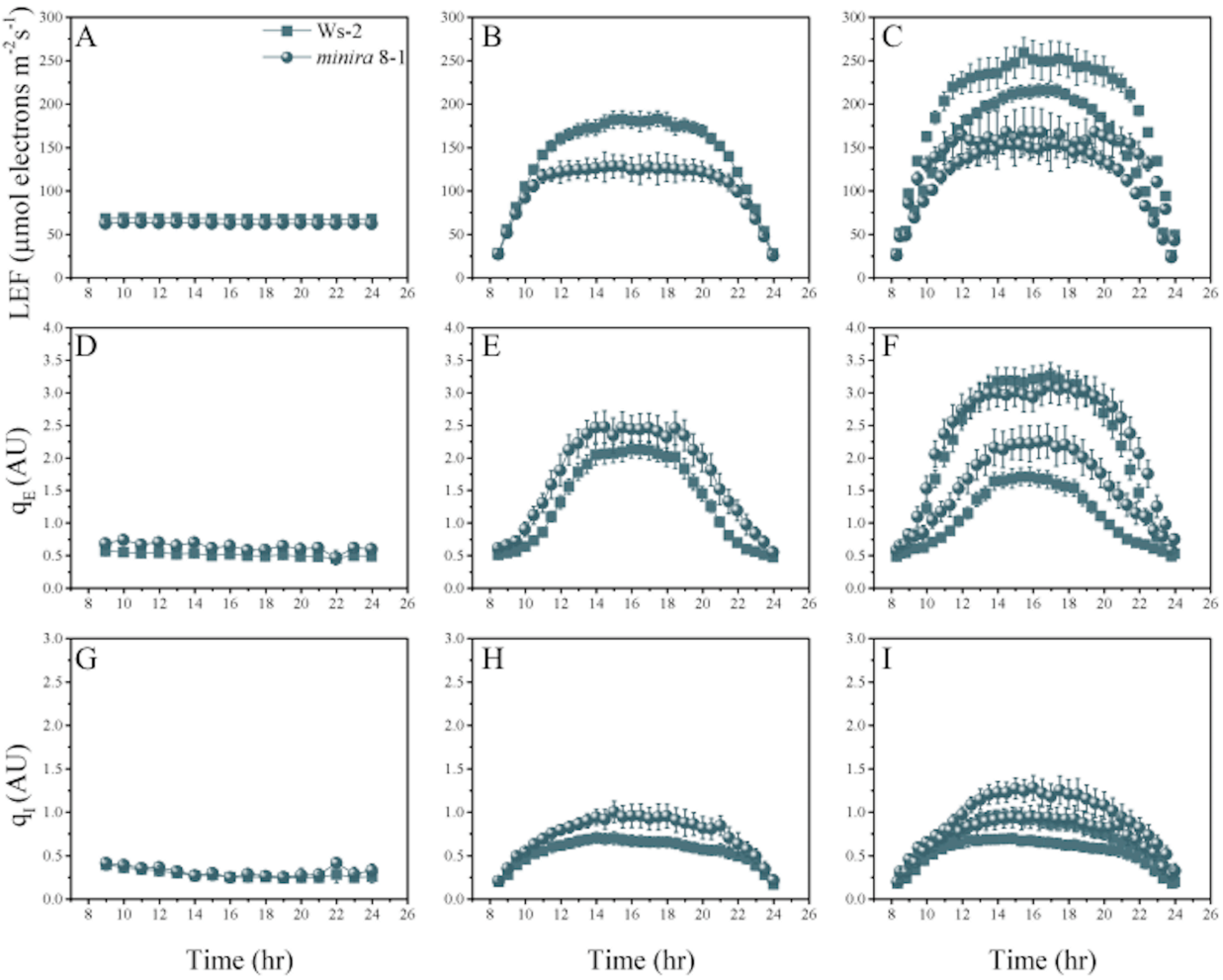

Supplemental Figure 2.6: Whole plant fluorescence imaging phenotyping of *minira* 8–1 mutant.
For details, please refer to the legend of Supplemental Figure 2.1.

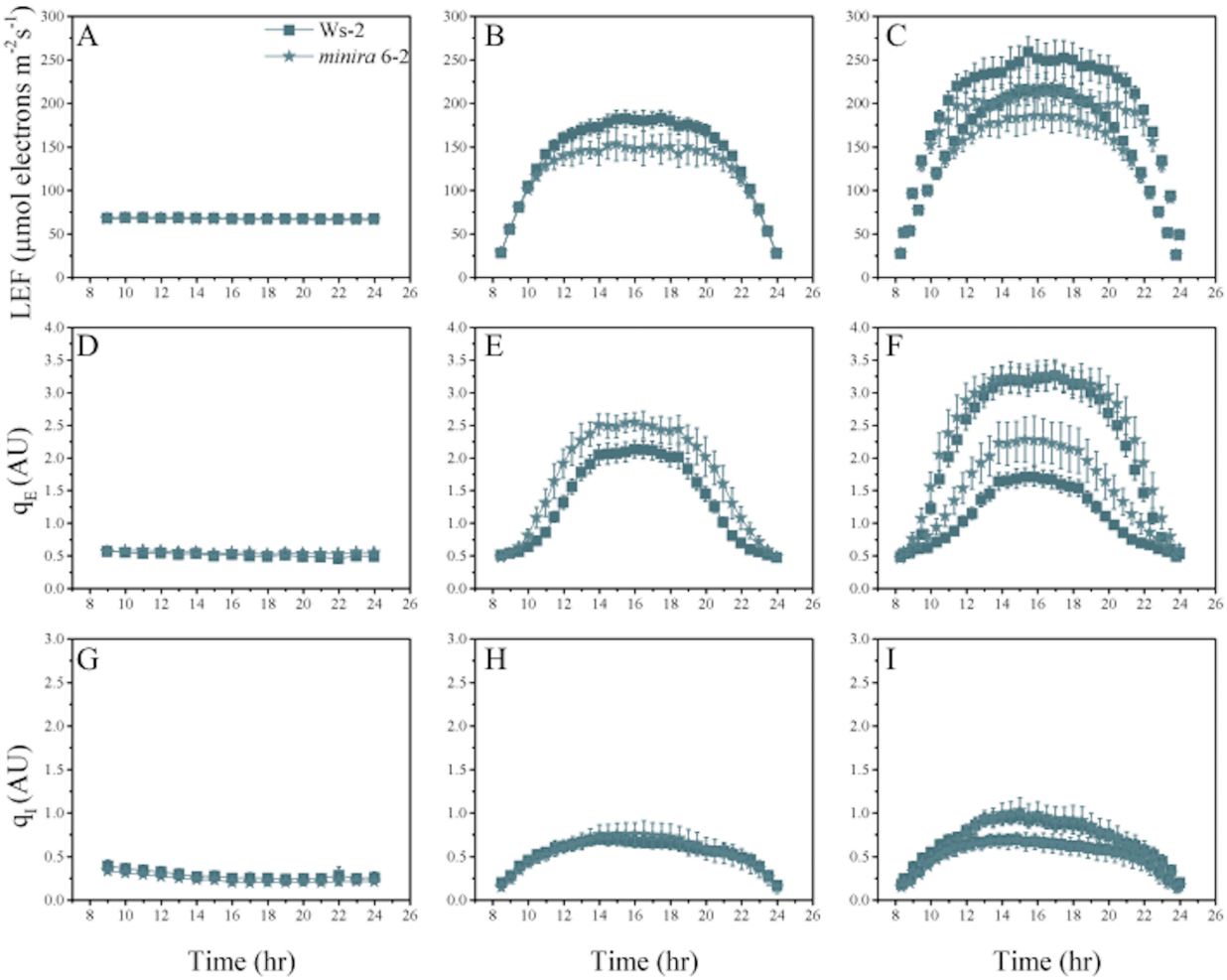

Supplemental Figure 2.7: Whole plant fluorescence imaging phenotyping of *minira* 6–2 mutant.

For details, please refer to the legend of Supplemental Figure 2.1.

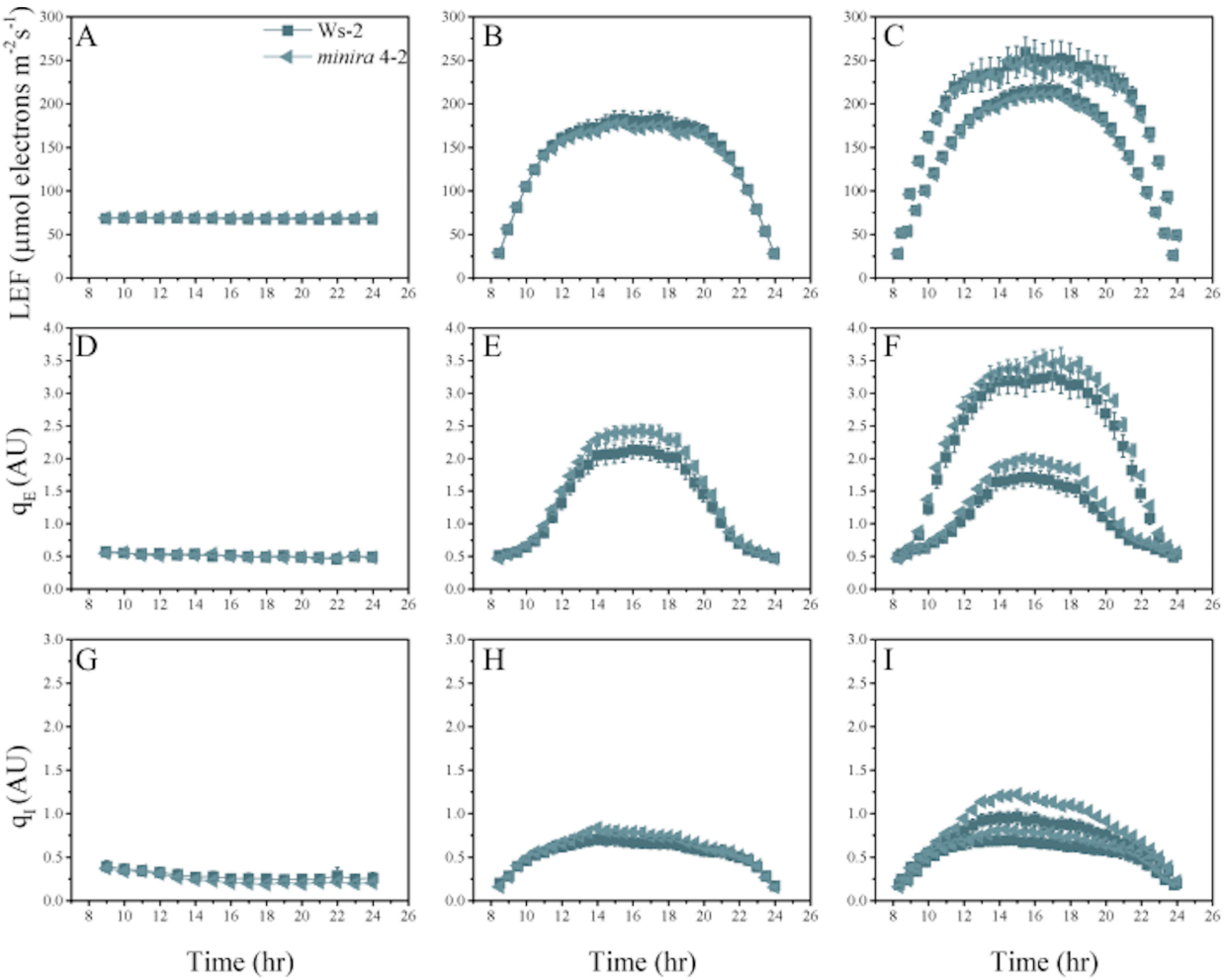

Supplemental Figure 2.8: Whole plant fluorescence imaging phenotyping of *minira* 4–2 mutant.

For details, please refer to the legend of Supplemental Figure 2.1.

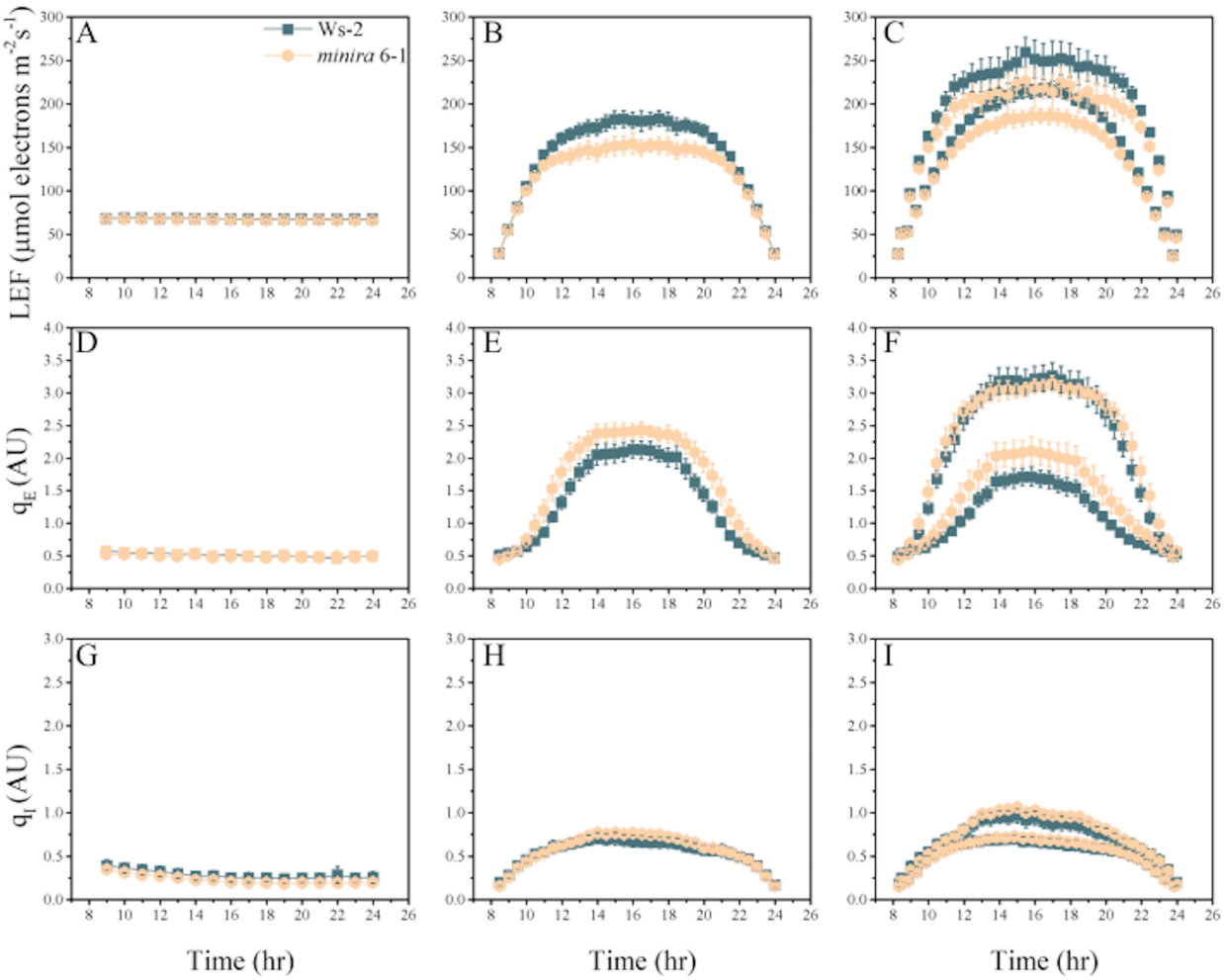

Supplemental Figure 2.9: Whole plant fluorescence imaging phenotyping of *minira* 6–1 mutant.

For details, please refer to the legend of Supplemental Figure 2.1.

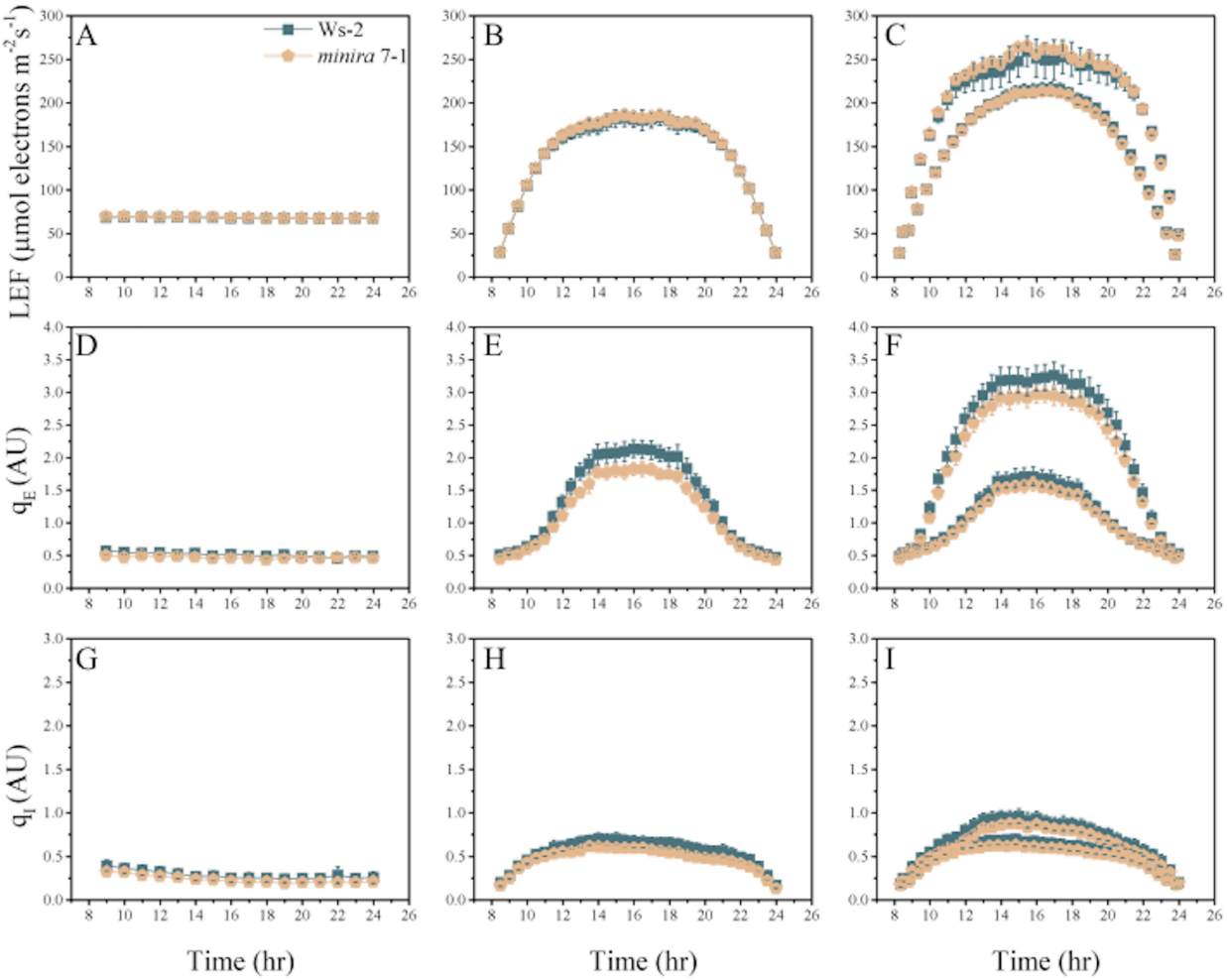

Supplemental Figure 2.10: Whole plant fluorescence imaging phenotyping of *minira* 7–1 mutant.

For details, please refer to the legend of Supplemental Figure 2.1.

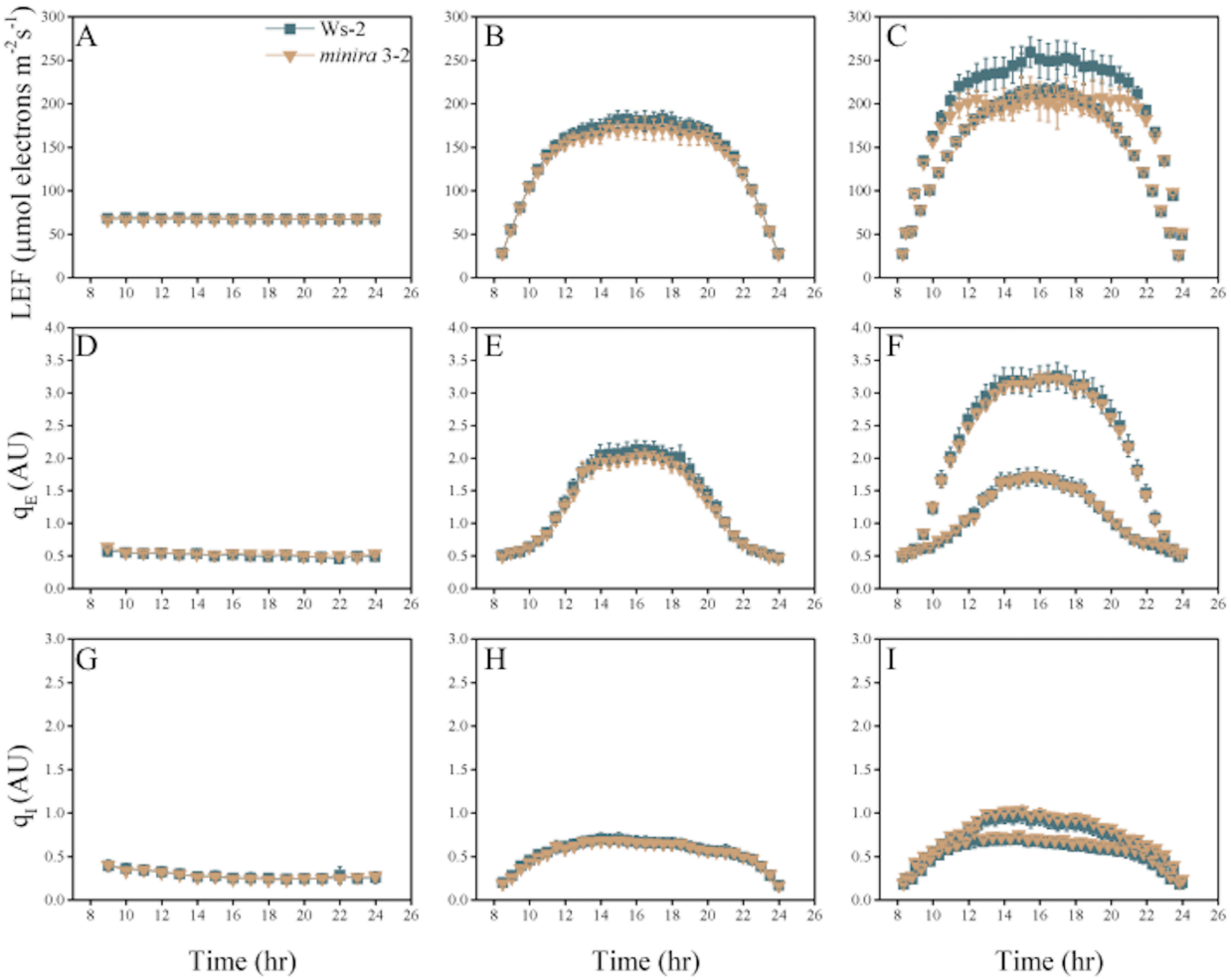

Supplemental Figure 2.11: Whole plant fluorescence imaging phenotyping of *minira* 3–2 mutant.

For details, please refer to the legend of Supplemental Figure 2.1.

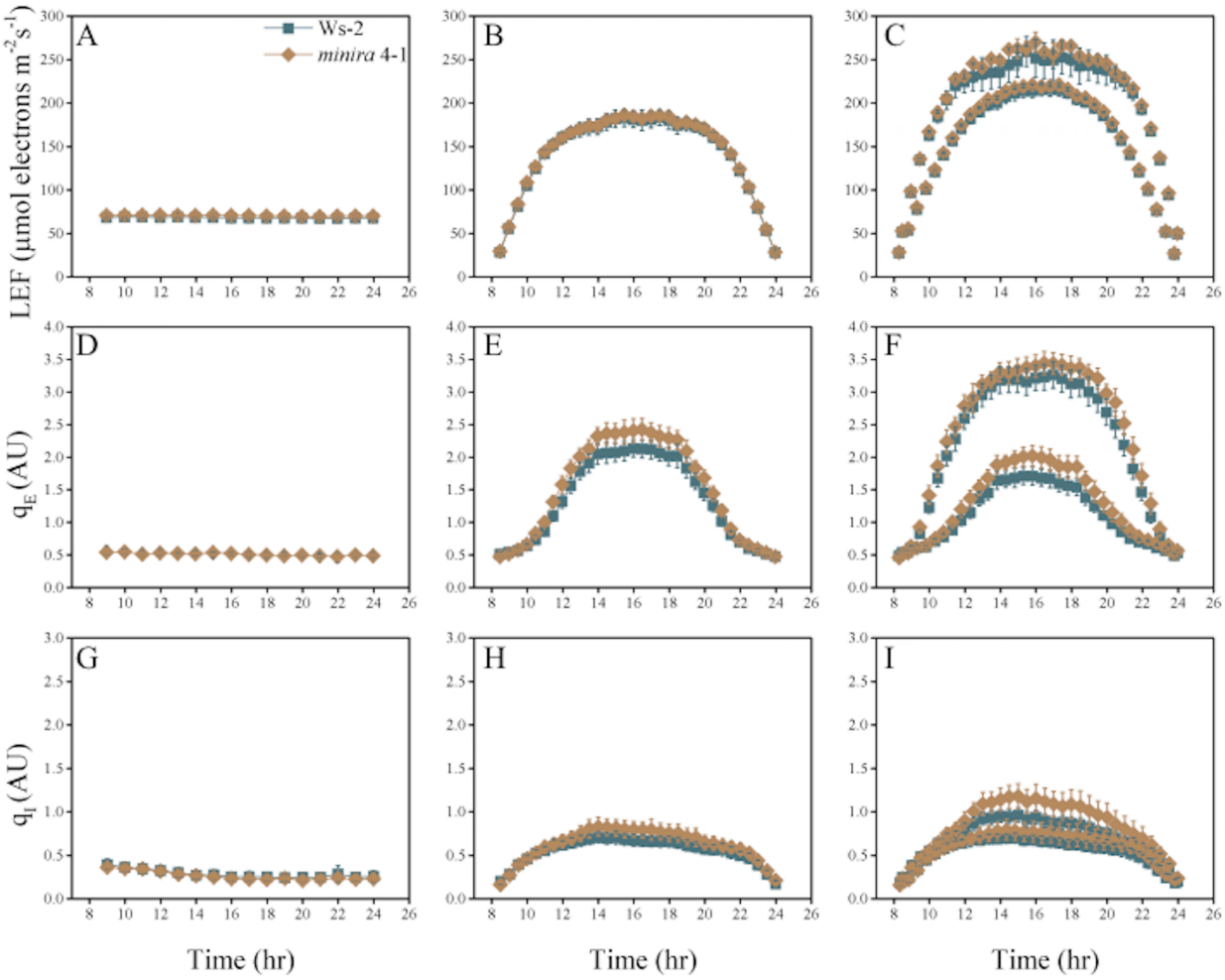

Supplemental Figure 2.12: Whole plant fluorescence imaging phenotyping of *minira* 4–1 mutant.

For details, please refer to the legend of Supplemental Figure 2.1.

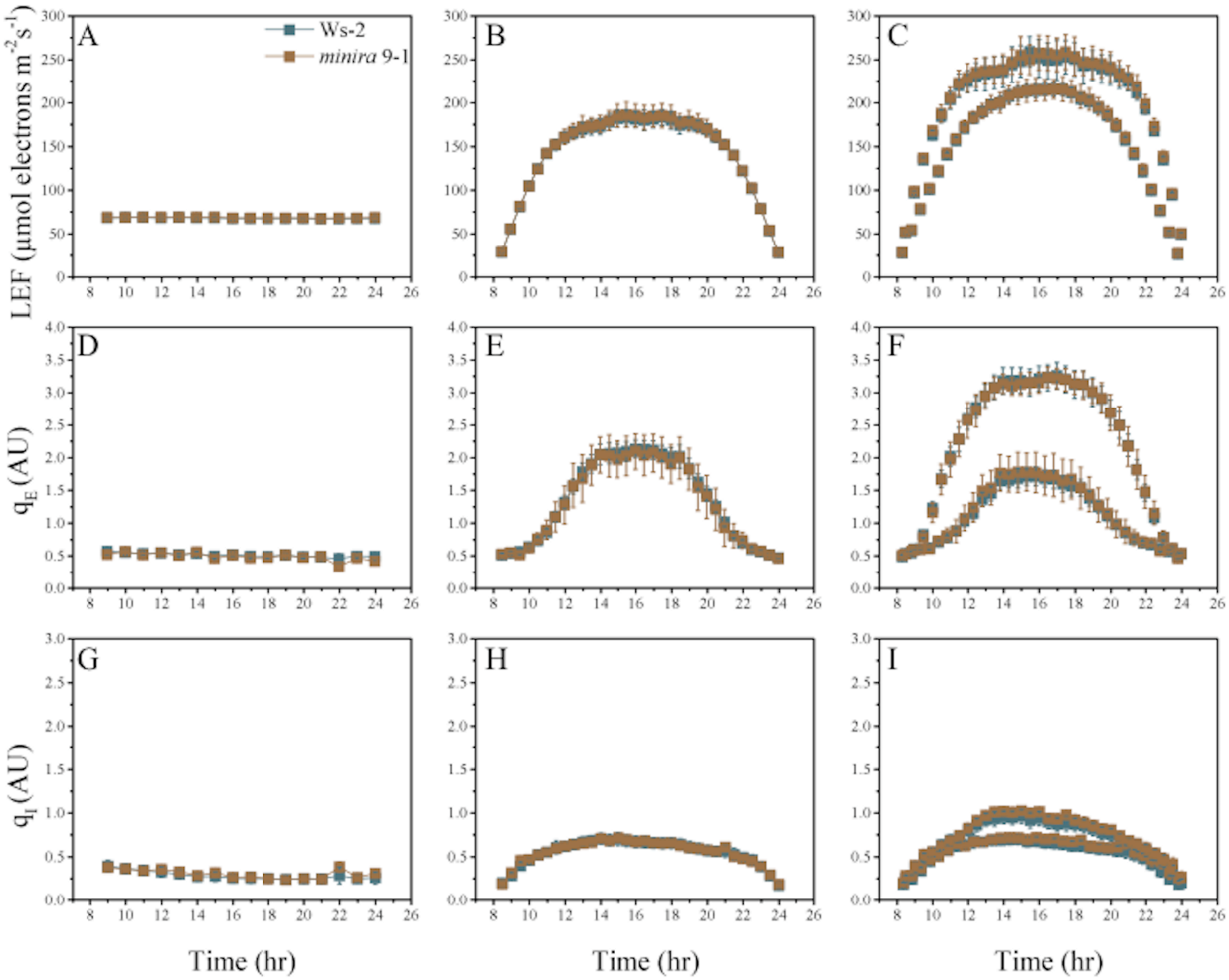

Supplemental Figure 2.13: Whole plant fluorescence imaging phenotyping of *minira* 9–1 mutant.

For details, please refer to the legend of Supplemental Figure 2.1.

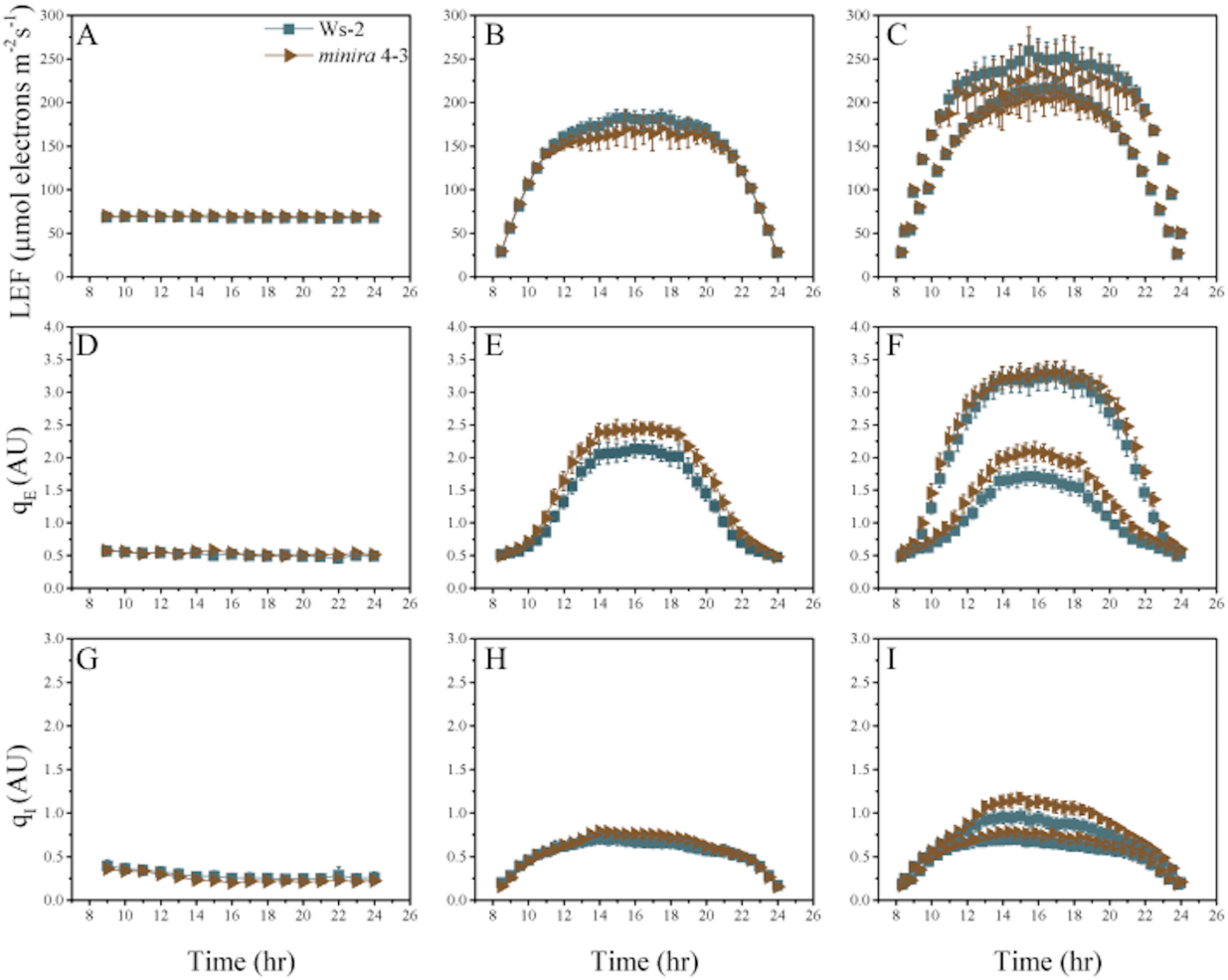

Supplemental Figure 2.14: Whole plant fluorescence imaging phenotyping of *minira* 4–3 mutant.

For details, please refer to the legend of Supplemental Figure 2.1.

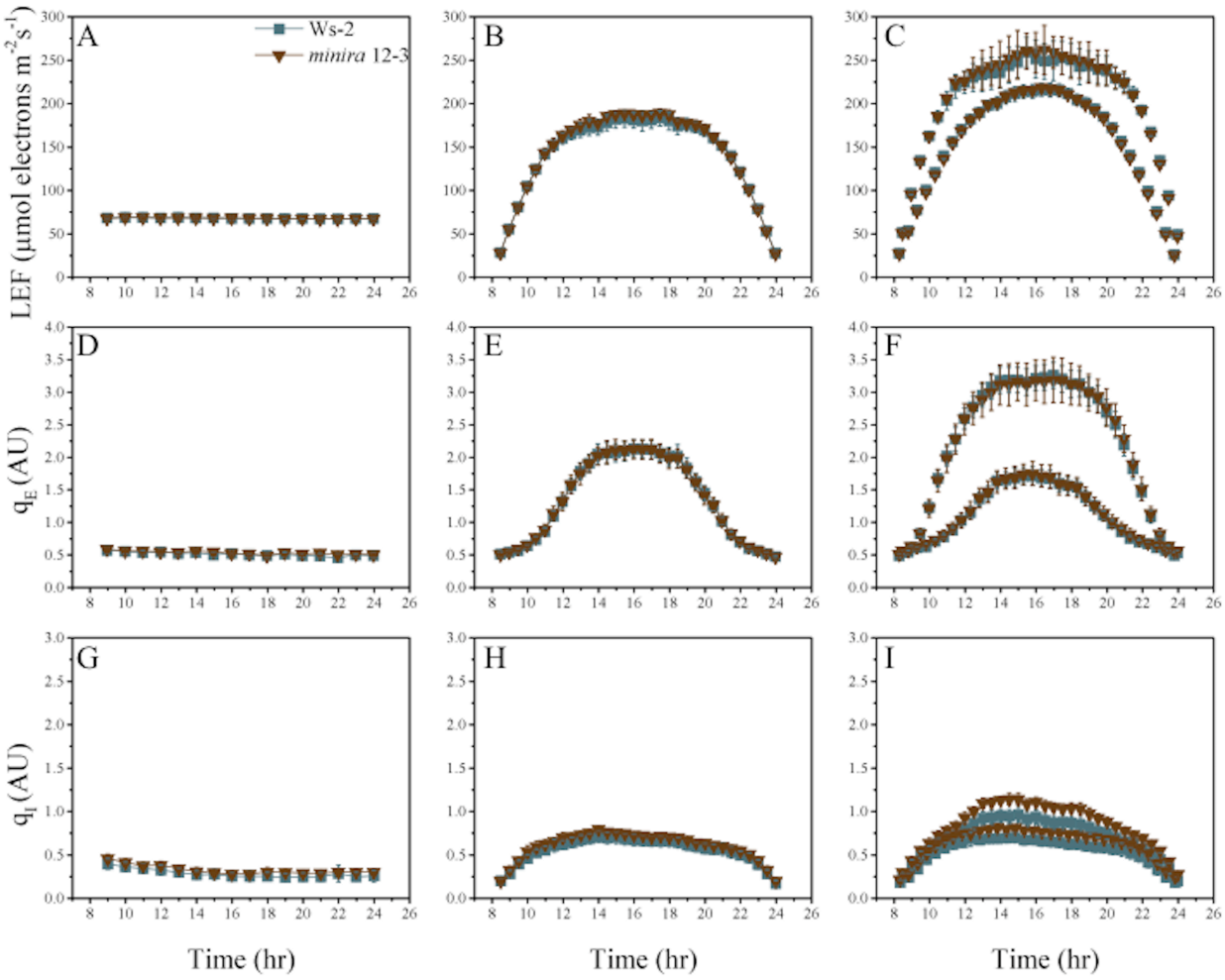

Supplemental Figure 2.15: Whole plant fluorescence imaging phenotyping of *minira* 12–3 mutant.

For details, please refer to the legend of Supplemental Figure 2.1.

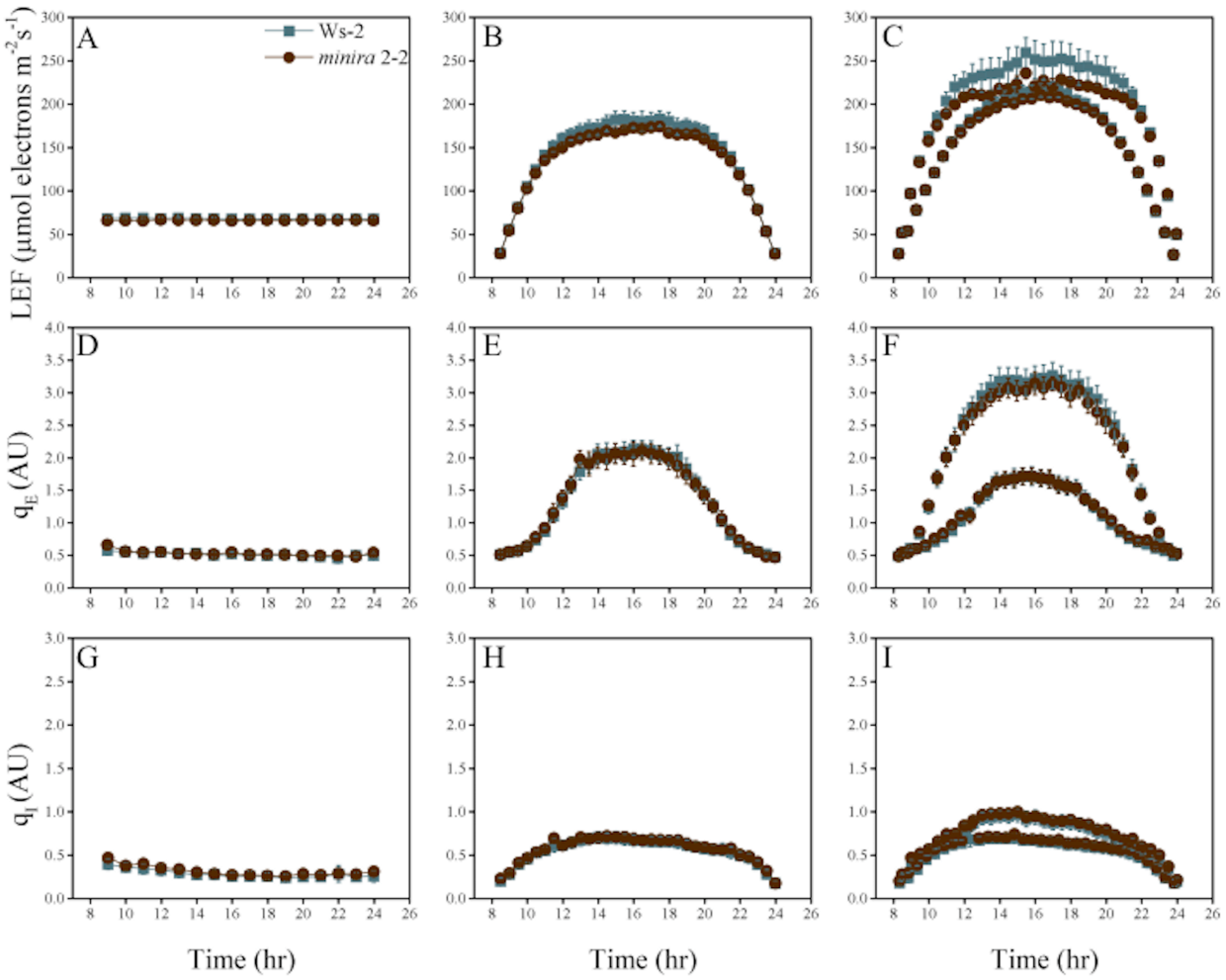

Supplemental Figure 2.16: Whole plant fluorescence imaging phenotyping of *minira* 2–2 mutant.
For details, please refer to the legend of Supplemental Figure 2.1.

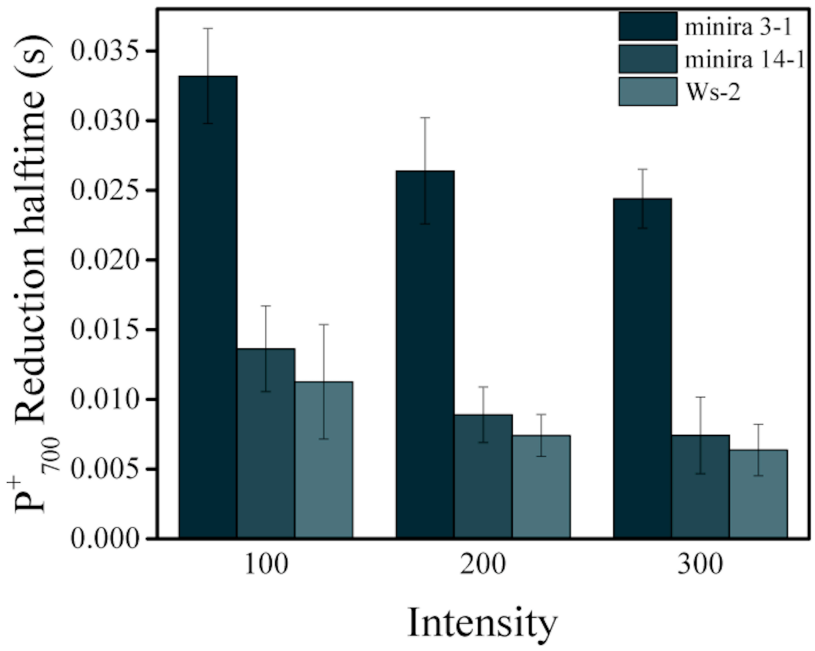

Supplemental Figure 2.17: Reduction kinetics of $P700^+$.
Light-dependent P700+ reduction half-times (mean ± s.d., n = 3) of wild type, *minira* 3–1 and *minira* 14–1 (A). Quenching of the 810 nm absorbance signal was followed during a brief dark interval and the half time of the first order decay determined at each light intensity.

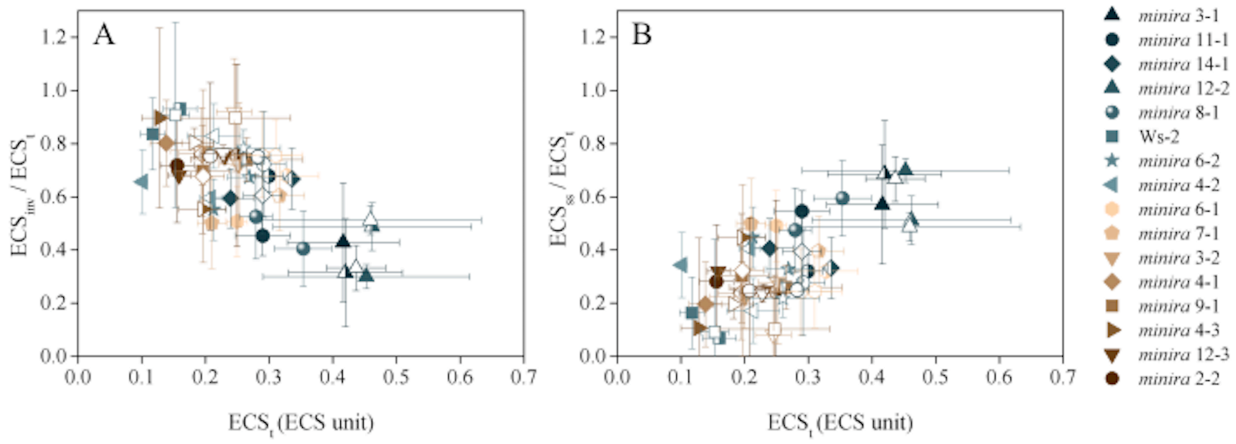

Supplemental Figure 2.18: The electric field component of the pmf dominates under high *pmf* conditions.
ECS measurements were performed to determine the partitioning of the light-driven *pmf* between ΔpH and $\Delta\psi$. Measurements were performed at 100 (solid symbols), 300 (half filled symbols), and 500 µmol photons $m^{-2}s^{-1}$ (open symbols) and the total pmf (ECS_t) as well as the composition of the *pmf* determined as in Figure 2.5. As the total *pmf* increases, the fraction of pmf stored as ECS_{inv} (proportional to ΔpH) (A) decreases linearly and is observed in all lines regardless of mutation, while the electric field (ECS_{ss}) (proportional to $\Delta\psi$) (B) increases linearly with total *pmf*, becoming a large fraction of the total *pmf* under high *pmf* conditions. Symbols represent the same plant for each light intensity (mean ± s.d., n = 3). ECS units were defined as the deconvoluted ΔA_{520} µg $chlorophyll^{-1}$ cm^2.

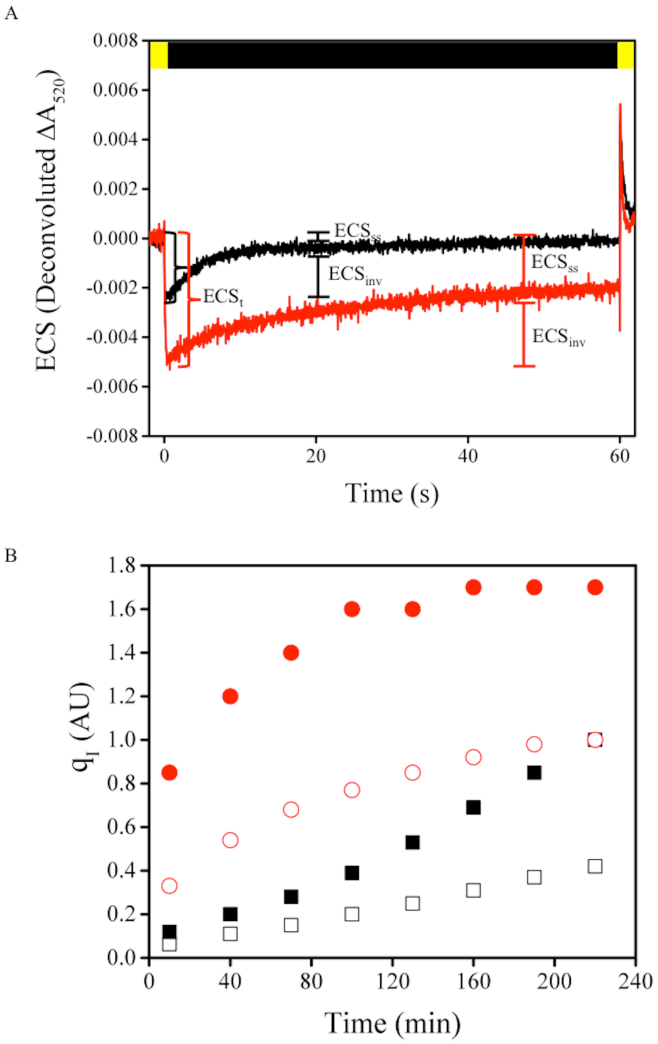

Supplemental Figure 2.19: Tobacco ATPC1 antisense knockdown increase Δ*ψ* partitioning under high *pmf* conditions.
The partitioning of the pmf in wild type Samsun (black) and ATPC1 (red) γ-subunit antisense line were determined from the deconvoluted ECS signal at ΔA_{520} nm (A). Following the light-dark transition (time 0 s), the ECS amplitude drop, which is proportional to the total *pmf*, is larger in the ATPC1 line due to the substantial knockdown of ATP synthase complexes and an inability to efflux protons from the lumen. The inversion of the ECS signal during the dark period, proportional to the ΔpH, represents a larger fraction of the *pmf* in the wild type than in ATPC1, indicating an increase in Δ*ψ* storage in the higher *pmf* ATPC1. Light conditions are represented above the traces and indicate the light (yellow) and dark (black) intervals. Leaf discs from another ATPC1 plant and Samsun were subjected to 600 µmol photons $m^{-2}s^{-1}$ light for the indicated times in the presence of water (open symbols) or lincomycin (closed symbols). Increases in q_I are more rapid in the higher *pmf* ATPC1 line when PSII repair is blocked with lincomycin.

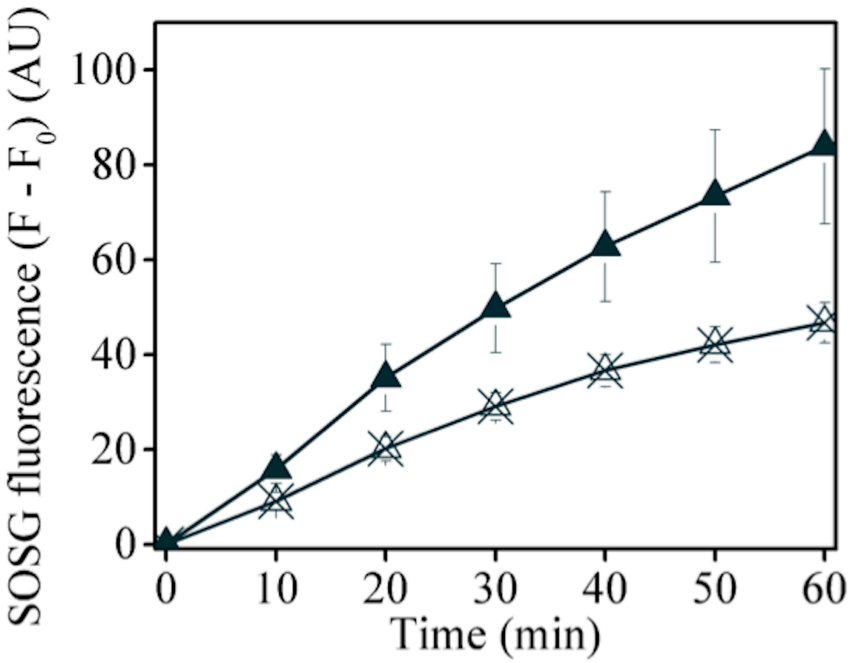

Supplemental Figure 2.20: Uncoupling Δψ decreases SOSG fluorescence in *minira* 3–1. *Minira* 3–1 leaves were vacuum infiltrated with either SOSG (solid triangles) or SOSG and 50 μM valinomycin (crossed triangles) to decrease the photosynthetic Δψ. Leaves were illuminated at a constant 100 μmol $m^{-2}s^{-1}$ intensity and SOSG fluorescence detected for 60 min.

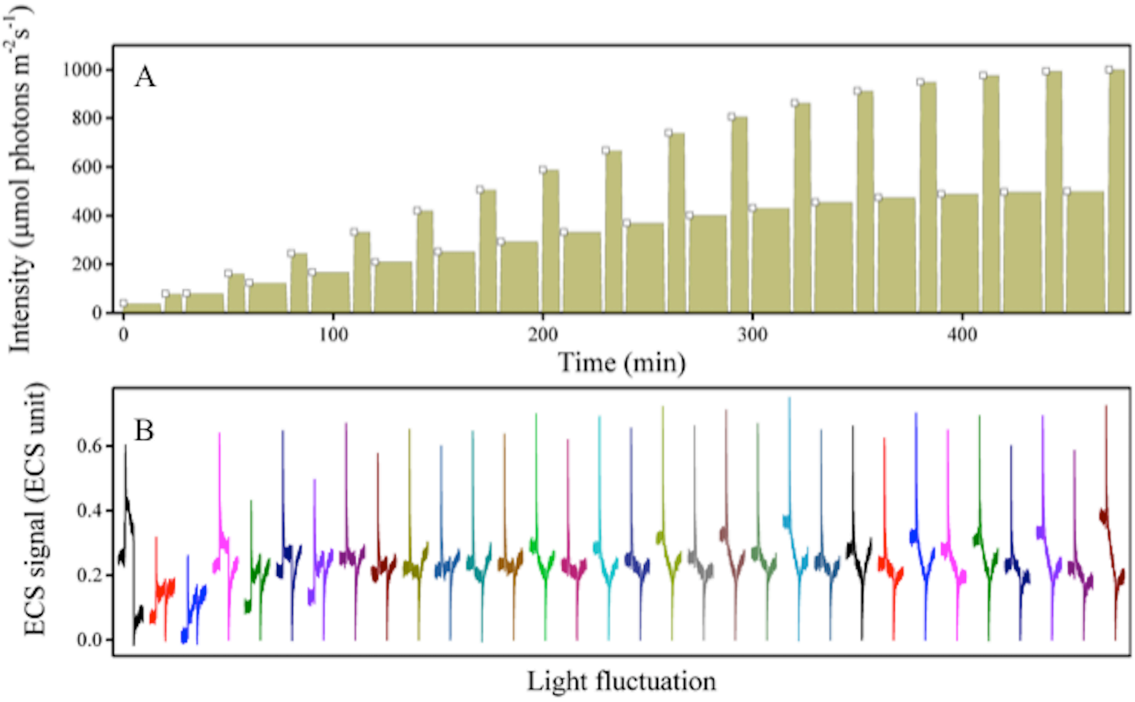

Supplemental Figure 2.21: Fluctuations in light intensity result in transient ECS spikes. Wild type plants were measured under fluctuating light (A) and the ECS measurements taken 10 s after each intensity fluctuation from lower to higher light (A, open squares). The resulting deconvoluted ΔA_{520nm} ECS signals show rapid, transient ECS 'spikes' induced by rapid $\Delta\psi$ transients before the ΔpH component can be altered (B). The upward spike represents the effect of rapidly increasing the light intensity. The downward spikes seen towards the ends of the traces reflect the transients that occur when the actinic light is switched to the lower light intensity at the end of the fluctuation. A rough estimate of the extent of the $\Delta\psi$ imposed by the spikes can be obtained by comparing the ECS signals with the calibration and results presented in Takizawa et al. (47), which estimated that the $\Delta\psi$ imposed by a saturating, single-turnover flash to thylakoids was about 40 mV. Based on this calibration value, the extent of basal *pmf* formed by equilibration with ATP (i.e. the dark *pmf* level or pmf_d) was estimated to be about 112 mV (Takizawa et al., 2007), 60 mV of which is stored in $\Delta\psi$ if the partitioning is 0.5. From the dark-interval relaxation kinetics of ECS under steady-state conditions (see Figure 2.7B and Supplemental Figure 2.17), we then expect an additional light-driven *pmf* under steady-state conditions to range from 150–200 mV, and given that the fraction of this *pmf* stored as $\Delta\psi$ ranged from 0.20–0.60, we estimate a range for steady-state light-driven $\Delta\psi$ between 30 and 120 mV. The transient spikes in $\Delta\psi$ generated during light fluctuations are likely to be essentially all stored in $\Delta\psi$ (see main text) and range in amplitude between 60–80 mV, so that the highest amplitude $\Delta\psi$ imposed during these conditions likely falls in the broad range between 150–260 mV. ECS units were defined as the deconvoluted ΔA_{520} µg chlorophyll^{-1} cm^2.

Table 2.1: Oligonucleotide sequences utilized for adapter ligation mutagenesis.

Mutation	*minira* #	Adaptor	Oligonucleotide sequences with mutated nucleotide underlined and in bold
I201V	*minira* 4	DMP 27	5′ GATCTGTGAC**G**TTAATGGAACCTGTGTGGATGCTG CGGAAGATGAGTTTTTCAGGTT 3′
		DMP 28	5′ AACCTGAAAAACTCATCTTCCGCAGCATCCACACA GGTTCCATTAA**C**GTCACA 3′
N202K	*minira* 5	DMP 29	5′ GATCTGTGACATTAA**A**GGAACCTGTGTGGATGCTG CGGAAGATGAGTTTTTCAGGTT 3′
		DMP 30	5′ AACCTGAAAAACTCATCTTCCGCAGCATCCACACA GGTTCC**T**TTAATGTCACA 3′
A209I	*minira* 6	DMP 31	5′ GATCTGTGACATTAATGGAACCTGTGTGGATGCT**A** **TC**GAAGATGAGTTTTTCAGGTT 3′
		DMP 32	5′ AACCTGAAAAACTCATCTTC**GAT**AGCATCCACACA GGTTCCATTAATGTCACA 3′
F213M	*minira* 7	DMP 33	5′ GATCTGTGACATTAATGGAACCTGTGTGGATGCTG CGGAAGATGAG**A**T**G**TTCAGGTT 3′
		DMP 34	5′ AACCTGAA**C**A**T**CTCATCTTCCGCAGCATCCACACA GGTTCCATTAATGTCACA 3′

Table 2.2: Oligonucleotide sequences utilized for adapter ligation mutagenesis to introduce secondary mutations.

Mutation	*minira* #	Adaptor	Oligonucleotide sequences with mutated nucleotide underlined and in bold
P194M	*minira* 2	DMP 23	5′ GTACACAAAGTTTGTCTCTTTGGTCAAATCAGA ACCCGTGATCCACACGCTACTGCCTTTATCA**AT G**AAAGGAGA 3′
		DMP 24	5′ GATCTCTCCTTT**CAT**TGATAAAGGCAGTAGCGT GTGGATCACGGGTTCTGATTTGACCAAAGAGAC AAACTTTGT 3′
E183D	*minira* 1	DMP 21	5′ GTACACAAAGTTTGTCTCTTTGGTCAAATCAGA **T**CCCGTGATCCACACGCTACTGCCTTTATCACC TAAAGGAGA 3′
		DMP 22	5′ GATCTCTCCTTTAGGTGATAAAGGCAGTAGCGT GTGGATCACGGG**A**TCTGATTTGACCAAAGAGAC AAACTTTGT 3′

Table 2.3: Oligonucleotide sequences utilized for splicing by overlap extension PCR.

Mutation	*minira* #	Region	Primer	Primer sequence
T218S	*minira* 8	Fragment 1	DMP49	5′ AACTGTCAATTTCCCTTCTTTACTCGTTAACCT 3′
			DMP 45	5′ TCCTGCAGCCCGGGAACAAAAAAAT 3′
		Fragment 2	DMP 50	5′ TGAGTTTTTCAGGTTAACGAGTAAAGAAGGG 3′
			DMP 46	5′ GCGGCCGCTCTAGACAAATCAAAC 3′
E220D	*minira* 9	Fragment 1	DMP51	5′ AACTGTCAATTTCCCGTCTTTTGTCGTTAAC 3′
			DMP 45	5′ TCCTGCAGCCCGGGAACAAAAAAAT 3′
		Fragment 2	DMP 52	5′ CAGGTTAACGACAAAAGACGGGAAATT 3′
			DMP 46	5′ GCGGCCGCTCTAGACAAATCAAAC 3′
T224A	*minira* 10	Fragment 1	DMP53	5′ GTCTCTCTTTCAACTGCCAATTTCCC 3′
			DMP 45	5′ TCCTGCAGCCCGGGAACAAAAAAAT 3′
		Fragment 2	DMP 54	5′ CGACAAAAGAAGGGAAATTGGCAGTTGA 3′
			DMP 46	5′ GCGGCCGCTCTAGACAAATCAAAC 3′
E228T	*minira* 11	Fragment 1	DMP55	5′ TGTTGGTGTCCTAAAAGTCGTTCTTTCAACTGT 3′
			DMP 45	5′ TCCTGCAGCCCGGGAACAAAAAAAT 3′
		Fragment 2	DMP 56	5′ GAAATTGACAGTTGAAAGAACGACTTTTAGGA 3′
			DMP 46	5′ GCGGCCGCTCTAGACAAATCAAAC 3′
I201V-N202K	*minira* 12	Fragment 1	DMP57	5′ CACACAGGTTCCTTTCACGTCACAGATCTC 3′
			DMP 45	5′ TCCTGCAGCCCGGGAACAAAAAAAT 3′
		Fragment 2	DMP 58	5′ GAGATCTGTGACGTGAAAGGAACCTGTGTG 3′
			DMP46	5′ GCGGCCGCTCTAGACAAATCAAAC 3′

Table 2.4: Synthetic gene constructs incorporating multiple ATPC2 mutations into ATPC1.

Domain	*minira* #	Synthetic gene fragment sequence with the new domain in bold. Restriction enzyme sites are underlined.
194-241	*minira* 16	aattaaTGTACACAAAGTTTGTCTCTTTGGTCAAATCAGAACCCGTG ATCCACACGCTACTGCCTTTA**TCGATGAAAGGAGAGTCTTGTGATGT** **GAAAGGTGAGTGTGTTGATGCTATCGAGGATGAGATGTTTAGGCTAA** **CGAGCAAAGATGGGAAGTTAGCTGTGGAAAGGACCAAGCTTGAAGTT** **GAGAAGCCTGAGATCTCACCGTTGATG**CAATTCGAGCAAGACCCTGT TCAGATTCTTGATGCTTTGTTGCCTCTGTATCTTAACAGTCAGATTC TTAGGGCATTACAGGAGTCATTGGCTAGTGAGCTTGCAGCTAGAATG AGTGCAATGAGTAGTGCTTCGGATAATGCATCGGATCTCAAGAAATC GCTTTCGATGGTGTATAATAGAAAGCGTCAAGCTAAGATTACTGGAG AGATTCTTGAGATTGTTGCTGGAGCTAATGCACAGGTTTGATTTGTC TAGAttaatt
213-228	*minira* 14	aattaaTGTACACAAAGTTTGTCTCTTTGGTCAAATCAGAACCCGTG ATCCACACGCTACTGCCTTTATCACCTAAAGGAGAGATCTGTGACAT TAATGGAACCTGTGTGGATGCTGCGGAAGATGAG**ATGTTTAGGCTAA** **CGAGCAAAGATGGGAAGTTAGCTGTGGAAAGGACC**ACTTTTAGGACA CCAACAGCTGATTTCTCGCCGATCTTGCAATTCGAGCAAGACCCTGT TCAGATTCTTGATGCTTTGTTGCCTCTGTATCTTAACAGTCAGATTC TTAGGGCATTACAGGAGTCATTGGCTAGTGAGCTTGCAGCTAGAATG AGTGCAATGAGTAGTGCTTCGGATAATGCATCGGATCTCAAGAAATC GCTTTCGATGGTGTATAATAGAAAGCGTCAAGCTAAGATTACTGGAG AGATTCTTGAGATTGTTGCTGGAGCTAATGCACAGGTTTGATTTGTC TAGAttaatt
I198S	*minira* 3	aattaaTGTACACAAAGTTTGTCTCTTTGGTCAAATCAGAACCCGTG ATCCACACGCTACTGCCTTTATCACCTAAAGGAGAGA**G**CTGTGACAT TAATGGAACCTGTGTGGATGCTGCGGAAGATGAGTTTTTCAGGTTAA CGACAAAAGAAGGGAAATTGACAGTTGAAAGAGAGACTTTTAGGACA CCAACAGCTGATTTCTCGCCGATCTTGCAATTCGAGCAAGACCCTGT TCAGATTCTTGATGCTTTGTTGCCTCTGTATCTTAACAGTCAGATTC TTAGGGCATTACAGGAGTCATTGGCTAGTGAGCTTGCAGCTAGAATG AGTGCAATGAGTAGTGCTTCGGATAATGCATCGGATCTCAAGAAATC GCTTTCGATGGTGTATAATAGAAAGCGTCAAGCTAAGATTACTGGAG AGATTCTTGAGATTGTTGCTGGAGCTAATGCACAGGTTTGATTTGTC TAGAttaatt

Table 2.5: Timing and light profile of imaging day 1.

Light Intensity Day 1	Duration at Intensity (min)	Time of Day
0	359.4	6:00
100	58	6:58
0	2	6:00
100	58	7:58
0	2	7:00
100	58	8:58
0	2	8:00
100	58	9:58
0	2	9:00
100	58	10:58
0	2	10:00
100	58	11:58
0	2	11:00
100	58	12:58
0	2	12:00
100	58	13:58
0	2	13:00
100	58	14:58
0	2	14:00
100	58	15:58
0	2	15:00
100	58	16:58
0	2	16:00
100	58	17:58
0	2	17:00
100	58	18:58
0	2	18:00
100	58	19:58
0	2	19:00
100	58	20:58
0	2	20:00
100	58	21:58
0	2	22:00

Table 2.6: Timing and light profile of imaging day 2.

Light Intensity Day 2	Duration at Intensity (min)	Time of Day
0	359.4	6:00
39	28	6:28
0	2	6:30
80	28	6:58
0	2	7:00
123	28	7:28
0	2	7:30
167	28	7:58
0	2	8:00
210	28	8:28
0	2	8:30
253	28	8:58
0	2	9:00
294	28	9:28
0	2	9:30
333	28	9:58
0	2	10:00
370	28	10:28
0	2	10:30
402	28	10:58
0	2	11:00
431	28	11:28
0	2	11:30
455	28	11:58
0	2	12:00
475	28	12:28
0	2	12:30
489	28	12:58
0	2	13:00
497	28	13:28
0	2	13:30
500	28	13:58
0	2	14:00
500	28	14:28
0	2	14:30
497	28	14:58
0	2	15:00
489	28	15:28

Table 2.6 (*continued*):

0	2	15:30
0	2	15:30
475	28	15:58
0	2	16:00
455	28	16:28
0	2	16:30
431	28	16:58
0	2	17:00
402	28	17:28
0	2	17:30
370	28	17:58
0	2	18:00
333	28	18:28
0	2	18:30
294	28	18:58
0	2	19:00
253	28	19:28
0	2	19:30
210	28	19:58
0	2	20:00
167	28	20:28
0	2	20:30
123	28	20:58
0	2	21:00
80	28	21:28
0	2	21:30
39	28	21:58
0	2	22:00

Table 2.7: Timing and light profile of imaging day 3.

Light Intensity Day 3	Duration at Intensity (min)	Time of Day
0	359.4	6:00
39	18	6:18
0	2	6:20
78	8	6:28
0	2	6:30
80	18	6:48
0	2	6:50
161	8	6:58
0	2	7:00
123	18	7:18
0	2	7:20
246	8	7:28
0	2	7:30
167	18	7:48
0	2	7:50
333	8	7:58
0	2	8:00
210	18	8:18
0	2	8:20
420	8	8:28
0	2	8:30
253	18	8:48
0	2	8:50
506	8	8:58
0	2	9:00
294	18	9:18
0	2	9:20
588	8	9:28
0	2	9:30
333	18	9:48
0	2	9:50
667	8	9:58
0	2	10:00
370	18	10:18
0	2	10:20
739	8	10:28
0	2	10:30
402	18	10:48

Table 2.7 (*continued*):

0	2	10:50
805	8	10:58
0	2	11:00
431	18	11:18
0	2	11:20
862	8	11:28
0	2	11:30
455	18	11:48
0	2	11:50
911	8	11:58
0	2	12:00
475	18	12:18
0	2	12:20
949	8	12:28
0	2	12:30
489	18	12:48
0	2	12:50
977	8	12:58
0	2	13:00
497	18	13:18
0	2	13:20
994	8	13:28
0	2	13:30
500	18	13:48
0	2	13:50
1000	8	13:58
0	2	14:00
500	18	14:18
0	2	14:20
1000	8	14:28
0	2	14:30
497	18	14:48
0	2	14:50
994	8	14:58
0	2	15:00
489	18	15:18
0	2	15:20
977	8	15:28
0	2	15:30
475	18	15:48

Table 2.7 (*continued*):

0	2	15:50
949	8	15:58
0	2	16:00
455	18	16:18
0	2	16:20
911	8	16:28
0	2	16:30
431	18	16:48
0	2	16:50
862	8	16:58
0	2	17:00
402	18	17:18
0	2	17:20
805	8	17:28
0	2	17:30
370	18	17:48
0	2	17:50
739	8	17:58
0	2	18:00
333	18	18:18
0	2	18:20
667	8	18:28
0	2	18:30
294	18	18:48
0	2	18:50
588	8	18:58
0	2	19:00
253	18	19:18
0	2	19:20
506	8	19:28
0	2	19:30
210	18	19:48
0	2	19:50
420	8	19:58
0	2	20:00
167	18	20:18
0	2	20:20
333	8	20:28
0	2	20:30
123	18	20:48

Table 2.7 (*continued*):

0	2	20:50
246	8	20:58
0	2	21:00
80	18	21:18
0	2	21:20
161	8	21:28
0	2	21:30
39	18	21:48
0	2	21:50
78	8	21:58
0	2	22:00

Table 2.8: Chlorophyll content of wild type (Ws-2) and *minira* leaves.

Genotype	Chlorophyll (μg cm^{-2})
Ws-2	16.55 ± 0.51
minira 2-2	13.00 ± 0.17*
minira 3-1	8.24 ± 1.62*
minira 3-2	13.04 ± 1.45
minira 4-1	14.55 ± 1.18
minira 4-2	14.05 ± 1.34
minira 4-3	14.99 ± 0.78
minira 6-1	13.64 ± 0.78*
minira 6-2	13.74 ± 0.85*
minira 7-1	13.48 ± 0.25*
minira 8-1	10.51 ± 1.53*
minira 9-1	12.53 ± 2.85
minira 11-1	11.98 ± 1.52*
minira 12-2	8.46 ± 2.28*
minira 12-3	12.28 ± 0.94*
minira 14-1	13.87 ± 1.65

Chapter 3

Hacking the thylakoid proton motive force for improved photosynthesis: modulating ion flux rates that control proton motive force partitioning into $\Delta\psi$ and ΔpH[2]

Geoffry A. Davis, A. William Rutherford, David M. Kramer

[2] This chapter was published as:
Davis, GA, Rutherford, AW, & Kramer, DM. 2017 Hacking the thylakoid proton motive force for improved photosynthesis: modulating ion flux rates that control proton motive force partitioning into $\Delta\psi$ and ΔpH. Philos Trans R Soc Lond B Biol Sci, 372(1730). doi: 10.1098/rstb.2016.0381

3.1 Abstract

There is considerable interest in improving plant productivity by altering the dynamic responses of photosynthesis in tune with natural conditions. This is exemplified by the 'energy-dependent' form of non-photochemical quenching (q_E), the formation and decay of which can be considerably slower than natural light fluctuations, limiting photochemical yield. In addition, we recently reported that rapidly fluctuating light can produce field recombination-induced photodamage (FRIP), where large spikes in electric field across the thylakoid membrane ($\Delta\psi$) induce photosystem II recombination reactions that produce damaging singlet oxygen ($^1O_2$). Both q_E and FRIP are directly linked to the thylakoid proton motive force (*pmf*), and in particular, the slow kinetics of partitioning *pmf* into its ΔpH and $\Delta\psi$ components. Using a series of computational simulations, we explored the possibility of 'hacking' *pmf* partitioning as a target for improving photosynthesis. Under a range of illumination conditions, increasing the rate of counter-ion fluxes across the thylakoid membrane should lead to more rapid dissipation of $\Delta\psi$ and formation of ΔpH. This would result in increased rates for the formation and decay of q_E while resulting in a more rapid decline in the amplitudes of $\Delta\psi$-spikes and decreasing $^1O_2$ production. These results suggest that ion fluxes may be a viable target for plant breeding or engineering. However, these changes also induce transient, but substantial mismatches in the ATP:NADPH output ratio as well as in the osmotic balance between the lumen and stroma, either of which may explain why evolution has not already accelerated thylakoid ion fluxes. Overall, though the model is simplified, it recapitulates many of the responses seen *in vivo*, while spotlighting critical aspects of the complex interactions between *pmf* components and photosynthetic processes. By making the programme available, we hope to enable the community of photosynthesis researchers to further explore and test specific hypotheses.

3.2 Introduction

This opinion/hypothesis paper was inspired by the recent Royal Society symposium on 'Enhancing photosynthesis in crop plants: targets for improvement' (http://www.rsc.org/events/download/Document/cee7d4f2-9ff1-477b-b155-3e2492577d77) that brought together experts in a range of photosynthetic processes. A prominent theme of several of the presentations was the sensitivity of photosynthesis to rapid, rather than gradual, changes in environmental conditions. Of particular interest was the kinetic mismatch between fluctuations in photosynthetically active radiation (PAR), which can change by orders of magnitude within a second, and the relatively slow onset of photoprotective mechanisms (123, 124). Indeed, there is growing evidence that this mismatch can sensitize both photosystem I (PSI) and photosystem II (PSII) to oxidative photodamage (36, 97). The focus of the present paper is the irreversible damage to PSII (to D1 and other subunits) due to singlet oxygen ($^1O_2$) generated by PSII charge recombination. It has also been proposed that the slow reversal of photoprotection mechanisms can lead to loss of photochemical productivity when light levels are suddenly decreased (125, 126). Thus, such kinetic mismatches appear to be good engineering targets for increasing the efficiency and resilience of photosynthesis. Here, we present an extended re-examination of one of the key processes that controls and regulates photosynthesis, the thylakoid proton motive force (*pmf*), its components, and some emerging effects on photosynthetic reaction centres.

The energy-storing processes of photosynthesis start with the capture of PAR by photoactive pigments, transfer of the energy to specialized chlorophyll molecules in PSI and PSII, inducing the transfer of electrons through a series of redox intermediates to ultimately generate NADPH from $NADP^+$ (127). The electron transfer steps are tightly coupled to proton transfer reactions into the thylakoid lumen, storing potential energy in the *pmf* to drive the

synthesis of ATP (61, 76). Both NADPH and ATP, in the correct ratios, are required for driving the assimilation of CO_2 and other cellular processes (121). The electron and proton transfer processes can be highly efficient, but when energy capture outpaces the capacity of photosynthesis—a situation that can occur at high light and/or under adverse environmental conditions—reactive intermediates can accumulate in the photosynthetic apparatus, leading to generation of reactive oxygen species (ROS), mainly $O_2^{-\bullet}$ in PSI and mainly $^1O_2$ in PSII, and these are responsible for oxidative photodamage. A range of photoprotective mechanisms have evolved to ameliorate photodamage and its effects, including non-photochemical quenching (NPQ) processes such as the q_E response (6), a complex cycle to repair damaged PSII (128), chloroplast movements (129), cyclic electron flow (130, 131), redox tuning to redirect back-reactions to non-ROS producing pathways (56, 132) and alternative electron acceptor systems (5, 133). Despite the diversity and complexity of these processes, in general, they result in the loss of light energy, for example, the decreased efficiency of light capture incurred by activation of NPQ (134), charge recombination (56) or the dissipation of redox energy when electrons are passed to the flavodiiron O_2 reductases (123). Consequently, photosynthetic organisms appear to be constantly balancing the trade-offs between efficient photochemistry and the avoidance of toxic side reactions.

In higher plants and green algae, the *pmf* plays a central role in regulating key photoprotective mechanisms, by responding to changes in both energy input and the physiological status of the chloroplast (61). It is, therefore, worthwhile to review the biophysical properties of the photosynthetic machinery that controls the partitioning of *pmf* into $\Delta\psi$ and ΔpH over different time-scales. In thermodynamic terms, the *pmf* can be described as the sum of two driving forces:

$$pmf = \Delta\psi + \frac{2.3RT}{F}\Delta pH \quad \text{(Eq. 1)}$$

where $\Delta\psi$ and ΔpH represent the differences in electric field, expression difference in volts, and pH, respectively, between the lumenal and stromal faces of the thylakoid membrane, R is the universal gas constant and F is Faraday's constant. Over a broad range of physiological conditions, $\Delta\psi$ and ΔpH appear to be thermodynamically and kinetically equivalent drivers of the ATP synthase (3, 4). On the other hand, storing *pmf* in $\Delta\psi$ and ΔpH has distinct impacts on cellular processes. Most notably, storing energy in ΔpH imposes a substantial change in pH in one or more cellular compartments. In mitochondria, *pmf* is held mainly as $\Delta\psi$, allowing enzymes to operate at optimal pH ranges. In chloroplasts, the build-up of ΔpH results in acidification of the thylakoid lumen, which acts to feedback regulate (or control) critical steps in the light reactions (reviewed in 5), including (i) the activation of the photoprotective q_E response (through activation of violaxanthin deepoxidase and protonation of PsbS (6)); and (ii) 'photosynthetic control' of electron flow at the cytochrome b_6f complex (reviewed in 13), preventing the accumulation of electrons on PSI that would otherwise lead to severe PSI photodamage (5, 47, 123, 124). There have also been proposals that PSII can be regulated or inhibited (13, 15) at low lumen pH, for example, by acid-induced release of Ca^{2+} from the oxygen-evolving complex (OEC), or by limiting electron flow by slowing of the OEC S-state transitions (15, 63).

Early work on isolated thylakoids suggested that *pmf* was stored mainly as ΔpH, but more recent work suggests that a pure ΔpH *pmf* is incompatible with the known pH dependencies of photosynthetic processes (13, 39). A range of *in vivo* studies (5, 36, 47, 70, 135-138) support the view that the *pmf* is actively partitioned into $\Delta\psi$ and ΔpH components to avoid severe

restrictions on b_6f activity or acid-induced damage to lumenal components, while balancing the needs for efficient energy storage and activation of lumen pH-responsive photoprotective processes (39). These arguments are supported by our simulations (below) and straightforward thermodynamic considerations, which indicate that: with ΔG_{ATP} (the free energy of hydrolysis of ATP) between 40 and 45 kJ mol^{-1}, a stromal pH of 7.8, and the coupling stoichiometry for protons/ATP, n, of 4.67, the maximal lumen pH (even before illumination) should range between 6 and 6.5 units, near or below the pK_a values that govern the activation of q_E and the control of cytochrome b_6f activity. In short, with 100% ΔpH, the photosynthetic electron transport chain should be strongly downregulated even at low light. Nevertheless, there are opposing views that maintain *pmf* is stored almost exclusively in ΔpH under steady-state conditions (139). It is worthwhile to note, however, that the phenomena discussed in this review are associated more with the dynamics of $\Delta\psi$ and ΔpH rather than their steady-state values.

In any case, the balancing of $\Delta\psi/\Delta$pH, and its kinetics, are dependent on the regulation of counter-ion homeostasis in the chloroplast (2), and recent work from several laboratories has identified putative components of these ion homeostatic machineries, including a thylakoid potassium channel (27), a K^+/H^+ antiporter (28), as well as transporters for other charged species (29-32, 140). There are also indications that the $\Delta\psi/\Delta$pH balance is controlled by the synthesis of membrane-permeable weak bases, such as putrescene, that effectively increase the proton buffering capacity of the lumen (54).

3.3 Interactions of the *pmf* with PSII: Importance for energy storage and photodamage.

The photosystems can be viewed as ‘energy traps' that capture energy from sunlight in the form of quasi-stable charge-separated states. To achieve this role, evolution has tuned the redox properties of reaction centre cofactors so that each progressive electron transfer reaction

occurs more rapidly than the decay by other routes (e.g. back-reactions or charge recombination), successively stabilizing the resulting charge-separated states and minimizing the losses to back-reactions or recombination to the point where quantum efficiency is near unity but at the cost of free energy losses at each step (56). Despite the high quantum yield of formation of stable charge-separated states, electron transfer back-reactions and charge recombination can occur, the rates of which depend on the energetics of the free energy gap, reorganizational energies and donor–acceptor distances between the oxidized and reduced components in the reaction centres (56, 141, 142). For PSII, the most important recombination reaction (both in terms of rates and consequences for photodamage) occurs from the $P_{680}^{+}Pheo^{-}$ radical pair state (with P_{680} oxidized and pheophytin reduced), which can be formed via both initial forward electron transfer, or by back-reactions via thermal activation of 'stable' intermediates in the PSII photocycle, e.g. $S_2Q_B^{-}$, the state formed when dark-adapted PSII undergoes a single photochemical reaction. Further thermal activation of $P_{680}^{+}Pheo^{-}$ can repopulate the P^{*} state, leading to essentially the full reversal of the initial light reactions, resulting in the emission of 'delayed fluorescence' (143), though owing to the high energy of activation this process has a low quantum efficiency (143). The intensity and temperature dependence of delayed fluorescence have been extensively used to estimate the energetics of reaction centres, and are potentially important probes for the more deleterious processes discussed below. More importantly for this discussion, the $P^{+}_{680}Pheo^{-}$ state can also decay non-radiatively, either directly to ground state, or via the triplet state of P_{680} ($^{3}P_{680}$) (144). In turn, $^{3}P_{680}$ can interact with molecular O_2 to form singlet O_2 ($^{1}O_2$), a highly ROS that can damage both PSII and other cellular components (93).

The rates and yield of back-reactions leading to $P_{680}^{+}Pheo^{-}$ recombination should be accelerated under any conditions that make the energy gaps between $P_{680}^{+}Pheo^{-}$ and the

subsequent radical pairs (e.g. $P_{680}^{+}Q_A^{-}$) shallower. For example, it is well known that when plants are treated with herbicides that are Q_B site inhibitors, such as 3-(3,4-dichlorophenyl)-1,1-dimethylurea (DCMU) or atrazine, which block electron transfer from Q_A^{-} to Q_B, the recombination reactions speed up by about 10- to 20-fold (99, 145), and the enhanced formation of $^1O_2$ triggers processes that can damage the cell. Our recent work describes a more physiological process that we term field recombination-induced photodamage (FRIP) in which large spikes in the photosynthetic $\Delta\psi$, such as those caused by rapid fluctuations in light intensity, destabilize the PSII photochemically generated charge pairs, accelerating PSII back-reactions, charge recombination and $^1O_2$ production (36). Our results suggest that FRIP represents both a limitation for energy storage as well as a limitation to productivity from losses due to photodamage, especially under rapidly fluctuating conditions found in nature.

3.4 Computational exploration of the effects of altering *pmf* storage kinetics on q_E and field recombination–induced photodamage.

NPQ and FRIP should both be sensitive to kinetic mismatches between the generation of $\Delta\psi$ and ΔpH and subsequent regulatory responses, and it is conceivable that engineering these processes could lead to improved photosynthesis. To test this possibility, we updated a previously published computational model for *pmf* (2, 146) that describes how the intrinsic biophysical properties of the thylakoid system impact the extent and kinetics of *pmf* storage in $\Delta\psi$ and ΔpH, and how these properties may affect the susceptibility of photosynthesis to photodamage under rapidly fluctuating conditions. While simplified, our model recapitulates many key features of the *pmf*. The biophysical bases of the current model are similar to those presented in other models (147), and thus using our parameters, one would expect similar results. The updated model includes the effects of $\Delta\psi$, ΔpH and Q_A redox state on FRIP. The code was

written in Python 3.5 using open source modules and is presented in the form of a detailed Jupyter (www.jupyter.org) notebook, which is included in the Appendix and freely available online at Github (www.github.com/protonzilla/Delta_Psi_Py), allowing the reader to download, modify, extend and explore variations of the simulations presented here. The details of the code and references to the parameter set are presented in the extensive annotation in the code and accompanying explanatory notes in the Appendix and on the Github site.

3.5 The effects of ΔpH and Δψ on PSII recombination and $^1O_2$ production *in vivo*.

As illustrated in figure 3.1a, the cofactors in PSII are situated such that charge separation reactions occur across the low dielectric of the thylakoid membrane, and thus the movement of electrons from P_{680} (near the luminal face), through pheophytin (Pheo) and to Q_A (near the stromal face) directly contribute to thylakoid Δψ. In addition, the oxidation of water at the OEC deposits protons into the lumen, while the reduction of plastoquinone (PQ) at the Q_B site takes up protons from the stroma, contributing to ΔpH. It follows that 'backpressure' from either of the *pmf* components could accelerate recombination reactions, as has been amply demonstrated in past work (38, 148). However, Δψ and ΔpH should have differential effects on recombination depending on the properties of the charge pair involved. The Δψ component will primarily affect the energetics of 'electrogenic' electron transfer reactions, i.e. those that occur vectorially across the thylakoid membrane, by shifting the equilibrium constant for these reactions towards the electron carrier closer to the lumenal side of the membrane (i.e. the positively charged side; figure 3.1b,c). The effect of Δψ on charge-separated states is dependent upon the physical distance between the redox cofactors and the perpendicular distance from the membrane edge, i.e. electron transfer between cofactors within the thylakoid membrane becomes progressively more destabilized by Δψ as the distance between charge-stable states spans larger distances

across the membrane. For example, electron transfer from $Pheo^-$ to Q_A moves a charge about halfway across the thylakoid dielectric, so that adding a $\Delta\psi$ of 120 mV should shift the free energy drop for this this reaction by about 60 meV, and alter the equilibrium constant for sharing the electron by a factor of about 10.

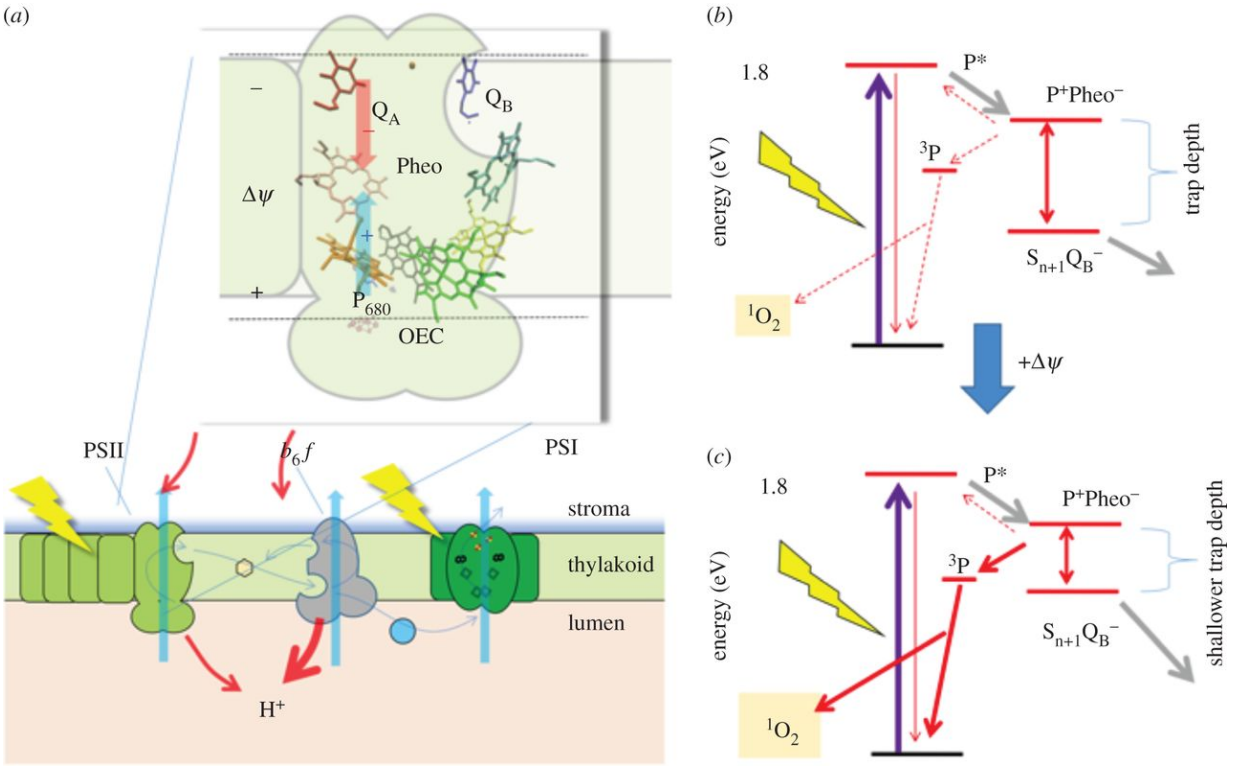

Figure 3.1: Photosynthetic electron transfer energetics are influenced by membrane orientation and membrane potential.
(a) PSII cofactors are oriented within the complex so that light-driven forward electron transfer induces the formation of a trans-thylakoid $\Delta\psi$. Subsequent proton uptake (red arrows) at Q_B and release at the oxygen-evolving complex will contribute to the ΔpH. During linear electron flow, additional $\Delta\psi$ (blue arrows) is generated by light-induced charge separation in photosystem I, while both $\Delta\psi$ and ΔpH are generated by the Q-cycle at the cytochrome b_6f complex. (b) The loss of free energy during PSII forward electron transfer energetically stabilizes (thick lines) the charge-separated state, impeding (thin lines) recombination. (c) Imposing either $\Delta\psi$ or ΔpH decreases this stabilization energy, increasing the rate of recombination, leading to the generation of $^3P_{680}$, which can interact with O_2 to form the toxic $^1O_2$ species.

The ΔpH component, on the other hand, should primarily affect recombination reactions that involve the uptake or deposition of protons into the aqueous compartments. The pH of the

stroma is thought to be relatively constant in the light, ranging between 7.0 in the dark to 8.0 in the light (149, 150). This pH change has a differential effect on Q_A^- versus Q_B^-, which are both located on the stromal side of the protein, during the initial dark–light transition in stromal pH. Q_A^- is unaffected by the light-induced alkalization of the stroma because no protonation reactions are involved in its redox chemistry. For Q_B^-, however, a proton is taken up when it is formed, and so a proton must be released when it is oxidized, thus favouring re-oxidation of Q_B^- with increasing stromal pH and destabilization of the semiquinone (151). This affect, however, is likely to remain constant during the course of the day in chloroplasts, as the stromal pH appears relatively stable. On the luminal side, a decreased lumen pH via proton transfer reactions will destabilize the OEC S-states if the redox transition involves proton release. Past work (16) suggests that, over the relevant lumenal pH range (approx. from 5.5 to 7.5), the proton release pattern is 1, 0, 1, 2 for transitions S0 → S1, S1 → S2, S2 → S3 and S3 → S4 → S0. The respective back-reactions should involve proton uptake by the OEC, and thus will be destabilized by low lumen pH. The S0 → S1 and S3 → S4 → S0 transitions are considered to be irreversible, so once formed should not be prone to recombination. S2 and S3 recombine with Q_A^- and Q_B^- (with the back-reaction via $P^+_{680}Pheo^-$ as the dominant pathway); however, because the S2 → S1 back-reaction does not involve a proton transfer its rate should be unaffected by lowering the lumen pH. Therefore, only PSII centres in the S3 state should display pH-dependent increases in recombination rates due to lowering the lumen pH (by 10-fold for a decrease of 1 pH unit). By contrast, $\Delta\psi$ should affect recombination for both S2 and S3 states. Under continuous light, the S-states are likely to be evenly distributed, so that $\Delta\psi$ should have about twice the effect of an energetically equivalent ΔpH on PSII recombination as it would affect approximately twice as many PSII centres.

The rate of recombination will also be affected by the redox state of the PSII electron acceptor Q_A, which is also influenced by the *pmf*. The reduced form, Q_A^-, accumulates when the rate of its photoreduction exceeds that of re-oxidation by downstream electron carriers, feeding electrons into the recombination pathways. Activation of q_E upon lowering the lumen pH as ΔpH builds up, results in decreases in the PSII excitation rate and thus the fraction of centres with Q_A^-. Antagonistically, pH-mediated downregulation of cytochrome b_6f turnover will slow the oxidation of PQH_2, increasing the fraction of centres with reduced Q_A^- as electron acceptors become limited.

3.6 Control of the extent and kinetics of *pmf* partitioning.

At the first level, the partitioning of *pmf* into $\Delta\psi$ and ΔpH is controlled by the biophysical properties of the chloroplast compartments. The electrical capacitance of the thylakoid membrane is small (approx. 0.6 μF cm^{-2}) (20) so that trans-thylakoid transfer of a single electron for each PSII centre can generate a rather large $\Delta\psi$ of about 30 mV, which is equivalent to an electric field across the membrane of about 50 000 V cm^{-1} (152) as seen in the simulations of *pmf* after a single turnover excitation of PSI and PSII (see Appendix, supplemental figure 3.1a). On the other hand, the proton buffering capacity (β) of the lumenal compartment is quite high (β ~ 0.03 M per pH) (22), so that the same single turnover flash should produce a very small change in lumen pH (approx. 0.001 units; Appendix, supplemental figure 3.1a). Changing the pH from 7 to 6 would require the deposition of 0.03 M of protons into the lumen (compared with approx. 10^{-6} M in the absence of lumen buffering groups).

These basic biophysical properties explain, in large part, why in early times (typically tens of seconds (2, 36)) after illumination, *pmf* is predominantly composed of $\Delta\psi$. As illustrated in figure 3.2a, and in the simulations in figure 3.3a.1–a.5, in a simple thylakoid membrane with

no counter-ion channels, *pmf* remains predominantly as $\Delta\psi$ indefinitely, because $\Delta\psi$ by itself is sufficient to force protons deposited in the lumen back out through the ATP synthase, resulting in only small net changes in lumen pH. This situation is the predominant mode of action for mitochondrial and plasma membrane ATP synthase activity (reviewed in 40) and likely allows pH-sensitive biochemical processes occurring in the internal spaces to proceed unhampered by large changes in proton concentrations. As shown in the simulation, the continuous presence of high $\Delta\psi$ (figure 3.3a.1) leads to destabilization of the PSII charge pairs, while the lack of ΔpH (figure 3.3a.2) prevents the formation of q_E (figure 3.3a.3), resulting in accumulation of reduced Q_A^- (figure 3.3a.4). The combination of these factors favours PSII back-reactions leading to $P^+_{680}Pheo^-$ recombination, producing large amounts of $^1O_2$ (figures 3.3a.4 and a.5)

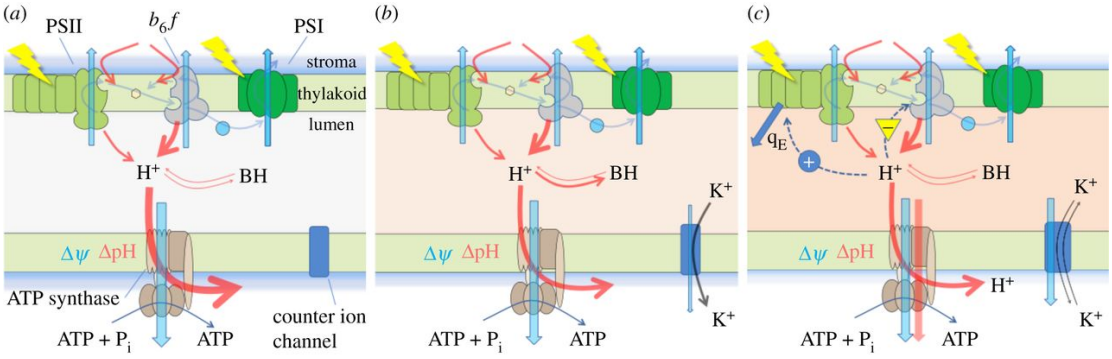

Figure 3.2: Illustration of the factors contributing to the balancing of *pmf* into $\Delta\psi$ and ΔpH during different phases of illumination.
The blue arrows on the upper thylakoid membrane show the directions of transmembrane electron flow that generates $\Delta\psi$, while the red arrows show the uptake and deposition of protons that generates ΔpH. The semi-transparent arrows passing over the ATP synthase indicate the relative contributions of $\Delta\psi$ (blue) and ΔpH (red) to the ATP synthase reaction. (a) At early times after illumination, *pmf* is stored predominantly in $\Delta\psi$, owing to the low electrical capacitance of the thylakoid membrane and the large proton buffering capacity of the lumen. The high $\Delta\psi$ effectively drives the efflux of protons from the lumen through the ATP synthase, maintaining a low ΔpH. (b) Activating counter-ion fluxes dissipates a fraction of $\Delta\psi$, allowing additional proton influx and less efflux, which gradually protonates lumenal buffering groups, forming a ΔpH. (c) Counter-ion fluxes establish ion gradients that eventually reach a local equilibrium with $\Delta\psi$, leading to a steady-state ratio of $\Delta\psi$:ΔpH. The generation of ΔpH is then capable of downregulating cytochrome b_6f turnover (triangle) as well as activating q_E (dark blue circle).

As illustrated in figure 3.2b, adding an ion channel to the thylakoid membrane allows counter-ions to move across the membrane, down the $\Delta\psi$ gradient. For example, the simulation in figure 3.3b.1–b.5 shows the movement of K^+ (figure 3.3b.3) in response to $\Delta\psi$, from the lumen to the stroma, progressively dissipating $\Delta\psi$ (figure 3.3b.1), while depleting the lumen of K^+. Anions, such as Cl^-, will also dissipate $\Delta\psi$, but in this case, they tend to accumulate in the lumen (153). In either case, the resulting loss of $\Delta\psi$ slows the efflux of protons through the ATP synthase, allowing additional protons to be transferred to the lumen. Over time, the accumulation of protons overcomes the lumen buffering capacity, increasing ΔpH (figure 3.3b.1–b.2) at the expense of $\Delta\psi$ (see discussion in 2, 76). As illustrated in figure 3.2c and simulated in figure 3.3b.1, ion fluxes cannot completely dissipate $\Delta\psi$ because the resulting counter-ion gradient will eventually prevent further movements, and the extent to which $\Delta\psi$ is dissipated will thus depend, in part, on the starting concentrations of these ions in the stroma and lumen as well as the presence of other ion transporters and proton buffers (see discussion in 2, 146). The simulation in figure 3.3b.1–b.5 began with stromal and lumenal K^+ concentration of 40 mM, and resulted in $\Delta\psi$:ΔpH of about 1:2 in the light. It is also clear from these simulations that, even in this simplified situation, $\Delta\psi$:ΔpH can change with conditions, as is evident by the fact that $\Delta\psi$:ΔpH increases as a result of the build-up of counter-ion gradients at higher *pmf* (see Appendix, supplemental figure 3.1). The simulations in column C will be discussed below.

In any case, allowing counter-ion flow results in dissipation of $\Delta\psi$ (figure 3.3b.1), the build-up of ΔpH that acidifies the lumen (figure 3.3b.2) and activates q_E (figure 3.3b.3), which decreases the fraction of reduced Q_A (figure 3.3b.4). The combined effect of these changes is a decrease in $^1O_2$ production when compared to the case with no counter-ion fluxes (figures 3.3b.4 and b.5), but at the expense of linear electron flow (LEF) (figure 3.3b.5).

From the above, we can conclude that the basic properties of the thylakoids allow $\Delta\psi$ to appear very rapidly upon illumination, whereas ΔpH is formed much more slowly, with a half time on the time-scale of several minutes (2), and that these kinetics are likely to affect the onset of photoprotective mechanisms. This kinetic mismatch can be exacerbated by the fact that at sub-saturating light, PSI and PSII centres will have access to relatively large pools of electron acceptors and donors, so that an abrupt increase in light may induce multiple turnovers, producing the large $\Delta\psi$ spikes that result in damaging back-reactions and recombination reactions.

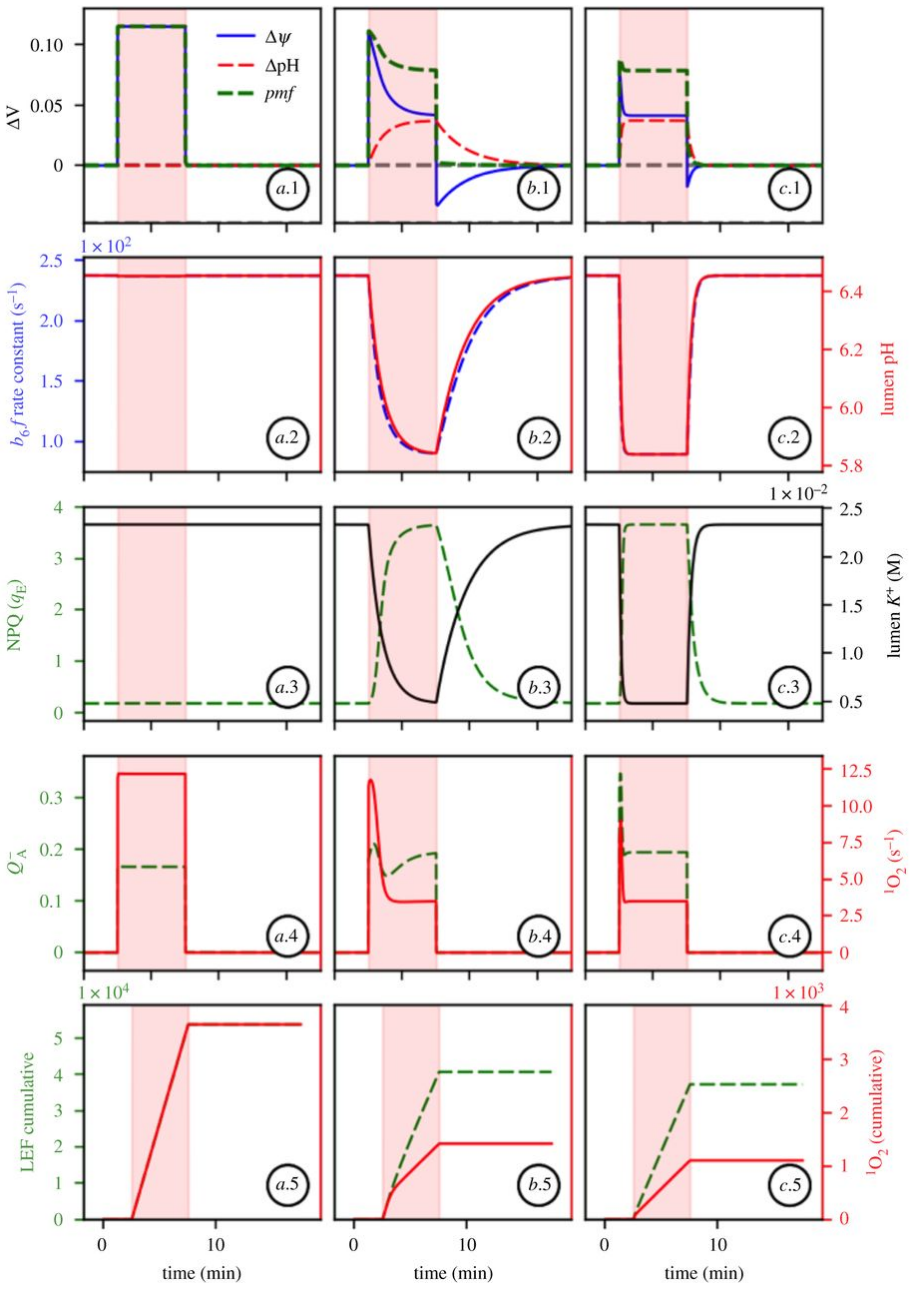

Figure 3.3: Simulated responses of thylakoid *pmf* components, linear electron flow, ion fluxes and $^1O_2$ production during a 5-min light pulse.

The simulations were performed using the DeltaPsi.py programme and initial values described in the Appendix. The timing and amplitude (maximum of 300 µmol photons m^{-2} s^{-1}) of the excitation light are indicated by the light red coloured blocks. Simulations were repeated with the thylakoid permeability to counter-ions set at 0 (a.1–a.5), 'normal' to approximately simulate the kinetics seen in leaves (b.1–b.5), and 'fast' (10-fold faster than normal, c.1–c.5). (1) Light-induced changes in *pmf* (green dashed curves), $\Delta\psi$ (blue solid curves) and ΔpH (red dashed curves), all expressed in units of volts, so that a ΔpH of one is equivalent to 0.06 V. (2) The lumen pH (red, solid curves) and the relative rate constant for oxidation of PQH_2 at the cytochrome b_6f complex (blue dashed curves). (3) The responses of q_E (NPQ, green dashed

Figure 3.3 (*continued*): curves) together with the concentration of counter-ions in the lumen, $[K^+]$ (black solid curves). (4) The fraction of Q_A in its reduced form (Q_A^-, green dashed curves) and the rate of $^1O_2$ production (red solid curves) due to FRIP (s^{-1} $PSII^{-1}$). (5) The cumulative LEF (green dashed curves) and $^1O_2$ production (solid red curves). Note that the *pmf* parameters are shown as light-induced changes, relative to dark values. A version of this figure without this offset, supplemental figure 3.2, shows that *pmf* in the dark is preferentially stored in ΔpH, but as *pmf* increases, it progressively favours $\Delta\psi$. LEF, linear electron flow.

Thylakoid properties also control the rate of ΔpH relaxation (and thus q_E recovery) when light is decreased, though the mechanism is more complex. As described in Cruz et al. (2, 61), when the light is switched off, electron flow in the reaction centres is inhibited, but proton efflux through the ATP synthase continues, which causes rapid changes in $\Delta\psi$ (in the opposite direction to that induced by light-driven electron flow). Because of the low thylakoid capacitance and high lumen β, the changes in $\Delta\psi$ are far larger than ΔpH, and continue until an 'inverted' $\Delta\psi$ is established. At this point, the total *pmf* ($\Delta\psi$ + ΔpH) is approximately equal to the backpressure from ATP hydrolysis (i.e. *pmf* ≈ ΔGATP/n), so the driving force for proton efflux is near zero, slowing down further proton efflux until counter-ion fluxes occur. When measuring $\Delta\psi$ changes in leaves using the electrochromic shift (ECS), this behaviour appears as the 'negative' ECS_{inv} phase, which is used to estimate light-induced ΔpH (2, 61), but it is important to note that these phases occur over the background level of $\Delta\psi$ from equilibration with ATP hydrolysis (ΔG_{ATP}) in the dark, as can be seen when the simulations are plotted without offsets in the *pmf* parameters (Appendix, supplemental figure 3.3).

Under natural field conditions in a plant canopy or an aquatic environment, light can fluctuate over a wide range of time-scales, from less than a second for wind-induced leaf movements or sunflecks and water focusing, seconds–minutes for changes in cloud cover, and hours for the position of the sun (66). Different regulatory processes contribute to photoprotection over these time-scales. Some photoprotection processes respond over the scale

of many minutes to hours (154), including the xanthophyll cycle reactions, the PSII photoinhibition/repair cycle and chloroplast movements. These slow processes are unable to respond to the more rapid fluctuations, but will approach steady-states reflecting the conditions averaged over the many minutes-to-hours time-scale. Antenna state-transitions respond over the medium times-scales, but appear to be more important in green algae than higher plants (155). Intriguingly, the remaining, rapidly responding photoprotective processes are all controlled (directly or indirectly) by lumen pH, most importantly the adjustment of q_E and the photosynthetic control of electron flow at the cytochrome b_6f complex, and are thus likely to be limited by the slow rates of ΔpH formation and decay.

This conclusion is in line with simulations in figure 3.3c.1–c.5, which shows that increasing the permeability of the thylakoid to counter-ions by 10-fold compared with 'normal', increased the rate of relaxation of $\Delta\psi$ (figure 3.2c.1), leading to faster onset of ΔpH (figure 3.3c.1 and c.2) and thus q_E (figure 3.3c.3). The overall effect is a decrease in $^1O_2$ production (figure 3.3c.4 and c.5) owing to both a decreased $\Delta\psi$ and Q_A^- (figure 3.3c.4). The potentially beneficial effects of increasing the permeability of the thylakoid to counter-ion movements can be seen by comparing figure 3.2b.5 and c.5, showing that the early, rapid accumulation of $^1O_2$ is strongly supressed as ΔpH builds up. However, there is also a trade-off in loss of LEF, caused by increased control of PQH_2 oxidation (figure 3.3b.4 and c.4).

The effects of counter-ion permeability on photosynthesis are highly dependent on the rates of fluctuation of the light, as is seen in the simulations in figure 4 that compare the effects of low frequency light changes (a 1 hour sine wave, figure 3.4a.1–2 and b.1–2) or high frequency light changes (a 1 h duration of a sine wave with period of 10 min, figure 3.4c.1–2 and d1–2). Overall, the lower frequency changes produced lower rates of $^1O_2$ production and increased

linear electron flow (LEF) relative to the higher frequency changes, consistent with the expected frequency dependence of saturation effects. Increasing counter-ion permeability 10-fold (figure 3.4b.1–2) had almost no effect on the simulated photosynthetic parameters under the slowly changing sinusoidal light. By contrast, the same change in counter-ion permeability had large effects under the higher frequency square wave illumination (figure 3.4d.1–2), causing a twofold decrease in $^1O_2$ under the fluctuating light, mainly due to the suppression of large $\Delta\psi$ spikes that occurred during the rapid increases in light intensity. This protection from $^1O_2$ production, however, comes at the cost of approximately 20% decrease in LEF compared with the low frequency changes.

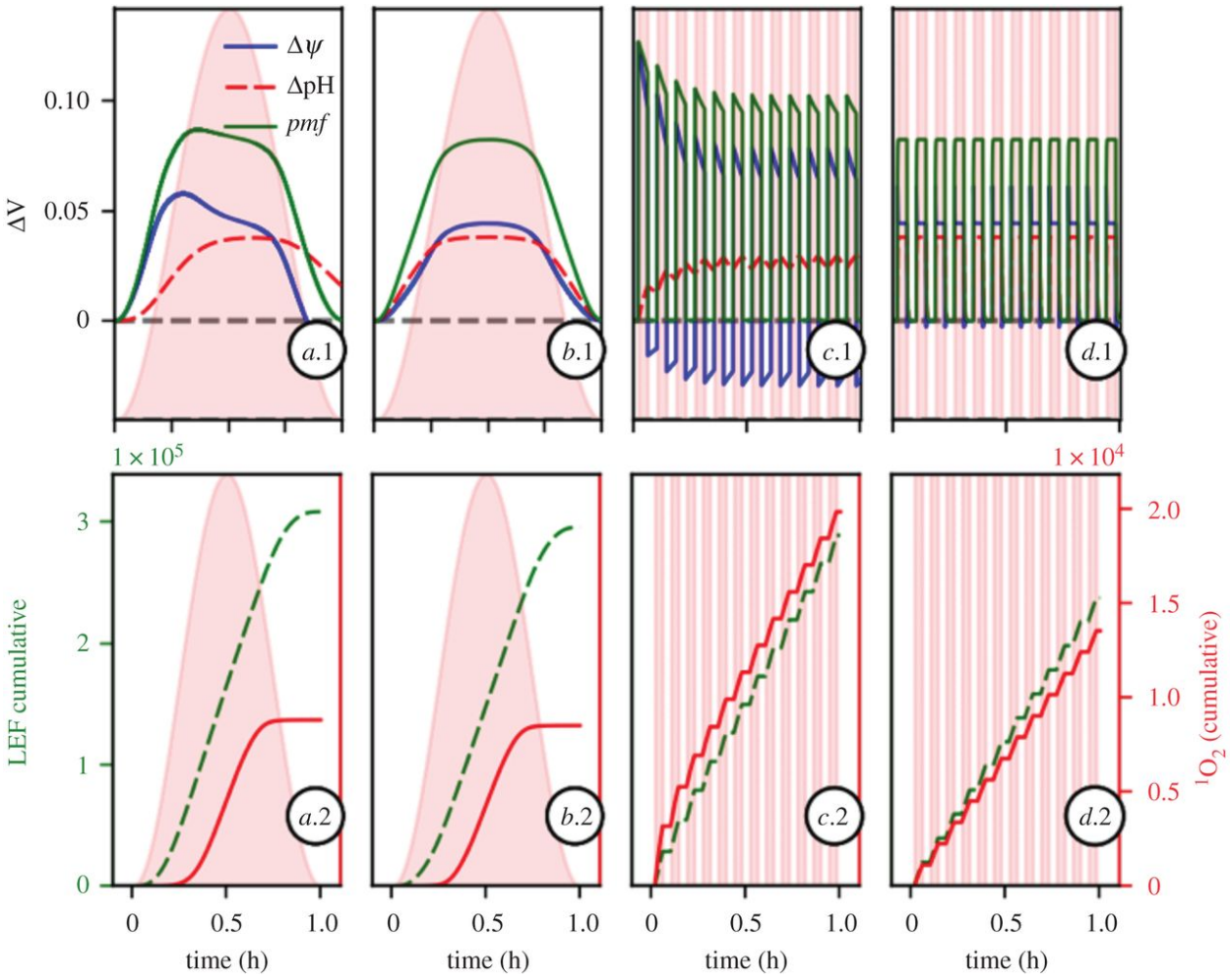

Figure 3.4: Simulated responses of thylakoid *pmf* components, linear electron flow (LEF) and $^1O_2$ production during a 1-h light sine wave.
Simulations and annotations were as in figure 3.3, but with illumination set to a 1-h sine wave (a.1, a.2, b.1, b.2) or a 1-h square wave (c.1, c.2, d.1, d.2) both with peak intensity of 300 µmol photons m^{-2} s^{-1}. Simulations were repeated with the thylakoid permeability to counter-ions set to 'normal' (a.1, a.2, c.1, c.2) or 'fast' (10-fold faster than normal, b.1, b.2, d.1, d.2). (a) Light-induced changes (with respect to the dark values) in *pmf*, Δψ and ΔpH, all expressed in units of volts, so that a ΔpH of one is equivalent to 0.06 V. (b) The cumulative LEF and $^1O_2$ productions. Full datasets for these simulations are presented in the Jupyter notebook in the Appendix, supplemental figure 3.3.

3.7 Can we improve photosynthesis by modifying *pmf* partitioning to make photosynthesis more robust?

The results from our model lead us to predict that increasing the rates of counter-ion fluxes across the thylakoid could, in principle, lead to improved photosynthetic performance,

though the improvement is predicted to be the long-term advantage of decreased photodamage rather than the short-term gain from increased LEF (65).

Given that the slow rates of ion fluxes are likely due at least in part to low protein levels of ion transporters in the thylakoids, a strategy of overexpressing the rate-limiting channels could be suggested. However, if better photosynthesis could be achieved this simply, plants might be expected to have already evolved more rapid ion fluxes than those measured in laboratories. Indeed, exploring these properties in natural populations may reveal precisely these sorts of variations.

On the other hand, increasing ion fluxes may lead to secondary, deleterious effects. A basic tenet of the model is that ΔpH cannot form without the movements of counter-ions, and thus, for each proton that accumulates in the lumen, approximately an equal number of counter-ion charges must be moved to dissipate the $\Delta\psi$. In effect, energy stored in $\Delta\psi$ is consumed, at least temporarily, in the movement of counter-ions, removing the ATP synthase driving force and preventing proton efflux through the ATP synthase. The diversion of protons away from ATP synthase efflux then allows protons to enter the lumen buffering pool, allowing ΔpH to form more rapidly as protons are no longer being driven out of the lumen by $\Delta\psi$ and the buffering capacity is overcome. Thus, one consequence of ΔpH formation will be a transient decrease in the LEF output ratio of ATP/NADPH due to the time-dependence of overcoming the lumen buffering capacity. Metabolic congestion and photodamage can occur if this ratio does not precisely match that needed to power assimilation, requiring alternative electron transfer processes, such as cyclic electron flow or the water–water cycle, to make up the balance (6). Our simulations suggest that a slow ΔpH formation (half time of about 4 min) results in a counter-ion related deficit of about 0.05 ATP per CO_2 fixed by assimilation, which should be easily remedied

by alternative electron transfer processes (figure 3.5). With a 10-fold faster ΔpH formation provided by increased counter-ion flux, the resulting ATP deficit caused by counter-ion movements can become severe, requiring a 10-fold higher input of ATP per CO_2 fixed (figure 3.5c), which may exceed the capacity for cyclic electron flow in some species.

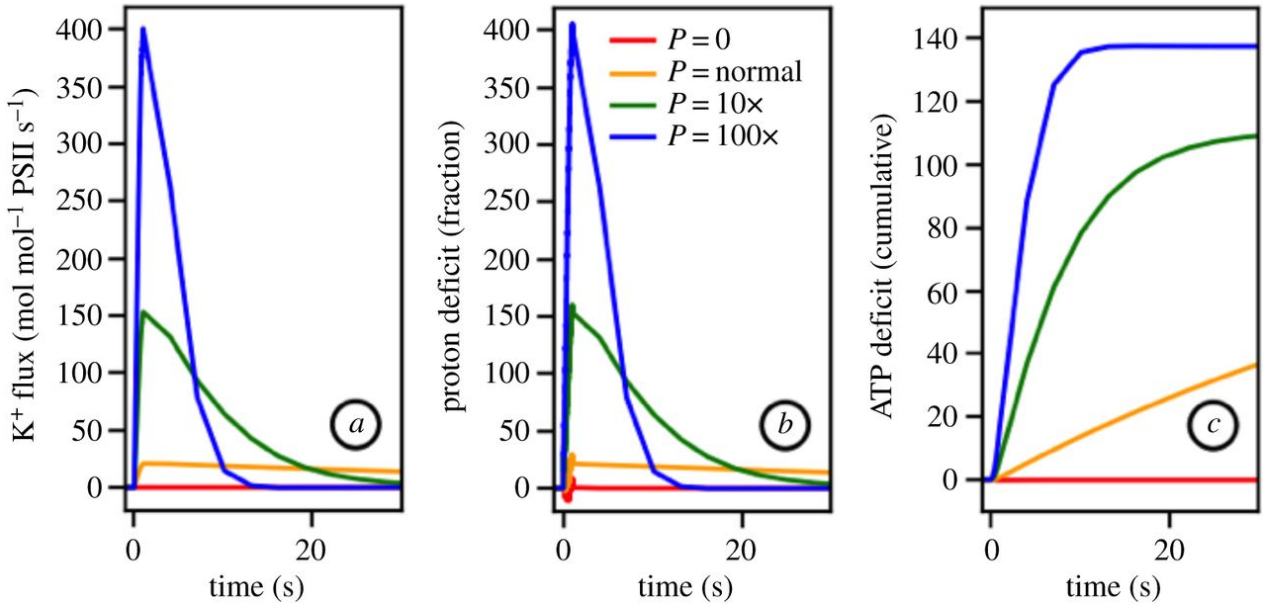

Figure 3.5: Effects of thylakoid counter-ion fluxes on the ATP/NADPH budget of photosynthesis.
Data are taken from the simulations performed in figure 3.3, with *x*-axis origin set to the beginning of illumination. (a) The light-induced flux of counter-ions (K^+), with positive values representing net flux out of the lumen. (b) The proton deficit, i.e. the protons deposited into the lumen but buffered so that they are unavailable to the ATP synthase. (c) The cumulative deficit in molecules of ATP relative to PSI turnover needed for CO_2 fixation by the Calvin–Benson cycle. The red, yellow, green and blue lines represent results with the thylakoid counter-ion permeability set to zero, 'normal' (figure 3.3), 10× normal and 100× normal, respectively.

The osmotic balance of the chloroplast compartments must also be finely tuned to maintain their structure and the function of proteins residing within each compartment, and even small osmotic imbalances can lead to swelling-induced loss of thylakoid stacking, or shrinkage-induced inhibition of the interactions of plastocyanin with PSI (2, 153, 156). Proton translocation

by itself should not appreciably affect the osmotic potential of the lumen because most protons are buffered. By contrast, counter-ion movements will very likely change the concentrations of free counter-ions, and thus have a colligative effect on the osmolarities of the lumen and stroma. It is interesting to note that loss of the chloroplast potassium KEA (the potassium–proton antiporter in the thylakoid membrane) transporters leads to swelling and disordering of the thylakoid structure (29), suggesting that fine-tuning of the thylakoid ion balance is critical for osmoregulation. It is also suggestive that Chlamydomonas cells are able to compensate for severe hyperosmotic shock-induced lumenal shrinkage, but only over the same time-scale as ΔpH formation, i.e. about 5–10 min (157). It is thus possible that the rate of *pmf* partitioning is limited by the need to prevent acute osmotic imbalances that could result in structural perturbations.

At this point, the model is not intended to reproduce all the reactions of photosynthesis. Nevertheless, using reasonable, published values for thylakoid properties (see Appendix), the model qualitatively reproduced the FRIP behaviours observed by Davis et al. (36), including light fluctuation-induced $\Delta\psi$ spikes, that result in increased recombination, $^1O_2$ production and the accumulation of photodamage.

This simplified model also suggests that accelerations in counter-ion fluxes will result in tuned increases in the rate of NPQ onset, which will have a potentially beneficial effect by decreasing $^1O_2$-related photodamage and accelerating q_E responses, but this will be at the cost of decreasing LEF. This suggestion is interesting in the light of the recent work of Kromdijk et al. (126), who reported that more rapid NPQ responses can increase plant yield by increasing PSII quantum efficiency (and thus LEF). Our simulations suggest an alternative explanation: that the underlying benefit of more rapid responses will be decreases in both ROS production and

photodamage, leading to more sustained photosynthesis and lower input costs over the long term. Interestingly, further modifications of photosynthetic parameters in our simulations show that the trade-off loss of LEF can be avoided by decreasing the pK_a for controlling the cytochrome b_6f complex to well below that for initiation of q_E, but this may lead to less control of electron flow at the cytochrome b_6f complex and over-reduction of PSI and subsequent PSI photodamage (5).

At the very least, recent results and the simulations they inspire suggest possible targets for plant improvement, and generate testable hypotheses. Ultimately, improving photosynthesis will require understanding the multiple constraints that life in the real world imposes on photosynthesis, as well as the multiple, interacting regulatory systems that have evolved to cope with them. Approaching this complex problem will require a larger scale investigation of the responses of *pmf* in a range of species, and under field-like conditions, as well as a deeper understanding of how the biophysical machinery of photosynthesis is integrated with the host organism to respond to the challenges of rapidly fluctuating environmental conditions.

From the simulations presented above, taking steps towards such an integrated view can reveal emergent properties of the system that were not apparent from studies of isolated complexes. Towards that end, it is hoped that future work (by us and others) will expand the model presented here to test the effects of important processes, including newly discovered ion transport systems and their regulation (158, 159), effects on thylakoid osmotic balance (160), the PSII damage/repair cycle (161, 162), the accumulation of electrons on the acceptor side of PSI (which can lead to irreversible PSI photodamage (163)), alternative modes of PSII regulation including the recent report of bicarbonate-mediated protective redox tuning (132), regulation of the ATP synthase, and the need for alternative electron transfer pathways.

Holistically, an expansive mechanistic model of photosynthetic regulation will likely provide immediate targets for testing the effects of engineered changes aimed at improving photosynthetic yields. When the model fails to replicate experimental results, it has the potential not only to focus attention on gaps in our understanding of photosynthesis and its regulation but also to provide insights that could help to fill these gaps.

3.8 Acknowledgements.

Work performed by G.A.D. and D.M.K. was supported by the US Department of Energy (DOE), Office of Science, Basic Energy Sciences (BES) under award number DE-FG02-91ER20021. A.W.R. was supported by the Biotechnology and Biological Sciences Research Council grant nos. BB/K002627/1 and BB/L011206/1 and the Royal Society Wolfson Research Merit Award.

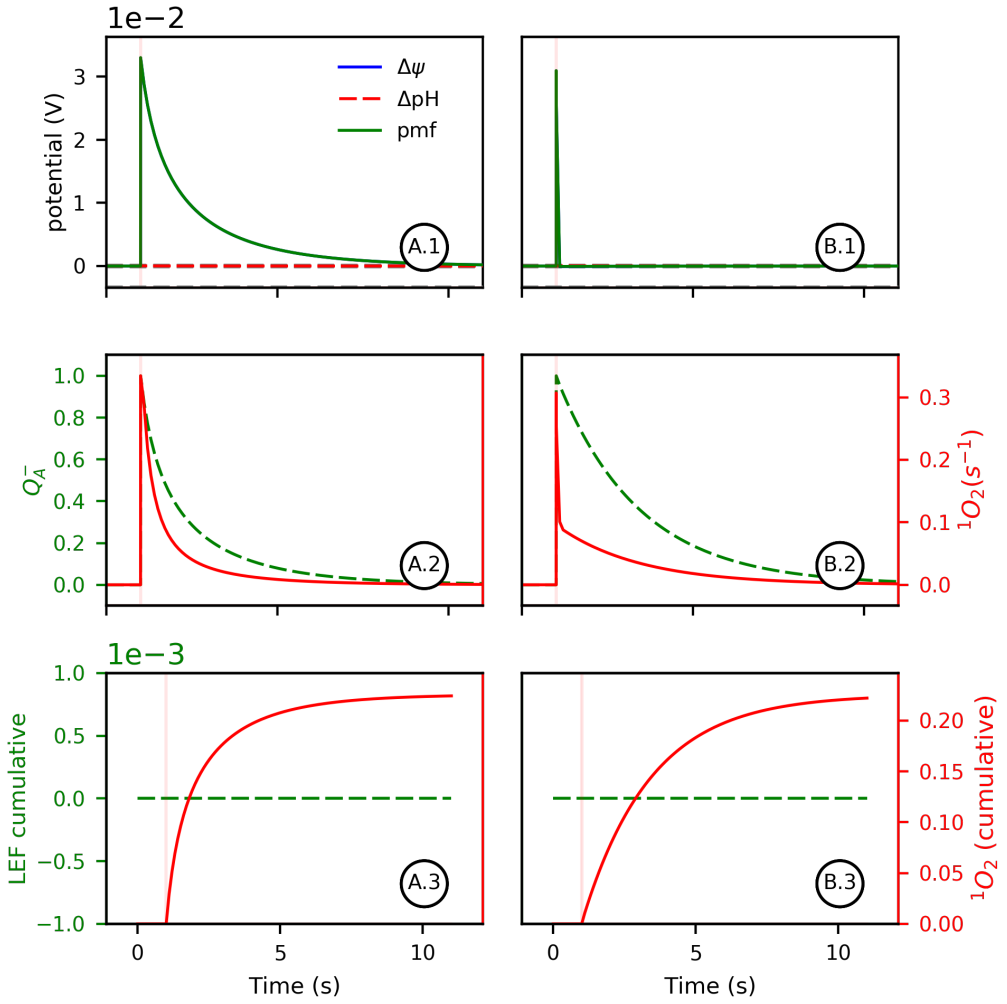

Supplemental Figure 3.1: Simulations of the amplitudes of *pmf* parameters induced by a single-turnover flash hitting all photosystem II (PSII), but no photosystem I (PSI). The simulations were set up to recapitulate the experiment performed in Davis et al. (36) (*c.f.* Figure 6). To obtain single turnover conditions, the rate constant for re-oxidation of Q_A^- was set to zero. Excitation of PSI was inhibited by setting its antenna size to zero. In Panels A.1 and A.2, the fluxes of counterions were also set to zero to reveal the electrogenic effects of both excitation and recombination. In Panels B.1 and B.2, the permeability of the thylakoid to counterions was set very high to simulate the effects of addition of KCl + valinomycin to rapidly dissipate flash-induced Δψ. Panel A.1 and B.1 show the effects on Δψ (blue solid line), ΔpH (red dashed line) and total *pmf* (green solid line). Panels A.2 and B.2 show the predicted concentration of the $S_2Q_A^-$ (green dashed line) and $^1O_2$ production (red dashed line). Panels A.3 and B.3 show the cumulative LEF and 1O2 production. As seen in Davis et al. and references within (36), the presence of a Δψ induced more rapid $^1O_2$ production. However, because all charge-separated states recombine through the same pathway, the cumulative levels of $^1O_2$ production for both conditions were the same.

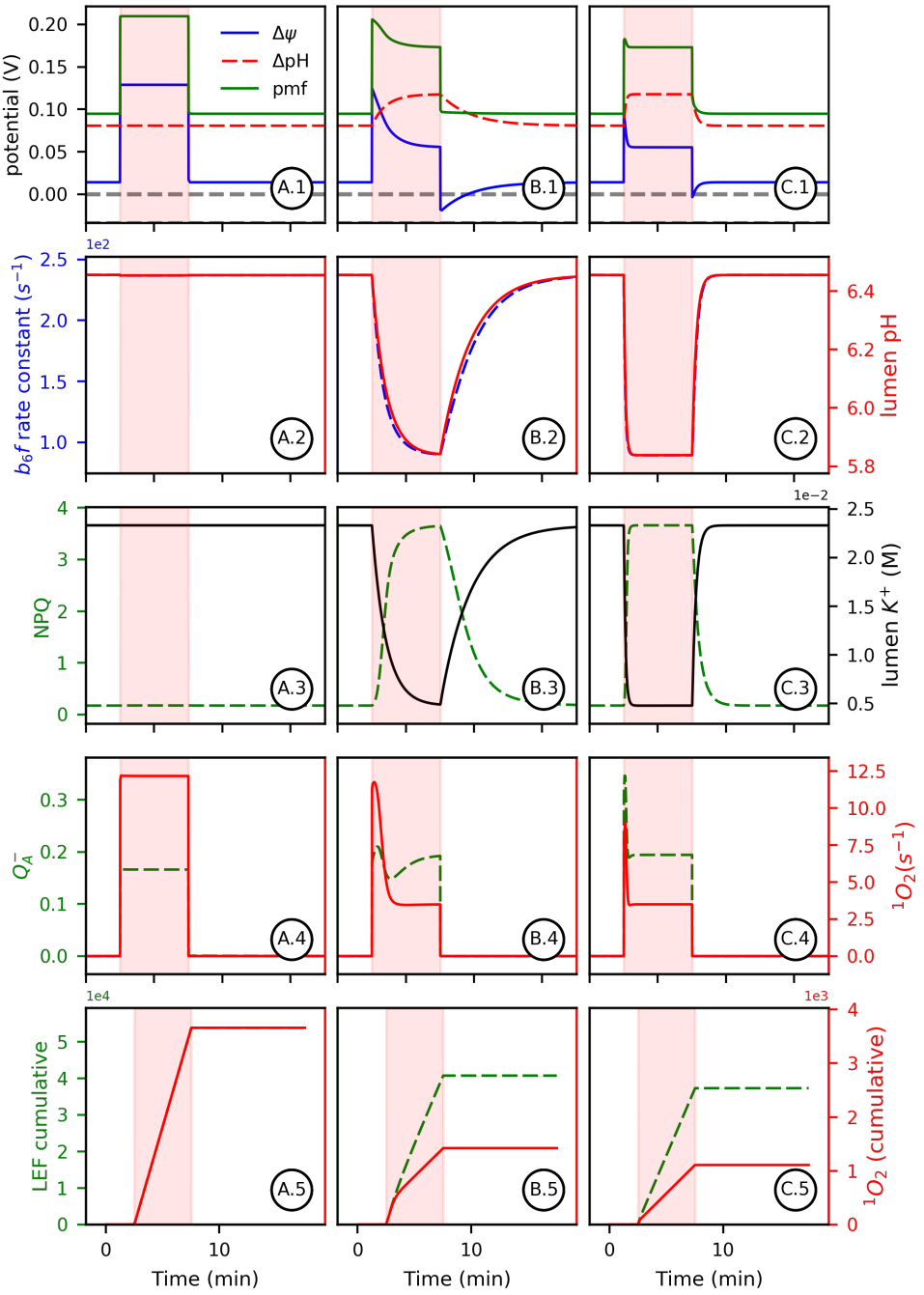

Supplemental Figure 3.2: Simulated responses of thylakoid *pmf* components, linear electron flow, ion fluxes, and 1O2 production during a 5-min light pulse.
The simulations are as in Figure 3.3, but the *pmf* parameters are not offset at time zero.

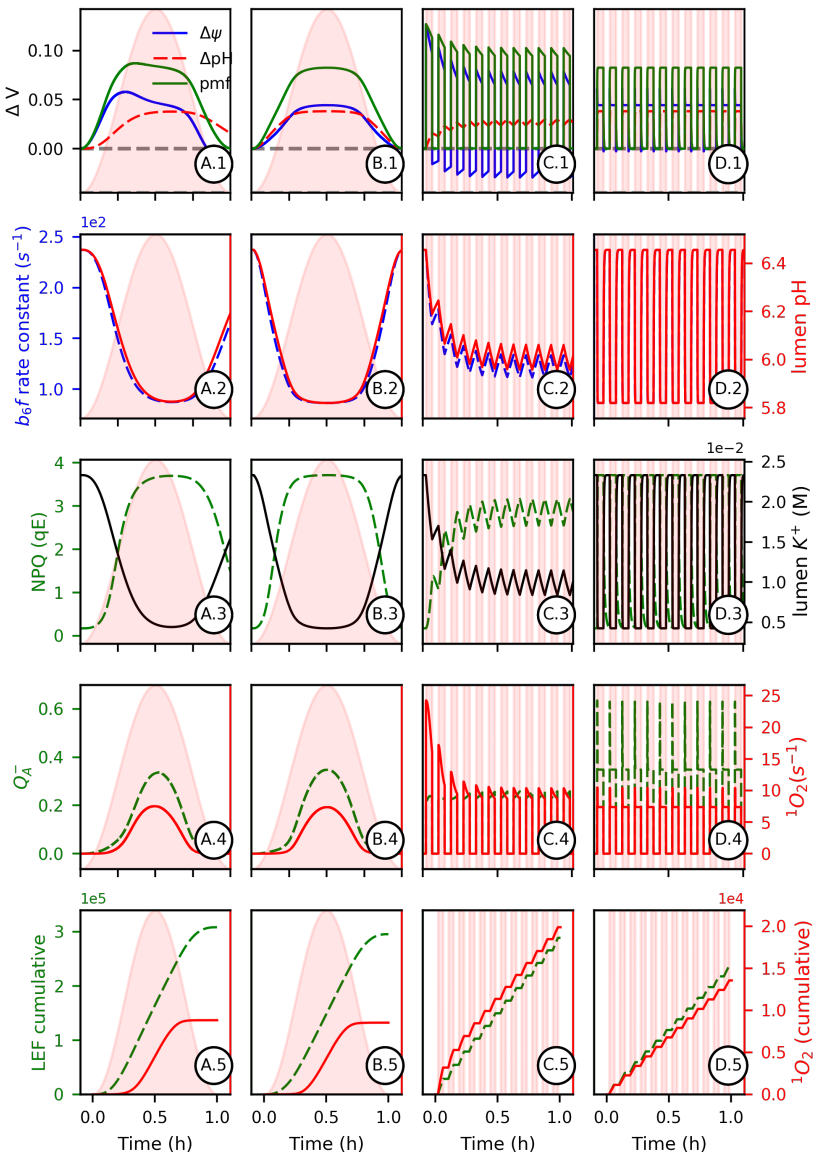

Supplemental Figure 3.3: Simulated responses of thylakoid *pmf* components, linear electron flow, and $^1O_2$ production during illumination with a 1-hour sine or square waves. The figure contains the full data set for the simulations described in Figure 3.4 in the main text. Simulations were performed as in Figure 3.3, but with illumination set to a one-hour sine wave (Panels in columns 1 and 2, starting with A, B) or a one-hour square wave (Panels in columns 3,4, starting with C, D) both with peak intensity of 300 µmol photons $m^{-2}s^{-1}$. Simulations were repeated with the thylakoid permeability to counter-ions set to "normal" (Panels in columns 1, 3, starting with A, C) or "fast" (10-fold faster than normal, panels in columns 2, 4, starting with B, D). The panels in row 1 show light-induced changes (with respect to the dark values) in *pmf*, Δψ, and ΔpH, all expressed in units of V, so that a ΔpH of one is equivalent of 0.06V. Row 2 shows the effect of the lumen pH on the turnover rate of cytochrome b_6f. Row 3 shows the responses of q_E together with the concentration of counter-ions in the lumen, $[K^+]$. Row 4 shows the fraction of Q_A in its reduced form (Q_A^-) and the rate of $^1O_2$ production due to FRIP (s^{-1} $PSII^{-1}$). Row 5 shows the cumulative LEF and $^1O_2$ productions.

Chapter 4

The electric field component of the photosynthetic proton motive force increases the yield of PSII recombination *in vivo* during light fluctuations

Geoffry A. Davis and David M. Kramer

4.1 Abstract

Photosystem II (PSII) functions as a water-plastoquinone oxidoreductase to mediate the capture and conversion of light into chemical energy during photosynthesis. This reaction mechanism requires two successive PSII turnovers to reduce plastoquinone and four turnovers to oxidize water, requiring coordination of multiple electron transfer steps occurring on the donor and acceptor sides of the protein complex to occur cooperatively for proper functioning. However, reversal of electron transfer (recombination) can occur, leading to side-reactions that produce a high yield of triplet chlorophyll and singlet oxygen, which result in irreversible oxidative damage and inactivation of PSII. These recombination events are suggested to be modulated *in vivo* by the extent of the electric field ($\Delta\psi$) across the thylakoid membrane, which destabilizes charge-separated states within PSII proportionally to the vectorial distance across the membrane. To identify the impact of $\Delta\psi$ on PSII recombination *in vivo*, delayed fluorescence was measured in intact *Arabidopsis thaliana* during fluctuations in light intensity to induce rapid, transient large $\Delta\psi$. Rapid increases in light intensity induced large, transient increases in the yield of PSII recombination, while static, high light did not increase PSII recombination yields. Using mutants deficient in activating photoprotective quenching mechanisms, PSII recombination occurs over a longer time than in wild type plants. Taken together, these results suggest that fluctuating light rapidly increases the yield of PSII recombination, which then decays relative to the depletion of $\Delta\psi$ and the concentration of PSII species available to recombine. The increases in PSII recombination under fluctuating light may explain the susceptibility of photosynthesis in natural, field conditions where rapid light fluctuations occur throughout the course of the day.

4.2 Introduction

Oxygenic photosynthesis in cyanobacteria, algae, and plants utilizes electrons generated from the oxidation of water to ultimately yield NADPH and ATP for cellular anabolism. This is accomplished by harvesting light in antenna pigments and funneling the excitation energy to special pair chlorophylls (P) within each of photosystem II (PSII) and photosystem I (PSI). PSII is a water–quinone oxidoreductase, utilizing the energy generated via excitation reaction center chlorophyll to oxidize water and reduce plastoquinol (PQH_2), releasing the protons into the thylakoid lumen during the water splitting process (164). The oxidation of PQH_2 by the cytochrome b_6f complex leads to additional proton deposition into the thylakoid lumen through the Q-cycle (10) and electron transfer to plastocyanin, which is used to re-reduce PSI following excitation and charge separation (165). Electrons from PSI are terminally transferred to ferredoxin and subsequently to $NADP^+$ to generate NADPH (127).

The deposition of protons into the lumen during electron transfer events generates a light-induced ΔpH across the thylakoid membrane. Acidification of the thylakoid lumen triggers regulatory processes that limit electron transfer at PSII. The availability of oxidized plastoquinone (PQ) for PSII electron transfer is limited by the rate of PQH_2 oxidation by the cytochrome b_6f complex, the turnover of which slows by a factor of 10 per pH unit decrease (11, 12), increasing the reduction state of the PQ pool and therefore limiting quinone substrate availability for PSII. This is counterbalanced in algae and higher plants by pH-mediated activation of the energy-dependent (q_E) form of nonphotochemical quenching (NPQ), which consists of protonation of the thylakoid membrane protein PsbS (7), as well as violaxanthin de-epoxidase protonation in the thylakoid lumen to activate the conversion of violaxanthin to zeaxanthin (166). Both components of q_E ultimately lead to excitation energy quenching in the

antenna pigments and decreased excitation pressure on PSII (6). Dissipation of ΔpH occurs predominantly via proton translocation by the thylakoid ATP synthase to produce ATP (40), however the critical activities of ion channels within the thylakoid membrane to modulate the partitioning of the transthylakoid proton motive force (*pmf*) between a ΔpH and electric field ($\Delta\psi$) are increasingly being identified (34, 35, 167).

The multifaceted complexity of electron transfer and *pmf* reactions across the thylakoid membrane *in vivo* leads to particular stresses on PSII. PSII is a multi-protein complex where the redox chemistry occurs across the membrane–bound reaction center core D1 and D2 subunits. Following the transfer of excitation energy from antenna pigments to PSII, excitation of chlorophyll molecules within the PSII (P*) core leads to primary charge separation through electron transfer from P_{680} to a nearby pheophytin (Pheo) molecule to form the $P_{680}^{+}Pheo^{-}$ state (Fig. 4.1). The initial charge separation is stabilized by subsequent electron transfer to the permanently bound quinone Q_A, and then to a secondary quinone Q_B. Re-reduction of P_{680}^{+} is mediated by a redox active tyrosine (Y_Z) that participates in the transfer of electrons from the PSII lumen-exposed oxygen-evolving complex (OEC), which goes through a series of at least four redox intermediates (S-states) to produce O_2 (17, 164).

PSII functions as a two-electron gate, requiring two successive PSII turnovers to fully reduce the quinone bound at Q_B, whereupon the quinol diffuses out of the PSII Q_B site into the thylakoid membrane. This sequential reduction of Q_B requires the semiquinone, Q_B^{-}, formed after the first PSII turnover to be held stably through a second PSII cycle. The forward 'productive' electron transfer routes are thermodynamically favorable, however, the reversal of charge–separated states, termed recombination, can occur due to various factors, and are mediated by the free-energy gap between the corresponding states, the physical distance between

redox carriers, and the reorganizational energy (56, 168). While electron back-reactions limit productivity by decreasing the overall efficiency of photosynthesis, PSII back-reactions are precarious *in vivo* due to the recombination of $P_{680}^{+}Q_A^{-}$ through Pheo as an intermediate, described as the indirect recombination pathway due rather than the direct recombination of Q_A^{-} to P_{680}^{+}. Indirect recombination from Q_A^{-}, or Q_B^{-} back to Q_A^{-} due to the relatively small equilibrium constant for sharing electrons between Q_A and Q_B (88), can generate both the initial charge separated singlet state ($^1[P_{680}^{+}Pheo^{-}]$) as well as produce a high yield of the triplet state ($^3[P_{680}^{+}Pheo^{-}]$) (141). The $^3[P_{680}^{+}Pheo^{-}]$ state decays to the triplet ground state chlorophyll (^3P), which has enough energy to interact with O_2 to generate singlet oxygen ($^1O_2$), which is highly reactive and proposed to irreversibly damage the D1 protein and lead to irreversible PSII photoinhibition (67, 96), requiring degradation of the damaged D1 and *de novo* synthesis of a new D1 protein to repair the damaged reaction center (128).

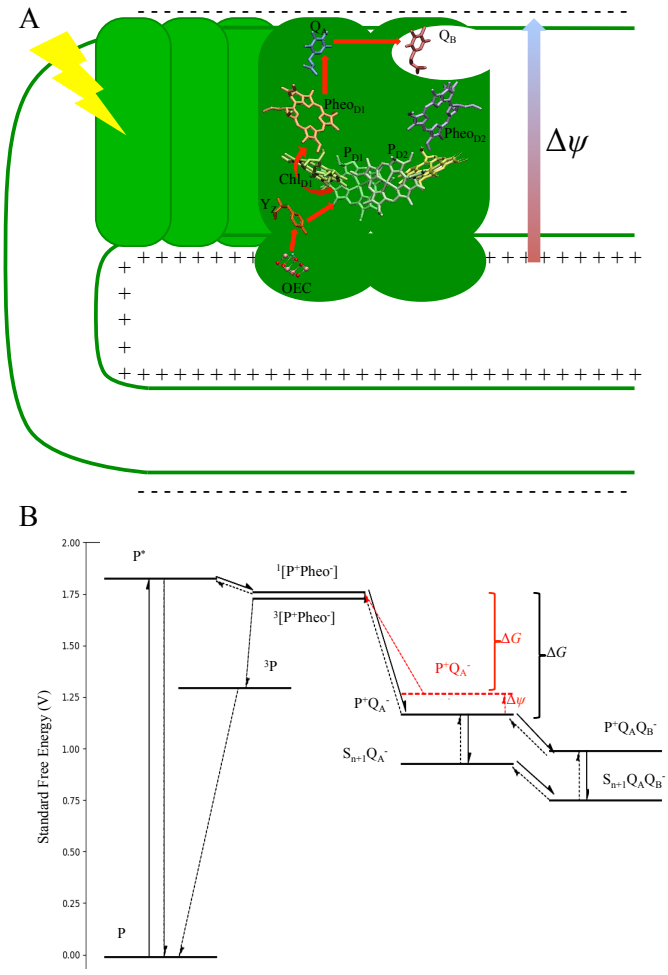

Figure 4.1: Photosystem II electron transfer reactions successively increase the distance of transmembrane charge separation.
Electron transfer within the PSII reaction center core D1 and D2 subunits occurs vectorially across the span of the thylakoid membrane (A). Light is capture in pigments within antenna proteins and the excitation energy funneled to the reaction center. Excitation of the core PSII chlorophylls (P^*) leads to the initial charge separated state $P_{680}^+Pheo^-$ along the D1 branch. The electron is subsequently transferred from $Pheo_{D1}$ to the bound quinone Q_A, followed by electron transfer to the terminal PSII electron acceptor Q_B. Re-reduction of P_{680}^+ is accomplished via the extraction of electrons from the Mn_4CaO_5 oxygen evolving complex (OEC) S-states through a redox active tyrosine (Y_Z). Secondary electron transfer reactions thermodynamically stabilize the productivity of forward electron transfer through successive electron transfer steps to lower potential redox carriers (B). Reversibility of electron transfer reactions (B, dashed lines) are mediated by the free energy difference between the charge separated species. Increasing transmembrane $\Delta\psi$ destabilizes the vectorial movement of charges across the membrane relative to the distance between cation and anion species. For simplicity this is illustrated for the effect on $P^+Q_A^-$ but will result in changes proportional to the distance between membrane bound charge separated species. A second PSII turnover is required to reduce Q_B^- to Q_BH_2, where it can then diffuse out of the Q_B site and exchange for oxidize PQ. Positions of PSII cofactors based on (169).

Reaction center back-reactions have been well studied *in vitro*, where the free energy gap between states can be experimentally manipulated. In isolated reaction centers or isolated thylakoid membranes, increases in the rate of electron recombination occurs when the free energy gap between $P^+Q_A^-$ and P^+Pheo^- (where P is the primary donor) is altered by substituting exogenous quinones (142), utilization of a salt-induced $\Delta\psi$ (26, 170), or application of external electric fields (171, reviewed in 102). *In vivo*, $\Delta\psi$ has been correlated with an increase in $^1O_2$, PSII damage, and photoinhibition (36), suggesting that *in vivo* the free energy gap of charge separated states in PSII are modulated by the partitioning of *pmf*, and the rate of electron recombination increases *in vivo* due to destabilization of charge separated states via $\Delta\psi$ (38, 172).

To directly test this possibility, millisecond timescale delayed fluorescence has been utilized to monitor PSII back-reactions *in vivo*. Delayed fluorescence (also referred to as delayed light emission) originates from repopulation of the excited P^* via recombination reactions from electrons already trapped by PSII (173, 174). Repopulation of P_{680}^* requires back-reaction from $^1[P_{680}^+Pheo^-]$, which can be generated by recombination from $P_{680}^+Q_A^-$. However, as discussed above, recombination from $P_{680}^+Q_A^-$ to $P_{680}^+Pheo^-$ generates both the singlet and triplet states, the latter of which forms with a higher yield (141). Therefore, monitoring the delayed fluorescence emission provides discreet information on the rate of PSII charge recombination as well as an estimate of the production of $^3[P^+Pheo^-]$ during these back-reactions. Along with the decreased frequency of forming $^1[P_{680}^+Pheo^-]$ via $P_{680}^+Q_A^-$ recombination relative to the triplet state, $^1[P_{680}^+Pheo^-]$ can directly decay to the ground state non-radiatively rather than through the energetically uphill repopulation of P^*. Although the emission of light as delayed fluorescence is approximately 100-fold lower than that of prompt fluorescence (175), its utility as a probe of

PSII recombination reactions *in vivo*. Utilizing delayed fluorescence as a probe of PSII recombination *in vivo* under environmental conditions can provide insight into mechanisms influencing PSII electron transfer reactions and photodamage *in vivo*, enhancing the capacity to predict stressors that will alter PSII photodamage rates through changes in electron recombination reactions.

4.3 Materials and Methods

4.3.1 Plant and growth conditions.

Arabidopsis thaliana plants were grown on soil at 21°C with 100 μmol photons $m^{-2}s^{-1}$ light under a 16:8 day:night cycle. Spectroscopic measurements were performed on plants three weeks after germination. *Arabidopsis thaliana* mutants lacking PsbS (*npq4*) (176) and violaxanthin de-epoxidase (*npq1*) (166) are both in the Col-0 background.

4.3.2 Spectroscopic measurements of delayed fluorescence, prompt fluorescence, and the electrochromic shift.

Measurements of chlorophyll fluorescence and the electrochromic shift were performed using a custom made spectrophotometer described previously (117) with modifications to utilize three detectors during each measurement. Individual detectors were used to measure electrochromic shift (ECS) transmission, the reference intensity of the measuring pulse prior to leaf absorption, and a photomultiplier tube (PMT) to measure both prompt and delayed fluorescence. Red actinic illumination was used in all experiments to minimize the effects of chloroplast movement on chlorophyll fluorescence parameters, as red light does not induce chloroplast movements (119). All measurements were performed under at room temperature under ambient conditions.

The ECS was measured at 520 nm using detectors positioned in line with the actinic and measuring light, and collected after passing through a BG18 bandpass filter as described previously (74). The amplitude and decay kinetics of the ECS were determined by fitting the dark interval relaxation kinetics to a first-order exponential decay to determine the total proton motive force (ECS_t) and the conductivity of the ATP synthase to protons (g_{H^+}) (74). The ECS was corrected for pigment variations by normalizing to the total chlorophyll per leaf area (36). Estimates of the redox state of Q_A (q_L) was determined 5 s, 15 s, and 30 s following each light transition (100).

Delayed chlorophyll fluorescence was measured using a PMT (R636-10, Hamamatsu, Inc.) with a commercially available socket assembly (C1392-57, Hamamatsu, Inc.). Delayed fluorescence was measured by interrupting the actinic illumination every 5 s with a 130 ms dark interval. During the 130 ms interval, data was sampled from the PMT every 200 us. The prompt fluorescence decay and ECS during the dark interval were measured simultaneously every 1ms with a 10 μs 520 nm measuring pulse. The timing and intensity of the measuring pulse were found to not alter the yield or kinetics of the delayed fluorescence signal.

4.3.3 Determination of delayed fluorescence yields.

Both delayed and prompt fluorescence originate from the same antenna pigments (177, 178), and therefore the relative yields of prompt and delayed fluorescence at a given time are equally impacted by the quenching processes occurring in the antenna at the time, e.g. the probability of measuring a photon emitted as delayed fluorescence is equal to the probability of measuring a photon emitted as prompt fluorescence under the same quenching conditions with the same detection unit. Therefore, the delayed fluorescence of each dark interval was normalized to the prompt fluorescence during the same dark interval by interpolating the prompt

fluorescence decay to each of the delayed fluorescence measurements in order to determine the yield of delayed fluorescence. The normalized delayed fluorescence signal was then integrated over the dark period to determine the delayed fluorescence yield. At each light intensity, a baseline offset was found to have occurred in the PMT proportional to the light intensity. Therefore the average of the last 5 measurements at each light intensity were subtracted from the calculated delayed fluorescence yields to proportionally correct each measurement for the offset caused by the actinic illumination.

4.4 Results

4.4.1 Abrupt increases in light intensity increase the yield of delayed fluorescence.

To determine the effect of light fluctuations on the delayed fluorescence yield (ΦDF), plants were subjected to a series of fluctuating actinic intensities, during which delayed fluorescence, prompt fluorescence, and ECS parameters were measured nearly simultaneously throughout the illumination period (Fig. 4.2). If P_{680}^* is repopulated via PSII recombination in the dark, relaxation to the ground state is accompanied by the release of the exciton back into the antenna pigment bed and can be measured as the delayed fluorescence signal if it is emitted as fluorescence by the antenna. The probability of measuring delayed fluorescence will not only depend upon the repopulation of P_{680}^*, but also upon the probability that after equilibration with the antenna pigments that excitation is not quenched but instead emitted as fluorescence. Therefore ΦDF can be determined by normalizing the delayed fluorescence to the prompt fluorescence at the same measurement time, as the probability of the antenna emitting a photon as fluorescence will be equivalent for both prompt and delayed fluorescence at the same given time.

As predicted by Davis et al. (36), rapid changes in light intensity produced short, rapid increases in the yield of delayed fluorescence when the light intensity is increased (Fig. 4.2A), indicating transient periods where PSII recombination reactions are increased. These increases in delayed fluorescence presumably arise from large, transient increases in $\Delta\psi$ across the thylakoid due to the low electrical capacitance of the thylakoid membrane (2, 20, 36). As can be seen from the *pmf* measured concurrently with the delayed fluorescence (Fig. 4.3B, D), increases in light intensity leads to a near instantaneous increase in the total *pmf*. While light fluctuations from one light intensity to a lower intensity were not expected to increase ΦDF due to the field induced recombination model, the rapid decrease in excitation pressure did not show a significant change in yield relative to the proceeding steady state yields even though the PSII excitation is rapidly decreased.

While it has been shown that photosynthesis is sensitive to light fluctuations (36, 60, 66, 75, 179), PSII photoinhibition is known to be linearly dependent upon the light intensity (78). As such, ΦDF was measured at 400 μmol $m^{-2}s^{-1}$ (Fig. 4.2B), approximately four times the growth light intensity, which is the average light intensity of the fluctuating light treatment. Similarly to the fluctuating light (Fig. 4.2A), upon the initial dark-light transition ΦDF increases before decreasing to near the detection limit. However, unlike under fluctuating light conditions, even at four times the growth light intensity and the same total quanta of the fluctuating light treatment, the yield of delayed fluorescence under constant light does not increase after the initial dark-light transition, and remains near the detection limit throughout the illumination period.

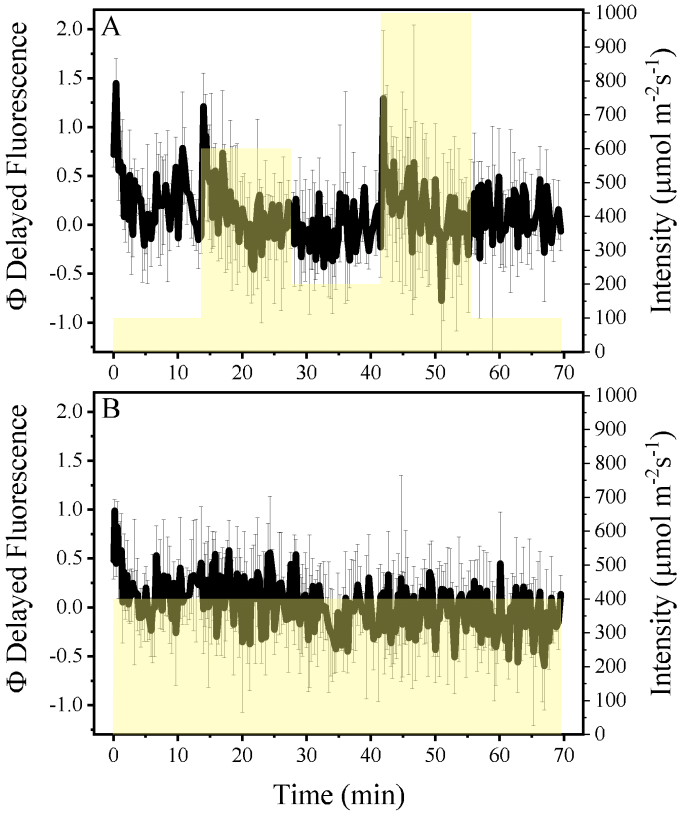

Figure 4.2: Fluctuating light increases PSII recombination *in vivo*.
Delayed and prompt fluorescence were measured every 5 s during 100 ms dark intervals in wild type Col-0 *Arabidopsis thaliana* leaves. For each dark interval, the yield of delayed fluorescence (ΦDF) was determined by integrating the DF/PF signals at each time point. During fluctuating light (A), transient increases in ΦDF occur immediately after each low light/high light transition. Following dark adaptation, light intensities were maintained for 14 minutes at 100, 600, 200, 1000, and 100 μmol $m^{-2}s^{-1}$ (yellow bars). Under static 400 μmol $m^{-2}s^{-1}$ light (B), ΦDF increases only during the initial induction following dark adaptation (mean ± s.d., *n*=4).

4.4.2 Alterations in the regulation of PSII Q_A redox state leads to changes in field-induced increases in recombination.

The redox state of Q_A, determining the availability of substrate Q_A^- for PSII recombination, is decreased *in vivo* by the regulation of exciton transfer from the antenna pigments to PSII cores by NPQ processes. In the Arabidopsis *npq4* mutant, which lacks PsbS, the pH-dependent q_E component of NPQ is severely compromised (176), leading to an increase

in the excitation pressure on PSII under conditions that would normally be limited by q_E. When subjected to fluctuating light (Fig. 4.3A), *npq4* plants experience increased PSII recombination relative to Col-0, reflected by a statistically higher ΦDF. Unlike Col-0, where the electric field induced increases in recombination decrease to background level in approximately 1-1.5 minutes, the increase in delayed fluorescence yield in *npq4* persists for 2.5-7 minutes. The long-lived increase in ΦDF does not appear to be a factor of an increase in light over growth intensity, as at 200 μmol $m^{-2}s^{-1}$ (2X growth light), there are not differences between *npq4* and Col-0, both of with have ΦDF near the detection limit. Arabidopsis plants lacking violaxanthin de-epoxidase (ΔVDE, *npq1*) are also deficient in q_E quenching, though not to the extent of *npq4* (180). Similarly to *npq4*, *npq1* plants exhibited a prolonged increase in ΦDF upon increases in light intensity, though the increased yield decreases faster than in *npq4* (Fig. 4.3C). Except for the transition from a dark adapted state, where the *pmf* stays elevated relative to Col-0, the total *pmf* between Col-0 and the two q_E mutants was not statistically significantly different following the light fluctuations (Fig. 4.3B, D), highlighting that the diminished ability to regulate excitation energy transfer to PSII to limit the accumulation of Q_A^- increases the recombination frequency relative to wild type.

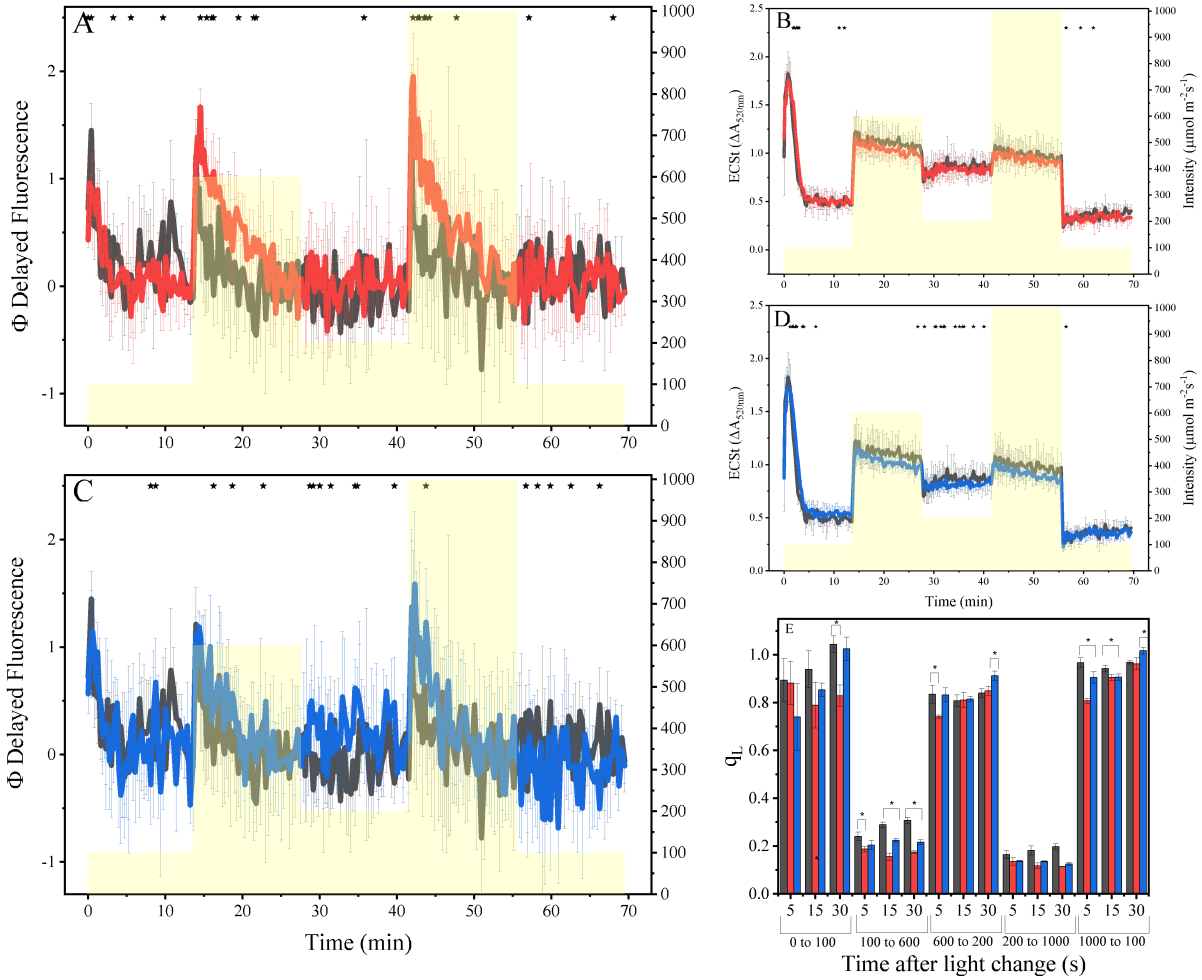

Figure 4.3: Deficiencies in pH-dependent NPQ antenna quenching increase ΦDF due to increased PSII center with Q_A^-.
Changes in PSII recombination due to an impaired ability to induce pH-dependent q_E quenching in Arabidopsis *npq4* (red, A and B) and *npq1* (blue, C, D) were assessed under fluctuating light. Light fluctuations were performed as in Fig. 4.2A. Col-0 (black) ΦDF from Fig. 4.1 shown as reference comparison. Increases in ΦDF are seen in both *npq4* (A) and *npq1* (B) following increases in light intensity (yellow bars). Total *pmf* (ECS_t) measured at the same time as ΦDF is not different from Col-0 following increases in light intensity in either *npq4* (B) or *npq1* (D). The fraction of centers with Q_A^- (q_L) (E) measured 5, 15, and 30s after each light fluctuation is increased in the q_E mutants after transitions to high light (mean ± s.d., n = 3-4) (*, $p < 0.05$).

4.5 Discussion

Regulation of the light reactions of photosynthesis is critical for prolonged maintenance of photosynthetic capacity. Multiple mechanisms have evolved to regulate PSII excitation pressure (57, 62) to limit photooxidative damage and the reduced photosynthetic capacity

incurred when reaction centers are inactivated (65). Even with multiple levels of regulation, photodamage to PSII leads to the rapid turnover of the reaction center D1 protein (128, 181).

While multiple mechanisms have been proposed to explain the cause(s) of PSII photodamage, most center on the generation of reactive oxygen species by PSII side reactions and subsequent protein damage caused by ROS (56, 67, 68). In the *Arabidopsis thaliana minira* mutants (36), alteration of the steady-state $\Delta\psi$ lead to an increase in $^1O_2$ production and PSII damage *in vivo*. This leads to the proposal that a large $\Delta\psi$ *in vivo*, experienced near continuously in *minira* mutants as well as during light fluctuations in wild type plants, can modulate PSII back reactions *in vivo* and increase the frequency of Q_A^- recombination, increasing $^1O_2$ production. To test this hypothesis, we utilized the yield of delayed fluorescence as a direct indicator of changes in PSII recombination reactions *in vivo*.

The high (near unity) quantum efficiency of PSII under optimal conditions leads to successful charge separation for nearly every exciton that reaches PSII (182). While the redox intermediates within PSII are poised to favor forward electron transfer reactions through successive decreases in midpoint potential and an increase in the donor/acceptor distance, non-productive recombination reactions can occur. While various methods have been employed to understand the energetics of PSII chemistry through mediating recombination reactions (reviewed in 174), we have utilized delayed fluorescence emission to monitor PSII recombination as it allows intact plants to be measured over prolonged periods of time. This allowed near continuous measurements of delayed fluorescence during the course of light treatments on intact Arabidopsis leaves.

Dark repopulation of P_{680}^* and emission of light as delayed fluorescence was observed in all plants tested upon a shift to higher light intensity (Figs. 4.2 and 4.3). Upon a high light

transition, an immediate increase in the *pmf* is observed (Fig. 4.3), which is predominantly held as $\Delta\psi$ due to the low electrical capacitance of the thylakoid membrane (2, 36, 167). The rapid increases in ΦDF decrease within minutes to minimal levels, likely responding to the combinatorial impact of a change in *pmf* partitioning that occurs from ion transport across the membrane to dissipate $\Delta\psi$ as well as the onset of q_E to decrease the fraction of PSII with Q_A^- (167).

The generation of $^1O_2$ via PSII acceptor side back reactions and ^3P production has been shown to correlate with the rate of PSII photoinhibition (36, 183, 184). Traditionally, PSII photoinhibition has been thoroughly characterized in a light-dependent manner, with increased photoinhibition being linearly dependent upon the light intensity (78). Similarly, $^1O_2$ generation has been shown to linearly increase with actinic illumination (185), and the overall $^1O_2$ production to be dependent upon the $P_{680}^+Q_A^-/P_{680}^+Pheo^-$ free energy gap (184, 185). Contrary to a linear light induction curve, the fluctuating light used above oscillates between lower and higher light intensities. As suggested by Davis et al. (36), low to high light transitions favoring transient $\Delta\psi$ spikes increased the yield of PSII recombination. However, an increase in irradiance over growth light (200 μmol $m^{-2}s^{-1}$ vs. 100 μmol $m^{-2}s^{-1}$) did not produce differences in ΦDF, consistent with a lack of $\Delta\psi$ generation during these transitions.

Photosynthesis is sensitive to natural light conditions, where rapid transitions in the available light intensity can occur throughout the day (66). Intriguingly, under standard laboratory (i.e. non-fluctuating) light conditions, the lack of regulating PSII excitation in *npq1* and *npq4* does not lead to a seed yield penalty, however growth under variable light in either a laboratory or field decreased seed yield in both *npq1* and *npq4* (66). During fluctuations in actinic light, both *npq1* and *npq4* experienced sustained increases in ΦDF relative to Col-0 (Fig.

4.3), indicating prolonged increased yields of PSII recombination through the indirect, ^3P generating pathway, potentially explaining the sensitivity of these mutants to long term growth under fluctuating light.

The electron transfer reactions of PSII occur on the order of nanoseconds to microseconds (164), requiring coordination of reactions occurring on both the donor and acceptor sides of PSII at different rates. The acceptor side of PSII is limited by the rate of Q_A^-/Q_B electron transfer and the availability of oxidized PQ to bind at the Q_B site (186). As ΔpH increases during photosynthesis, the turnover rate of cytochrome b_6f decreases (11, 12), shifting the PQ/PQH_2 ratio and limiting the availability of oxidized PQ, increasing the lifetime of Q_A^- if the quinol exchange range becomes limiting, and increasing the likelihood of $P_{680}^+Q_A^-$ recombination. Concurrently, activation of q_E via PsbS and VDE protonation as the ΔpH increases should relieve some of the excitation pressure on PSII by quenching excitation energy in the antenna pigments rather than transferring it to PSII. However, the electron transfer rates of PSII are much faster than the buildup of ΔpH (2), which initially requires overcoming the buffering capacity of the thylakoid membrane (22). The generation of $\Delta\psi$, however, can be generated rapidly, as the low electrical capacitance of the thylakoid membrane leads to the generation of $\Delta\psi$ via the trans-thylakoid movement of electrons by the reaction centers (20). This kinetic mismatch in the timing of $\Delta\psi$ generation versus the pH-dependent processes that help protect reaction centers from over-excitation (discussed in 167) has been proposed to increase the rate of PSII photodamage and the generation of $^1O_2$ (36). Utilizing delayed fluorescence as a direct indicator of the yield of PSII recombination, the same conditions that generate rapid increases in *pmf* and $\Delta\psi$ leads to enhanced PSII recombination. While the generation of ΔpH lags compared to $\Delta\psi$ generation following a high-light fluctuation, results from mutants deficient

in q_E induction suggest that regulating the PSII excitation pressure in steady-state to minimize the concentration of Q_A^- decreases ΦDF immediately after the light fluctuation due to the decreased availability of states available to recombine.

Recombination from Q_A^- in PSII is dependent upon four main factors: 1) presence of Q_A^-, 2) the redox state of the quinone at the Q_B site, 3) the free energy difference between $P_{680}^+Q_A^-$ / $P_{680}^+Pheo^-$, and 4) the PSII donor side existing in an S-state capable of recombination from Q_A^- (S2 and S3) (187). Under continuous illumination, due to PSII misses that fail to advance the S-state (17), within seconds the population of PSII within the leaf will become asynchronous between the S-states, with each state being approximately equally represented. This leads to approximately 50% of PSII being capable of Q_A^- recombination at a given time due to the donor side availability (167). The free energy difference between $P_{680}^+Q_A^-$ and $P_{680}^+Pheo^-$ is modulated by the trans-thylakoid $\Delta\psi$, which can be modified by the movement of ions across the membrane, but is large following abrupt changes in light intensity (2, 36). These large $\Delta\psi$ spikes are enough to increase the recombination frequency from Q_A^- in wild type Col-0 plants (Fig. 4.1A).

Characterization of specific recombining states during near–continuous measurements of delayed fluorescence, both as performed in the current work or with a phosphoriscope, has proven difficult to ascertain. Due to the total PSII population becoming asynchronous between both the PSII donor side and acceptor side reduction states, multiple pathways for Q_A^- recombination, as well as the continuation of forward electron transfer during the measuring interval if the Q_B site is not blocked, delayed fluorescence under continuous illumination is the result of a multitude of states (188). The rates of PSII donor side electron transfer reactions vary depending on the S-state, however, within 10 μs 80% of PSII will progress from $Y_ZP_{680}^+$ to

$Y_Z^+P_{680}$ (189), and within ~1 ms reduction of Y_Z^+ and advancement of the S-state will have occurred (16). Therefore, after the first 1-2 measurements of delayed fluorescence obtained in our experiments, re-population of P_{680}^* will require equilibrium reactions occurring on both on the donor and acceptor sides of PSII. However, the yield of delayed fluorescence represents a fraction of the total PSII recombination routes, which primarily proceed via repopulation of $P680^+Pheo^-$ (145) (Fig 4.1). When recombining via this indirect route, van Mieghem et al. found 66-75% of Q_A^- recombination occurred by generation of $^3[P_{680}^+Pheo^-]$ rather than $^1[P_{680}^+Pheo^-]$ at 20K (141). Using an externally applied electric field, de Grooth and van Gorkom found that only ~3% of Q_A^- recombination repopulated P_{680}^*, suggesting that the delayed fluorescence measured in the current experiments during light fluctuations represents less ~5% of the total yield of PSII recombination, the majority of which is presumed to proceed via a route that favors generation of ^3P. Under these conditions, if the assumption that a large increase in ^3P and $^1O_2$ generation is correct (36), an increase in PSII photodamage should occur rapidly after a low light to high light transition, which could explain the increased sensitivity of photosynthesis to natural light conditions. As delayed fluorescence can be measured non-destructively, an increased understanding of the relationship between delayed fluorescence and PSII damage will allow the targeted manipulation of photosynthetic processes to minimize the detrimental effects of the $\Delta\psi$-mediated increases in PSII recombination following light fluctuations while maintaining photosynthetic efficiency.

4.6 Acknowledgements

Work performed by G.A.D. and D.M.K. was supported by the US Department of Energy (DOE), Office of Science, Basic Energy Sciences (BES) under award number DE-FG02-91ER20021.

Chapter 5

Natural variation in the activation and dissipation of nonphotochemical quenching in *Arabidopsis thaliana* subjected to fluctuating light

Geoffry A. Davis, John E. Froehlich, David M. Kramer

5.1 Abstract

Improving the productivity of photosynthesis in natural, field conditions requires an improvement in our current understanding of factors mediating the onset and dissipation of photosynthetic regulatory processes. Feedback regulation of the light reactions of photosynthesis is mediated by the buildup and subsequent dissipation of a light-induced pH gradient (ΔpH) across the thylakoid membrane, which subsequently induces nonphotochemical energy quenching (NPQ) by light-harvesting antenna pigments and downregulates the rate of electron transfer through the photosystems. The kinetics of ΔpH generation and photosynthetic repression combined with the kinetics of removing these limitations leads to periods of light availability that are not being optimally utilized by photosynthesis for energy production during natural, fluctuating light conditions. To identify genetic factors mediating variation in the onset, dissipation, and total steady-state NPQ during light fluctuations, the *Arabidopsis thaliana* multi-parent advanced generation inter-cross (MAGIC) population was subjected to high-throughput chlorophyll fluorescence phenotyping under fluctuating light to determine time-dependent quantitative trail loci (QTL) for photosynthetic regulation. QTL were identified that showed a time-dependent emergence and disappearance relative to fluctuations in light intensity. Utilizing this high-throughput phenotyping approach combined with the identified QTL, alterations in the onset and dissipation of NPQ could be manipulated to improve plant productivity in field conditions.

5.2 Introduction

Increases in crop productivity during the 20th century, the so-called Green Revolution, were driven primarily by increases in the partitioning of biomass into grain (harvest index) (190). While improvements in biomass accumulation depend upon the initial utilization of light by photosynthesis, increases in the efficiency of photosynthesis have not necessarily been improved with breeding for improved harvest index (191). Meeting the increased global demand for food by 2050 (192) will require substantial gains in yield per hectare; with crop breeding producing plants that are near the theoretical upper limit in harvest index (193, 194), improvements in photosynthetic efficiency, which is far from the theoretical biological limit (103, 195), are promising avenues for the improvement of crops (196).

Under natural field conditions, plants experience a variety of biotic and abiotic factors that influence their overall productivity. Photosynthetic light reactions, although dependent on light availability for the production of cellular energy, are sensitive to the abrupt fluctuations in light intensity experienced in nature from cloud cover and other physical shading that lead to rapid changes in the incident light intensity upon a leaf (60, 66, 75, 197). These light intensity fluctuations have been shown impact the yield of plants relative to laboratory conditions under which the basic processes of photosynthesis are usually studied (66), necessitating an improvement of our understanding of the operation and regulation of the light reactions under natural, environmental light conditions.

Oxygenic photosynthesis in cyanobacteria, algae, and plants utilizes multiple membrane–localized protein complexes in series to mediate the overall transfer of electrons from water to ferredoxin and NADPH (127). The electron transfer processes of photosynthesis are stabilized and coupled to the transfer of protons into the thylakoid lumen, generating a light-induced proton

gradient (ΔpH) across the thylakoid membrane which is utilized by the thylakoid ATP synthase to generate ATP (76). As the thylakoid lumen pH decreases, protonation of lumen-exposed residues of specific proteins leads to feedback regulation of the light reactions (61). Quinol oxidation by cytochrome b_6f decreases 10-fold per pH unit decrease, which slows electron transfer from photosystem II (PSII) (11, 12). Thermal dissipation of absorbed light as heat, termed nonphotochemical quenching (NPQ), is initiated via protonation of violaxanthin de-epoxidase (VDE) (62) and protonation of the thylakoid membrane protein PsbS (7). The activation of these NPQ processes decreases the excitation pressure on PSII, preventing the over-reduction of PSII electron acceptors (6).

While the ΔpH component of the thylakoid proton motive force (*pmf*) has well-established roles in regulating photosynthesis, the electric field ($\Delta\psi$) component of the *pmf* has emerged as a regulator of electron transfer reactions *in vivo* as well (36). As the thylakoid $\Delta\psi$ increases, the vectorial transfer of electrons within protein complexes becomes increasingly thermodynamically destabilized (38), leading to an increase in reverse electron transfer reactions (i.e. recombination), which can result in the production of reactive oxygen species (ROS) and damage to the photosystems resulting in photoinhibition (56). While NPQ results in photoprotection of PSII by decreasing the excitation pressure, the kinetics of ΔpH generation are limited by the high buffering capacity of the thylakoid lumen (22), while $\Delta\psi$ generation kinetics are much more rapid due to the low electrical capacitance of the membrane (20). These kinetic imbalances result in short periods where $\Delta\psi$ dominates the *pmf* composition prior to ΔpH buildup, which in turn leads to a kinetic lag prior to NPQ activation where PSII is subject to high excitation pressure as well as increased probability of electron recombination and ROS production (167).

While the kinetics of NPQ induction may limit plant productivity by increasing the probability of $\Delta\psi$-induced photoinhibition, the NPQ dissipation kinetics have also been suggested to limit plant productivity (125, 198, 199). Upon a decrease in light intensity, slow relaxation of NPQ can limit productivity by sustaining exciton quenching in the antenna and limiting PSII excitation under the now low-light condition, leading to less net photosynthesis during the time required to dissipate the quenching state. Genetic engineering of NPQ has proven one potential avenue to circumvent these losses and improve biomass accumulation (126).

The dramatic impacts that the kinetic mismatches between light intensity changes and NPQ induction/dissipation impose on plant productivity may have lead, over evolutionary time, to divergence in the kinetics of NPQ induction and deactivation. Variation in the overall capacity for NPQ exists between species (200, 201), between shade vs. high-light grown plants (201, 202), and within a species (203-205). However, while natural variation in photosynthetic parameters has been observed within different genetic accessions of the same species, a correlation between maximum rates of photosynthesis (measured under saturating light) does not necessarily correlate positively with biomass accumulation (206-208). Although the accumulation of biomass by photosynthetic organisms begins with the transformation of light into chemical energy, the multifaceted regulatory processes determining the partitioning of accumulated biomass could be one explanation for inconsistent or lack of correlation between photosynthesis and biomass accumulation (209). However it is also possible that the technical challenges of measuring photosynthesis under non-static conditions have limited the potential identification of genetic factors influencing photosynthesis under more natural conditions. To overcome this hurdle, we have utilized chlorophyll fluorescence imaging under dynamic environmental conditions (75) in combination with an *Arabidopsis thaliana* multi-parent

advanced generation inter-cross (MAGIC) population (210) to map natural variation in photosynthesis during light fluctuations. This approach allows photosynthetic measurements to be obtained simultaneously for dozens of plants under non-static conditions that can be precisely manipulated to rapidly phenotype plants under environmental conditions.

5.3 Materials and Methods

5.3.1 Plant materials and growth conditions

The MAGIC lines (210) as well as the 19 parental accessions were obtained from the Arabidopsis Biological Resource Center (http://abrc.osu.edu). Freshly propagated seed was generated for each genotype prior to phenotyping experiments. Plants were grown on soil at 100 μmol photons $m^{-2}s^{-1}$ for a 16 hr/8 hr light/dark photoperiod at 22°C.

5.3.2 Chlorophyll fluorescence imaging

Whole-plant chlorophyll fluorescence imaging was performed on plants 21 days after germination in custom outfitted growth chambers (75). To minimize any potential phenotypic variation due to any differences in circadian rhythm, all plants were imaged during the first hour of illumination during the photoperiod. During the imaging procedure, the light intensity was maintained for 10 min at each of five intensities: 100, 600, 200, 1000, and 100 μmol photons $m^{-2}s^{-1}$ (Fig. 5.1). For high-density measurements of steady-state fluorescence (ϕ_f), F_o was measured after 8 hours of dark adaptation corresponding to the "night" portion of the photoperiod. At the start of the light portion of the photoperiod, measurements of ϕ_f were obtained every 30 s over the course of illumination. The fluorescence yield in the light (ϕ_{fs}) at each point was normalized to the minimum fluorescence yield in the dark F_o. Variations in quantitative trait loci (QTL) identification did not occur with or without normalization to F_o.

For measurements of photosynthetic parameters derived from pulse amplitude modulation, F_V/F_M was measured 30 s prior to the onset of actinic illumination after 8 hours of dark adaptation corresponding to the "night" portion of the photoperiod. Upon actinic illumination, chlorophyll fluorescence images were acquired every 2 min during illumination using saturation pulse methods (75, 211).

At least three replicates for each genotype were measured for each of the photosynthetic parameters was used for QTL analysis. Due to lack of germination or survival until the measuring stage, some MAGIC genotypes did not have at least three biological replicates, and the genotypes were removed from subsequent QTL analysis. Fluorescence images were analyzed using open source image analysis software (ImageJ, NIH) modified in house to calculate photosynthetic parameters over whole plant averages.

5.3.3 QTL analysis

QTL analysis was performed using the HAPPY R software package as in Kover et al. (210). Briefly, this utilizes experimentally tested markers and a genetic map to construct a mosaic genome for each MAGIC genotype. Using a probabilistic hidden Markov model, the founding genotype for each of 1,260 single nucleotide variations (SNPs) is tested and determined for each genotype. The likelihood of no QTL being present at each phenotype was tested by fitting a fixed-effect linear model corresponding to a standard genome scan with up to 18 degrees of freedom and performing an analysis of variance (ANOVA). The statistical significance for each locus was summarized by the negative logarithm of the ANOVA p-value ($-\log_{10} p$). The genome-wide significance thresholds were independently determined for each measurement time point by repeating the genome scan with 1000 permutations. To minimize the identification of

false positive QTL, a QTL was only defined if the $-\log_{10}p$ value of the locus was above the permutation derived 95% genome-wide significance threshold.

5.3.4 Protein extraction and western blotting

Analysis of proteins with known involvement in NPQ was performed using total leaf protein from each of the 19 *Arabidopsis thaliana* MAGIC founder accessions as in Livingston et al. (118). To minimize variation in protein levels due to developmental differences between leaves (212), and due to the variation in number of rosette leaves between the different accessions, proteins were extracted from three pooled biological replicates of the youngest fully expanded leaf of 21 day-old plants. Determination of specific proteins was performed by separating 20 μg of total leaf proteins via SDS-PAGE under reducing conditions followed by transfer to polyvinylidene difluoride (PVDF) membrane. NPQ proteins were analyzed using antibodies specific to each protein, anti-violaxanthin de-epoxidase (α-VDE, PHY1225S, PhytoAB, Redwood City, CA, USA), anti-zeaxanthin epoxidase (α-ZEP, PHY0499, PhytoAB, Redwood City, CA, USA), and anti-PsbS (α-PsbS, AS09 533, Agrisera, Vannas, Sweden) and detected using an anti-rabbit secondary antibody conjugated to alkaline phosphatase. Samples were developed via addition of BCIP/NBT substrates (Sigma-Aldrich, St. Louis, MO, USA).

5.4 Results

5.4.1 Variation in NPQ kinetics between Arabidopsis accessions

To discover underlying factors regulating photosynthesis under conditions mimicking natural field stresses, NPQ was assayed over time during the course of fluctuating light in the 19 *Arabidopsis thaliana* founding accessions used to create the Arabidopsis MAGIC population (Fig. 5.1) (210, 213). Rather than compare the extent of NPQ in low light versus high light, the dynamics of NPQ changes during fluctuating light was used, as the rapid induction of NPQ

following an increase in irradiance is proposed to decrease the probability of PSII photodamage (167) while the rate of NPQ relaxation when the irradiance decreases will alter the capability of PSII to utilize the non-inhibitory light (126). During light fluctuations (Fig. 5.1A), the 19 MAGIC founders display a range of NPQ phenotypes that represent all three potential scenarios for NPQ regulation: fast vs. slow induction, fast vs. slow dissipation, and altered steady-state NPQ extent (Fig. 5.1B, C).

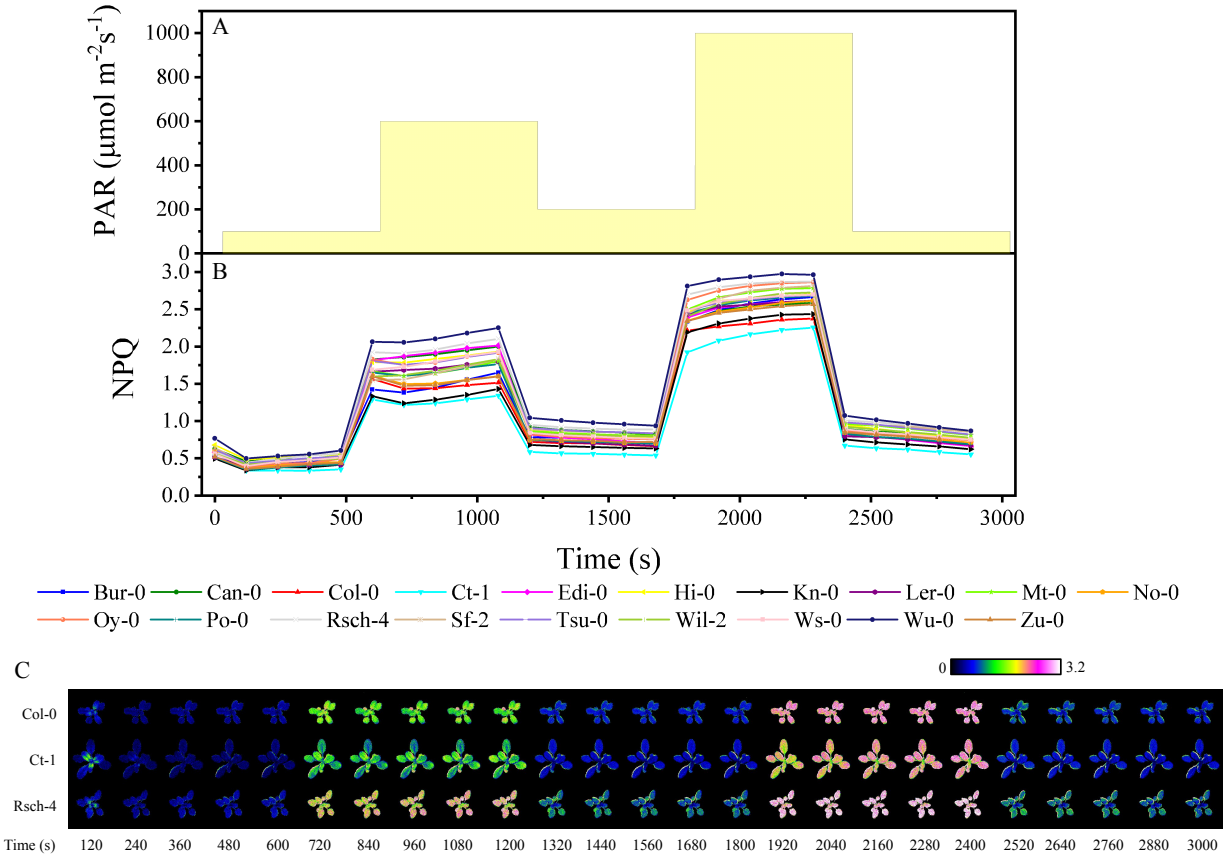

Figure 5.1: The 19 founding parental accessions of the Arabidopsis MAGIC population display a range of NPQ induction and dissipation kinetics during fluctuating light. Chlorophyll fluorescence imaging of NPQ in the 19 founding *Arabidopsis thaliana* accessions of the MAGIC population was carried out during fluctuations in light intensity (A). Light intensities were: 100, 600, 200, 1000, and 100 µmol photons $m^{-2}s^{-1}$. The light was maintained at each intensity for 10 min. Following dark-adaptation corresponding to the normal "night" portion of the photoperiod, the maximum quantum yield of PSII photochemistry was measured to obtain F_M. The imaging period corresponded to the first hour of light during the photoperiod, with the first 5 measurements (100 µmol photons $m^{-2}s^{-1}$) occurring at growth light intensity. NPQ was measured every 2 min in the light (B) averaged over whole plant rosettes (C). For visualization,

Figure 5.1 (*continued*): standard deviation is not shown in B (mean, n = 6-8). False-color NPQ images of representative plants of 3 accessions (Col-0, Ct-1, Rsch-4) over the course of the imaging procedure (C) show time-dependent changes in NPQ as well as total NPQ differences.

To investigate potential causes of NPQ variation among the founding genotypes, differences in the key regulators of the pH-dependent component of NPQ (q_E) were assessed (Fig. 5.2). Alterations in PsbS or VDE within the population could explain differences in the ability of plants to induce NPQ (8), while alterations to zeaxanthin epoxidase (ZEP) to relieve xanthophyll dependent q_E quenching component could be a factor in dissipating NPQ at low light (166). Among the 19 founding accessions, the protein content of PsbS is approximately the same among each plant (Fig. 5.2C), suggesting that differences in NPQ extents during the fluctuating light experiment is not due to alteration of PsbS protein levels. However, enzymes responsible for the conversion of xanthophyll pigments do show differences in the level of protein content relative to total leaf protein (Fig. 5.2A, B). Although measured at different developmental stages (21 day-old plants in current work versus ~12 day-old plants in Gan et al.), Gan et al. also found that the transcripts for VDE (*AT1G08550*) and ZEP (*AT5G67030*) were differentially expressed within the founding accessions, suggesting that regulation of the VDE/ZEP ratio *in vivo* represents at least one strategy that natural populations have evolved to regulate NPQ (47). Contrary to RIL analysis where phenotypic differences require binary parental differences, most of the founding accessions show no differences in the protein levels of any of the three components, but still have altered NPQ dynamics relative to the other accessions, indicating that multiple factors influence the extent and rates of NPQ and will be present in the MAGIC population.

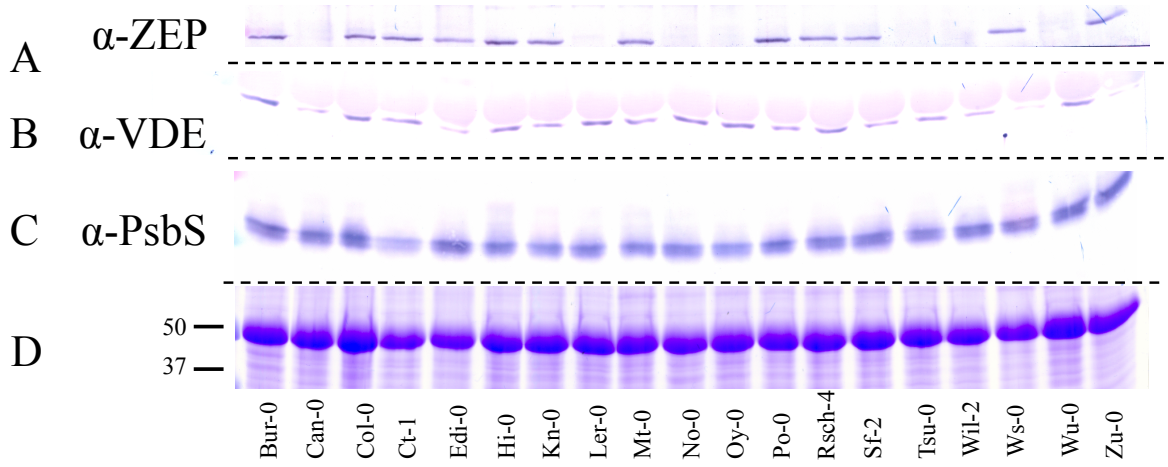

Figure 5.2: Differential content of proteins mediating the rapidly reversible pH-dependent q_E component of NPQ Arabidopsis accessions.
Total leaf protein was extracted from 21 day-old plants for each Arabidopsis founding accession. Protein levels for ZEP (A), VDE (B), and PsbS (C) were determined from 20 µg of total leaf protein using antibodies specific to each protein. Coomassie staining of 20 µg of the same protein samples (D) was performed to ensure equal loading across samples.

5.4.2 QTL mapping of NPQ kinetics

To elucidate factors influencing photosynthetic responses to fluctuating light, 379 MAGIC genotypes were measured under the same conditions as the founding accessions (Fig. 5.3). Similar to the founders, different dynamics of NPQ induction, dissipation, and total extent were present across the phenotypes of the MAGIC population. QTL analysis of NPQ identified 71 QTLs above the genome-wide 95% significance threshold at 19 of the measurement times (Fig. 5.4, Table 5.1). Over the entire experimental period, this represents 21 unique QTL identifications, as the same QTL could be identified multiple times at different measurements. During the measuring period, the photochemical yield of PSII (ΦII) was determined at the same time as NPQ, however no QTLs were observed for ΦII. Transformation of the ΦII data to estimate linear electron flow ($\Phi II * PAR * PSII_{cross\text{-}section} * A$), estimating a $PSII_{cross\text{-}section}$ of 0.5 and leaf absorptivity of 0.8 for all plants, also yielded no QTL. Future analyses measuring the

specific light absorption parameters for each MAGIC genotype could better define QTL related specifically to PSII photochemistry.

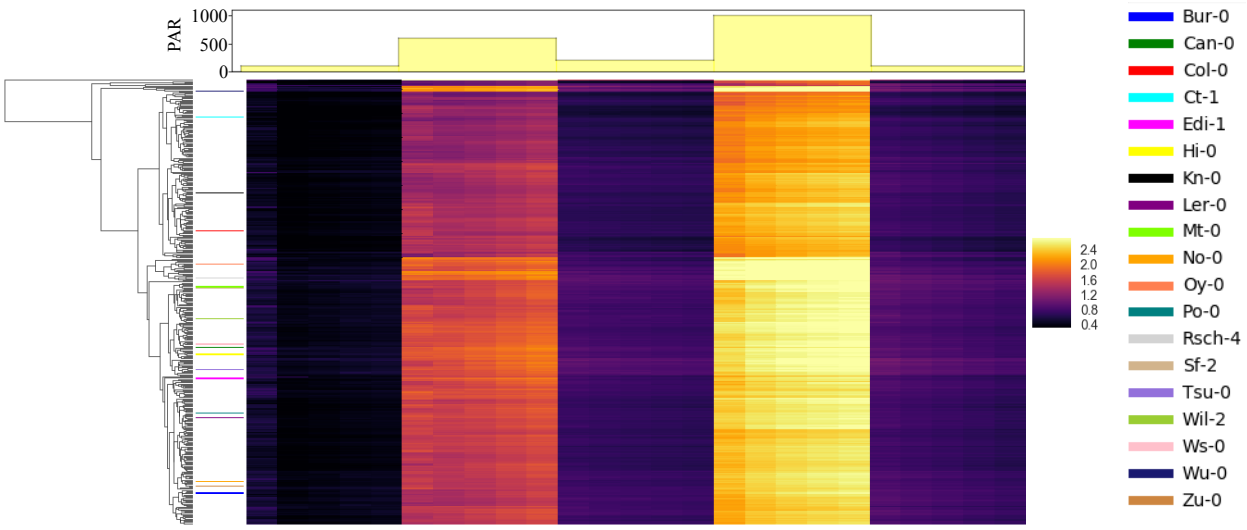

Figure 5.3: Kinetics of NPQ responses in the Arabidopsis MAGIC population under fluctuating light.
Whole plant chlorophyll fluorescence imaging was used to phenotype the NPQ responses of the MAGIC population over a fluctuating light time course. The mean NPQ at each time point of n = 3-4 biological replicates of each MAGIC genotype is clustered by the total phenotype over the course of the experiment. The position of each founding accession is indicated by the colored bar next to the dendrogram. Accession colors are the same as in Fig. 5.1.

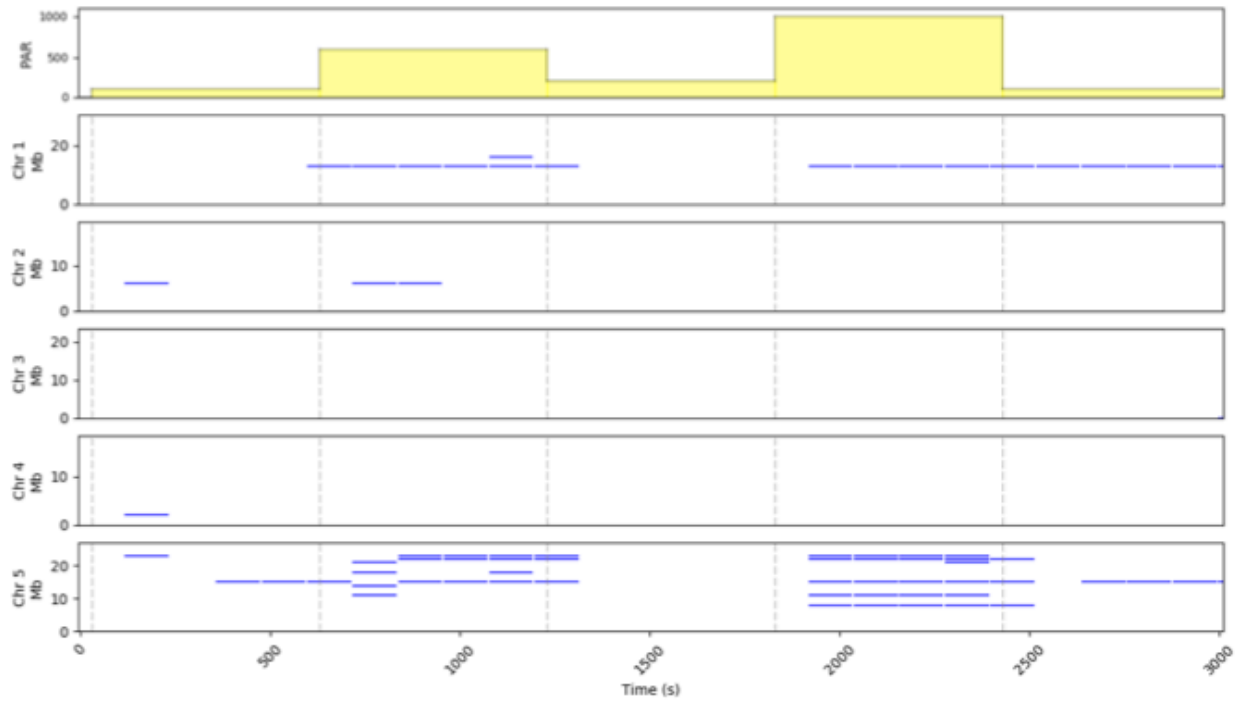

Figure 5.4: Time-dependent identification of NPQ QTL during fluctuating light in Arabidopsis MAGIC lines.
QTL analysis of NPQ phenotypes of the MAGIC population were determined every 2 min during a fluctuating light treatment, resulting in 5 NPQ measurements per light intensity. The peak positions of QTLs with $-\log_{10}p$-values $\geq$ 95% genome-wide significance are shown relative to the position in the *Arabidopsis thaliana* Col-0 reference genome at the time at which they are significant until the next measured time point. Vertical dashed lines indicate the changes in light intensity.

5.4.3 QTL mapping of rapid responses to light fluctuations

Utilizing pulse amplitude modulated (PAM) fluorometry, the extent of different photosynthetic processes can be determined (211). However, the high intensity of light used during the saturating pulses to fully reduce PSII limits how rapidly the pulses can be applied; as the interval between saturation pulses decreases, damage to photosynthetic proteins begins to occur, decreasing the ability to measure how rapidly processes change following a disturbance. Another limitation of using chlorophyll fluorescence as a probe of photosynthesis is that information about the function of PSII is obtained while other processes of the light reactions,

pmf extent and composition, b_6f turnover, PSI redox state, and ATP synthase activity, are not directly observed.

To increase the capacity to measure rapid changes in photosynthesis, the yield of chlorophyll fluorescence (ϕ_f) was measured every 30 s during the fluctuating light regime separately from experiments measuring NPQ. The ϕ_f is determined by the rate constant of fluorescence relative to the rate constants for all of the processes that compete for excitation energy:

$$\phi_f = \frac{k_f}{k_f + k_{qE} + k_{qI} + k_{qT} + k_{pc}[q_L] + k_{isc} + k_d} \quad \text{(Eq. 1)}$$

where k_f is the rate of fluorescence, k_{qE} the rate of energy-dependent nonphotochemical quenching q_E, k_{qE} the rate of photoinhibitory nonphotochemical quenching q_I, k_{qT} the rate of state transition nonphotochemical quenching, k_{isc} the rate of non-radiative decay due to intersystem crossing, k_d the rate of non-radiative decay, k_{pc} the rate of photochemistry, and q_L the fraction of PSII open reaction centers (PSII with oxidized Q_A). In higher plants, quenching due to antenna state transitions appears to be minimal (155).

k_{qE} is a composite rate of the various processes that mediate the total q_E response, the rates of pH-regulated PsbS quenching, pH-mediated activation of VDE and conversion of violaxanthin into zeaxanthin, and the activity of zeaxanthin epoxidase to convert zeaxanthin to violaxanthin (146). The redox state of Q_A (q_L) is also regulated by pH-dependent downregulation of cytochrome b_6f turnover, increasing the fraction of Q_A^- as the thylakoid lumen pH decreases.

The photosynthetic *pmf* is composed of both a ΔpH and $\Delta\psi$ (2, 39, 135, 137), with the partitioning regulated by the activity of thylakoid ion channels (34, 35). While the ΔpH has a well-studied role in regulating photosynthesis to limit photodamage, a large $\Delta\psi$, which occurs following light fluctuations to a higher light intensity, has been shown to promote photodamage

through reactive oxygen species production (36). Therefore the kinetics of $\Delta\psi$ dissipation and ΔpH generation to mediate photosynthetic regulation following light transitions could be a limiting factor for plant productivity (167). Therefore, although the photosynthetic *pmf* cannot be imaged directly, changes in ϕ_f following light fluctuations will respond proportionally to changes in ΔpH generation or relaxation due to the direct regulation of quenching processes by the lumen pH.

To follow the response of ϕ_f to light fluctuations, ϕ_f was imaged every 30 s during the fluctuating light treatment (Fig. 5.5) in 422 MAGIC genotypes. To differentiate ϕ_f variation due to time–dependent kinetic changes due to light fluctuations from intrinsic variations in fluorescence yield which could have shifted amplitudes but identical kinetics, ϕ_f was normalized to the first measurement after each light intensity shift to determine how rapidly each genotype responded to changes in light intensity. Changes in ϕ_f did not follow a simple exponential decay over time, limiting the ability to fit the ϕ_f response of each genotype and utilize the corresponding decay rate as a phenotype for QTL analysis. Instead, the amplitude of ϕ_f change from the normalized t_0 of each light change was determined (Fig. 5.5A), and this phenotype used to determine time-dependent QTL (Fig. 5.5C). As the composition of the thylakoid ΔpH changes following a light fluctuation, the dual regulation of q_E and b_6f turnover mediates the concentration of PSII with Q_A^-, which is reflected in the amplitude of ϕ_f - $\phi_{f\,t0}$, with how rapidly ϕ_f changes from the light fluctuation proportionally reflecting how rapidly ΔpH changes.

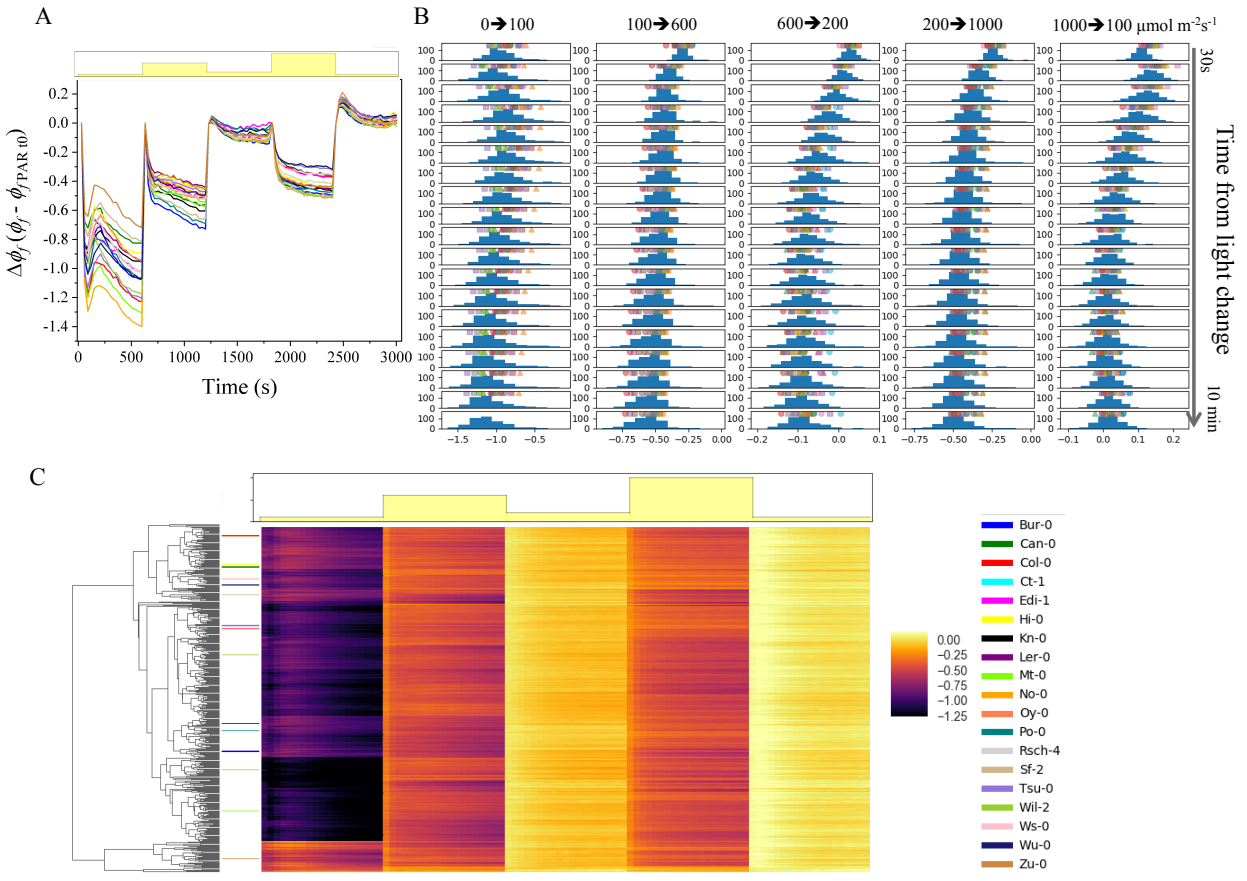

Figure 5.5: The kinetics and amplitude of chlorophyll fluorescence quenching varies among the Arabidopsis MAGIC founders and MAGIC population during light fluctuations. Using the same light intensity changes as the NPQ measurements (Fig. 5.1) chlorophyll fluorescence (ϕ_f) was measured every 30 s in the Arabidopsis founding accessions (A). To quantify the changes in ϕ_f over time, each ϕ_f measurement was normalized to the first measurement within each light intensity. Variation in the phenotypes within the MAGIC population (B) for the change in ϕ_f show broad distributions from the mean of the population as well as shifts in the mean of the population upon transitions from high light to low light. The mean of each founding accession is indicated by colored symbols above each histogram. The mean ϕ_f - $\phi_{f\,t0}$ at each time point of n = 3-4 biological replicates of each MAGIC genotype is clustered by the total phenotype over the course of the experiment (C). The position of each founding accession is indicated by the colored bar next to the dendrogram. For visualization, the first measurement at each light intensity, used for normalizing, are not shown (all values = 1). Colors of each founding accession are maintained throughout each of A, B, and C.

Analysis of the variation in the change in ϕ_f over time identified 129 QTL above the genome-wide 95% significance threshold (Fig. 5.6, Table 5.2). Over the course of the fluctuating light regime, multiple instances occur of a QTL centered at the same locus, narrowing the total

number of QTL to 57 unique QTL peaks. Surprisingly, most of the identified unique QTL (50/57) were only identified upon the recovery from high light to low light. Following transitions from lower light intensity to high light, only seven unique QTL peaks were identified. While increases in light intensity were presumed to lead to the greatest changes in the ϕ_f relative to the initial values, a possible explanation for the large differences between the conditions leading to QTL identification is the variation in mean phenotypes within the MAGIC population under these conditions. The distribution of phenotypes over time is less divergent from the mean following low light to high light fluctuations than the transition from high light to low light (Fig. 5.5B). During the initial induction of photosynthesis from overnight dark adaptation, an early responding QTL centered at 5.14 Mb on chromosome 1 was identified at 90-180 s following the beginning of the photoperiod, with a late responding photosynthetic induction QTL identified at 9-9.5 min after the beginning of the photoperiod, potentially identifying QTL representing constitutive photosynthetic differences between the genotypes. The transition to 1,000 μmol photons $m^{-2}s^{-1}$, above the normal light saturation for Arabidopsis, identified five closely localized QTL on chromosome 1, cumulatively explaining ~10-15% of the total phenotypic variance at each time point.

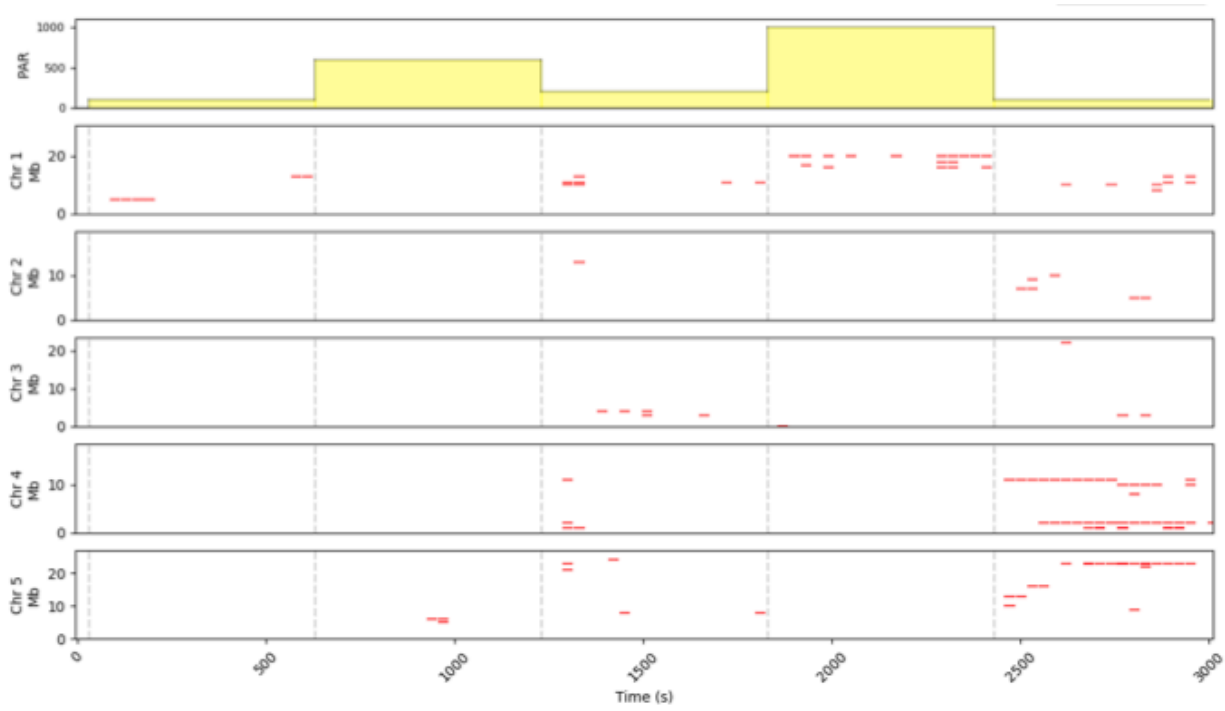

Figure 5.6: Time-dependent changes in the amplitude of ϕ_f quenching during light fluctuations.
To determine how rapidly photosynthesis responds to changes in light intensity, QTL analysis was performed on the amplitude of ϕ_f every 30 s relative to the first ϕ_f measurement at each light intensity. The peak positions of QTLs with $-\log_{10} p$-values $\geq$ 95% genome-wide significance are shown relative to the position in the *Arabidopsis thaliana* Col-0 reference genome at the time at which they are significant until the next measured time point. Vertical dashed lines indicate the times at which the light intensity changes.

5.5 Discussion

The utility of *Arabidopsis thaliana* as a genetic model allows many phenotypes to be analyzed and understood at the genetic level (214). The major contributors regulating the light reactions of photosynthesis in the green lineage have been well characterized at the molecular level *in vitro* and *in vivo*, with mutants in *Arabidopsis thaliana* and *Chlamydomonas reinhardtii* identifying many of the specific proteins involved in pH-mediated regulation of photosynthesis (reviewed in 5). However, while analysis of knockout mutants for specific genes clearly identifies the role of that gene in physiological processes, the *in vivo* regulation in terms on/off

rates, total extent, and changes due to acclimation are lost when using only knockouts to understand the regulation (215). Under most laboratory conditions, where plants are undergoing minimal if any stress, the regulatory significance underpinning physiological processes can be lost. While laboratory conditions have helped dissect many of the molecular mechanisms of NPQ regulation of photosynthesis (166, 176, 216), understanding the regulation of photosynthesis in environmental conditions requires further progress (60, 75).

The regulation of excitation pressure reaching PSII complexes within leaves is mediated by feedback regulation from the light-generated ΔpH, modulating the redox state PSII electron acceptors by decreasing excitation energy transfer via q_E activation and decreasing electron transfer via regulation of b_6f quinol oxidation (5). These processes help minimize the amount of PSII photodamage, which irreversibly inhibits the damaged PSII complex and requires degradation and *de novo* synthesis of a new D1 subunit to maintain photosynthetic integrity (128). While protease activities and *de novo* protein synthesis have an energetic (ATP) cost, of larger concern to plant productivity is the decreased photosynthetic capacity that occurs while the PSII complex is inactive (65). Therefore, while downregulation of photosynthesis via NPQ and electron transfer regulation limit the output of photosynthesis, the evolution of these photoprotective processes and distribution among photosynthetic organisms suggests that the benefits of dampening photosynthesis outweigh the negative growth productivity due to enhanced photodamage (66).

The protection of photosynthesis under high light intensities, however, limits photosynthetic capabilities as soon as the light intensity decreases (195, 199). Conversely, due to kinetic limitations that limit the buildup of ΔpH versus $\Delta\psi$ (2), slow induction of q_E is suggested to increase PSII photodamage (36, 167). Taken together, improvements in overall photosynthetic

yields could be accomplished by increasing the rate at which q_E induction occurs while simultaneously increasing q_E dissipation when it is no longer necessary.

To identify factors that would allow both of these conditions to occur, variation in *Arabidopsis thaliana* natural populations was utilized to identify QTL involved in rapid photosynthetic responses to light fluctuations. Although many of the core genes of the photosynthetic reaction centers are encoded by the chloroplast genome, natural diversity of nuclear genomes has been utilized to improve the understanding of photosynthetic regulation and factors that are involved in modulating the basic bioenergetics processes of the light reactions (203, 204, 217). Whole plant chlorophyll fluorescence phenotypes for both NPQ as well as changes in ϕ_f quenching identified time-dependent fluctuating light QTL in the Arabidopsis MAGIC population (Figs. 5.4, 5.6). While variations in NPQ leading to the identification of QTL were present at most time points (Fig. 5.4), changes in ϕ_f relative to the light intensity fluctuations primarily appear after high light to low light transitions (Fig. 5.6). The time-dependence of these QTL relative to when the light fluctuates is most apparent for how rapidly ϕ_f quenching changes. After a light fluctuation from 600 to 200 μmol photons $m^{-2}s^{-1}$, early QTL on chromosomes 1, 2, 4, and 5 appear within 30 s of the light intensity change and are not longer present 90 s after the light decrease, while late QTL on chromosomes 3 and 5 emerge after ~3 minutes (Fig. 5.6).

Using a multi-parent population, as was done in the present work, the increased nucleotide polymorphism and crossover frequency obtained using genome-wide association panels is approached, while maintaining limited genome structure complexity provided by recombinant inbred lines (RIL) (210, 213). As such, within the MAGIC founding accessions, variation in NPQ processes is likely mediated in part by *cis*-regulation of the protein levels of

VDE and ZEP (Fig. 5.2) in some founding accessions as well as the progeny. Altering the ratio of VDE/ZEP has been suggested as a strategy to alter the apparent pH-dependency of q_E activation (47), allowing rapid q_E activation with decreased ZEP levels such as is seen in Wu-0 (Figs. 5.1, 5.2). Further analysis of xanthophyll pigment compositions and pigment changes over time will help clarify how much the altered protein contents mediate NPQ phenotypic variation. Similar to other analyses of natural populations, variation in PsbS protein content does not explain the variation in NPQ within the founding accessions (205, 215). Advantageously, relative to a RIL population, using a multi-parental mapping population the phenotypes are not limited to binary phenotypes of the two parental lines used to generate a RIL population. As such, although VDE/ZEP levels may be one route used to modulate NPQ dynamics in Arabidopsis, founding accessions with no apparent differences in the level of NPQ component proteins still display a range of NPQ phenotypes (e.g. Ct-1 vs. Rsch-4 in Fig. 5.1), suggesting that other factors regulating NPQ could be identifiable within the QTL.

The identification of photosynthetic QTL in a time-dependent manner during fluctuating light conditions helps shift the strategies for identifying mechanisms utilized to maintain photosynthesis under natural conditions (197). Although genomic variation within the founding accessions of the MAGIC population is similar to the global Arabidopsis nucleotide diversity, polymorphisms that generate amino acid changes in protein coding genes are underrepresented (213). Within the MAGIC founders, 80% of the predicted proteins have major isoform frequencies of at least 15/19, meaning that each polymorphism causing a functional protein change is likely to be represented in 4 or fewer of the 19 lines, effectively recapitulating RIL population structures of bi-allelic changes at most loci conferring function protein changes. Further refinement of the QTL mapping regions combined with candidate allele testing will help

provide evidence for alleles within the population contributing to rapid photosynthesis responses to light fluctuations. These can subsequently be tested for their impact on yield under field conditions (126) as well as used in marker-assisted breeding in crop species to boost the initial steps of plant anabolism in order to increase yield (218). Incremental improvements in the initial steps of photosynthesis under dynamic light conditions facilitated by the rapid, high-throughput phenotyping utilized in this study, combined with genetic identification and implementation of beneficial alleles, will help drive increases in plant productivity.

5.6 Acknowledgements

We would like to thank Linda Savage for initial discussions on planting strategy for screening the MAGIC population. Work performed by G.A.D. and D.M.K. was supported by the US Department of Energy (DOE), Office of Science, Basic Energy Sciences (BES) under award number DE-FG02-91ER20021.

Table 5.1: List of QTLs identified for time-dependent NPQ responses to fluctuating light.

Time (s)	Intensity (μmol photons $m^{-2}s^{-1}$)	Time since light change (s)	Peak Position	Chromosome	90% Confidence Interval		logP
					lower	upper	
120	100	120	2902408	4	2502452	3006991	3.76
120	100	120	6647145	2	6154830	6647145	3.60
120	100	120	23247571	5	23246477	23248880	3.60
360	100	360	15047966	5	14694836	15439873	4.38
480	100	480	15047966	5	13832746	15750717	4.63
600	100	600	13201153	1	11850168	13832436	4.49
600	100	600	15047966	5	13832746	15439873	4.28
720	600	120	13090494	1	11399904	17679130	6.88
720	600	120	14935674	5	12512173	16337385	6.40
720	600	120	21864028	5	19397857	23246248	5.64
720	600	120	18166800	5	17341215	18765193	4.43
720	600	120	11067093	5	10525858	12183470	4.00
720	600	120	6025716	2	5666979	6647145	3.94
840	600	240	22023651	5	17538410	23247571	7.26
840	600	240	13090494	1	11399904	17876791	6.92
840	600	240	15298812	5	12426277	16429063	6.61
840	600	240	23798428	5	23705688	23810485	4.32
840	600	240	6025716	2	5666979	6647145	4.18
960	600	360	22023651	5	19106920	23247571	7.01
960	600	360	15048131	5	12576814	16337385	6.42
960	600	360	13090494	1	11412672	17679130	5.83
960	600	360	23798428	5	23705688	23810485	4.27
1080	600	480	22023651	5	18266506	23247571	7.02
1080	600	480	15298812	5	12576814	16429063	6.55
1080	600	480	13090494	1	11412672	16134927	5.74
1080	600	480	16872100	1	16251782	17679130	4.48
1080	600	480	23798428	5	23559674	23810485	4.49
1080	600	480	18166800	5	17461027	18241539	3.99
1200	600	600	15298812	5	12681159	16429063	6.36
1200	600	600	22023651	5	18278591	23247571	6.78
1200	600	600	13090494	1	11466186	15525445	5.12
1200	600	600	23798428	5	23559674	23810485	4.25
1920	1000	120	13201153	1	11037687	17876791	7.87
1920	1000	120	15048131	5	12512173	16337385	5.34
1920	1000	120	22023651	5	21021855	22610276	4.96
1920	1000	120	8978323	5	8360127	9481360	4.09

Table 5.1 (*continued*):

Time (s)	Intensity (μmol photons $m^{-2}s^{-1}$)	Time since light change (s)	Peak Position	Chromosome	90% Confidence Interval		logP
					lower	upper	
1920	1000	120	23098340	5	22697296	23246477	3.67
2040	1000	240	13201153	1	11070732	17876791	8.34
2040	1000	240	15048131	5	12512173	16186076	5.36
2040	1000	240	22023651	5	21021921	22610276	4.92
2040	1000	240	8978323	5	0	9481360	4.18
2040	1000	240	11067093	5	10525702	12183470	3.90
2040	1000	240	23098340	5	22697296	23246477	3.79
2160	1000	360	13201153	1	11159782	17876791	8.16
2160	1000	360	15048131	5	12681159	16186076	4.90
2160	1000	360	22023651	5	21243342	22610276	4.56
2160	1000	360	8978323	5	0	9481360	3.91
2160	1000	360	11067093	5	10525858	11613391	3.61
2160	1000	360	23246248	5	22697296	23246477	3.58
2280	1000	480	13201153	1	11159782	17876791	7.97
2280	1000	480	15048131	5	12681159	15750933	4.79
2280	1000	480	22023651	5	21701553	22397775	4.48
2280	1000	480	8978323	5	0	9481360	3.80
2280	1000	480	21398449	5	21243342	21398449	3.61
2280	1000	480	23246248	5	22697296	23246477	3.59
2280	1000	480	11067093	5	10525858	11613391	3.54
2400	1000	600	13201153	1	11399904	17876791	7.53
2400	1000	600	15048131	5	12681159	15750933	4.76
2400	1000	600	22023651	5	21701553	22397775	4.39
2400	1000	600	8978323	5	8810481	9481360	3.72
2520	100	120	13540607	1	12892642	13832436	3.81
2640	100	240	13832180	1	12208016	13832436	4.28
2640	100	240	15298812	5	14935674	15439873	3.77
2760	100	360	13832180	1	12208016	14160452	4.52
2760	100	360	15298812	5	14694836	15439873	3.98
2880	100	480	13201153	1	11850168	16128552	4.82
2880	100	480	15298812	5	13832746	15439873	4.36
3000	100	600	13201153	1	12208016	14160452	4.46
3000	100	600	15298812	5	13832746	15439873	4.06

Table 5.2: List of QTLs identified for time-dependent changes in ϕ_f amplitude.

Time (s)	Intensity (μmol photons $m^{-2}s^{-1}$)	Time since light change (s)	Peak Position	Chromosome	90% Confidence Interval		logP
					lower	upper	
90	100	90	5148226	1	5095611	5206772	3.66
120	100	120	5148226	1	4992111	5206986	3.81
150	100	150	5148226	1	4947328	5290747	3.99
180	100	180	5148226	1	4992111	5206986	3.73
570	100	570	13201153	1	12208016	13201153	3.64
600	100	600	13201153	1	12208016	13201153	3.76
930	600	330	6416383	5	6415440	6708110	3.59
960	600	360	6416383	5	6222069	6899955	3.91
960	600	360	5996219	5	5829162	5996219	3.62
1290	200	90	2902408	4	2695395	4197470	4.66
1290	200	90	10423538	1	8974265	10841461	4.38
1290	200	90	1585202	4	1243348	2510399	4.39
1290	200	90	23798306	5	23300895	24816019	3.84
1290	200	90	11412672	1	11159782	12093566	3.67
1290	200	90	21701553	5	21398449	21701553	3.68
1290	200	90	11268000	4	10659145	11470264	3.62
1320	200	120	13979309	2	13319028	15244621	4.40
1320	200	120	13090494	1	11655539	13217139	3.67
1320	200	120	1553591	4	1243348	1585202	3.65
1320	200	120	10423538	1	8974265	10547614	3.50
1320	200	120	11412672	1	11215275	11553534	3.50
1380	200	180	4073395	3	3679535	4073911	3.93
1410	200	210	24295906	5	23903662	24816019	3.50
1440	200	240	8541646	5	7315346	8978323	3.87
1440	200	240	4073911	3	3991976	4073911	3.78
1500	200	300	4073911	3	3679286	4073911	4.06
1500	200	300	3344784	3	2903318	3610515	3.93
1650	200	450	3344784	3	2903318	3580015	4.02
1710	200	510	11466186	1	11159852	11850168	3.49
1800	200	600	11215275	1	11159782	11553534	3.66
1800	200	600	8810481	5	8001188	9628385	3.63
1860	1000	60	297887	3	276915	819034	4.08
1860	1000	60	965025	3	819454	965025	4.08
1890	1000	90	20135840	1	19502363	20310446	3.99
1920	1000	120	20135840	1	19502363	20510777	4.54

Table 5.2 (*continued*):

Time (s)	Intensity (μmol photons $m^{-2}s^{-1}$)	Time since light change (s)	Peak Position	Chromosome	90% Confidence Interval		logP
					lower	upper	
1920	1000	120	17679130	1	17148697	19434966	3.91
1980	1000	180	20135840	1	19502363	20310446	4.00
1980	1000	180	16871886	1	16134927	16872100	3.74
2040	1000	240	20135840	1	19778790	20171160	3.60
2160	1000	360	20135840	1	19778790	20310446	3.65
2280	1000	480	20135840	1	19502363	20310446	3.94
2280	1000	480	16871886	1	16134927	17179544	3.82
2280	1000	480	18943964	1	17474215	19397107	3.67
2310	1000	510	20135840	1	19502363	20310446	4.06
2310	1000	510	16871886	1	16134927	16872100	3.80
2310	1000	510	18629407	1	17474215	19434966	3.74
2340	1000	540	20135840	1	19502363	20310446	3.97
2370	1000	570	20135840	1	19502363	20310446	3.81
2400	1000	600	16871886	1	16134927	16872100	3.66
2400	1000	600	20135840	1	19778790	20310446	3.64
2460	100	60	11268000	4	9952391	11786400	4.46
2460	100	60	13832746	5	12681159	15439873	4.23
2460	100	60	10525702	5	9628385	10910094	3.86
2490	100	90	11268000	4	9199369	13576430	6.97
2490	100	90	7722418	2	7544501	7722418	4.33
2490	100	90	13832746	5	13597330	17130805	4.09
2520	100	120	11268000	4	9199369	13670757	7.88
2520	100	120	16351105	5	14973938	17907459	4.14
2520	100	120	7722418	2	7643146	7722418	3.94
2520	100	120	9579136	2	9249015	10127320	3.70
2550	100	150	11268000	4	9199369	13670757	7.07
2550	100	150	16947516	5	15744761	18048533	3.93
2550	100	150	2902408	4	2803493	2907158	3.80
2580	100	180	11577769	4	9630919	13078462	6.48
2580	100	180	10127320	2	9249015	11142985	3.92
2580	100	180	2902408	4	2803493	3001617	3.85
2610	100	210	11268000	4	9630919	12900417	6.25
2610	100	210	2902408	4	2803493	3001617	3.75
2610	100	210	10423538	1	9973305	10720291	3.67

Table 5.2 (*continued*):

Time (s)	Intensity (μmol photons $m^{-2}s^{-1}$)	Time since light change (s)	Peak Position	Chromosome	90% Confidence Interval		logP
					lower	upper	
2610	100	210	22606285	3	21773266	22627912	3.65
2610	100	210	23248880	5	23247571	23248880	3.45
2640	100	240	11577769	4	9630919	12900417	5.26
2640	100	240	2902408	4	2803493	3129542	4.13
2670	100	270	11577769	4	9952391	11984761	4.70
2670	100	270	2902408	4	2695395	3924075	4.59
2670	100	270	23705688	5	23253768	24357567	3.94
2670	100	270	23247571	5	23246477	23248880	3.64
2670	100	270	1585202	4	1243079	1585202	3.63
2700	100	300	2902408	4	2695395	3924075	4.75
2700	100	300	11580131	4	9952391	11878383	4.36
2700	100	300	23798306	5	23253768	24357567	3.90
2700	100	300	1585202	4	1241726	1585202	3.70
2700	100	300	1132454	4	1125812	1132454	3.63
2730	100	330	2907158	4	2803493	3924075	4.07
2730	100	330	11580131	4	9952391	11878383	4.01
2730	100	330	23300895	5	23246477	24295906	3.96
2730	100	330	10423538	1	9516375	10720291	3.57
2760	100	360	2902408	4	2695395	4253906	4.63
2760	100	360	10777260	4	9952391	11878383	4.41
2760	100	360	23798428	5	23253768	24357567	3.87
2760	100	360	23247571	5	23246477	23247571	3.76
2760	100	360	1585202	4	1241726	1585202	3.61
2760	100	360	1585202	4	1241726	1585202	3.61
2760	100	360	3991976	3	2967872	4073911	3.56
2760	100	360	1132454	4	1125812	1237935	3.56
2790	100	390	10777260	4	9952391	11822736	4.44
2790	100	390	2902408	4	2803493	3535626	3.84
2790	100	390	5666979	2	3939356	6025716	3.74
2790	100	390	8482332	4	8177688	8482332	3.55
2790	100	390	9105481	5	8894881	9481360	3.53
2790	100	390	23810485	5	23705451	24357567	3.53
2820	100	420	23810485	5	23248880	25069184	4.33

Table 5.2 (*continued*):

Time (s)	Intensity (μmol photons $m^{-2}s^{-1}$)	Time since light change (s)	Peak Position	Chromosome	90% Confidence Interval		logP
					lower	upper	
2820	100	420	5666979	2	3939356	6647145	3.79
2820	100	420	2902408	4	2803493	3924075	3.75
2820	100	420	23247571	5	23246477	23247571	3.72
2820	100	420	10302880	4	10043931	10977564	3.62
2820	100	420	22697296	5	21864028	23012412	3.58
2820	100	420	3344784	3	2903318	3578598	3.53
2850	100	450	23798428	5	23253768	24816019	4.10
2850	100	450	2907158	4	2803493	3924075	3.98
2850	100	450	10423538	1	9516375	11553534	3.87
2850	100	450	10302880	4	10042015	10777260	3.67
2850	100	450	8974265	1	8969354	9362052	3.61
2880	100	480	2907158	4	2695395	4933872	4.80
2880	100	480	1585202	4	1241726	1613368	3.65
2880	100	480	13217139	1	12646750	13217139	3.63
2880	100	480	1132454	4	1128719	1237935	3.61
2880	100	480	23798428	5	23396016	24357567	3.63
2880	100	480	11412672	1	11159782	11466186	3.58
2910	100	510	2907158	4	2588286	5291404	5.72
2910	100	510	1585202	4	1238602	2441130	4.02
2910	100	510	23798428	5	23400832	24357567	3.69
2910	100	510	1132454	4	1128719	1132454	3.57
2940	100	540	2907158	4	2695395	4803015	4.37
2940	100	540	13217139	1	12646750	13217139	3.58
2940	100	540	11003558	4	11001770	11470264	3.58
2940	100	540	10777260	4	10613944	10977564	3.55
2940	100	540	23798428	5	23705451	24357567	3.54
2940	100	540	11412672	1	11159782	11412672	3.46
3000	100	600	2907158	4	2803493	3924075	3.78

Chapter 6

Conclusions and future directions

Geoffry A. Davis

6.1 Abstract.

The work in this chapter is to contextualize the concepts presented within this dissertation as a whole as well as in the larger field of photosynthesis research. Questions that have emerged from the work presented in this dissertation and how they can be projected forward to better understand how photosynthesis occurs within cells in natural environments are discussed.

6.2 Conclusions.

Advances in crop yield over the last century have not occurred simultaneously with increases in photosynthetic capacity (see Chapter 5). While this is not in itself a problem, the discrepancies between theoretically maximal photosynthetic yields of the light reactions versus the actualized potentials of crop species provides opportunities to nudge photosynthesis closer to optimum potentials. While the core electron transfer processes of the photosynthetic light reactions are well characterized from atomistic to mechanist levels, many of the regulatory factors that act on the core electron and proton transfer complexes are poorly understood in their cellular and physiological context. This is due to a number of factors, including, but not limited to, long growth cycles of certain species, technical challenges of certain measurements, as well as a small (but expanding) repertoire of plant model organisms.

To overcome some of these challenges, high-throughput photosynthetic phenotyping instruments have been developed by multiple groups to gain mechanistic insight from large datasets of responses to stress (see Chapters 2 and 5). Expanding the methodologies used to measure photosynthetic parameters, combined with the increasing amount of genetic information available for photosynthetic organisms, can lead to improvements in our understanding of what processes limit photosynthesis under natural conditions, how those processes are regulated, and if there are ways that it could be improved to minimize those limitations.

6.3 Future directions.

The large impact that $\Delta\psi$ imposes on photosystem (PSII) electron transfer reactions (see Chapters 2, 3, 4) leads us to believe that photosynthetic organisms have evolved mechanisms to minimize the photodamage potential of $\Delta\psi$ and increases in recombination. The core electron transfer proteins of PSII are highly conserved across oxygenic photosynthetic organisms (219), as well as being mechanistically and structurally conserved between PSII and anoxygenic reaction centers (220). However, unlike eukaryotic photosynthetic organisms, which usually posses a single copy of the *psbA* gene to produce D1, cyanobacteria often possess multiple *psbA* genes (219). A potential advantage of maintaining multiple *psbA* genes is the ability to tune PSII activity for environmental conditions. As such, specific mutations in D1 have been associated with alteration in the D1 pheophytin hydrogen bonding network, leading to alterations in PSII recombination and photodamage (145, 184). Whether these canonical "high light" *psbA* isoforms are adaptive advantages to minimize PSII recombination in fluctuating light environments could provide one avenue to minimize light fluctuation induced PSII photodamage.

Unlike cyanobacteria, higher plant chloroplast genomes contain a single *psbA* gene, preventing any direct modulation of the free-energy gaps via protein subunit replacement. However, the rapid and consistent increases in PSII recombination during fluctuating light (Chapter 4) leads to the proposal that organisms have either evolved mechanisms to minimize the severity of rapid $\Delta\psi$ increases, and/or that mechanisms have evolved to rapidly respond to the oxidative stress that occurs after $\Delta\psi$ mediated increases in reactive oxygen species. While it appears that regulating the redox state of Q_A via nonphotochemical quenching (NPQ) is one mechanism to minimize the duration of increased PSII recombination yields (Chapter 4), other mechanisms may exist to minimize photodamage from fluctuating light (Chapter 3).

Identification of QTL that appear in a time-dependent manner (Chapter 5) may represent alleles responsible for mediating immediate versus late responses to fluctuating light, which could be tested via allele swapping between ecotypes via CRISPR/Cas9 targeted gene replacement. To more specifically identify mechanisms related to PSII recombination, delayed fluorescence could be measured in the *Arabidopsis thaliana* multi-parent advanced generation inter-cross (MAGIC) population under fluctuating light. Similarly to the prompt chlorophyll fluorescence analysis (Chapter 5), a camera with a higher sensitivity could be used to measure changes in the yield of delayed fluorescence following fluctuating light treatments to map QTL responsible for differences in PSII recombination yield as well as differences in how rapidly the increased PSII recombination is relieved. This would be complementary to the analysis already performed, as overlapping QTL could provide better mechanistic insight for the causative allele.

The sensitivity of NPQ mutants to fluctuating light (Chapter 4) suggests that regulation of steady-state NPQ quenching is important to minimize the levels of Q_A^- in the event of an immediate increase in light intensity. If Q_A^- is minimized, potential photosynthetic productivity is limited, however, the plant may remain better protected during light fluctuations. The cost benefit tradeoffs for plant yield in rapidly regulating Q_A^- via NPQ could also be analyzed in the MAGIC population. Under short term fluctuations, variations in the kinetics and extent of NPQ existed within the MAGIC founding accessions as well as the mapping population. Long-term fluctuating growth under dynamic, fluctuating light utilizing chlorophyll fluorescence imaging during vegetative growth would allow both QTL analysis of photosynthetic and yield parameters over developmental stages, but also provide a large, genetically diverse but naturally occurring dataset of evolutionarily tuned photosynthetic responses to fluctuating growth. This would

provide information to suggest whether protection from $\Delta\psi$-induced photodamage or rapid relaxation of NPQ provide greater yield benefits under natural light conditions.

APPENDIX

A.1 Description of DeltaPsi.py code for simulating the light reactions of photosynthesis.[3]

DeltaPsi.py is a program for first-order, exploratory simulations of the effects of capacitance, proton buffering capacity and counter-ion movements on the thylakoid proton motive force (*pmf*), trans-thylakoid electric field ($\Delta\psi$), stroma-lumen pH difference (ΔpH**)**, linear electron flow (LEF), the ratio of ATP/NADPH produced by LEF, the activation and recovery of the lumen pH-dependent form of nonphotochemical quenching (NPQ), termed q_E, photosystem II (PSII) activity and recombination rates and $^1O_2$ production.

The code is based on the simulations in (2) because simulations using this code were validated by the review process in both the original publication and in a separate, follow up publications (146). The following describes changes in this version.

1) The code was updated to run on modern, open-source, cross-platform and freely-available Python platform. Examples below were performed using the open source Jupyter notebook platform (www.jupyter.org), but code can also be run on any Python platform.
2) To provide the maximal transparency and allow others to repeat and modify our code and simulations, the full code is made available on GitHub (www.github.com/protonzilla/Delta_Psi_Py) with extensive annotation. Readers are encouraged to fork the code and add their modifications, improvements and tests. It is hoped that these open source tools will provide the capacity to extend or modify and extend and validate the simulations, especially to test new hypotheses.

[3] This section originally published as electronic supplemental material for:
Davis, GA, Rutherford, AW, & Kramer, DM. 2017 Hacking the thylakoid proton motive force for improved photosynthesis: modulating ion flux rates that control proton motive force partitioning into $\Delta\psi$ and ΔpH. Philos Trans R Soc Lond B Biol Sci, 372(1730). doi: 10.1098/rstb.2016.0381

3) A more efficient ODE solver, odeint (scipy.integrate.odeint: https://docs.scipy.org/doc/scipy-0.18.1/reference/generated/scipy.integrate.odeint.html), was used to increase the speed and accuracy of the simulations.

3) Several improvements in the formulae were made to include several recent advances, as outlined in the following.

a) Explicit simulation of Q_A and plastoquinone (PQ) redox states were included to simulate PSII quantum yields and to account for the effects of $\Delta\psi$ on PSII recombination reactions.

b) The lumen pH-dependence of the xanthophyll cycle and the protonation of PsbS were updated to simulate the pH dependencies reported in Takizawa et al. (47) and Zaks et al. (146).

c) The effects of lumen pH on plastoquinol (PQH_2) oxidation at the cytochrome b_6f complex were included to account for the observed "photosynthetic control" of electron transfer by the lumen pH, using the model and pK_a values reported in (47).

d) The driving force for ATP synthase reaction (and thus the efflux of protons) is now taken as being equal to the difference in the proton motive force (*pmf*) and the free energy storage in ATP (ΔG_{ATP}) divided by n, the stoichiometry of H^+ translocated through the ATP synthase over the number of molecules of ATP formed, as described in more detail below.

e) A more realistic model for the kinetics of the cytochrome b_6f complex was developed, to account for the thermodynamic and kinetic effects of *pmf* components on these reactions. In particular, the code now considers the b_6f complex to be fully reversible, so that both $\Delta\psi$ and ΔpH alter the equilibrium constant.

f) An equation was derived and implemented to calculate the quantum efficiency of PSII based on NPQ and Q_A redox state.

A.1.2 Description of updated code.

The following describes the equations used in the simulations, focusing especially on those that extend the previous versions. Details of the calculations are embedded in the code and described in the code and the text.

A.1.2.1 The *pmf* and its partitioning into Δψ and ΔpH.

The theory and equations used to describe *pmf* components are essentially as described in earlier work by Cruz et al., (2) and Zaks et al. (146), with two updates. First, the new code allows for addition of antiporters or symporters, as described in the code for KEA3, which is proposed to act as a K^+/H^+ antiporter in the thylakoid membrane (28, 158):

the KEA reaction looks like this:

$$H^+_{lumen} + K^+_{stroma} \rightleftharpoons H^+_{stroma} + K^+_{lumen} \quad \text{(Eq. 1)}$$

where H^+_{lumen}, H^+_{stroma}, K^+_{lumen}, and K^+_{stroma} represent protons in the lumen and stroma and K^+ ions in the lumen and stroma, respectively. The reaction is electroneutral, so the forward reaction will depend on $\Delta[H^+]$and $\Delta[K^+]$ as:

$$v_{KEA} = v_{KEA}\,([H^+_{lumen}] \cdot [K^+_{stroma}] - [H^+_{stroma}][\,[K^+_{lumen}]) \quad \text{(Eq. 2)}$$

v_KEA = k_KEA*(Hlumen*Kstroma - Hstroma*Klumen) (Python)

where H^+_{lumen} (Hlumen), H^+_{stroma} (Hstroma), K^+_{lumen} (Klumen), K^+_{stroma} (Kstroma) are the concentrations of free H^+ and K^+ ions in the lumen and stroma, respectively.

Next, the following is used to calculate K^+ flux, which depends on the permeability of electrogenic K^+ channels and the KEA reaction. The permeability of K^+ through the K^+ channel

is perm_K. The K^+ flux through the electrogenic channel depends on both the K^+ concentration gradient and the electric field, i.e. $\Delta\tilde{\mu}_{K^+}$,

$$\Delta\tilde{\mu}_{K^+} = .06(\log_{10}\left(\frac{[K^+]_{stroma}}{[K^+]_{lumen}}\right) - \Delta\psi \text{ (Eq. 3)}$$

K_deltaG=(.06*np.log10(Kstroma/Klumen) - Dy) (Python)

where K_deltaG $= \Delta\tilde{\mu}_{K^+}$ and Dy=$\Delta\psi$, the transthylakoid electric field (stroma-lumen) in V. The instantaneous net change in lumen $[K^+]$ per unit time is given by:

$$\frac{d[K^+]}{dt} = v_{KEA} + P_{K^+}\Delta\tilde{\mu}_{K^+}([K^+]_{lumen} + [K^+]_{stroma})/2 \text{ (Eq. 3)}$$

net_Klumen = perm_K * K_deltaG*(Klumen+Kstroma)/2 + v_KEA (Python)

where net_Klumen = $\frac{d[K^+]}{dt}$. In this simplified form, we assume that the flux through the K^+ channel is proportional to the driving force and the average concentration of K^+ in the stroma and lumen.

A.1.2.2 PSII recombination reactions and singlet O_2 production.

Earlier work (e.g. (221-223) shows that both $\Delta\psi$ and ΔpH should increase PSII recombination rates, and thus should increase $^1O_2$ production. We derived an equation for estimating recombination rate in PSII is described in Davis et al. (36) considering the effects of ΔpH and $\Delta\psi$ on energetics of electron sharing between redox intermediates:

$$v_{recomb} = [S_2Q_A^-] * k_{recomb}10^{(f_{\Delta\psi}\frac{-\Delta\psi}{0.06} + f_{pH}\cdot\Delta pH)} \quad \text{(eq. 4)}$$

v_recomb = k_recomb*QAm*(10**(fraction_Dy_effect *Dy/.06 +

fraction_pH_effect*(7.0-pHlumen)) (Python)

where v_{recomb} is the rate of recombination, $[S_2Q_A^-]$ is the concentration of PSII centers with reduced Q_A and the oxygen evolving complex in the S_2 state, k_{recomb} the intrinsic rate of recombination from $S_2Q_A^-$ in the absence of $\Delta\psi$ and ΔpH, ΔE_{stab} the stabilization free energy of

the charge separated state, expressed in eV (36), $f_{D\psi}$ (fraction_Dy_effect) and f_{DpH} (fraction_pH_effect) represents the fraction of quasi-stable S-states (that are able to recombine) and are sensitive to $\Delta\psi$ and ΔpH respectively (see text for more detail).

A.1.2.3 Normalizations of parameters.

One (trivial) difference with our earlier model Cruz et al., (2) is that content and concentration parameters are normalized to PSII content rather than thylakoid surface area. This will make it easier to account for lumen volume changes. We use the general parameters from the literature, as reviewed in Cruz et al., (2), including the following. From Cruz et al., 2001 "...we estimated that there were approximately 2×10^{-13} mol of PSI and PSII cm^{-2}" of thylakoid membrane, or 6 X 10^{10} PSII complexes cm^{-2}. If all PSII centers were hit, on average there would be 6 x 10^{10} cm^{-2} protons delivered into the lumen.

2×10^{-13} mol of PSII cm^{-2} thylakoid membrane

6.02 x 10^{23} molecules per mole × 10^{-13} moles of PSII cm^{-2} thylakoid membrane

1.2 x 10^{11} PSII centers per cm^{-2} thylakoid membrane

1.2 x 10^{11} protons cm^{-2}, into 0.8 10^{-9} L cm^{-2} i.e. 23 10-6 moles/L are moved, equivalent to a change in the concentration of protons (both bound and unbound) of 2.3 10^{-5} moles or about 12 μM.

With 0.8 x 10^{-9} L lumen volume cm^{-2} thylakoid membrane, yield 1.2x10^{11} PSII centers per cm^{-2} thylakoid membrane, or 6.7x 10^{-21} L per PSII center. Therefore, one turnover of PSII should introduce about 1.7 10^{-24} moles H+ /6.7 10^{-21} L equivalent to a change in concentration of about 2.5 10^{-4} M.

Given the large lumen buffering capacity, β=0.03 M/pH unit (22), the vast majority of these protons become buffered, and a single turnover flash should yield a ΔpH change of only

about 0.008 units. On the other hand, the capacitance of the thylakoid membrane is expected to be small, about 0.6 μF/cm^2 (see text) so that moving one charge per PSII center should produce a substantial $\Delta\psi$,

Hitting all PSII centers with a single turnover flash should move 1.2 x 10^{11} charges cm^{-2} or 1.2 x 10^{11} charges/6.242×10^{18} charges coulomb^{-1} =1.9E-8 C, and with 1.9E-8C/0.6 E-6C/V, and thus:

$$\Delta\psi(\text{flash})=0.033\ \text{V}$$

We use this value to indicate the effective $\Delta\psi$ for a transthylakoid movement of one charge per PSII equivalent.

A1.2.4 The reactions of the cytochrome *b_6f* complex.

The overall reaction for the cytochrome *b_6f* complex is takes to be:

$$PQH_2 + PC(ox) \leftarrow b_6f \rightarrow PQ + pmf + PC(red)\ \text{(Eq. 6)}$$

where PQ and PQH_2 are the oxidized and reduced forms of plastoquinone, PC(ox) and PC(red) are the oxidized and reduced forms of plastocyanin, and *pmf* is the proton motive force. There are several factors to consider. First, there is a kinetic effect of lumen pH on the binding of PQH_2 to the Rieske Fe_2S_2 protein (224), with a pK_a near 6-6.5 (see (47) and references within), so that:

$$b_6f(H^+) \leftrightarrow b_6f(\text{active}),\ \text{pKreg}\sim6.5\ \text{(Eq. 7)}$$

where b_6f(active) is the deprotonated, active and $b_6f(H^+)$ is inactive forms of the complex. This is a kinetic constraint, likely related to the deprotonation of a His residue on the Rieske FeS protein, see Crofts and Wang (224) for a detailed description of the experimental bases of this interpretation in the cytochrome bc1 complexes. The term, pKreg, describes the pH-dependence

of activation of the cytochrome b_6f complex. The empirically measured value is between 6.0 and 6.5 (47).

Next, we need to consider the redox states of PQH_2, PC as well as the $\Delta\psi$ and ΔpH components of *pmf*. Because the Q-cycle releases 2 H^+ into the lumen for each electron passed from PQH_2 to PC, there should be a thermodynamic constraint to the forward reaction:

$$0.5PQH_2 + b_6f(active) + PC(ox) \text{ --}k\_b6f\rightarrow PQ + b_6f(H^+) + PC(red) + 2H^+(\text{lumen}) \quad \text{(Eq. 8)}$$

This is somewhat simplified in that the intermediate reactions involving electron transfer through the low potential cytochrome b chain are ignored and it is assumed that the electron from the semiquinone generated in the Q_o site of the complex is immediately transferred to PQ, so that while one PQ is produced during the Q_o site reaction, it is partially reduced with the net effect of oxidation of a 0.5 PQH_2.

The forward rate constant is k_b6f, but the reaction is reversible, so that:

$$0.5PQH_2 + b_6f(active) + PC(ox) \leftarrow k\_b6f\_reverse\text{-- } PQ + b_6f(H^+) + PC(red) + 2H_{in} \quad \text{(Eq. 9)}$$

k_b6f_reverse is a function of *pmf* because the Q-cycle in the forward direction works against both ΔpH and $\Delta\psi$. Note that this thermodynamic effect is in addition to the kinetic effect on the deprotonation of the Rieske protein. We simulate this as follows:

$$K_{eq,b_6f} = E_m\left(\frac{PC_{ox}}{PC_{red}}\right) - E_m\left(\frac{PQ}{PQH_2}\right) - n \cdot pmf \quad \text{(Eq. 10)}$$

$$\text{Keq\_b6f} = E_m(\text{Pc(ox)/PC(red)}) - E_m(\text{PQ/PQH}_2) - n*pmf \text{ (Python)}$$

where K_{eq,b_6f} is the equilibrium constant for the forward reaction, and E_m(Pc(ox)/PC(red))=) = 0.370 V and E_m(PQ/PQH_2)=0.11 V at pH=7, are the effective redox midpoint potentials for the PC and PQ couples at pH=7, but are pH-dependent so that:

$$E_m(PQ/PQH_2) = 0.11\ V - (7\text{-}pH_{lumen}) * 0.06 \quad \text{(Eq. 12)}$$

In other words, the overall equilibrium constant is determined by the redox potentials of the donor and acceptor together and the *pmf*. We use unity as the scaling factor for the *pmf* contributions because one proton translocated to the lumen per e^- transferred (together with one e^- charge moved from the p- to the n-side) equilibrium.

$$k_{b_6f,reverse} = \frac{k_{b_6f,forward}}{K_{eq,b_6f}} \quad \text{(Eq.13)}$$

k_b6f_reverse = k_b6f / Keq_b6f (Python)

In principle, we could simulate the effects of changing PQH_2 and PC redox states in two ways, either using the simulated concentrations of PQH_2 and PC together with the standard $E^{'0}$ (E_m) values, or accounting for the concentrations in the E_m values. We chose the former because it better fits the form of the ODE equations and is a bit simpler to calculate. Thus,

$$v_{b6f} = [PQH_2][PC_{ox}]k_{b_6f,forward} - [PQ][PC_{red}]\, k_{b_6f,reverse} \quad \text{(eq. 14)}$$

v_b6f=[PQH2]*[PC_ox]*k_b6f - [PQ]*[PC_red]*k_b6f_reverse (Python)

The midpoint potential of PC is pH-independent under our conditions, but E'0(PQ/PQH2) = 0.11 V at pH=7, but pH-dependent (see Eq. 12) so that:

$$K_{eq,b_6f} = E_m\left(\frac{PC_{ox}}{PC_{red}}\right) - E_m\left(\frac{PQ}{PQH_2}\right) - n \cdot pmf = 0.370 - 0.11 + .06 * (\text{pHlumen} - 7.0) - n \cdot \text{pmf}$$ (Eq. 15)

Keq_b6f = E'0(Pc_ox/PC_red) - E'0(PQ/PQH2) - pmf = 0.370 - 0.11 + .06 * (pHlumen - 7.0) – pmf (Python)

So, the full set of equations in Python is:

Em7_PC=0.37 Em_PC=Em7_PC Em7_PQH2 = 0.11 Em_PQH2= Em7_PQH2 + 0.06*(pHlumen-7.0) #(Eq. 16)

Keq_b6f = 10**((Em_PC - Em_PQH2 - pmf)/.06) #(Eq. 17)

k_b6f_reverse = k_b6f / Keq # (Eq. 18)

v_b6f=PQH2*PC_ox* k_b6f - PQ*PC_red*k_b6f_reverse # (Eq. 19)

A.1.2.5 Calculating Phi2.

The following is a derivation for determining Phi2 from NPQ and Q_A redox state. The equations and derivations are based on those presented in Kramer et al. (100).

Recall that NPQ is the ratio of:

$$NPQ = \frac{k_{NPQ}}{k_f + k_d}$$ (Eq. 20)

where k_{NPQ}, k_f and k_d are the intrinsic rate constants for NPQ, fluorescence and non-radiative decay of excitons in the photosynthetic antenna. Also, maximal PSII quantum yield is:

$$\phi_{II,max} = \frac{k_{pc}}{k_d + k_f + k_{pc}} \sim 0.8$$ (Eq. 21)

$$\frac{1}{\phi_{II,max}} = \frac{k_d+k_f+k_{pc}}{k_{pc}} = 1 + \frac{k_d+k_f}{k_{pc}} \text{ (Eq. 22)}$$

$$\frac{k_{pc}}{k_d+k_f} = \frac{1}{\frac{1}{\phi_{II,max}}-1} \sim 4.88 \text{ (Eq. 23)}$$

where k_{pc} is the maximal rate constant for PSII photochemistry.

The realized ϕ_{II} at any time is given by:

$$\phi_{II} = \frac{[Q_A]k_{pc}}{k_d+k_f+k_{NPQ}+[Q_A]k_{pc}} \text{ (Eq. 24)}$$

where $[Q_A]$ is the fraction of open PSII centers with oxidized Q_A.

$$\frac{1}{\phi_{II}} = \frac{k_d+k_f+k_{NPQ}+[Q_A]k_{pc}}{[Q_A]k_{pc}} = 1 + \frac{k_d+k_f+k_{NPQ}}{[Q_A]k_{pc}} = 1 + \frac{k_d+k_f}{[Q_A]k_{pc}} + \frac{k_{NPQ}}{[Q_A]k_{pc}} = 1 + \frac{k_d+k_f}{[Q_A]k_{pc}} + \frac{NPQ(k_f+k_d)}{[Q_A]k_{pc}}$$

(Eq. 25)

$$[Q_A]\left(\frac{1}{\phi_{II}} - 1\right) = \frac{k_d+k_f}{k_{pc}} + \frac{NPQ(k_f+k_d)}{k_{pc}} = \frac{k_d+k_f}{k_{pc}}(1 + NPQ) = \frac{(1+NPQ)}{4.88} \text{ (Eq. 26)}$$

$$\frac{1}{\phi_{II}} - 1 = \frac{(1+NPQ)}{4.88[Q_A]} \text{ (Eq. 27)}$$

$$\frac{1}{\phi_{II}} = \frac{(1+NPQ)}{4.88[Q_A]} + 1 \text{ (Eq. 28)}$$

$$\phi_{II} = \frac{1}{\frac{(1+NPQ)}{4.88[Q_A]}+1} \text{ (Eq. 29)}$$

In Python, this translates to:

```
def Calc_Phi2(QA, NPQ):
Phi2=1/(1+(1+NPQ)/(4.88*QA))
return Phi2
```

REFERENCES

REFERENCES

1. Mitchell, P., *Chemiosmotic coupling in oxidative and photosynthetic phosphorylation.* Biol Rev Camb Philos Soc, 1966. **41**(3): p. 445-502.

2. Cruz, J.A., et al., *Contribution of electric field (Δψ) to steady-state transthylakoid proton motive force (pmf) in vitro and in vivo. Control of pmf parsing into Δψ and ΔpH by ionic strength.* Biochemistry, 2001. **40**(5): p. 1226-37.

3. Hangarter, R.P. and N.E. Good, *Energy thresholds for ATP synthesis in chloroplasts.* Biochim Biophys Acta, 1982. **681**(3): p. 397-404.

4. Gräber, P., U. Junesch, and G.H. Schatz, *Kinetics of proton-transport-coupled ATP-synthesis in chloroplasts. Activation of the ATPase by an artificially generated ΔpH and Δψ.* Berichte Der Bunsen-Gesellschaft-Physical Chemistry Chemical Physics, 1984. **88**(7): p. 599-608.

5. Strand, D.D. and D.M. Kramer, *Control of Non-Photochemical Exciton Quenching by the Proton Circuit of Photosynthesis*, in *Non-Photochemical Quenching and Energy Dissipation in Plants, Algae and Cyanobacteria*, B. DemmigAdams, et al., Editors. 2014, Springer: Dordrecht. p. 387-408.

6. Müller, P., X.P. Li, and K.K. Niyogi, *Non-photochemical quenching. A response to excess light energy.* Plant Physiol, 2001. **125**(4): p. 1558-66.

7. Li, X.P., et al., *Regulation of photosynthetic light harvesting involves intrathylakoid lumen pH sensing by the PsbS protein.* J Biol Chem, 2004. **279**(22): p. 22866-74.

8. Johnson, M.P. and A.V. Ruban, *Arabidopsis plants lacking PsbS protein possess photoprotective energy dissipation.* Plant J, 2010. **61**(2): p. 283-9.

9. Pinnola, A. and R. Bassi, *Molecular mechanisms involved in plant photoprotection.* Biochem Soc Trans, 2018. **46**(2): p. 467-482.

10. Sacksteder, C.A., et al., *The proton to electron stoichiometry of steady-state photosynthesis in living plants: A proton-pumping Q cycle is continuously engaged.* Proc Natl Acad Sci U S A, 2000. **97**(26): p. 14283-8.

11. Hope, A.B., P. Valente, and D.B. Matthews, *Effects of pH on the kinetics of redox reactions in and around the cytochrome bf complex in an isolated system.* Photosynthesis Research, 1994. **42**(2): p. 111-120.

12. Nishio, J.N. and J. Whitmarsh, *Dissipation of the proton electrochemical potential in intact chloroplasts (II. The pH gradient monitored by cytochrome f reduction kinetics).* Plant Physiol, 1993. **101**(1): p. 89-96.

13. Kramer, D.M., C.A. Sacksteder, and J.A. Cruz, *How acidic is the lumen?* Photosynthesis Research, 1999. **60**(2-3): p. 151-163.

14. Fisher, N., M.K. Bowman, and D.M. Kramer, *Electron Transfer Reactions at the Qo Site of the Cytochrome bc1 Complex: The Good, the Bad, and the Ugly*, in *Cytochrome Complexes: Evolution, Structures, Energy Transduction, and Signaling*, W.A. Cramer and T. Kallas, Editors. 2016, Springer Netherlands: Dordrecht. p. 419-434.

15. Zaharieva, I., J.M. Wichmann, and H. Dau, *Thermodynamic limitations of photosynthetic water oxidation at high proton concentrations.* J Biol Chem, 2011. **286**(20): p. 18222-8.

16. Vinyard, D.J. and G.W. Brudvig, *Progress Toward a Molecular Mechanism of Water Oxidation in Photosystem II.* Annu Rev Phys Chem, 2017.

17. Kok, B., B. Forbush, and M. McGloin, *Cooperation of charges in photosynthetic O2 evolution-I. A linear four step mechanism.* Photochem Photobiol, 1970. **11**(6): p. 457-75.

18. Takizawa, K., A. Kanazawa, and D.M. Kramer, *Depletion of stromal P(i) induces high 'energy-dependent' antenna exciton quenching (q_E) by decreasing proton conductivity at CF(O)-CF(1) ATP synthase.* Plant Cell Environ, 2008. **31**(2): p. 235-43.

19. Kanazawa, A. and D.M. Kramer, *In vivo modulation of nonphotochemical exciton quenching (NPQ) by regulation of the chloroplast ATP synthase.* Proc Natl Acad Sci U S A, 2002. **99**(20): p. 12789-94.

20. Junge, W. and H.T. Witt, *On ion transport system of photosynthesis - investigations on a molecular level.* Zeitschrift Fur Naturforschung Part B-Chemie Biochemie Biophysik Biologie Und Verwandten Gebiete, 1968. **B 23**(2): p. 244-&.

21. Van Kooten, O., J.F. Snel, and W.J. Vredenberg, *Photosynthetic free energy transduction related to the electric potential changes across the thylakoid membrane.* Photosynth Res, 1986. **9**(1-2): p. 211-27.

22. Junge, W., et al., *The buffering capacity of the internal phase of thylakoids and the magnitude of the pH changes inside under flashing light.* Biochim Biophys Acta, 1979. **546**(1): p. 121-41.

23. Vredenberg, W.J. and L.N. Dusens, *Light-induced changes in absorbancy and fluorescence of chlophyllous pigments associated with the pigment systems 1 and 2 in blue-green algae.* Biochim Biophys Acta, 1965. **94**: p. 355-70.

24. Vredenberg, W.J., *Light-induced changes in membrane potential of algal cells associated with photosynthetic electron transport.* Biochem Biophys Res Commun, 1969. **37**(5): p. 785-92.

25. Hind, G., H.Y. Nakatani, and S. Izawa, *Light-dependent redistribution of ions in suspensions of chloroplast thylakoid membranes.* Proc Natl Acad Sci U S A, 1974. **71**(4): p. 1484-8.

26. Barber, J. and W.J. Varley, *Stimulation of delayed light emission by salt gradients and estimation of relative ionic permeabilities of the thylakoid membranes.* Journal of Experimental Botany, 1972. **23**(74): p. 216-&.

27. Carraretto, L., et al., *A thylakoid-located two-pore K+ channel controls photosynthetic light utilization in plants.* Science, 2013. **342**(6154): p. 114-8.

28. Armbruster, U., et al., *Ion antiport accelerates photosynthetic acclimation in fluctuating light environments.* Nat Commun, 2014. **5**: p. 5439.

29. Kunz, H.H., et al., *Plastidial transporters KEA1, -2, and -3 are essential for chloroplast osmoregulation, integrity, and pH regulation in Arabidopsis.* Proc Natl Acad Sci U S A, 2014. **111**(20): p. 7480-5.

30. Herdean, A., et al., *The Arabidopsis thylakoid chloride channel AtCLCe functions in chloride homeostasis and regulation of photosynthetic electron transport.* Front Plant Sci, 2016. **7**: p. 115.

31. Herdean, A., et al., *A voltage-dependent chloride channel fine-tunes photosynthesis in plants.* Nat Commun, 2016. **7**: p. 11654.

32. Schneider, A., et al., *The evolutionarily conserved protein PHOTOSYNTHESIS AFFECTED MUTANT71 is required for efficient manganese uptake at the thylakoid membrane in Arabidopsis.* Plant Cell, 2016. **28**(4): p. 892-910.

33. Carraretto, L., et al., *Ion channels in plant bioenergetic organelles, chloroplasts and mitochondria: from molecular identification to function.* Mol Plant, 2016. **9**(3): p. 371-95.

34. Armbruster, U., et al., *The regulation of the chloroplast proton motive force plays a key role for photosynthesis in fluctuating light.* Curr Opin Plant Biol, 2017. **37**: p. 56-62.

35. Spetea, C., et al., *An update on the regulation of photosynthesis by thylakoid ion channels and transporters in Arabidopsis.* Physiol Plant, 2017. **161**(1): p. 16-27.

36. Davis, G.A., et al., *Limitations to photosynthesis by proton motive force-induced photosystem II photodamage.* Elife, 2016. **5**.

37. Vos, M.H., H.J. van Gorkom, and P.J. van Leeuwen, *An electroluminescence study of stabilization reactions in the oxygen-evolving complex of Photosystem II.* Biochim Biophys Acta, 1991. **1056**(1): p. 27-39.

38. Crofts, A.R., C.A. Wraight, and D.E. Fleischman, *Energy conservation in the photochemical reactions of photosynthesis and its relation to delayed fluorescence.* FEBS Lett, 1971. **15**(2): p. 89-100.

39. Kramer, D.M., J.A. Cruz, and A. Kanazawa, *Balancing the central roles of the thylakoid proton gradient.* Trends Plant Sci, 2003. **8**(1): p. 27-32.

40. von Ballmoos, C., A. Wiedenmann, and P. Dimroth, *Essentials for ATP synthesis by F1F0 ATP synthases.* Annu Rev Biochem, 2009. **78**: p. 649-72.

41. Silverstein, T.P., *An exploration of how the thermodynamic efficiency of bioenergetic membrane systems varies with c-subunit stoichiometry of F_1F_0 ATP synthases.* J Bioenerg Biomembr, 2014. **46**(3): p. 229-41.

42. von Ballmoos, C., G.M. Cook, and P. Dimroth, *Unique rotary ATP synthase and its biological diversity.* Annu Rev Biophys, 2008. **37**: p. 43-64.

43. Kaim, G. and P. Dimroth, *ATP synthesis by F-type ATP synthase is obligatorily dependent on the transmembrane voltage.* EMBO J, 1999. **18**(15): p. 4118-27.

44. Pogoryelov, D., et al., *Engineering rotor ring stoichiometries in the ATP synthase.* Proc Natl Acad Sci U S A, 2012. **109**(25): p. E1599-608.

45. Seelert, H., et al., *Structural biology. Proton-powered turbine of a plant motor.* Nature, 2000. **405**(6785): p. 418-9.

46. Kramer, D.M. and A.R. Crofts, *Activation of the chloroplast ATPase measured by the electrochromic change in leaves of intact plants.* Biochim Biophys Acta, 1989. **976**(1): p. 28-41.

47. Takizawa, K., et al., *The thylakoid proton motive force in vivo. Quantitative, non-invasive probes, energetics, and regulatory consequences of light-induced pmf.* Biochim Biophys Acta, 2007. **1767**(10): p. 1233-44.

48. Kashket, E.R., *Proton motive force in growing Streptococcus lactis and Staphylococcus aureus cells under aerobic and anaerobic conditions.* J Bacteriol, 1981. **146**(1): p. 369-76.

49. Booth, I.R., *Regulation of cytoplasmic pH in bacteria.* Microbiol Rev, 1985. **49**(4): p. 359-78.

50. Pogoryelov, D., et al., *The oligomeric state of c rings from cyanobacterial F-ATP synthases varies from 13 to 15.* J Bacteriol, 2007. **189**(16): p. 5895-902.

51. Pogoryelov, D., et al., *The c15 ring of the Spirulina platensis F-ATP synthase: F1/F0 symmetry mismatch is not obligatory.* EMBO Rep, 2005. **6**(11): p. 1040-4.

52. Dimroth, P., G. Kaim, and U. Matthey, *Crucial role of the membrane potential for ATP synthesis by F(1)F(o) ATP synthases.* J Exp Biol, 2000. **203**(Pt 1): p. 51-9.

53. Giersch, C., et al., *Energy charge, phosphorylation potential and proton motive force in chloroplasts.* Biochim Biophys Acta, 1980. **590**(1): p. 59-73.

54. Ioannidis, N.E., et al., *Evidence that putrescine modulates the higher plant photosynthetic proton circuit.* PLoS One, 2012. **7**(1): p. e29864.

55. de Grooth, B.G. and H.J. van Gorkom, *External electric field effects on prompt and delayed fluorescence in chloroplasts.* Biochim Biophys Acta, 1981. **635**(3): p. 445-56.

56. Rutherford, A.W., A. Osyczka, and F. Rappaport, *Back-reactions, short-circuits, leaks and other energy wasteful reactions in biological electron transfer: redox tuning to survive life in O(2).* FEBS Lett, 2012. **586**(5): p. 603-16.

57. Niyogi, K.K. and T.B. Truong, *Evolution of flexible non-photochemical quenching mechanisms that regulate light harvesting in oxygenic photosynthesis.* Curr Opin Plant Biol, 2013. **16**(3): p. 307-14.

58. Kirilovsky, D. and C.A. Kerfeld, *The orange carotenoid protein in photoprotection of photosystem II in cyanobacteria.* Biochim Biophys Acta, 2012. **1817**(1): p. 158-66.

59. Avenson, T.J., J.A. Cruz, and D.M. Kramer, *Modulation of energy-dependent quenching of excitons in antennae of higher plants.* Proc Natl Acad Sci U S A, 2004. **101**(15): p. 5530-5.

60. Kramer, D.M. and J.R. Evans, *The importance of energy balance in improving photosynthetic productivity.* Plant Physiol, 2011. **155**(1): p. 70-8.

61. Cruz, J.A., et al., *Plasticity in light reactions of photosynthesis for energy production and photoprotection.* J Exp Bot, 2005. **56**(411): p. 395-406.

62. Demmig-Adams, B. and W.W. Adams, *Photoprotection and other responses of plants to high light stress.* Annual Review of Plant Physiology and Plant Molecular Biology, 1992. **43**: p. 599-626.

63. Krieger, A. and E. Weis, *The role of calcium in the pH-dependent control of photosystem II.* Photosynthesis Research, 1993. **37**(2): p. 117-130.

64. Gross, E.L., et al., *Stability of plastocyanin to acid pH.* Biophysical Journal, 1994. **66**(2): p. A272-A272.

65. Raven, J.A., *The cost of photoinhibition.* Physiol Plant, 2011. **142**(1): p. 87-104.

66. Kulheim, C., J. Agren, and S. Jansson, *Rapid regulation of light harvesting and plant fitness in the field.* Science, 2002. **297**(5578): p. 91-3.

67. Keren, N. and A. Krieger-Liszkay, *Photoinhibition: molecular mechanisms and physiological significance.* Physiol Plant, 2011. **142**(1): p. 1-5.

68. Tyystjarvi, E., *Photoinhibition of Photosystem II.* Int Rev Cell Mol Biol, 2013. **300**: p. 243-303.

69. Takahashi, S., H. Bauwe, and M. Badger, *Impairment of the photorespiratory pathway accelerates photoinhibition of photosystem II by suppression of repair but not acceleration of damage processes in Arabidopsis.* Plant Physiol, 2007. **144**(1): p. 487-94.

70. Rott, M., et al., *ATP synthase repression in tobacco restricts photosynthetic electron transport, CO2 assimilation, and plant growth by overacidification of the thylakoid lumen.* Plant Cell, 2011. **23**(1): p. 304-21.

71. Kohzuma, K., et al., *Thioredoxin-insensitive plastid ATP synthase that performs moonlighting functions.* Proc Natl Acad Sci U S A, 2012. **109**(9): p. 3293-8.

72. Dal Bosco, C., et al., *Inactivation of the chloroplast ATP synthase gamma subunit results in high non-photochemical fluorescence quenching and altered nuclear gene expression in Arabidopsis thaliana.* J Biol Chem, 2004. **279**(2): p. 1060-9.

73. Inohara, N., et al., *Two genes, atpC1 and atpC2, for the gamma subunit of Arabidopsis thaliana chloroplast ATP synthase.* J Biol Chem, 1991. **266**(12): p. 7333-8.

74. Sacksteder, C.A. and D.M. Kramer, *Dark-interval relaxation kinetics (DIRK) of absorbance changes as a quantitative probe of steady-state electron transfer.* Photosynth Res, 2000. **66**(1-2): p. 145-58.

75. Cruz, J.A., et al., *Dynamic Environmental Photosynthetic Imaging Reveals Emergent Phenotypes.* Cell Syst, 2016. **2**(6): p. 365-377.

76. Avenson, T.J., et al., *Regulating the proton budget of higher plant photosynthesis.* Proc Natl Acad Sci U S A, 2005. **102**(27): p. 9709-13.

77. Nishiyama, Y. and N. Murata, *Revised scheme for the mechanism of photoinhibition and its application to enhance the abiotic stress tolerance of the photosynthetic machinery.* Appl Microbiol Biotechnol, 2014.

78. Tyystjarvi, E. and E.M. Aro, *The rate constant of photoinhibition, measured in lincomycin-treated leaves, is directly proportional to light intensity.* Proc Natl Acad Sci U S A, 1996. **93**(5): p. 2213-8.

79. Joliot, P. and R. Delosme, *Flash-induced 519 nm absorption change in green algae.* Biochim Biophys Acta, 1974. **357**(2): p. 267-84.

80. Joliot, P., R. Delosme, and A. Joliot, *515 nm Absorption changes in Chlorella at short times (4--100 mus) after a flash.* Biochim Biophys Acta, 1977. **459**(1): p. 47-57.

81. Bailleul, B., et al., *Electrochromism: a useful probe to study algal photosynthesis.* Photosynth Res, 2010. **106**(1-2): p. 179-89.

82. Kramer, D.M., T.J. Avenson, and G.E. Edwards, *Dynamic flexibility in the light reactions of photosynthesis governed by both electron and proton transfer reactions.* Trends Plant Sci, 2004. **9**(7): p. 349-57.

83. Pätsikkä, E., et al., *Excess copper predisposes photosystem II to photoinhibition in vivo by outcompeting iron and causing decrease in leaf chlorophyll.* Plant Physiol, 2002. **129**(3): p. 1359-67.

84. Diner, B. and P. Joliot, *Effect of the transmembrane electric field on the photochemical and quenching properties of photosystem II in vivo.* Biochim Biophys Acta, 1976. **423**(3): p. 479-98.

85. Satoh, K. and S. Katoh, *Induction kinetics of millisecond-delayed luminescence in intact Bryopsis chloroplasts.* Plant and Cell Physiology, 1983. **24**(6): p. 953-962.

86. Rappaport, F., et al., *A new electrochemical gradient generator in thylakoid membranes of green algae.* Biochemistry, 1999. **38**(7): p. 2040-7.

87. Johnson, G.N., A.W. Rutherford, and A. Krieger, *A change in the midpoint potential of the quinone Q_A in Photosystem II associated with photoactivation of oxygen evolution.* Biochim Biophys Acta, 1995. **1229**(2): p. 202-207.

88. Robinson, H.H. and A.R. Crofts, *Kinetics of the oxidation-reduction reactions of the photosystem-II quinone acceptor complex, and the pathway for deactivation.* Febs Letters, 1983. **153**(1): p. 221-226.

89. Dall'Osto, L., et al., *Zeaxanthin protects plant photosynthesis by modulating chlorophyll triplet yield in specific light-harvesting antenna subunits.* J Biol Chem, 2012. **287**(50): p. 41820-34.

90. Ramel, F., et al., *Light-induced acclimation of the Arabidopsis chlorina1 mutant to singlet oxygen.* Plant Cell, 2013. **25**(4): p. 1445-62.

91. Shumbe, L., et al., *Singlet oxygen-induced cell death in Arabidopsis under high-light stress is controlled by OXI1 kinase.* Plant Physiol, 2016. **170**(3): p. 1757-71.

92. Koh, E. and R. Fluhr, *Singlet oxygen detection in biological systems: uses and limitations.* Plant Signal Behav, 2016: p. 0.

93. Krieger-Liszkay, A., C. Fufezan, and A. Trebst, *Singlet oxygen production in photosystem II and related protection mechanism.* Photosynth Res, 2008. **98**(1-3): p. 551-64.

94. Telfer, A., *Singlet oxygen production by PSII under light stress: mechanism, detection and the protective role of beta-carotene.* Plant Cell Physiol, 2014. **55**(7): p. 1216-23.

95. Telfer, A., A. Pascal, and A. Gall, *Carotenoids in Photosynthesis*, in *Carotenoids*, G. Britton, S. Liaaen-Jensen, and H. Pfander, Editors. 2008, Birkhäuser Basel. p. 265-308.

96. Keren, N., et al., *Mechanism of photosystem II photoinactivation and D1 protein degradation at low light: the role of back electron flow.* Proc Natl Acad Sci U S A, 1997. **94**(4): p. 1579-84.

97. Allahverdiyeva, Y., et al., *Cyanobacterial oxygenic photosynthesis is protected by flavodiiron proteins.* Life (Basel), 2015. **5**(1): p. 716-43.

98. Zhang, S., K. Apel, and C. Kim, *Singlet oxygen-mediated and EXECUTER-dependent signalling and acclimation of Arabidopsis thaliana exposed to light stress.* Philos Trans R Soc Lond B Biol Sci, 2014. **369**(1640): p. 20130227.

99. Krieger-Liszkay, A. and A.W. Rutherford, *Influence of herbicide binding on the redox potential of the quinone acceptor in photosystem II: relevance to photodamage and phytotoxicity.* Biochemistry, 1998. **37**(50): p. 17339-44.

100. Kramer, D.M., et al., *New fluorescence parameters for the determination of Q_A redox state and excitation energy fluxes.* Photosynth Res, 2004. **79**(2): p. 209-18.

101. Finazzi, G., et al., *Ions channels/transporters and chloroplast regulation.* Cell Calcium, 2015. **58**(1): p. 86-97.

102. van Gorkom, H.J., *Electroluminescence.* Photosynth Res, 1996. **48**(1-2): p. 107-16.

103. Blankenship, R.E., et al., *Comparing photosynthetic and photovoltaic efficiencies and recognizing the potential for improvement.* Science, 2011. **332**(6031): p. 805-9.

104. Gust, D., et al., *Engineered and artificial photosynthesis: Human ingenuity enters the game.* Mrs Bulletin, 2008. **33**(4): p. 383-387.

105. Milo, R., *What governs the reaction center excitation wavelength of photosystems I and II?* Photosynth Res, 2009. **101**(1): p. 59-67.

106. Shockley, W. and H.J. Queisser, *Detailed balance limit of efficiency of p-n junction solar cells.* Journal of Applied Physics, 1961. **32**(3): p. 510-&.

107. Marosvolgyi, M.A. and H.J. van Gorkom, *Cost and color of photosynthesis.* Photosynth Res, 2010. **103**(2): p. 105-9.

108. Miyashita, H., et al., *Chlorophyll d as a major pigment.* Nature, 1996. **383**(6599): p. 402-402.

109. Kuhl, M., et al., *Ecology: a niche for cyanobacteria containing chlorophyll d.* Nature, 2005. **433**(7028): p. 820.

110. Gan, F., et al., *Extensive remodeling of a cyanobacterial photosynthetic apparatus in far-red light.* Science, 2014. **345**(6202): p. 1312-7.

111. Behrendt, L., et al., *Chlorophyll f-driven photosynthesis in a cavernous cyanobacterium.* ISME J, 2015. **9**(9): p. 2108-11.

112. Cotton, C.A., et al., *Photosynthetic constraints on fuel from microbes.* Front Bioeng Biotechnol, 2015. **3**: p. 36.

113. Hadi, M.Z., et al., *Simple and versatile selection of Arabidopsis transformants.* Plant Cell Reports, 2002. **21**(2): p. 130-135.

114. Clough, S.J. and A.F. Bent, *Floral dip: a simplified method for Agrobacterium-mediated transformation of Arabidopsis thaliana.* Plant J, 1998. **16**(6): p. 735-43.

115. Seigneurin-Berny, D., et al., *Purification of intact chloroplasts from Arabidopsis and spinach leaves by isopycnic centrifugation.* Curr Protoc Cell Biol, 2008. **Chapter 3**: p. Unit 3 30.

116. Porra, R.J., W.A. Thompson, and P.E. Kriedemann, *Determination of accurate extinction coefficients and simultaneous equations for assaying chlorophylls a and b extracted with four different solvents: verification of the concentration of chlorophyll standards by atomic absorption spectroscopy.* Biochim Biophys Acta, 1989. **975**(3): p. 384-394.

117. Hall, C.C., et al., *Photosynthetic measurements with the Idea Spec: an integrated diode emitter array spectrophotometer/fluorometer.* Photosynthesis: Research for Food, Fuel and Future (15th International Conference on Photosynthesis) 2013: p. 184-188.

118. Livingston, A.K., et al., *An Arabidopsis mutant with high cyclic electron flow around photosystem I (hcef) involving the NADPH dehydrogenase complex.* Plant Cell, 2010. **22**(1): p. 221-33.

119. Cazzaniga, S., et al., *Interaction between avoidance of photon absorption, excess energy dissipation and zeaxanthin synthesis against photooxidative stress in Arabidopsis.* Plant J, 2013. **76**(4): p. 568-79.

120. Krause, G.H. and P. Jahns, *Pulse Amplitude Modulated Chlorophyll Fluorometry and its Application in Plant Science*, in *Advances in Photosynthesis and Respiration*, B.R.a.P. Green, W. W., Editor. 2003, Kluwer Academic: Dordrecht, The Netherlands. p. 373-399.

121. Baker, N.R., J. Harbinson, and D.M. Kramer, *Determining the limitations and regulation of photosynthetic energy transduction in leaves.* Plant Cell Environ, 2007. **30**(9): p. 1107-25.

122. Ragas, X., et al., *Singlet oxygen photosensitisation by the fluorescent probe Singlet Oxygen Sensor Green.* Chem Commun (Camb), 2009(20): p. 2920-2.

123. Allahverdiyeva, Y., et al., *Flavodiiron proteins Flv1 and Flv3 enable cyanobacterial growth and photosynthesis under fluctuating light.* Proc Natl Acad Sci U S A, 2013. **110**(10): p. 4111-6.

124. Suorsa, M., et al., *PGR5 ensures photosynthetic control to safeguard photosystem I under fluctuating light conditions.* Plant Signal Behav, 2013. **8**(1): p. e22741.

125. Murchie, E.H. and K.K. Niyogi, *Manipulation of photoprotection to improve plant photosynthesis.* Plant Physiol, 2011. **155**(1): p. 86-92.

126. Kromdijk, J., et al., *Improving photosynthesis and crop productivity by accelerating recovery from photoprotection.* Science, 2016. **354**(6314): p. 857-861.

127. Eberhard, S., G. Finazzi, and F.A. Wollman, *The dynamics of photosynthesis.* Annu Rev Genet, 2008. **42**: p. 463-515.

128. Aro, E.M., I. Virgin, and B. Andersson, *Photoinhibition of Photosystem II. Inactivation, protein damage and turnover.* Biochim Biophys Acta, 1993. **1143**(2): p. 113-34.

129. Kasahara, M., et al., *Chloroplast avoidance movement reduces photodamage in plants.* Nature, 2002. **420**(6917): p. 829-32.

130. Yamori, W. and T. Shikanai, *Physiological functions of cyclic electron transport around Photosystem I in sustaining photosynthesis and plant growth.* Annu Rev Plant Biol, 2016. **67**: p. 81-106.

131. Strand, D.D., N. Fisher, and D.M. Kramer, *Distinct Energetics and Regulatory Functions of the Two Major Cyclic Electron Flow Pathways in Chloroplasts*. Chloroplasts: Current Research and Future Trends, ed. H. Kirchhoff. 2016, Wymondham: Caister Academic Press. 89-100.

132. Brinkert, K., et al., *Bicarbonate-induced redox tuning in Photosystem II for regulation and protection.* Proc Natl Acad Sci U S A, 2016. **113**(43): p. 12144-12149.

133. Allahverdiyeva, Y., et al., *Photoprotection of photosystems in fluctuating light intensities.* J Exp Bot, 2015. **66**(9): p. 2427-36.

134. Niyogi, K.K., *Safety valves for photosynthesis.* Curr Opin Plant Biol, 2000. **3**(6): p. 455-60.

135. Aronsson, H., et al., *Monogalactosyldiacylglycerol deficiency in Arabidopsis affects pigment composition in the prolamellar body and impairs thylakoid membrane energization and photoprotection in leaves.* Plant Physiol, 2008. **148**(1): p. 580-92.

136. Cruz, J.A., et al., *Storage of light-driven transthylakoid proton motive force as an electric field (Δψ) under steady-state conditions in intact cells of Chlamydomonas reinhardtii.* Photosynth Res, 2005. **85**(2): p. 221-33.

137. Fristedt, R., et al., *The thylakoid membrane protein CGL160 supports CF1CF0 ATP synthase accumulation in Arabidopsis thaliana.* PLoS One, 2015. **10**(4): p. e0121658.

138. Tikhonov, A.N., *Energetic and regulatory role of proton potential in chloroplasts.* Biochemistry (Mosc), 2012. **77**(9): p. 956-74.

139. Johnson, M.P. and A.V. Ruban, *Rethinking the existence of a steady-state Δψ component of the proton motive force across plant thylakoid membranes.* Photosynth Res, 2014. **119**(1-2): p. 233-42.

140. Duan, Z., et al., *A bestrophin-like protein modulates the proton motive force across the thylakoid membrane in Arabidopsis.* J Integr Plant Biol, 2016. **58**(10): p. 848-858.

141. van Mieghem, F., et al., *Charge recombination reactions in photosystem II. I. Yields, recombination pathways, and kinetics of the primary pair.* Biochemistry, 1995. **34**(14): p. 4798-813.

142. Woodbury, N.W., et al., *Radical-pair energetics and decay mechanisms in reaction centers containing anthraquinones, naphthoquinones or benzoquinones in place of ubiquinone.* Biochim Biophys Acta, 1986. **851**(1): p. 6-22.

143. Goltsev, V., et al., *Delayed fluorescence in photosynthesis.* Photosynth Res, 2009. **101**(2-3): p. 217-32.

144. Rutherford, A.W., D.R. Paterson, and J.E. Mullet, *A light-induced spin-polarized triplet detected by EPR in photosystem II reaction centers.* Biochim Biophys Acta, 1981. **635**(2): p. 205-14.

145. Rappaport, F., et al., *Kinetics and pathways of charge recombination in photosystem II.* Biochemistry, 2002. **41**(26): p. 8518-27.

146. Zaks, J., et al., *A kinetic model of rapidly reversible nonphotochemical quenching.* Proc Natl Acad Sci U S A, 2012. **109**(39): p. 15757-62.

147. Tikhonov, A.N. and A.V. Vershubskii, *Computer modeling of electron and proton transport in chloroplasts.* Biosystems, 2014. **121**: p. 1-21.

148. Jursinic, P., *Investigation of double turnovers in photosystem II charge separation and oxygen evolution with excitation flashes of different duration.* Biochim Biophys Acta, 1981. **635**(1): p. 38-52.

149. Heldt, W.H., et al., *Alkalization of the chloroplast stroma caused by light-dependent proton flux into the thylakoid space.* Biochim Biophys Acta, 1973. **314**(2): p. 224-41.

150. Wu, W. and G.A. Berkowitz, *Stromal pH and photosynthesis are affected by electroneutral K and H exchange through chloroplast envelope ion channels.* Plant Physiol, 1992. **98**(2): p. 666-72.

151. Rutherford, A.W., et al., *Thermoluminescence as a probe of photosystem II. The redox and protonation states of the secondary acceptor quinone and the O2-evolving enzyme.* Biochim Biophys Acta, 1984. **767**(3): p. 548-556.

152. Avenson, T.J., et al., *Integrating the proton circuit into photosynthesis: progress and challenges.* Plant Cell and Environment, 2005. **28**(1): p. 97-109.

153. Kirchhoff, H., et al., *Dynamic control of protein diffusion within the granal thylakoid lumen.* Proc Natl Acad Sci U S A, 2011. **108**(50): p. 20248-53.

154. Demmig-Adams, B., et al., *Non-Photochemical Fluorescence Quenching in Contrasting Plant Species and Environments*, in *Non-Photochemical Quenching and Energy*

Dissipation in Plants, Algae and Cyanobacteria, B. DemmigAdams, et al., Editors. 2014, Springer: Dordrecht. p. 531-552.

155. Mekala, N.R., et al., *Plants actively avoid state transitions upon changes in light intensity: role of light-harvesting complex II protein dephosphorylation in high light.* Plant Physiol, 2015. **168**(2): p. 721-34.

156. Kirchhoff, H., U. Mukherjee, and H.J. Galla, *Molecular architecture of the thylakoid membrane: lipid diffusion space for plastoquinone.* Biochemistry, 2002. **41**(15): p. 4872-82.

157. Cruz, J.A., et al., *Inhibition of plastocyanin to P_{700}^+ electron transfer in Chlamydomonas reinhardtii by hyperosmotic stress.* Plant Physiol, 2001. **127**(3): p. 1167-79.

158. Armbruster, U., et al., *Regulation and levels of the thylakoid K^+/H^+ antiporter KEA3 shape the dynamic response of photosynthesis in fluctuating light.* Plant Cell Physiol, 2016. **57**(7): p. 1557-1567.

159. Wang, C., et al., *Fine-tuned regulation of the K+ /H+ antiporter KEA3 is required to optimize photosynthesis during induction.* Plant J, 2017. **89**(3): p. 540-553.

160. Puthiyaveetil, S., B. van Oort, and H. Kirchhoff, *Surface charge dynamics in photosynthetic membranes and the structural consequences.* Nat Plants, 2017. **3**: p. 17020.

161. Jarvi, S., M. Suorsa, and E.M. Aro, *Photosystem II repair in plant chloroplasts--Regulation, assisting proteins and shared components with photosystem II biogenesis.* Biochim Biophys Acta, 2015. **1847**(9): p. 900-9.

162. Kirchhoff, H., *Structural constraints for protein repair in plant photosynthetic membranes.* Plant Signal Behav, 2013. **8**(4): p. e23634.

163. Tiwari, A., et al., *Photodamage of iron-sulphur clusters in photosystem I induces non-photochemical energy dissipation.* Nat Plants, 2016. **2**: p. 16035.

164. Vinyard, D.J., G.M. Ananyev, and G.C. Dismukes, *Photosystem II: the reaction center of oxygenic photosynthesis.* Annu Rev Biochem, 2013. **82**: p. 577-606.

165. Nelson, N. and A. Ben-Shem, *Structure, function, and regulation of plant photosystem I.* Advances in Photosynthesis and Respiration:THE LIGHT-DRIVEN PLASTOCYANIN: FERREDOXIN OXIDOREDUCTASE, ed. J.H. Golbeck. Vol. 24. 2006: Springer, Po Box 17, 3300 Aa Dordrecht, Netherlands. 71.

166. Niyogi, K.K., A.R. Grossman, and O. Bjorkman, *Arabidopsis mutants define a central role for the xanthophyll cycle in the regulation of photosynthetic energy conversion.* Plant Cell, 1998. **10**(7): p. 1121-34.

167. Davis, G.A., A.W. Rutherford, and D.M. Kramer, *Hacking the thylakoid proton motive force for improved photosynthesis: modulating ion flux rates that control proton motive force partitioning into Δψ and ΔpH.* Philos Trans R Soc Lond B Biol Sci, 2017. **372**(1730).

168. Schatz, G.H., H. Brock, and A.R. Holzwarth, *Kinetic and energetic model for the primary processes in photosystem II.* Biophys J, 1988. **54**(3): p. 397-405.

169. Umena, Y., et al., *Crystal structure of oxygen-evolving photosystem II at a resolution of 1.9 A.* Nature, 2011. **473**(7345): p. 55-60.

170. Dau, H. and K. Sauer, *Electric field effect on chlorophyll fluorescence and its relation to Photosystem II charge separation reactions studied by a salt-jump technique.* Biochim Biophys Acta, 1991. **1098**(1): p. 49-60.

171. Arnold, W. and J. Azzi, *Mechanism of delayed light production by photosynthetic organisms and a new effect of electric fields on chloroplasts.* Photochemistry and Photobiology, 1971. **14**(3): p. 233-&.

172. Fleischman, D.E., *Luminescence in photosynthetic bacteria.* Photochemistry and Photobiology, 1971. **14**(3): p. 277-&.

173. Strehler, B.L. and W. Arnold, *Light production by green plants.* Journal of General Physiology, 1951. **34**(6): p. 809-820.

174. Tyystjarvi, E. and I. Vass, *Light emission as a probe of charge separation and recombination in the photosynthetic apparatus: Relation of prompt fluorescence to delayed light emission and thermoluminescence.* Chlorophyll a Fluoerescence: Signature of Photosynthesis, 2004. **19**: p. 363-388.

175. Jursinic, P. and Govindjee, *Effects of hydroxylamine and silicomolybdate on the decay in delayed light emission in the 6-100 microsecond range after a single 10 ns flash in pea thylakoids.* Photosynthesis Research, 1982. **3**(3): p. 161-178.

176. Li, X.P., et al., *A pigment-binding protein essential for regulation of photosynthetic light harvesting.* Nature, 2000. **403**(6768): p. 391-5.

177. Grabolle, M. and H. Dau, *Energetics of primary and secondary electron transfer in Photosystem II membrane particles of spinach revisited on basis of recombination-fluorescence measurements.* Biochim Biophys Acta, 2005. **1708**(2): p. 209-18.

178. Hideg, E., M. Kobayashi, and H. Inaba, *The far red induced slow component of delayed light from chloroplasts is emitted from Photosystem II : Evidence from emission spectroscopy.* Photosynth Res, 1991. **29**(2): p. 107-12.

179. Suorsa, M., et al., *PROTON GRADIENT REGULATION5 is essential for proper acclimation of Arabidopsis photosystem I to naturally and artificially fluctuating light conditions.* Plant Cell, 2012. **24**(7): p. 2934-48.

180. de Bianchi, S., et al., *Regulation of plant light harvesting by thermal dissipation of excess energy.* Biochem Soc Trans, 2010. **38**(2): p. 651-60.

181. Li, L., et al., *Protein degradation rate in Arabidopsis thaliana leaf growth and development.* Plant Cell, 2017. **29**(2): p. 207-228.

182. Wraight, C.A. and R.K. Clayton, *The absolute quantum efficiency of bacteriochlorophyll photooxidation in reaction centres of Rhodopseudomonas spheroides.* Biochim Biophys Acta, 1974. **333**(2): p. 246-60.

183. Hideg, E., et al., *Photoinhibition of photosynthesis in vivo results in singlet oxygen production detection via nitroxide-induced fluorescence quenching in broad bean leaves.* Biochemistry, 1998. **37**(33): p. 11405-11.

184. Rehman, A.U., et al., *Characterization of singlet oxygen production and its involvement in photodamage of Photosystem II in the cyanobacterium Synechocystis PCC 6803 by histidine-mediated chemical trapping.* Biochim Biophys Acta, 2013. **1827**(6): p. 689-98.

185. Fufezan, C., A.W. Rutherford, and A. Krieger-Liszkay, *Singlet oxygen production in herbicide-treated photosystem II.* FEBS Lett, 2002. **532**(3): p. 407-10.

186. de Wijn, R. and H.J. van Gorkom, *Kinetics of electron transfer from Q_A to Q_B in photosystem II.* Biochemistry, 2001. **40**(39): p. 11912-22.

187. Rutherford, A.W., A.R. Crofts, and Y. Inoue, *Thermoluminescence as a probe of Photosystem II photochemistry. The origin of the flash-induced glow peaks.* Biochim Biophys Acta, 1982. **682**(3): p. 457-465.

188. Jursinic, P.A., *Delayed fluorescence: Current concepts and status*, in *Light Emission by Plants and Bacteria*, Govindjee, Amesz J., and Fork D.C., Editors. 1986, Academic Press: Orlando, Florida. p. 291-328.

189. Jeans, C., M.J. Schilstra, and D.R. Klug, *The temperature dependence of $P680^+$ reduction in oxygen-evolving photosystem II.* Biochemistry, 2002. **41**(15): p. 5015-23.

190. Reynolds, M.P., S. Rajaram, and K.D. Sayre, *Physiological and genetic changes of irrigated wheat in the post-green revolution period and approaches for meeting projected global demand.* Crop Science, 1999. **39**(6): p. 1611-1621.

191. Watanabe, N., J.R. Evans, and W.S. Chow, *Changes in the photosynthetic properties of Australian wheat cultivars over the last century.* Australian Journal of Plant Physiology, 1994. **21**(2): p. 169-183.

192. Alexandratos, N. and J. Bruinsma, *World Agriculture Towards 2030/2050: The 2012 Revision No. 12-03*, F.a.A. Organization, Editor 2012: Rome.

193. Long, S.P. and D.R. Ort, *More than taking the heat: crops and global change.* Curr Opin Plant Biol, 2010. **13**(3): p. 241-8.

194. Ray, D.K., et al., *Recent patterns of crop yield growth and stagnation.* Nat Commun, 2012. **3**: p. 1293.

195. Long, S.P., et al., *Can improvement in photosynthesis increase crop yields?* Plant Cell Environ, 2006. **29**(3): p. 315-30.

196. Ort, D.R., et al., *Redesigning photosynthesis to sustainably meet global food and bioenergy demand.* Proc Natl Acad Sci U S A, 2015. **112**(28): p. 8529-36.

197. Kaiser, E., A. Morales, and J. Harbinson, *Fluctuating light takes crop photosynthesis on a rollercoaster ride.* Plant Physiol, 2018. **176**(2): p. 977-989.

198. Werner, C., et al., *Effects of photoinhibition on whole-plant carbon gain assessed with a photosynthesis model.* Plant Cell and Environment, 2001. **24**(1): p. 27-40.

199. Zhu, X.G., et al., *The slow reversibility of photosystem II thermal energy dissipation on transfer from high to low light may cause large losses in carbon gain by crop canopies: a theoretical analysis.* J Exp Bot, 2004. **55**(400): p. 1167-75.

200. Demmig-Adams, B., *Survey of thermal energy dissipation and pigment composition in sun and shade leaves.* Plant and Cell Physiology, 1998. **39**(5): p. 474-482.

201. Johnson, G.N., et al., *The dissipation of excess excitation energy in British plant species.* Plant Cell and Environment, 1993. **16**(6): p. 673-679.

202. Brugnoli, E., A. Cona, and M. Lauteri, *Xanthophyll cycle components and capacity for non-radiative energy dissipation in sun and shade leaves of Ligustrum ovalifolium exposed to conditions limiting photosynthesis.* Photosynthesis Research, 1994. **41**(3): p. 451-463.

203. van Rooijen, R., et al., *Natural variation of YELLOW SEEDLING1 affects photosynthetic acclimation of Arabidopsis thaliana.* Nat Commun, 2017. **8**(1): p. 1421.

204. Oakley, C.G., et al., *Genetic basis of photosynthetic responses to cold in two locally adapted populations of Arabidopsis thaliana.* J Exp Bot, 2018. **69**(3): p. 699-709.

205. Jung, H.S. and K.K. Niyogi, *Quantitative genetic analysis of thermal dissipation in Arabidopsis.* Plant Physiol, 2009. **150**(2): p. 977-86.

206. Driever, S.M., et al., *Natural variation in photosynthetic capacity, growth, and yield in 64 field-grown wheat genotypes.* J Exp Bot, 2014. **65**(17): p. 4959-73.

207. Qu, M., et al., *Leaf photosynthetic parameters related to biomass accumulation in a global rice diversity survey.* Plant Physiol, 2017. **175**(1): p. 248-258.

208. Jahn, C.E., et al., *Genetic variation in biomass traits among 20 diverse rice varieties.* Plant Physiol, 2011. **155**(1): p. 157-68.

209. Fischer, R.A., et al., *Wheat yield progress associated with higher stomatal conductance and photosynthetic rate, and cooler canopies.* Crop Science, 1998. **38**(6): p. 1467-1475.

210. Kover, P.X., et al., *A Multiparent Advanced Generation Inter-Cross to fine-map quantitative traits in Arabidopsis thaliana.* PLoS Genet, 2009. **5**(7): p. e1000551.

211. Baker, N.R., *Chlorophyll fluorescence: a probe of photosynthesis in vivo.* Annu Rev Plant Biol, 2008. **59**: p. 89-113.

212. Bielczynski, L.W., et al., *Leaf and plant age affects photosynthetic performance and photoprotective capacity.* Plant Physiol, 2017. **175**(4): p. 1634-1648.

213. Gan, X., et al., *Multiple reference genomes and transcriptomes for Arabidopsis thaliana.* Nature, 2011. **477**(7365): p. 419-23.

214. Provart, N.J., et al., *50 years of Arabidopsis research: highlights and future directions.* New Phytol, 2016. **209**(3): p. 921-44.

215. Mishra, Y., et al., *Arabidopsis plants grown in the field and climate chambers significantly differ in leaf morphology and photosystem components.* BMC Plant Biol, 2012. **12**: p. 6.

216. Niyogi, K.K., O. Bjorkman, and A.R. Grossman, *Chlamydomonas xanthophyll cycle mutants identified by video imaging of chlorophyll fluorescence quenching.* Plant Cell, 1997. **9**(8): p. 1369-1380.

217. Flood, P.J., J. Harbinson, and M.G. Aarts, *Natural genetic variation in plant photosynthesis.* Trends Plant Sci, 2011. **16**(6): p. 327-35.

218. Bazakos, C., et al., *New strategies and tools in quantitative genetics: how to go from the phenotype to the genotype.* Annu Rev Plant Biol, 2017. **68**: p. 435-455.

219. Cardona, T., J.W. Murray, and A.W. Rutherford, *Origin and evolution of water oxidation before the last common ancestor of the Cyanobacteria.* Mol Biol Evol, 2015. **32**(5): p. 1310-28.

220. Cardona, T., et al., *Charge separation in photosystem II: a comparative and evolutionary overview.* Biochim Biophys Acta, 2012. **1817**(1): p. 26-43.

221. Crofts, A.R., C.A. Wraight, and D.E. Fleischmann, *Energy conservation in photochemical reactions of photosynthesis and its relation to delayed fluorescence.* Febs Letters, 1971. **15**(2): p. 89-100.

222. Jursinic, P., Govindjee, and C.A. Wraight, *Memrane-potential and microsecond to millisecond delayed light-emission after a single excitation flash in isolated chloroplasts* Photochemistry and Photobiology, 1978. **27**(1): p. 61-71.

223. Wagner, H., et al., *Light emission originating from photosystem II radical pair recombination is sensitive to zeaxanthin related non-photochemical quenching (NPQ).* J Photochem Photobiol B, 2006. **83**(3): p. 172-9.

224. Crofts, A.R. and Z. Wang, *How rapid are the internal reactions of the ubiquinol:cytochrome c 2 oxidoreductase?* Photosynth Res, 1989. **22**(1): p. 69-87.